Patricia Wildberger

Shining new light on enzymatic glycosyl and phosphoryl transfer reactions

Mechanistic insights from structure-function studies and new biocatalytic applications for the synthesis of high-value glycosides

PhD Thesis

Graz University of Technology

Institute of Biotechnology and Biochemical Engineering
Univ.-Prof. Dipl.-Ing. Dr.techn. Bernd Nidetzky

Graz, October 2013

Statutory Declaration

I declare that I have authored this thesis independently, that I have not used other than the declared sources/resources, and that I have explicitly marked all material which has been quoted either literally or by content from the used sources.

Graz, _____ _____

Date Signature

Abstract

Carbohydrates are the most abundant organic molecules in nature and are characterized by their enormous structural complexity and functional diversity. The synthesis and cleavage of glycosidic bonds in glycoconjugates, oligosaccharides and polysaccharides is catalyzed by a specific group of enzymes, the carbohydrate-active enzymes (CAZymes). Among them are sucrose phosphorylase from *Leuconostoc mesenteroides* and cellobiose phosphorylase from *Cellulomonas uda*, enzymes responsible for the cleavage of glycosidic bonds through substitution of phosphate. Both enzymes are supposed to serve a catabolic role *in vivo*, fueling the energy metabolism of the cell with glucose 1-phosphate produced from sucrose or cellobiose, respectively. Site-directed mutagenesis of active-site residues was used to thoroughly investigate structure-function relationships in sucrose phosphorylase intended to gain insights on the molecular level of substrate specificity, substrate binding and catalysis. Furthermore, the spectrum of glucosylated products synthesized by sucrose phosphorylase was broadened. When sucrose was used as donor and glyceric acid amide as alternative acceptor to phosphate, sucrose phosphorylase catalyzed the highly regio- and stereoselective as well as efficient single-step synthesis of the novel osmolyte (*R*)-2-*O*-*α*-D-glucopyranosyl glyceric acid amide. Cellobiose phosphorylase was investigated in respect of its donor substrate specificity, by probing a substrate analogue, the endocyclic enitol glucal, as alternative to cellobiose. Glucal was utilized as substrate and the 2-deoxy glucosyl moiety was transferred to phosphate, thereby catalyzing the single-step synthesis of 2-deoxyglucose 1-phosphate, a substrate for chemical mutagenesis studies. Finally, we investigated the activity spectrum of glucose-1-phosphatase from *Escherichia coli*, an enzyme classified as hydrolase and described to cleave phosphoric monoester bonds. In our studies we were able to elucidate the potential of glucose-1-phosphatase to transfer the phosphoryl group from glucose 1-phosphate to an acceptor different to water. When glucose 1-phosphate was provided as donor and fructose as acceptor, glucose-1-phosphatase catalyzed the synthesis of fructose 1-phosphate. By coupling the phosphoryl transfer activity of glucose-1-phosphatase to the glucosyl transfer activity of sucrose phosphorylase, the high-value metabolite fructose 1-phosphate was synthesized from the commodity products sucrose and phosphate in an efficient one-pot, two-step cascade reaction.

Zusammenfassung

Kohlenhydrate sind die in der Natur am weitesten verbreiteten organischen Moleküle und zeichnen sich durch ihre enorme strukturelle Komplexität und funktionelle Vielfalt aus. Die Bildung und Spaltung von glycosidischen Bindungen in Glycokonjugaten, Oligosacchariden und Polysacchariden wird von einer bestimmten Gruppe von Enzymen, den kohlenhydrataktiven Enzymen (CAZymes), katalysiert. Zu ihnen zählen Saccharose Phosphorylase aus *Leuconostoc mesenteroides* und Cellobiose Phosphorylase aus *Cellulomonas uda*, Enzyme, die glycosidische Bindungen spalten und die Glycosylgruppe auf Phosphat übertragen. Beide Enzyme sind *in vivo* in katabolische Prozesse involviert, indem sie, ausgehend von Saccharose bzw. Cellobiose, dem Zellstoffwechsel Glucose 1-Phosphat zur Verfügung stellen. Mittels ortsgerichteter Mutagenese wurden ausgewählte Aminosäurereste im aktiven Zentrum von Saccharose Phosphorylase substituiert, um Struktur-Funktions-Beziehungen zu untersuchen und um zum besseren Verständnis von molekularen Vorgängen auf Ebene der Substratspezifität, Substratbindung und Katalyse beizutragen. Zudem konnte das Produktspektrum erweitert werden. Ausgehend von Saccharose als Donorsubstrat und Glyzerinsäureamid als alternativer Akzeptor zu Phosphat katalysierte Saccharose Phosphorylase die hoch regio- und stereoselektive sowie effiziente, einstufige Synthese von (*R*)-2-*O*-α-D-Glucopyranosylglyzerinsäureamid. Cellobiose Phosphorylase wurde in Bezug auf die Donorsubstratspezifität untersucht. Als Substratanalogon wurde das endozyklische Enitol Glucal getestet, das von Cellobiose Phosphorylase verwertet und im Zuge der Reaktion auf Phosphat übertragen wurde. Das Reaktionsprodukt, das im einstufigen Syntheseverfahren produziert wurde, wurde als 2-Deoxy-Glucose 1-Phosphat, ein Substrat für chemische Mutagenesestudien, identifiziert. Schließlich haben wir uns auf Glucose-1-Phosphatase aus *Escherichia coli*, ein Enzym, das als Hydrolase klassifiziert und als Phosphorsäuremonoester-spaltendes Enzym beschrieben wird, konzentriert und das Aktivitätsspektrum untersucht. Im Zuge dessen konnten wir zeigen, dass Glucose-1-Phosphatase die Phosphatgruppe von Glucose 1-Phosphat nicht nur auf Wasser, sondern auch auf alternative Akzeptoren überträgt. Ausgehend von Glucose 1-Phosphat als Donor und Fructose als Akzeptor katalysierte Glucose-1-Phosphatase die einstufige Synthese von Fructose 1-Phosphat. Durch Kopplung der Phosphoryltransferaktivität von Glucose-1-Phosphatase und der Glucosyltransferaktivität von Saccharose Phosphorylase konnte ein effizientes biokatalytisches Syntheseverfahren, bestehend aus einer zweistufigen Reaktionskaskade, entwickelt werden, um ausgehend von den leicht und günstig zugänglichen Substraten Saccharose und Phosphat, den hochpreisigen Metaboliten Fructose 1-Phosphat herzustellen.

Acknowledgements

Over the past three years I have faced many ups and down. There have been sweet successes and bitter setbacks, which have brought me to where I am today. It is with a certain ambivalence that this important part of my life is coming to a close.

I am grateful to all the people who have helped me to reach my goals and the place I have finally made it to. I would like to thank these people for their excellent guidance, advice, enriching discussions and hands-on help in the lab. Without their constant support and encouragement, I would not be where I am today.

Contents

1 Extended abstract

Biocatalysis has emerged as an environmentally friendly alternative to traditional catalysts and can be exploited for a variety of processes, from the synthesis of fine chemicals (1) to the generation of novel biofuels (2). Natural evolution has evolved a remarkable set of enzymes catalyzing a range of chemical transformations, usually with high catalytic efficiencies, tight substrate specificities and complete regio- and stereospecificities (3, 4). Whilst these properties turn enzymes into ideal catalysts for catalyzing their natural reaction, some of these properties are orthogonal for catalyzing non-natural reactions. Protein engineering provides a way to broaden the scope of enzyme catalyzed reactions, thereby intending to enhance their *ex vivo* synthetic utility (5). State of the art engineering-approaches of the present "third wave of biocatalysis" (6) include 1) rational design (3), the identification of distinct point mutations based on protein structure or homology models and 2) directed evolution combined with screening or selection (7, 8) for randomly introducing mutations and searching for hits. Both methods, previously considered as two opposing approaches being unique and exclusive, succeeded in generating a remarkable range of new enzyme properties (3, 9, 10). Currently, (semi)rational design and random approaches are converging to optimize hand-in-hand biocatalysts in a less labour-intensive and more time-efficient manner (11, 12). Still in its infancy is the *de novo* design (13-15), the computational design of enzymes for catalyzing reactions which cannot be catalyzed by any known naturally occurring enzyme. At present, results from rational design and directed evolution studies as well as of combinations thereof help to deepen our understanding on relationships between enzyme structure and activity, thereby providing the basis for predictive enzyme engineering and the future *de novo* design of tailored biocatalysts.

The work presented in this thesis contributes to a better understanding of enzyme structure and function by thoroughly characterizing structure-function relationships of selected enzymes catalyzing transglycosylation and transphosphorylation reactions. Site-directed mutagenesis and substrate analogues were used to study structure-function relationships. Furthermore, the selected enzymes were exploited for biocatalytic processes for the synthesis of high-value glycosides. Sucrose phosphorylase from *Leuconostoc mesenteroides* (SPase, EC 2.4.1.7) and cellobiose phosphorylase from *Cellulomonas uda* (CPase, EC 2.4.1.20) were chosen as representatives of glycosyl transferring enzymes; two members of the

haloacid dehydrogenase-like phosphatase family, HAD4 and HAD13 and glucose 1-phosphatase from *Escherichia coli* (G1Pase, EC 3.1.3.10) were selected from the pool of phosphoryl transferring enzymes. All five enzymes have in common that they utilize glucose 1-phosphate as donor substrate, either catalyzing the transfer of the glucosyl (SPase, CPase) or the phosphate group (HAD4, HAD13, G1Pase) to a corresponding acceptor substrate.

Enzymatic glucosyl transfer

SPase is a retaining bacterial disaccharide phosphorylase from the glycoside hydrolase family 13 (GH-13) (16, 17) that catalyzes the reversible conversion of sucrose and phosphate to glucose 1-phosphate and fructose (16). The proposed reaction mechanism is a double displacement-like reaction mechanism that involves the formation of a β-glucosyl enzyme intermediate. In the first step, the glucosyl moiety of sucrose is transferred to the enzyme, resulting in the formation of the β-glucosyl enzyme intermediate. In the next step, the glucosyl moiety is transferred from the β-glucosyl enzyme intermediate to the natural acceptor phosphate, thereby synthesizing glucose 1-phosphate. Whereas SPase's function *in vivo* is to fuel the energy metabolism of the cell with glucose 1-phosphate, SPase can be exploited *in vitro* for the synthesis of a diverse range of glucosides, among which some of them entered the cosmetic industry (18) or are used in the fine-chemical sector (17, 19, 20). The property that transforms SPase into a highly attractive transglucosylation catalyst is its ability to utilize sucrose as cheap and readily accessible donor substrate combined with its ability to transfer the glucosyl group from sucrose to a broad range of acceptors (instead of phosphate as natural acceptor). However, the spectrum of synthesized glucosides is limited by SPase's strict specificity for donor substrates with a glucosyl moiety (like sucrose, glucose 1-phosphate and to less extent glucose 1-fluoride). To understand how strict specificity for glucosyl donor substrates is achieved, SPase's active-site architecture was thoroughly investigated. The accessibility of the crystal structure of sucrose phosphorylase from *Bifidobacterium adolescentis*, with sucrose bound as ligand, enables to descry active-site residues interacting with the glucosyl moiety of sucrose. Firstly, a network of charged hydrogen bonds seems to be responsible for accommodating the glucosyl moiety of the donor substrate at subsite -1. Interestingly, the C4-OH of the glucosyl moiety is engaged in strong hydrogen bonding interactions with two active-site residues of opposite charge (Asp49 and Arg395). To evaluate their contribution on substrate binding and/or catalysis, both residues were substituted, thereby generating D49A and R395L. A detailed kinetic analysis revealed that substitution of Asp49 and Arg395 resulted in impaired substrate binding, significantly decreased catalytic activities and transition state destabilization. Although Asp49 and Arg395 are interacting

with the glucosyl moiety of the donor substrate at subsite -1, the structural disruptions caused by the substitutions relayed to proximal parts inside and outside of the catalytic subsite -1, thereby providing an unexpected opportunity to gain insight into binding recognition at subsite +1, the subsite where the leaving group/nucleophile binds. This result suggests that the two neighbouring subsites show a certain degree of synergism in catalytic function, which was partially impaired upon substitution of Asp49 and Arg395.

Secondly, an aromatic motif (Phe52) is present at the catalytic subsite of SPase, which is positioned at the B-face of the glucopyranosyl ring of the substrate. To analyse the role of Phe52 on substrate binding and/or catalysis, Phe52 was mutated to Ala and Asn, respectively, thereby generating F52A and F52N. Both mutants were characterized by free energy profile analysis for catalytic glucosyl transfer from sucrose to phosphate. Phe52's role could be addressed to selective transition state stabilization. Each of the two oxocarbenium-ion like transition states, flanking the β-glucosyl enzyme intermediate, were found to require stabilization from Phe52 most probably by forming cation-π interactions between the oxocarbenium-ion like transition state and the π-electron cloud of the aromatic ring.

To expand the general understanding on aromatic-carbohydrate interactions at the catalytic subsite of enzymes from family GH-13, a follow-up study was performed to examine the influence of Phe52 on the functionality of the catalytic triad. Therefore, each residue of the catalytic triad was substituted on the F52A template by Ala, thereby generating the F52A-D196A (nucleophile), F52A-E237A (acid-base catalyst) and F52A-D295A (transition-state stabilizer) mutant. Kinetic analysis of the doubly mutated enzymes supplemented by molecular docking studies provided new insights on how decisive the conformation of glucose 1-phosphate is for catalysis. The disposition in which the phosphate moiety is "tucked-under" the sugar is proposed to be the reactive conformation of glucose 1-phosphate required by SPase for functional catalysis.

Finally, the spectrum of glucosides synthesized by SPase was broadened, by demonstrating SPase's transglucosylation potential towards glyceric acid amide as acceptor. A biocatalytic process was established which started from sucrose as donor substrate and a racemic mixture of glyceric acid amide as acceptor substrate. The reaction resulted in the synthesis of a regio- and diastereomerically pure product in near theoretical yield. A combination of NMR analysis, molecular docking studies and chiroptical techniques was used to identify the reaction product as (*R*)-2-*O*-α-D-glucopyranosyl glyceric acid amide, a novel osmolyte, which is proposed to act as protectant against heat denaturation of biological macromolecules. The synthesis of (*R*)-2-*O*-α-D-glucopyranosyl glyceric acid amide is the first evidence that SPase catalyzes a transglucosylation reaction with complete regio- and stereoselectivity. As a side-effect of chiral synthesis of (*R*)-2-*O*-α-D-glucopyranosyl glyceric acid amide, the

non-converted enantiomer can be obtained in good yield, thereby suggesting a chiral resolution strategy via stereo-selective transglucosylation.

CPase is an inverting bacterial disaccharide phosphorylase from family GH-94 that catalyzes the reversible conversion of cellobiose and phosphate to glucose 1-phosphate and glucose. The proposed reaction mechanism is a single displacement-like reaction mechanism that proceeds through an oxocarbenium-ion like transition state. A close relative to CPase, cellobiose phosphorylase from *Cellvibrio gilvus*, was shown to utilize the endocyclic enitol glucal as alternative substrate to cellobiose and to transfer the 2-deoxy-D-glucosyl moiety to different acceptor sugars, thereby synthesizing transfer products having a β-(1→4) glycosidic structure. The availability of 2-deoxy-D-glucosyl saccharides is of interest as these substrates are considered as valuable tools for investigating substrate recognition, binding and catalysis in various carbohydrate processing enzymes. To understand the mechanism of glucal utilization, we carefully investigated the reaction with glucal by employing CPase as biocatalyst. By using glucal as donor and phosphate as acceptor substrate, we were able to synthesize 2-deoxy-α-D-glucose 1-phosphate, a substance which is difficult to obtain chemically, in a single-step transformation and in a yield of 40% based on the initial substrate concentration. The proposed enzymatic mechanism for the synthesis of 2-deoxy-α-D-glucose 1-phosphate involves first substrate activation by protonation at C2 prior to or concomitant with nucleophilic attack of phosphate oxygen on C1. We probed the stereoselectivity of the protonation event and provided evidence that the proton transfer occurred from below the substrate ring in a *re* side attack on C2. Finally, we added glucose to the reaction of glucal and phosphate and could show that catalytic concentrations of phosphate stimulated the regioselective 2-deoxy-D-glucosyl transfer from glucal to the 4-hydroxyl of D-glucose to synthesize 2-deoxy-β-D-glucosyl-(1→4)-D-glucose in a yield of up to 60%.

Enzymatic phosphoryl transfer

HAD4, HAD13 and G1Pase are enzymes classified as phosphatases either belonging to the haloacid dehalogenase-like phosphatase family (HAD4, HAD13) (21) or the histidine acid phosphatase family (22), respectively. The proposed reaction mechanism of the three enzymes is a double displacement-like reaction mechanism that proceeds either through a phosphoaspartate (HAD4, HAD13) or a phosphohistidine (G1Pase) intermediate. In our study the three phosphatases were benchmarked by their hydrolytic activities towards several donor substrates and were tested to possess synthetic next to their hydrolytic activity. Whereas HAD4 and HAD13 were found to catalyze exclusively hydrolysis reactions, evidence could be provided that G1Pase transfers the phosphate group to an acceptor different to water. In contrast to conventional activated donor substrates for phosphoryl transfer, like nucleoside

triphosphate and pyrophosphate, G1Pase utilizes glucose 1-phosphate, which was not yet considered as potential donor for phosphoryl transfer reactions. Next to elucidating G1Pase's phosphoryl transfer activity, the newly-discovered function was exploited for the synthesis of fructose 1-phosphate in a single-step enzymatic conversion from glucose 1-phosphate and fructose. Under optimized conditions, the enzymatic conversion resulted in a remarkable yield of 67%. In a further step, the reaction of G1Pase was coupled to the reaction of SPase, thereby elaborating an one-pot, two-step cascade reaction to synthesize fructose 1-phosphate from the cheap commodity products sucrose and phosphate in a yield of up to 63%. Moreover, we could tap the full potential of G1Pase by exploiting its promiscuity to acceptors different from fructose, thereby gaining access to various sugar phosphates in single enzymatic conversions starting from glucose 1-phosphate and the respective carbohydrate acceptor.

References

1. Schulze B, Wubbolts MG. 1999. Biocatalysis for industrial production of fine chemicals. Curr Opin Biotechnol 10:609-615.

2. Alcalde M, Ferrer M, Plou FJ, Ballesteros A. 2006. Environmental biocatalysis: from remediation with enzymes to novel green processes. Trends Biotechnol 24:281-287.

3. Toscano MD, Woycechowsky KJ, Hilvert D. 2007. Minimalist active-site redesign: teaching old enzymes new tricks. Angew Chem Int Ed Engl 46:3212-3236.

4. Hudlicky T, Reed JW. 2009. Applications of biotransformations and biocatalysis to complexity generation in organic synthesis. Chem Soc Rev 38:3117-3132.

5. Kazlauskas RJ, Bornscheuer UT. 2009. Finding better protein engineering strategies. Nat Chem Biol 5:526-529.

6. Bornscheuer UT, Huisman GW, Kazlauskas RJ, Lutz S, Moore JC, Robins K. Engineering the third wave of biocatalysis. Nature 485:185-194.

7. Turner NJ. 2009. Directed evolution drives the next generation of biocatalysts. Nat Chem Biol 5:567-573.

8. Jäckel C, Kast P, Hilvert D. 2008. Protein design by directed evolution. Annu Rev of Biophys 37:153-173.

9. Tracewell CA, Arnold FH. 2009. Directed enzyme evolution: climbing fitness peaks one amino acid at a time. Curr Opin Chem Biol 13:3-9.

10. Lutz S. 2010. Beyond directed evolution - semi-rational protein engineering and design. Curr Opin Biotechnol 21:734-743.

11. Otten LG, Hollmann F, Arends IW. Enzyme engineering for enantioselectivity: from trial-and-error to rational design? Trends Biotechnol 28:46-54.

12. Quin MB, Schmidt-Dannert C. Engineering of biocatalysts: from evolution to creation. ACS Catal 1:1017-1021.

13. Barrozo A, Borstnar R, Marloie G, Kamerlin SCL. 2012. Computational protein engineering: bridging the gap between rational design and laboratory evolution. Int J Mol Sci:12428-12460.

14. Jiang L, Althoff EA, Clemente FR, Doyle L, Rothlisberger D, Zanghellini A, Gallaher JL, Betker JL, Tanaka F, Barbas CF, Hilvert D, Houk KN, Stoddard BL, Baker D. 2008. De novo computational design of retro-aldol enzymes. Science 319:1387-1391.

15. Siegel JB, Zanghellini A, Lovick HM, Kiss G, Lambert AR, St Clair JL, Gallaher JL, Hilvert D, Gelb MH, Stoddard BL, Houk KN, Michael FE, Baker D. 2010. Computational design of an enzyme catalyst for a stereoselective bimolecular Diels-Alder reaction. Science 329:309-313.

16. Goedl C, Schwarz A, Minani A, Nidetzky B. 2007. Recombinant sucrose phosphorylase from *Leuconostoc mesenteroides*: characterization, kinetic studies of transglucosylation, and application of immobilised enzyme for production of α-D-glucose 1-phosphate. J Biotechnol 129:77-86.

17. Goedl C, Sawangwan T, Wildberger P, Nidetzky B. 2010. Sucrose phosphorylase: a powerful

transglucosylation catalyst for synthesis of α-D-glucosides as industrial fine chemicals. Biocatal Biotransform 28:10-21.

18. Goedl C, Sawangwan T, Mueller M, Schwarz A, Nidetzky B. 2008. A high-yielding biocatalytic process for the production of 2-*O*-(α-D-glucopyranosyl)-*sn*-glycerol, a natural osmolyte and useful moisturizing ingredient. Angew Chem Int Ed Engl 47:10086-10089.

19. Luley-Goedl C, Sawangwan T, Brecker L, Wildberger P, Nidetzky B. 2010. Regioselective *O*-glucosylation by sucrose phosphorylase: a promising route for functional diversification of a range of 1,2-propanediols. Carbohyr Res 345:1736-1740.

20. Sawangwan T, Goedl C, Nidetzky B. 2009. Single-step enzymatic synthesis of (*R*)-2-*O*-α-D-glucopyranosyl glycerate, a compatible solute from micro-organisms that functions as a protein stabiliser. Org Biomol Chem 7:4267-4270.

21. Kuznetsova E, Proudfoot M, Gonzalez CF, Brown G, Omelchenko MV, Borozan I, Carmel L, Wolf YI, Mori H, Savchenko AV, Arrowsmith CH, Koonin EV, Edwards AM, Yakunin AF. 2006. Genome-wide analysis of substrate specificities of the *Escherichia coli* haloacid dehalogenase-like phosphatase family. J Biol Chem 281:36149-36161.

22. Rigden DJ. 2008. The histidine phosphatase superfamily: structure and function. Biochem J 409:333-348.

2 Probing enzyme-substrate interactions at the catalytic subsite of *Leuconostoc mesenteroides* sucrose phosphorylase with site-directed mutagenesis: the roles of Asp^{49} and Arg^{395}

Biocatalysis and Biotransformation, May–June 2012; 30(3): 326–337

informa
healthcare

ORIGINAL ARTICLE

Probing enzyme–substrate interactions at the catalytic subsite of *Leuconostoc mesenteroides* sucrose phosphorylase with site-directed mutagenesis: the roles of Asp^{49} and Arg^{395}

PATRICIA WILDBERGER, ANAMARIA TODEA & BERND NIDETZKY

Institute of Biotechnology and Biochemical Engineering, Graz University of Technology, Petersgasse 12/1, Graz, Austria

Abstract

Sucrose phosphorylase is a bacterial α-transglucosidase that catalyses glucosyl transfer from sucrose to phosphate, releasing D-fructose and α-D-glucose 1-phosphate as the product of the first (*enzyme glucosylation*) and second (*enzyme deglucosylation*) step of the enzymatic reaction, respectively. The transferred glucosyl moiety of sucrose is accommodated at the catalytic subsite of the phosphorylase through a network of charged hydrogen bonds whereby a highly conserved residue pair of Asp and Arg points towards the equatorial hydroxyl at C_4. To examine the role of this 'hyperpolar' binding site for the substrate 4-OH, we have mutated Asp^{49} and Arg^{395} of *Leuconostoc mesenteroides* sucrose phosphorylase individually to Ala (D49A) and Leu (R395L), respectively, and also prepared an 'uncharged' double mutant harbouring both site-directed substitutions. The efficiency for enzyme glucosylation from sucrose was massively decreased in purified preparations of D49A (10^7-fold) and R395L (10^5-fold) as compared to wild-type enzyme. The double mutant was not active above the detection limit. Enzyme deglucosylation to phosphate proceeded relatively efficient in D49A as well as R395L, about 500-fold less than in the wild-type phosphorylase. Substrate inhibition by phosphate and a loss in selectivity for reaction with phosphate as compared to water were new features in the two mutants. Asp^{49} and Arg^{395} are both essential in the catalytic reaction of *L. mesenteroides* sucrose phosphorylase.

Keywords: *sucrose phosphorylase, glycoside hydrolase family GH-13, glycosyltransferase, catalytic mechanism, glucosyl transfer, covalent intermediate*

Introduction

Family GH-13 of the glycoside hydrolase families constitutes a large and functionally very diverse group of hydrolases and transglycosidases that all act on α-glucosidic substrates, catalysing hydrolysis or rearrangement of the glycosidic bond in different natural saccharides such as maltodextrins, starch, α,α-trehalose and sucrose (α-D-glucopyranosyl 2-β-D-fructofuranoside) (Stam et al. 2006). The economic relevance of enzymatic conversions of starch (van der Maarel et al. 2002) and sucrose (Buchholz & Seibel 2008) into value-added commodity products has raised considerable interest in the elucidation of structure–function relationships for various members of family GH-13 (Sauer et al. 2000), particularly the ones that have known or potential applications as industrial catalysts. Of note, family GH-13 contains an array of starch processing enzymes that are all utilised in large-scale biotransformations (Buchholz & Seibel 2008). Engineering of the properties of these enzymes for enhanced performance (e.g. stability, activity, specificity) under conditions of industrial manufacturing is a clear goal of process optimisation (van der Veen et al. 2004, 2006). Enzymes of family GH-13 adopt a $(\beta/\alpha)_8$ barrel fold (Brayer et al. 1995; Brzozowski & Davies 1997; Abad et al. 2002), like that shown in Figure 1A for SPase, and share a highly conserved catalytic site in which three carboxylic acid residues are key in promoting the enzymatic reaction (Nielsen & Borchert 2000; MacGregor et al. 2001; Mirza et al. 2001, 2006; Sprogøe et al. 2004). A double displacement-like catalytic mechanism is utilised that involves formation and breakdown of a β-glucosyl enzyme intermediate on an aspartate side chain in the active site, acting as catalytic nucleophile (Voet & Abeles 1970; Davies & Wilson 1999; Uitdehaag et al. 1999).

Correspondence: Bernd Nidetzky, Institute of Biotechnology and Biochemical Engineering, Graz University of Technology, Petersgasse 12/1, Graz, Austria. Tel: +43-316-873-8400. Fax: +43-316-873-8434. E-mail: bernd.nidetzky@tugraz.at

ISSN 1024-2422 print/ISSN 1029-2446 online © 2012 Informa UK, Ltd.
DOI: 10.3109/10242422.2012.674720

Sucrose phosphorylase (SPase) is a somewhat unusual member of family GH-13 that catalyses glucosyl transfer to phosphate (P_i), a negatively charged acceptor molecule that is usually expelled from the relevant subsite in glycoside hydrolases (Rydberg et al. 2002). The net reaction of SPase therefore is conversion of sucrose and P_i into D-fructose and α-D-glucose 1-phosphate (Glc1P), as shown in Scheme 1 (Goedl et al. 2007). However, SPase is able to utilise a large number of other acceptor molecules (e.g. sugar alcohols) in place of P_i, making the enzyme an attractive transglucosylation catalyst for the synthesis of different α-glucosides (Goedl et al. 2010). Glucosylation of glycerol to yield the natural osmolyte α-D-glucosyl-*sn*-glycerol has recently been developed into an industrial application for SPase (Goedl et al. 2008).

SPase is an enzyme of bacterial origin (Weimberg & Doudoroff 1954; Russell et al. 1988; van den Broek et al. 2004; Lee et al. 2006; Goedl et al. 2010) and the available amino acid sequences have previously been categorised into sub-family 18 of family GH-13 (Stam et al. 2006). Crystal structures of SPase from *Bifidobacterium adolescentis* (*Ba*SPase) have been determined for the free enzyme (Sprogøe et al. 2004), the enzyme–sucrose complex, and the β-glucosyl enzyme intermediate (Mirza et al. 2006), as shown in Figure 1A, B and C, respectively. The structural evidence provides detailed information about substrate binding recognition in SPase catalysis. Figure 1B shows how the transferred glucosyl moiety is accommodated at sugar-binding subsite −1 of the enzyme. In addition to the residues that are directly involved in the catalytic reaction as general acid–base (Glu) (Mirza et al. 2006; Schwarz et al. 2007) and nucleophile (Asp) (Schwarz & Nidetzky 2006), there are several amino acids that provide charged hydrogen bonding interactions with non-reacting parts of the glucosyl substrate (Mirza et al. 2006). Sequence comparison reveals that these interactions are highly conserved among the sucrose phosphorylases, as shown in Figure 2, and they are usually also present across the entire family GH-13 (see Supporting Figure S1 available online at http://www.informahealthcare.com/bab/doi/10.3109/10242422.2012.674720). For example, the Asp interacting with the hydroxyls at C_2 and C_3 of the glucosyl moiety belongs to the active-site signature of family GH-13 enzymes (Janecek et al. 1997). It is often referred to as a 'transition state stabiliser', and its role in SPase catalysis has been examined using site-directed Asp → Glu and Asp → Asn replacements in the enzyme from *Leuconostoc mesenteroides* (*Lm*SPase) (Mueller & Nidetzky 2007a). SPase and related enzymes from family GH-13 are highly specific for transferring a glucosyl residue. A small structural

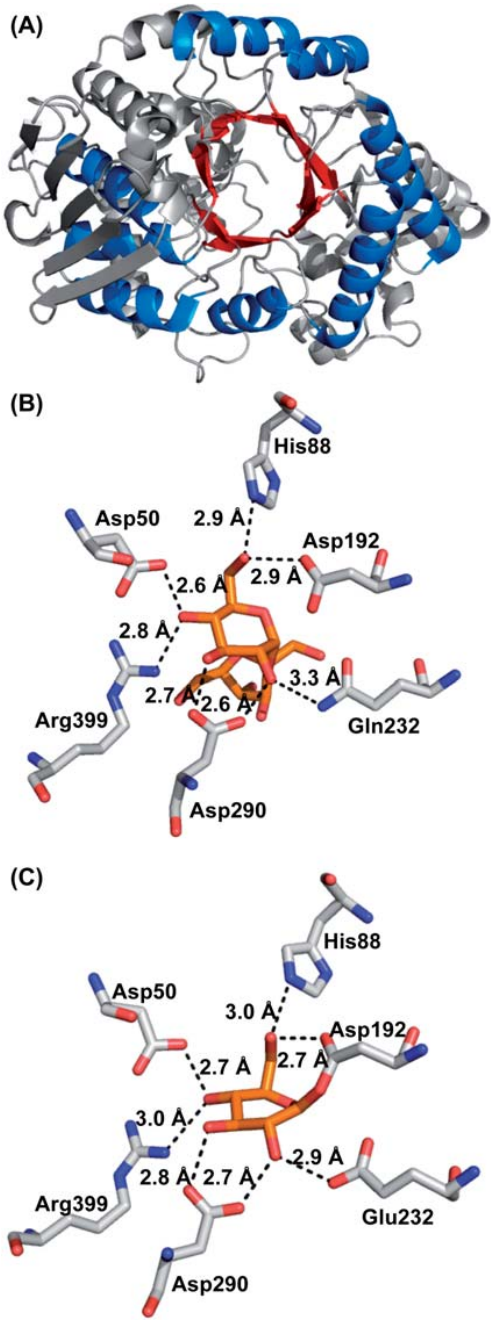

Figure 1. Structural view of substrate binding in sucrose phosphorylase. (A) Three-dimensional fold of the protein subunit of *Ba*SPase derived from the crystal structure of the dimeric enzyme (PDB-entry 1r7a, molecule A). (B) and (C) Close up views of the accommodation of a glucosyl residue in the substrate binding site of *Ba*SPase bound with sucrose (PDB-entry 2gdu, molecule A) and the β-glucosyl enzyme intermediate (PDB-entry 2gdv, molecule A). Residues forming hydrogen bonds with the glucopyranosyl moiety (orange) are displayed. Note: Arg^{190} and His^{289} interacting with the hydroxy groups at C_2 and C_3 are not shown for clarity reasons. The shown residues of *Ba*SPase are highly conserved in other sucrose phosphorylases (Figure 2).

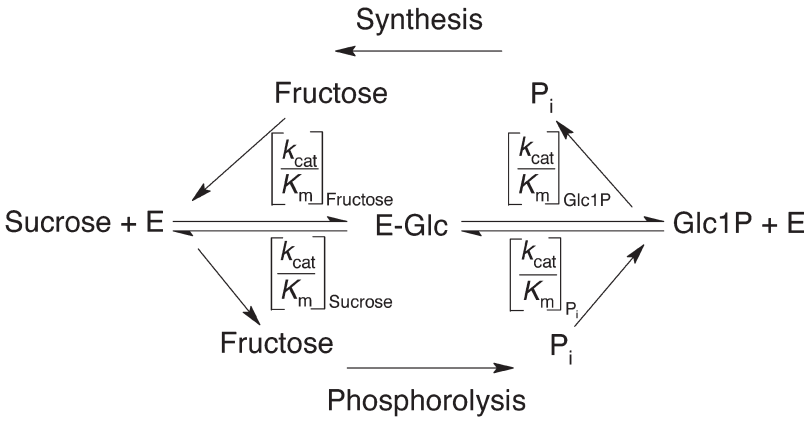

Scheme 1. Reaction mechanism of sucrose phosphorylase in two catalytic steps via a covalent glucosyl–enzyme intermediate (E-Glc).

change in the substrate such as that resulting from epimerisation at C_2 (*mannosyl* as compared to *glucosyl*), for example, was shown to lead to loss by several orders of magnitude in phosphorylase catalytic efficiency (Mueller and Nidetzky 2007a).

Figure 1B and C reveals an additional feature of substrate binding recognition in SPase that is of a general interest. The equatorial C_4–OH of the glucosyl substrate is accommodated in an extremely polar binding site where two residues of opposite charge (Asp^{49}, Arg^{395}) are engaged in strong hydrogen bonding interactions with the sugar hydroxyl. The importance of the two conserved residues in the different steps of reaction of *Lm*SPase has not been previously analysed using mutagenesis. There is, however, some precedence within family GH-13 that results from work with deoxy substrate analogues in which the C_4–OH of the transferred glucosyl moiety had been replaced by hydrogen (Frandsen et al. 2002). Using three different α-glucosidases cleaving the α-1,6-glycosidic linkage in isomaltosides, Svensson and co-workers have shown that the catalytic efficiency for hydrolysis was decreased by about three orders of magnitude as result of substrate deoxygenation at C_4 (Frandsen et al. 2002). Sequence comparison reveals that the α-glucosidases used in the previous study contain an aspartic acid homologous to Asp^{50} of SPase but they do not have Arg^{399}. Non-covalent bonding of the glucosyl 4-OH with the conserved Asp and perhaps other residues of the catalytic subsite of the α-glucosidases seems to be important for substrate binding and/or catalysis. The research reported herein was performed to examine kinetic consequences resulting from individual and combined site-directed substitutions of the relevant Asp and Arg residues in SPase from *L. mesenteroides* (Asp^{49}, Arg^{395}).

Materials and methods

Phusion high-fidelity DNA polymerase was obtained from Finnzymes. All other materials used have been described elsewhere (Goedl et al. 2007).

Site-directed mutagenesis and enzyme preparation

Point mutations $Asp^{49} \rightarrow$ Ala (D49A) and $Arg^{395} \rightarrow$ Leu (R395L) were introduced using a reported two-stage PCR protocol (Wang & Malcolm 1999) in

Enzyme	Asp C_4–OH	His C_6–OH	Arg C_2–OH	Asp C_4–OH	Glu C_2–OH	His C_2–OH & C_3–OH	Asp C_2–OH & C_3–OH	Arg C_4–OH
*Lm*SPase	STG--D[49]RGFAP	DFMINH[89]ISRES	GANLIR[395]LDAFA	NLIRLD[196]AFAYA	AEILPE[234]IHEHY	TTLDTH[259]DGIGV	TLDTHD[260]GIGVV	STKEGR[399]NINRH
*La*SPase	STG--D[49]RGFAP	DFMINH[89]ISRQS	GADIIR[395]LDAFA	DIIRLD[196]AFAYA	AMILPE[234]IHEHY	TTLDTH[259]DGIGV	TLDTHD[260]GIGVV	KTKEGR[399]NINRH
*Stm*SPase	STG--D[49]RGFAP	DFMINH[89]ISRQS	GCDLIR[395]LDAFA	DLIRLD[196]AFAYA	AEILPE[234]IHEHY	TTLDTH[259]DGIGV	TLDTHD[260]GIGVV	STKEGR[399]NINRH
*Ba*SPase	PFDGAD[50]AGFDP	DAIVNH[89]MSWES	HVSYIR[395]LDAVG	SYIRLD[196]AVGYG	LEILIE[234]VHSYY	TVLDTH[259]DGIGV	VLDTHD[260]GIGVI	KTNNGR[399]DINRH
*Bl*SPase	PFDGAD[50]AGFDP	DAIVNH[89]MSWES	HVRYIR[395]LDAVG	RYIRLD[196]AVGYG	LEILIE[234]VHSYY	TVLDTH[259]DGIGV	VLDTHD[260]GIGVI	RTNNGR[399]DINRH
*Av*SPase	PIDGAD[50]AGFDP	DLIVNH[89]VSAQS	NVTAIR[395]LDAAG	TAIRLD[196]AAGYA	MEVLVE[234]IHSYY	TVLDTH[259]DGIGV	VLDTHD[260]GIGVI	KTGVGR[399]DINRH

Figure 2. Partial multiple sequence alignment of sucrose phosphorylases from different organisms showing positional conservation of all amino acids that provide charged hydrogen bonding interactions with the glucosyl moiety. The partial sequences shown are sucrose phosphorylases from *Leuconostoc mesenteroides* (*Lm*SPase; BAA14344.1), *Lactobacillus acidophilus* (*La*SPase; AAO21868.1), *Streptococcus mutans* UA159 (*Stm*SPase; AAN58596.1), *Bifidobacterium adolescentis* (*Ba*SPase; AAO33821.1), *Bifidobacterium longum* JCM 1217 (*Bl*SPase; BAF62433.1) and *Agrobacterium vitis* (*Av*SPase; CAA80424.1). Alignment was performed by using the Clustal 2.0.12 alignment tool. Conserved residues are shaded in grey.

which a pASK-IBA7+ (IBA GmbH) expression vector encoding wild-type *Lm*SPase was used as template (Wildberger et al. 2011). The following pairs of oligonucleotide primers were used to amplify the entire plasmid with *Pfu* DNA polymerase for D49A and *Phusion* High-Fidelity DNA polymerase for R395L, respectively, whereby the mismatched codons are indicated in bold. D49A: 5′-TCAACAGGT**GCA**CGCGGT-3′ (forward), 5′-ACCGCG**TGC**ACCTGTTGA-3′ (reverse); R395L: 5′-AATATTAAC**TTG**CATTACTATACG-3′ (forward), 5′-CGTATAGTAATG**CAA**GTTAATATT-3′ (reverse). In stage one for the substitution of D49A, two separate PCRs with the forward and reverse primer, respectively, were performed. Each PCR consisted of a pre-heating step at 95°C for 60 s and was followed by four reaction cycles (50 s at 95°C; 50 s at 49°C; 10 min at 72°C). In stage two, the two PCRs were combined and continued for 18 reaction cycles (50 s at 95°C; 50 s at 49°C; 10 min at 72°C) followed by a final extension step at 72°C for 10 min. In the first stage for substitution of R395L, the two separate PCRs with the forward and reverse primer, underwent a pre-heating step at 98°C for 30 s followed by six reaction cycles (15 s at 98°C; 20 s at 51°C; 180 s at 72°C). In the second stage, the two PCRs were combined and continued for 30 reaction cycles (15 s at 98°C; 20 s at 51°C; 3 min at 72°C) followed by a final extension step at 72°C for 5 min. Based on D49A and R395L, a doubly mutated enzyme, termed D49A-R39L, was generated. The R395L plasmid served as template for substitution of Asp^{49} by Ala. The PCR was carried out in the same way as described above for the creation of D49A.

In all cases (D49A, R395L and D49A-R395L), the final amplification product was subjected to parental template digest by *DpnI*. Sequenced plasmid vectors harbouring the mutagenised gene were transformed into *Escherichia coli* BL21-Gold (DE3) cells, and recipient strains were grown at 37°C in Lysogeny broth (LB)-medium containing 0.15 mg/L ampicillin. Induction of gene expression and recombinant protein production was carried out as reported elsewhere (Wildberger et al. 2011).

The vector pASK-IBA7+ encodes wild-type *Lm*SPase that has *Strep*-tag II fused to the N-terminus of the enzyme. The likewise *Strep*-tagged mutants were purified by gravity flow *Strep*-Tactin Sepharose column chromatography at 4°C. All buffers were degassed and filtered using 0.45-µm cellulose-acetate filters (Sartorius). The *E. coli* cell extract was passed through a 1.2-µm cellulose-acetate filter (Sartorius) before loading on a *Strep*-Tactin Sepharose column (binding capacity 300 nmol/mL; bed volume 5 mL). The column was equilibrated with buffer W (100 mM Tris/HCl, 150 mM NaCl, 1 mM EDTA, pH 8.0) for 5 column volumes. Cell extract was applied and the column was washed with buffer W for 5 column volumes. Affinity bound enzyme, identified as a 59 kDa protein band in SDS–PAGE, was eluted with buffer E (100 mM Tris/HCl, 150 mM NaCl, 1 mM EDTA, 2.5 mM desthiobiotin, pH 8.0) for 4 column volumes. Pooled fractions were concentrated and desalted using a Vivaspin ultrafiltration tube (10 kDa cutoff; Vivascience) and again concentrated to about 5–15 mg/mL in 50 mM MES buffer, pH 7.0. Stock solutions of wild-type and mutants were stored at − 20°C. Purification was monitored by SDS–PAGE.

Assays

Enzyme activity in the direction of sucrose phosphorolysis (see Scheme 1, lower panel) was determined at 30°C using a continuous coupled enzymatic assay with phosphoglucomutase and glucose-6-phosphate dehydrogenase (Goedl et al. 2007). Protein concentration was measured with the BioRad dye-binding method referenced against BSA. Glucose was determined using an assay with hexokinase and glucose-6-phosphate dehydrogenase (Goedl et al. 2007). Glucose in the presence of fructose was determined using an assay with glucose oxidase and peroxidase (Goedl et al. 2008). Glc1P was assayed using phosphoglucomutase and glucose-6-phosphate dehydrogenase (Goedl et al. 2007). P_i was determined colorimetrically at 850 nm (Goedl et al. 2007).

Analytical method for sucrose detection

Reaction mixtures containing D49A (0.6 mg/mL) or R395L (0.5 mg/mL), 20 mM Glc1P and 100 mM fructose in 50 mM MES buffer (pH 7.0) were incubated at 30°C for 72 h and analysed for sucrose synthesis by high performance anion exchange chromatography with pulsed amperometric detection (HPAE-PAD). The analysis was performed using a Dionex BioLC system (Dionex Corporation, Sunnyvale, CA, USA) equipped with a CarboPac PA10 column (4 × 250 mm) and an Amino Trap guard column (4 × 50 mm) thermostated at 30°C. Sucrose was detected with an ED50A electrochemical detector using a gold working electrode and a silver/silver chloride reference electrode by applying the predefined waveform for carbohydrates. Elution was carried out at a flow rate of 1 mL/min with the following method: isocratic flow of 52 mM NaOH for 20 min, followed by an isocratic flow of 100 mM NaOH and 100 mM NaOAc for 5 min and a linear gradient from 100 mM NaOAc to 400 mM NaOAc

applied within 15 min in an isocratic background of 100 mM NaOH. The column was washed for 10 min with 52 mM NaOH. Under the conditions applied, sucrose eluted after 12.5 min.

Initial-rate studies and steady-state kinetic analysis

Reactions were performed at 30°C in 50 mM MES buffer, pH 7.0, and monitored by product formation (phosphorolysis: Glc1P; synthesis: P_i) in discontinuous assays. The typical concentrations of D49A and R395L were 0.5 and 0.3 mg/mL, respectively and an incubation time of 1 h was used. Glucosyl donor and acceptor concentrations were varied in a suitable range: sucrose (5–800 mM), P_i (0.01–250 mM), Glc1P (1–900 mM) and fructose (10–800 mM). Control reactions lacking the enzyme or one of the substrates were performed in all cases, and enzymatic initial rates were corrected as required. Kinetic parameters (V_{max}, K_m) were obtained from nonlinear fits of data to Equation (1). When substrate inhibition occurred, initial velocities were fitted to Equation (2). k_{cat} is defined in Equation (3).

$$v = V_{\max} \cdot \frac{S}{(K_m + S)} \quad (1)$$

$$v = V_{\max} \cdot \frac{S}{\left(K_m + S \cdot \frac{(1+S)}{K_i}\right)} \quad (2)$$

$$k_{cat} = \frac{V_{\max}}{E} \quad (3)$$

where ν is the observed reaction rate [mM/min], V_{max} is the maximal initial rate [mM/min], S is the substrate concentration [mM], K_m is the apparent Michaelis–Menten constant [mM], K_i is the substrate–inhibition constant [mM], k_{cat} is the catalytic constant [s^{-1}] and E is the total molar enzyme concentration based on a molecular mass of 59 kDa for the wild-type *Lm*SPase subunit [mM]. When enzyme was not saturable with substrate and an independent determination of V_{max} and K_m therefore not possible, V_{max}/K_m was obtained from data acquired under substrate-limited reaction conditions where the rate increases in linear dependence on substrate concentration. The decrease in k_{cat}/K_m can be expressed as loss of transition state stabilisation energy (Equation (4)):

$$\Delta\Delta G^{\#} = -RT \cdot \ln([k_{cat}/K_m]_{mut}/[k_{cat}/K_m]_{wt}) \quad (4)$$

where $\Delta\Delta G^{\#}$ is the free energy change [kJ/mol], $[k_{cat}/K_m]_{mut}$ is the catalytic efficiency of the mutants, $[k_{cat}/K_m]_{wt}$ is the catalytic efficiency of the wild-type enzyme, R is the gas constant [8.31 J mol^{-1} K^{-1}] and T is the temperature [303.15 K].

Hydrolysis as side reaction

In the absence of a suitable nucleophile. *Lm*SPase displays hydrolase activity towards sucrose and Glc1P under conditions in which a suitable nucleophile (P_i or fructose) is lacking. The hydrolytic activities of the wild-type *Lm*SPase and mutants towards Glc1P (100 mM) and sucrose (500 mM) were determined at 30°C in 50 mM MES buffer, pH 7.0, using discontinuous assays. Reactions were carried out using 0.5 mg/mL D49A, 0.3 mg/mL R395L and 0.1 mg/mL wild-type *Lm*SPase. The release of glucose was measured using a coupled enzyme assay with glucose oxidase and peroxidase (see subsection Assays).

In the presence of a suitable nucleophile. To test whether hydrolysis occurs even under conditions of the presence of P_i, wild-type *Lm*SPase and mutants were incubated with 500 mM sucrose and varying concentrations of P_i at 30°C in 50 mM MES buffer, pH 7.0. P_i concentrations were varied at five levels (1, 10, 50, 100 and 300 mM) for D49A and R395L, and at four levels (10, 50, 100 and 300 mM) for wild-type *Lm*SPase. Reactions were carried out using 0.1–0.5 mg/mL D49A, 0.01–0.3 mg/mL R395L and 0.1–10 μg/mL wild-type *Lm*SPase. Samples were taken every half hour up to 8 h (50 mM P_i) or every hour for up to 5 h (all other P_i concentrations). To determine the hydrolytic activity (k_{catH}), the release of glucose was measured by using the coupled enzyme assay with glucose oxidase and peroxidase (see subsection Assays). To determine the phosphorolytic activity (k_{catP}), the release of Glc1P was measured, by using the coupled enzyme assay with phosphoglucomutase and glucose-6-phosphate dehydrogenase (see subsection Assays) and the ratio of k_{catH}/k_{catP} was calculated. Our used assays for measuring glucose and Glc1P had a limit of detection of 0.01 mM.

Results and discussion

Site directed mutagenesis

Asp^{50} and Arg^{399} of *Ba*SPase are highly conserved among the known sucrose phosphorylases (Figure 2). To characterise their roles in enzymatic glucosyl transfer to and from P_i, we have performed site-directed mutagenesis on the homologous residues in *Lm*SPase, Asp^{49} and Arg^{395}, and prepared the D49A and R395L variants of the enzyme. A double mutant harbouring both substitutions was also made, and Figure 3 shows an SDS–polyacrylamide gel of the isolated mutants along with the wild-type enzyme that was produced and purified in exactly the same way as the mutants. The choice of residue substitution

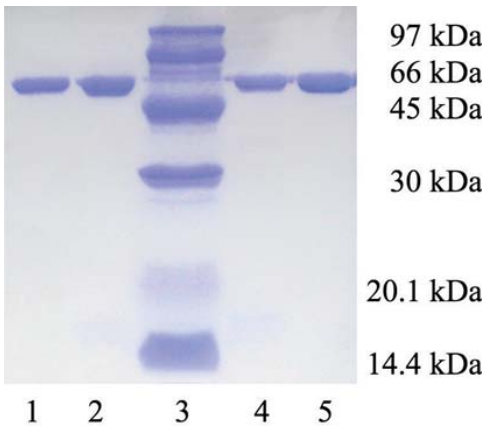

Figure 3. Enzyme purification monitored by SDS–PAGE. Lane 1: D49A; 2: R395L; 3: molecular mass standard; 4: D49A-R395L; 5: *Lm*SPase wild-type.

Asp → Ala and Arg → Leu was primarily based on the consideration that the original hydrogen bond to the glucosyl C_4 hydroxy group (Figure 1B and C) should be disrupted as a result of the site-specific replacement. However, we were also mindful of the fact that each substitution alters the properties of the binding site for the C_4 hydroxy group, both in terms of polarity and net charge. Of note, the overall neutral net charge of the binding site in the wild-type enzyme is re-installed in the double mutant. The purified mutants were suitably stable and could be stored frozen at a concentration of ≥ 5 mg/mL (50 mM MES buffer, pH 7.0) for at least several weeks without substantial loss of activity.

Kinetic characterisation of LmSPase mutants

We first evaluated the specific activity of each mutant in the standard assay for phosphorolysis of sucrose (Goedl et al. 2007). Compared to the wild-type enzyme whose specific activity was 98 U/mg under the conditions used (Wildberger et al. 2011), the R395L mutant was 650-fold less active. The specific activity of D49A was even lower than that of R395L, reflecting a 50,000-fold activity loss in comparison to the specific activity of wild-type *Lm*SPase. These results suggest that both Asp^{49} and Arg^{395} have an important role for substrate binding and/or catalysis by *Lm*SPase.

The double mutant displayed a further loss of specific activity in comparison to D49A and R395L, showing an almost 300,000-fold decrease in activity compared to the wild-type enzyme. It is clear therefore that the second mutation, Asp^{49} → Ala or Arg^{395} → Leu, on the relevant single mutant R395L or D49A brings about a significant additional disruptive effect on the enzyme activity. However, the combined effect of the two substitutions in the double mutant was substantially smaller than the effect that could have been expected from the two individual mutations ($50{,}000 \times 650 = 10^{7.5}$), suggesting that the two site-directed replacements are not completely independent one of another. It would seem that especially the replacement Asp^{49} → Ala destroys the function of the binding site composed of Asp^{49} and Arg^{395}. Considering that the double mutation reverts the imbalance in site effective net charge that was introduced by each of the single mutations (D49A: net charge +1; R395L: net charge −1; D49A-R395L: net charge 0; wild-type enzyme: net charge 0), it is interesting that the second mutation did not in any way 'repair' the damage resulting from a single mutation. Antagonism of two single mutations in a doubly mutated enzyme has been observed previously (Mildvan 2004), and reversal of charge perturbation in the functional site is probably one important reason for it (see for example, Kratzer & Nidetzky 2005).

We realised that the specific activity of D49A-R395L would be too low to perform a more detailed kinetic characterisation of the double mutant. We therefore attempted to restore activity in the double mutant through the addition of external reagents. The reagents chosen for potential 'chemical rescue' were meant to compensate for the loss of the carboxylate side chain of Asp^{49}. Acetate, formate, bromide and chloride were tested, each in a concentration of 100 mM using the sodium salt. The notion underlying the experiment was that the reagent might bind at the site vacated by the substitution of Asp^{49} by Ala and thus restores part of the function of the original side chain (for the general case, see Peracchi 2001, 2008). Halides have previously been shown to serve in rescuing the activity of mutants in which carboxylate side chains had been removed by mutagenesis (Hayden et al. 1999). The rate-enhancing effect of the external reagents was generally borderline significant (≤ 1.3-fold), except that of formate, which reached a still modest value of 5. Kinetic analysis of the D49A-R395L mutant was therefore not pursued, and we also abandoned chemical rescue studies of the D49A mutant.

A steady-state kinetic analysis for phosphorolysis and synthesis of sucrose was performed with the single mutants D49A and R395L. The results are summarised in Table I along with the relevant kinetic data for the wild-type enzyme, which were taken from one of our recent papers (Wildberger et al. 2011). Interpretation is done on the basis of the Ping-pong bi-bi kinetic mechanism of wild-type *Lm*SPase (Goedl & Nidetzky 2009). In this mechanism,

the catalytic efficiency (k_{cat}/K_m) for the glucosyl donor and acceptor substrate represents the formation and breakdown of the covalent glucosyl–enzyme intermediate, respectively, as a kinetically isolated step (Scheme 1).

Enzyme glucosylation: reaction with glucosyl donor substrates. Formation of the β-glucosyl enzyme intermediate occurs in either direction of the enzymatic reaction from sucrose (phosphorolysis) or Glc1P (synthesis) as the glucosyl donor substrate (Scheme 1). In phosphorolysis, the initial rate of reaction catalysed by D49A and R395L showed a linear dependence on the sucrose concentration up to a very high level of 800 mM. This finding suggested that the K_m for sucrose had increased more than 82-fold (= 800/9.8) in both mutants as compared to the K_m for the wild-type enzyme (Table I) and that it had been raised to a value far outside of the experimental range. In the absence of saturation at high sucrose concentration, only a catalytic efficiency and no turnover number could be determined from the initial rate measurements. Expressed in k_{cat}/K_m terms, the D49A mutant showed a dramatically reduced efficiency for enzyme glucosylation from sucrose that was about 7×10^6-fold lower than that of wild-type *Lm*SPase. The k_{cat}/K_m of R395L for reaction with sucrose was not as strongly affected as that of D49A, even though it was decreased by about 40,000-fold as compared to the corresponding k_{cat}/K_m for the wild-type enzyme. The kinetic analysis for reaction with sucrose reinforces the notion that Asp[49] and Arg[395] are both highly important for activity of *Lm*SPase, more specifically for promoting glucosylation of the enzyme in the direction of phosphorolysis. Loss of substrate binding affinity, impaired positioning of sucrose for catalysis and

Table I. Kinetic parameters for phosphorolysis and synthesis of sucrose catalysed by wild-type *Lm*SPase (Wildberger et al. 2011) and the D49A and R395L mutants thereof.

Reaction		Wild-type	D49A	R395L
Phosphorolysis of sucrose				
Glucosylation from sucrose[a]	k_{cat} [s^{-1}]	117	n.a.	n.a.
	K_m [mM]	9.8	n.a.	n.a.
	k_{cat}/K_m [s^{-1} mM^{-1}]	12	1.8×10^{-6}	3.1×10^{-4}
	$\Delta\Delta G$ [kJ/mol]	–	40	27
Deglucosylation by P_i[b]	k_{cat} [s^{-1}]	145	2.0×10^{-3}	0.2
	K_m [mM]	6.0	4.0×10^{-2}	2.4
	k_{cat}/K_m [s^{-1} mM^{-1}]	24	5.0×10^{-2}	8.3×10^{-2}
	K_i [mM]	–	46	55
	$\Delta\Delta G$ [kJ/mol]	–	16	14
Synthesis of sucrose				
Glucosylation from Glc1P[c]	k_{cat} [s^{-1}]	39	4.0×10^{-2}	0.4
	K_m [mM]	4.5	676	140
	k_{cat}/K_m [s^{-1} mM^{-1}]	8.3	5.9×10^{-5}	2.9×10^{-3}
	$\Delta\Delta G$ [kJ/mol]	–	30	20
Deglucosylation by fructose[d]	k_{cat} [s^{-1}]	47	1.8×10^{-2}	0.2
	K_m [mM]	13	387	180
	k_{cat}/K_m [s^{-1} mM^{-1}]	3.7	4.7×10^{-5}	1.1×10^{-3}
	$\Delta\Delta G$ [kJ/mol]	–	28	21
Hydrolysis				
Hydrolysis of sucrose[e]	k_{cat} [s^{-1}]	3.3[a]	2.0×10^{-3}	2.0×10^{-2}
Hydrolysis of Glc1P[f]	k_{cat} [s^{-1}]	1.6[b]	1.0×10^{-3}	7.0×10^{-3}
Hydrolysis of sucrose in presence of P_i[g]				
Hydrolysis	k_{cat} [s^{-1}]	1.6	1.0×10^{-3}	2.0×10^{-3}
Phosphorolysis	k_{cat} [s^{-1}]	90	1.0×10^{-3}	2.5×10^{-1}

The S.D. for k_{cat}, K_m and k_{cat}/K_m was equal to or smaller than 9.3%, 24.4% and 1.0% of the reported values respectively, with the exception of [a]11% and [b]20%. The S.D. for K_i was equal to or smaller than 18.7%. [a]Sucrose was varied at 14 levels between 0.01 and 120 mM for the wild-type enzyme (Wildberger et al. 2011). For D49A, sucrose was varied at 8 levels between 50 and 800 mM. For R395L, sucrose was varied at 10 levels between 5 and 800 mM. P_i was constant at 50 mM. [b]P_i concentration was varied at 17 levels between 0.01 and 140 mM for the wild-type enzyme (Wildberger et al. 2011). For the mutants, P_i was varied at 16 levels between 0.01 and 250 mM. Sucrose was constant at 500 mM. [c]Glc1P was varied at 12 levels between 0.5 and 250 mM for the wild-type enzyme (Wildberger et al. 2011). For both mutants, Glc1P was varied at 11 levels between 1 and 900 mM. Fructose was constant at 100 mM. [d]Fructose was varied at 12 levels between 1 and 200 mM (Wildberger et al. 2011). For the mutants, fructose was varied at 16 levels between 10 and 800 mM. Glc1P was constant at 100 mM. [e]Hydrolysis of sucrose was determined under conditions when no P_i was present. Sucrose was used at 500 mM. [f]Hydrolysis of Glc1P was determined under conditions when no fructose was present. Glc1P was used at 100 mM. [g]Hydrolysis of sucrose was determined under conditions when P_i was present. Sucrose was used at 500 mM, P_i was used at 50 mM.

decrease in ability to stabilise the oxocarbenium ion-like transition state of the reaction could all be responsible for the dramatic lowering of catalytic efficiency in the two mutants.

Enzyme glucosylation from Glc1P was also impaired strongly in the D49A and R395L mutants. However, the kinetic consequences resulting from the mutations were not completely uniform when the reaction with Glc1P was compared to the reaction with sucrose. First of all, initial rates in the direction of synthesis showed a saturable (hyperbolic) dependence of the concentration of Glc1P, allowing for an independent determination of k_{cat} and K_m. Secondly, the disruptive effect of mutation of Asp^{49} and Arg^{395} expressed in fold decrease in k_{cat}/K_m was lower by about two orders of magnitude in the reaction with Glc1P as compared to the reaction with sucrose. In other words, the damage that each of the mutations did on enzyme glucosylation was less severe in synthesis than it was in phosphorolysis. The leaving group of the glucosyl donor substrate, P_i in Glc1P as compared to fructose in sucrose, and the way that the respective leaving group is accommodated in the enzyme appears to have an important influence on the expression of kinetic consequences resulting from the individual site-directed mutations. The structural disruption in D49A and R395L therefore seems not to be strictly local, and there might be a correspondence between the interaction with the glucosyl C_4–OH at the catalytic subsite and interactions between the enzyme and the leaving group at subsite + 1 (see later). We can furthermore calculate from the data in Table I that the loss in k_{cat}/K_m for D49A and R395L was distributed between up to 150-fold increases in K_m and near 1000-fold decreases in k_{cat}. As noted before, R395L was less strongly affected in all its kinetic parameters than D49A.

Enzyme deglucosylation: reaction with acceptor substrates. We begin by analysing enzyme deglucosylation to fructose. Table I shows that k_{cat}/K_m for the reaction with fructose was decreased by several orders of magnitude in both mutants as compared to the corresponding k_{cat}/K_m for wild-type *Lm*SPase. The severity of the disruptive effect on k_{cat}/K_m (fructose) was comparable to that observed on k_{cat}/K_m (Glc1P). The dependence of the initial rate on the concentration of fructose was hyperbolic in both mutants, so that both k_{cat} and K_m could be determined in each case. The losses in catalytic efficiency are explained as the result of up to 30-fold increases in K_m and up to 2611-fold decreases in k_{cat}. The somewhat larger effect of the mutations on k_{cat} than on K_m in the direction of synthesis under conditions where enzyme glucosylation or deglucosylation was analysed supports the idea that replacement of Asp^{49} and Arg^{395} does, in fact, damage the steps of catalysis, not just substrate binding. We emphasise that even though initial rates in the synthesis direction were measured as release of P_i from Glc1P, productive glucosyl transfer from the mutated enzyme to fructose was confirmed by direct determination of the sucrose formed in the reaction. The putative disaccharide product synthesized in the reaction of each mutant co-eluted with the authentic sucrose standard in high-performance anion exchange chromatography.

Figure 4 shows the dependence of the initial rate of phosphorolysis of sucrose catalysed by D49A and R395L on the concentration of P_i. In contrast to the wild-type enzyme that displayed 'normal' Michaelis–Menten behaviour when assayed with P_i as the variable substrate under otherwise identical conditions (data not shown), both mutants were subject to a marked substrate inhibition by P_i. Fit of the data with Equation (2) gave a similar substrate inhibition constant of around 50 mM for both mutants. We interpret the substrate inhibition by P_i to originate from binding of P_i to the free enzyme, thereby preventing glucosylation of the enzyme by sucrose from taking place. Non-productive binding of P_i to the β-glucosyl enzyme intermediate would also interfere with reaction and manifest itself in a lowering of k_{cat} by the fraction of non-productively bound enzyme. However, it would not produce substrate inhibition. Wild-type *Lm*SPase appears to have evolved a structural mechanism that disfavours binding of P_i to the free enzyme (see later). Another interesting feature of the mutated enzymes was that their K_m for P_i was decreased, in D49A by two orders of magnitude, in

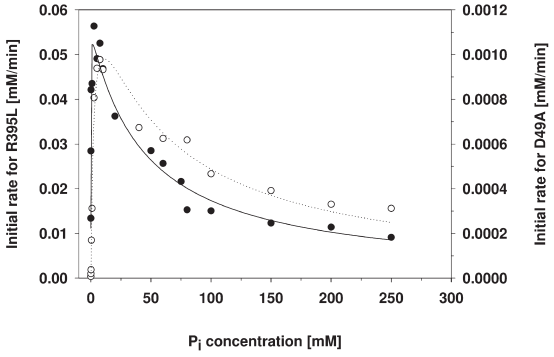

Figure 4. Michaelis–Menten plot for the determination of kinetic parameters for phosphorolysis of sucrose catalysed by D49A (●) and R395L (○). Initial rates were recorded from Glc1P release using a discontinuous assay. P_i was varied at 16 levels between 0.01 and 250 mM. Sucrose was kept constant at 500 mM. Lines are fits of Equation (3) to the data.

comparison to the corresponding K_m for the wild-type enzyme. The calculated k_{cat} values were, however, extremely low (Table I), consistent with the notion that the catalytic events during enzyme deglucosylation had been strongly disrupted as a result of the mutations.

Glucosyl transfer to water: hydrolysis as a side reaction

We first examined hydrolysis of sucrose and Glc1P under conditions where P_i or fructose was lacking as nucleophile for reaction in phosphorolysis and synthesis, respectively. Apparent catalytic constants ($^{app}k_{cat}$) for glucosyl donor hydrolysis were determined at a single constant substrate concentration and are summarised in Table I. The wild-type enzyme has previously been shown to promote hydrolysis of sucrose and Glc1P at approximately 2–3% of the level of activity for enzymatic conversion of the same donor substrates in the presence of the naturally preferred nucleophiles. The hydrolysis $^{app}k_{cat}$ for the mutated enzymes was lower than the corresponding $^{app}k_{cat}$ for wild-type *Lm*SPase by about two (R395L) and three (D49A) orders of magnitude. The relative decrease in (apparent) turnover number resulting from the use of water instead of P_i or fructose as nucleophile of the reaction was 20-fold or greater and therefore comparable between the two mutants and the wild-type enzyme. Therefore, this implies that the selectivity for transferring the glucosyl residue from the enzyme to P_i or fructose as compared to transferring the same glucosyl residue to water had not been altered in *Lm*SPase as a result of the site-directed replacement of Asp^{49} and Arg^{395}.

However, we were also interested in determining the extent of competition between water and P_i under conditions of phosphorolysis of sucrose. In other words, we wanted to examine the possible occurrence of a true 'error hydrolysis' as an accompaniment to the normal glucosyl transfer to P_i. Figure 5 displays an analysis in which the initial rate of release of Glc1P (*phosphorolysis*) and glucose (*hydrolysis*) from sucrose was measured at a variable concentration of P_i. Remarkably enough, the wild-type enzyme showed a low level of erroneous hydrolysis that accounted for about 2% of the total glucosyl transfer catalysed and was independent of the P_i concentration used in the range 10–300 mM. The D49A mutant, by contrast, had completely lost the ability of the wild-type enzyme to discriminate between water and P_i as acceptor substrate. The ratio of the rates of hydrolysis and phosphorolysis was about unity for the D49A mutant, and this was constant over a wide range of P_i concentrations. The K_m of P_i for the D49A mutant is given in Table I as 40 μM. Therefore, this K_m implies that the β-glucosyl

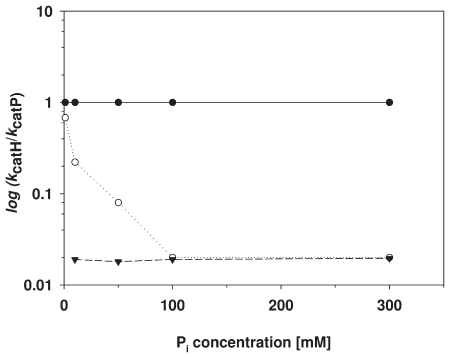

Figure 5. Ratio of hydrolytic (k_{catH}) and phosphorolytic (k_{catP}) activities of wild-type *Lm*SPase (▼) and mutants (D49A (●), R395L (○)) towards sucrose in the presence of varying concentrations of P_i (WT: 10, 50, 100 and 300 mM; mutants: 1, 10, 50, 100 and 300 mM).

enzyme intermediate of D49A mutant was completely saturated with P_i under the conditions described in Figure 5. The observed ratio of reaction rates thus represents an intrinsic property of this enzyme complex to undergo conversion via glucosyl transfer to water and P_i. The selectivity of D49A for reaction with P_i is low. The R395L mutant differs from the D49A mutant in that discrimination between reaction with P_i and water seems to occur mainly at the level of binding of the nucleophile to the β-glucosyl enzyme intermediate. The selectivity ratio decreased as the P_i concentration was increased (Figure 5) to eventually reach the value seen in wild-type *Lm*SPase.

Structural interpretation of the consequences of substitution of Asp^{49} and Arg^{395}

Using Equation (4), the kinetic data in Table I can be used to calculate the amount of Gibbs free energy ($\Delta\Delta G^{\#}$) that is no longer available for stabilisation of the transition states flanking the β-glucosyl enzyme intermediate once Asp^{49} or Arg^{395} has been substituted by site-directed mutagenesis. The calculated losses of transition state stabilisation energy in the two mutants as compared to the wild-type enzyme are large and seem to exceed by far the typical value of $\Delta\Delta G^{\#} \approx 14.5$–$18.5$ kJ/mol) that one would maximally expect for the removal of a charged hydrogen bond between an enzyme side chain and a non-reacting hydroxy group of the substrate. There is useful evidence from work on the selective modification of the interacting sites on the enzyme (point mutation; for two seminal papers, see Fersht et al. 1985; Wells & Fersht 1985), the substrate (synthetic substitution of the relevant hydroxy group by hydrogen or fluorine; e.g. Street et al. 1986; Frandsen et al.

2002) or both (e.g. Sierks & Svensson 1992; Sierks & Svensson 2000) that support this rough upper limit to the energetic contribution of a single hydrogen bond to transition stabilisation.

The very large $\Delta\Delta G^{\#}$ values associated with enzyme glucosylation from sucrose in both mutants, however, especially in the D49A mutant, are probably best explained by a structural disruption caused by the mutations that was not strictly local but relayed to proximal parts inside and outside of the catalytic subsite where the glucosyl residue is accommodated. Comparison of the specific activities in phosphorolysis direction for the single mutants with the corresponding specific activity for the D49A-R395L double mutant supports the suggestion that mutation of Asp^{49} has probably resulted in an essentially complete destruction of the functionality of the binding site for the C_4 hydroxy group, disrupting not only the hydrogen bond from Asp^{49} but also that from Arg^{395}.

Moreover, consequences of the two mutations expressed in terms of $\Delta\Delta G^{\#}$ (enzyme glucosylation) were highly dependent on the leaving group of the glucosyl donor substrate, being up to 10 kJ/mol (D49A) or 7 kJ/mol (R395L) smaller when Glc1P was utilised instead of sucrose. This result suggests that there is a certain degree of synergism in catalytic function between the subsite that binds the glucosyl residue and the neighbouring subsite that binds the leaving group; and that the cooperation between the two subsites is decreased as a result of the substitution of Asp^{49} and Arg^{395} through the occurrence of a proximally disruptive effect. Of note, the work of Frandsen et al. (2002) provides an estimate for the energetic consequence in the transition state of enzyme glucosylation in GH-13 α-glucosidases that results from complete removal of hydrogen bonding with the glucosyl C_4 hydroxy group due to the use of a deoxygenated donor substrate. These $\Delta\Delta G^{\#}$ values are in the order of □20 kJ/mol and substantially lower than $\Delta\Delta G^{\#}$ values for reaction of D49A and R395L mutants with sucrose (Table I), supporting the notion that the effect of the mutations goes beyond destruction of the hydrogen bonding at C_4. Even though this conclusion invalidates the use of the kinetic data in Table I for measurement of the hydrogen bond strength with the C_4 hydroxyl in *Lm*SPase, the results have an important bearing on our understanding of the role of communication between the two phosphorylase subsites on recognition and specificity of the enzyme, as follows.

It has been suggested from crystal structures of *Ba*SPase (Sprogøe et al. 2004; Mirza et al. 2006) that the enzyme must undergo a protein conformational change at subsite + 1 to switch between utilisation of fructose and P_i as leaving group/nucleophile of the reaction. The residues mainly involved in this conformational change are Arg^{137}, Asp^{338} and Tyr^{340} (*Lm*SPase numbering), and their proposed roles in binding recognition and catalysis have been confirmed by mutagenesis (Mueller & Nidetzky 2007a). Structural plasticity at subsite + 1 is suggested to be responsible for two salient features of the D49A and R395L mutants that are not present in the wild-type enzyme: substrate inhibition by P_i, and strong competition from water for reaction with the β-glucosyl enzyme intermediate.

Superimposition of the structure of free *Ba*SPase (Sprogøe et al. 2004) with the structure of the enzyme–sucrose complex (Mirza et al. 2006) (Supporting Figure S2 available online at http://www.informahealthcare.com/bab/doi/10.3109/10242422.2012.674720) reveals that binding of sucrose does not induce conformational changes at either one of the two subsites of the enzyme. This finding implies that *Ba*SPase is structurally preorganised already in the free enzyme to bind an α-glucosyl donor substrate that contains a fructose leaving group. Of note, the structure of free *Ba*SPase has the main phosphate-binding residues (Arg^{137}, Tyr^{340}) pointing out of subsite + 1, suggesting that the enzyme should be able to discriminate against formation of a non-productive binary complex with P_i. The timing of binding of P_i, that seems to be so very well-orchestrated with respect to formation of the β-glucosyl enzyme intermediate in wild-type *Lm*SPase, has probably been messed up as result of mutations of Asp^{49} and Arg^{395}. Accumulation of the enzyme–phosphate complex at high P_i levels in the steady state appears to be a plausible reason for the onset of substrate inhibition by P_i in the mutated phosphorylases. Both D49A and R395L mutants would seem to favour a 'phosphate-binding ready' conformation of the free enzyme that is not present in wild-type *Lm*SPase.

Why is deglucosylation to P_i affected (up to 210-fold) less strongly by mutation of Asp^{49} and Arg^{395} than the deglucosylation to fructose? We think that the structural requirements for binding of P_i are by far less stringent than those for binding of fructose. One could imagine multiple reactive conformations of the P_i molecule while for fructose, there probably exists only a single conformation that leads to glucosyl transfer. Therefore, small structural changes at subsite −1 caused by the proximally disruptive effect of substitution of Asp^{49} or Arg^{395} could simply be more easily tolerated, through alternative conformations, in the reaction with P_i as compared to the reaction with fructose. The notion of an alternatively bound P_i acceptor substrate would be consistent with observations for the D49A mutant where water shows an unusually strong competition with bound P_i for reaction with the β-glucosyl enzyme intermediate.

Conclusion

The evidence presented herein portrays Asp^{49} or Arg^{395} as essential residues of glucosyl transfer to and from P_i catalysed by *Lm*SPase and by extension due to sequence conservation, other sucrose phosphorylases. The proximally disruptive effects of site-directed substitution of Asp^{49} by Ala and Arg^{395} by Leu provided an unexpected opportunity to gain further insight into binding recognition of the leaving group/nucleophile at subsite +1 of the enzyme. The results reveal how important it may be for the wild-type enzyme to discriminate against binding of P_i to the free phosphorylase in order to prevent substrate inhibition by P_i from taking place.

Declaration of interest: The authors report no conflicts of interest. The authors alone are responsible for the content and writing of the paper. Financial support from the Austrian Science Funds FWF (project L586-B03 to B.N.) is gratefully acknowledged.

References

Abad MC, Binderup K, Rios-Steiner J, Arni RK, Preiss J, Geiger JH. 2002. The X-ray crystallographic structure of *Escherichia coli* branching enzyme. J Biol Chem 277:42164–42170.

Brayer GD, Luo Y, Withers SG. 1995. The structure of human pancreatic α-amylase at 1.8 Å resolution and comparisons with related enzymes. Protein Sci 4:1730–1742.

Brzozowski AM, Davies GJ. 1997. Structure of the *Aspergillus oryzae* α-amylase complexed with the inhibitor acarbose at 2.0 Å resolution. Biochemistry 36:10837–10845.

Buchholz K, Seibel J. 2008. Industrial carbohydrate biotransformations. Carbohydr Res 343:1966–1979.

Davies GJ, Wilson KS. 1999. Trapped in the act of catalysis. Nat Struct Biol 6:406–408.

Fersht AR, Shi JP, Knill-Jones J, Lowe DM, Wilkinson AJ, Blow DM, et al. 1985. Hydrogen bonding and biological specificity analysed by protein engineering. Nature 314:235–238.

Frandsen TP, Palcic MM, Svensson B. 2002. Substrate recognition by three family 13 yeast α-glucosidases. Eur J Biochem 269:728–734.

Goedl C, Nidetzky B. 2009. Sucrose phosphorylase harbouring a redesigned, glycosyltransferase-like active site exhibits retaining glucosyl transfer in the absence of a covalent intermediate. Chem Bio Chem 10:2333–2337.

Goedl C, Sawangwan T, Mueller M, Schwarz A, Nidetzky B. 2008. A high-yielding biocatalytic process for the production of 2-*O*-(α-D-glucopyranosyl)-*sn*-glycerol, a natural osmolyte and useful moisturizing ingredient. Angew Chem Int Ed 47: 10086–10089.

Goedl C, Sawangwan T, Wildberger P, Nidetzky B. 2010. Sucrose phosphorylase: a powerful transglucosylation catalyst for synthesis of α-D-glucosides as industrial fine chemicals. Biocatal Biotransform 28:10–21.

Goedl C, Schwarz A, Minani A, Nidetzky B. 2007. Recombinant sucrose phosphorylase from *Leuconostoc mesenteroides*: characterization, kinetic studies of transglucosylation, and application of immobilised enzyme for production of α-D-glucose 1-phosphate. J Biotechnol 129:77–86.

Hayden BM, Dean JL, Martin SR, Engel PC. 1999. Chemical rescue of the catalytically disabled clostridial glutamate dehydrogenase mutant D165S by fluoride ion. Biochem J 340: 555–560.

Janecek S, Svensson B, Henrissat B. 1997. Domain evolution in the α-amylase family. J Mol Evol 45:322–331.

Kim MI, Kim HS, Jung J, Rhee S. 2008. Crystal structures and mutagenesis of sucrose hydrolase from *Xanthomonas axonopodis pv. glycines*: insight into the exclusively hydrolytic amylosucrase fold. J Mol Biol 380:636–647.

Kratzer R, Nidetzky B. 2005. Electrostatic stabilization in a preorganized polar active site: the catalytic role of Lys-80 in *Candida tenuis* xylose reductase (AKR2B5) probed by site-directed mutagenesis and functional complementation studies. Biochem J 389:507–515.

Lee JH, Yoon SH, Nam SH, Moon YH, Moon YY, Kim D. 2006. Molecular cloning of a gene encoding the sucrose phosphorylase from *Leuconostoc mesenteroides* B-1149 and the expression in *Escherichia coli*. Enzyme Microb Technol 39:612–620.

MacGregor EA, Janecek S, Svensson B. 2001. Relationship of sequence and structure to specificity in the α-amylase family of enzymes. Biochim Biophys Acta 1546:1–20.

Mildvan AS. 2004. Inverse thinking about double mutants of enzymes. Biochemistry 43:14517–14520.

Mirza O, Skov LK, Remaud-Simeon M, Potocki de Montalk G, Albenne C, Monsan P, Gajhede M. 2001. Crystal structures of amylosucrase from *Neisseria polysaccharea* in complex with D-glucose and the active site mutant Glu328Gln in complex with the natural substrate sucrose. Biochemistry 40:9032–9039.

Mirza O, Skov LK, Sprogøe D, van den Broek LA, Beldman G, Kastrup JS, Gajhede M. 2006. Structural rearrangements of sucrose phosphorylase from *Bifidobacterium adolescentis* during sucrose conversion. J Biol Chem 281:35576–35584.

Mueller M, Nidetzky B. 2007a. The role of Asp-295 in the catalytic mechanism of *Leuconostoc mesenteroides* sucrose phosphorylase probed with site-directed mutagenesis. FEBS Lett 581:1403–1408.

Mueller M, Nidetzky B. 2007b. Dissecting differential binding of fructose and phosphate as leaving group/nucleophile of glucosyl transfer catalyzed by sucrose phosphorylase. FEBS Lett 581:3814–3818.

Nielsen JE, Borchert TV. 2000. Protein engineering of bacterial α-amylases. Biochim Biophys Acta 1543:253–274.

Peracchi A. 2001. Enzyme catalysis: removing chemically 'essential' residues by site-directed mutagenesis. Trends in Biochem Sci 26:497–503.

Peracchi A. 2008. How (and why) to revive a dead enzyme: the power of chemical rescue. Curr Chem Biol 2:32–49.

Russell RR, Mukasa H, Shimamura A, Ferretti JJ. 1988. *Streptococcus mutans* gtfA gene specifies sucrose phosphorylase. Infect Immun 56:2763–2765.

Rydberg EH, Li C, Maurus R, Overall CM, Brayer GD, Withers SG. 2002. Mechanistic analyses of catalysis in human pancreatic α-amylase: detailed kinetic and structural studies of mutants of three conserved carboxylic acids. Biochemistry 41: 4492–4502.

Sauer J, Sigurskjold BW, Christensen U, Frandsen TP, Mirgorodskaya E, Harrison M, Roepstorff P, Svensson B. 2000. Glucoamylase: structure/function relationships, and protein engineering. Biochim Biophys Acta 1543:275–293.

Schwarz A, Brecker L, Nidetzky B. 2007. Acid-base catalysis in *Leuconostoc mesenteroides* sucrose phosphorylase probed by site-directed mutagenesis and detailed kinetic comparison of wild-type and Glu237-->Gln mutant enzymes. Biochem J 403: 441–449.

Schwarz A, Nidetzky B. 2006. Asp-196-->Ala mutant of *Leuconostoc mesenteroides* sucrose phosphorylase exhibits altered

stereochemical course and kinetic mechanism of glucosyl transfer to and from phosphate. FEBS Lett 580:3905–3910.

Shirai T, Hung VS, Morinaka K, Kobayashi T, Ito S. 2008. Crystal structure of GH13 α-glucosidase GSJ from one of the deepest sea bacteria. Proteins Struct Funct Bioinf 73: 126–133.

Sierks MR, Svensson B. 1992. Kinetic identification of a hydrogen bonding pair in the glucoamylase-maltose transition state complex. Protein Eng 5:185–188.

Sierks MR, Svensson B. 2000. Energetic and mechanistic studies of glucoamylase using molecular recognition of maltose OH groups coupled with site-directed mutagenesis. Biochemistry 39:8585–8592.

Sprogøe D, van den Broek LA, Mirza O, Kastrup JS, Voragen AG, Gajhede M, Skov LK. 2004. Crystal structure of sucrose phosphorylase from *Bifidobacterium adolescentis*. Biochemistry 43:1156–1162.

Stam MR, Danchin EG, Rancurel C, Coutinho PM, Henrissat B. 2006. Dividing the large glycoside hydrolase family 13 into subfamilies: towards improved functional annotations of α-amylase-related proteins. Protein Eng Des Sel 19:555–562.

Street IP, Armstrong CR, Withers SG. 1986. Hydrogen bonding and specificity. Fluorodeoxy sugars as probes of hydrogen bonding in the glycogen phosphorylase-glucose complex. Biochemistry 25:6021–6027.

Uitdehaag JC, Kalk KH, van Der Veen BA, Dijkhuizen L, Dijkstra BW. 1999. The cyclization mechanism of cyclodextrin glycosyltransferase (CGTase) as revealed by a γ-cyclodextrin-CGTase complex at 1.8-Å resolution. J Biol Chem 274:34868–34876.

van den Broek LA, van Boxtel EL, Kievit RP, Verhoef R, Beldman G, Voragen AG. 2004. Physico-chemical and transglucosylation properties of recombinant sucrose phosphorylase from *Bifidobacterium adolescentis* DSM20083. Appl Microbiol Biotechnol 65:219–227.

van der Maarel MJ, van der Veen B, Uitdehaag JC, Leemhuis H, Dijkhuizen L. 2002. Properties and applications of starch-converting enzymes of the α-amylase family. J Biotechnol 94: 137–155.

van der Veen BA, Potocki-Veronese G, Albenne C, Joucla G, Monsan P, Remaud-Simeon M. 2004. Combinatorial engineering to enhance amylosucrase performance: construction, selection, and screening of variant libraries for increased activity. FEBS Lett 560:91–97.

van der Veen BA, Skov LK, Potocki-Veronese G, Gajhede M, Monsan P, Remaud-Simeon M. 2006. Increased amylosucrase activity and specificity, and identification of regions important for activity, specificity and stability through molecular evolution. FEBS J 273:673–681.

Voet JG, Abeles RH. 1970. The mechanism of action of sucrose phosphorylase. Isolation and properties of a β-linked covalent glucose-enzyme complex. J Biol Chem 245:1020–1031.

Wang W, Malcolm BA. 1999. Two-stage PCR protocol allowing introduction of multiple mutations, deletions and insertions using QuikChange Site-Directed Mutagenesis. Biotechniques 26:680–682.

Weimberg R, Doudoroff M. 1954. Studies with three bacterial sucrose phosphorylases. J Bacteriol 68:381–388.

Wells TNC, Fersht AR. 1985. Hydrogen bonding in enzymatic catalysis analysed by protein engineering. Nature 316: 656–657.

Wildberger P, Luley-Goedl C, Nidetzky B. 2011. Aromatic interactions at the catalytic subsite of sucrose phosphorylase: their roles in enzymatic glucosyl transfer probed with Phe52-->Ala and Phe52-->Asn mutants. FEBS Lett 585:499–504.

Zhang D, Li N, Lok SM, Zhang LH, Swaminathan K. 2003. Isomaltulose synthase (*Pal*I) of *Klebsiella sp. LX3*. Crystal structure and implication of mechanism. J Biol Chem 278: 35428–35434.

Supplementary material are available online.

Supporting Figures S1 and S2

SUPPLEMENTARY INFORMATION FOR

Probing enzyme-substrate interactions at the catalytic subsite of *Leuconostoc mesenteroides* sucrose phosphorylase with site-directed mutagenesis: the roles of Asp^{49} and Arg^{395}

Patricia Wildberger, Anamaria Todea and Bernd Nidetzky*

Institute of Biotechnology and Biochemical Engineering, Graz University of Technology, Petersgasse 12/1, A-8010 Graz, Austria

*Corresponding author
E-mail: bernd.nidetzky@tugraz.at; Tel. +43-316-873-8400; Fax +43-316-873-8434

Enzyme	Asp C_4-OH	His C_6-OH	Arg C_2-OH	Asp C_6-OH	Glu C_2-OH	His C_2-OH & C_3-OH	Asp C_2-OH & C_3-OH	Arg C_4-OH
Amylosucrase (Mirza et al. 2001)	PEGKSD^{151}GGYAV	DFIFNH^{155}TSNEH	GVDILR^{296}MDAVA	DILRMD^{294}AVAFI	PDQVVQ^{344}YIGQ-	HTAWVN^{199}YVRSH	TAWVNY^{196}VRSHD	RWAHRP^{522}RYNEA
Sucrose hydrolase (Kim et al. 2008)	RAGDND^{136}GGFAV	DFVLNH^{180}TADDH	GVEAFR^{278}LDSTA	EAFRLD^{288}STAYL	MTQLPD^{332}YFGSG	HCAWLS^{188}YVRCH	CAWLSY^{287}VRCHD	RWLHRP^{520}AMDWQ
α-Glucosidase (Shirai et al. 2008)	P--NAD^{59} NGYDI	DLVINH^{103}TSDEH	GIDGFR^{197}IDAIS	DGFRID^{199}AISHI	YDIMTV^{254}GEANG	KRTLTK^{307}WQKGL	RTLTKW^{308}QKGLE	PWIKVN^{438}ENYRT
Isomaltulose synthase (Zhang et al. 2003)	P--NTD^{193}NGYDI	DVVINH^{145}TSDQH	GVSGMR^{239}FDTVA	SGMRFD^{241}TVATY	YDVATA^{297}GEIFG	RQIISK^{350}MDVTV	QIISKM^{351}DVTVG	PWFHIN^{483}PNYVE
Sucrose phosphorylase (Sprogøe et al. 2004)	PFDGAD^{50} AGFDP	DAIVNH^{85}MSWES	HVSYIR^{190}LDAVG	SYIRLD^{196}AVGYG	LEILIP^{232}VHSYY	TVLDTH^{209}DGIGV	VLDTHD^{290}GIGVI	-----R^{399}DINRH

Supplementary Figure S1. Partial multiple sequence alignment of selected glucoside hydrolases and transglucosidases from family GH-13 showing partial positional conservation of amino acids that provide charged hydrogen bonding interactions with the glucosyl moiety of their substrate. The partial sequences shown are amylosucrase from *Neisseria polysaccharea* (AAT15258.1), sucrose hydrolase from *Xanthomonas axonopodis pv. glycines* (AAQ93678.1), α-glucosidase from *Geobacillus sp. HTA-462* (BAE48285.1), isomaltulose synthase from *Klebsiella sp. LX3* (AAK82938.1) and sucrose phosphorylase from *Bifidobacterium adolescentis* (AAO33821.1).

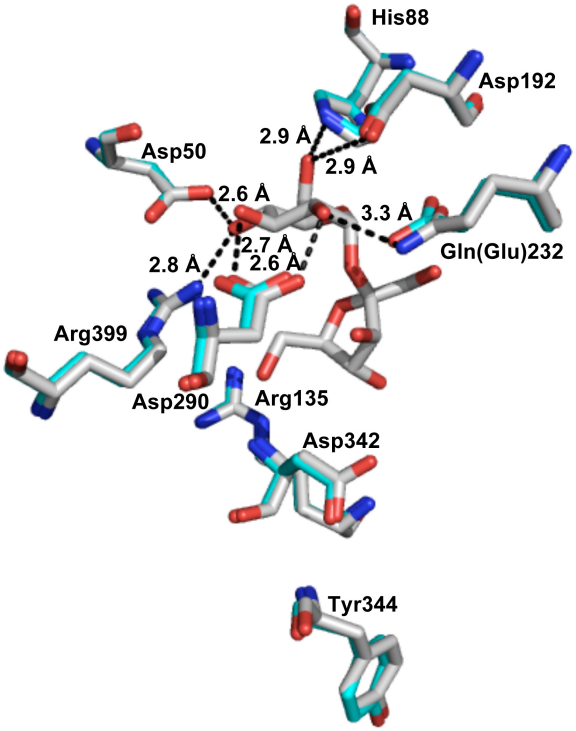

Supplementary Figure S2. Structural overlay of the catalytic subsites in free (blue; PDB entry 1r7a molecule A) and sucrose bound (grey; PDB entry 2gdu, molecule A) BaSPase. The residues interacting with the glucopyranosyl moiety of sucrose are shown. Furthermore, the residues involved in the conformational change at subsite -1 between utilisation of fructose and phosphate as leaving group/nucleophile are displayed. The figure reveals that there are no significant conformational changes at both subsites in response to binding of sucrose.

3 Aromatic interactions at the catalytic subsite of sucrose phosphorylase: Their roles in enzymatic glucosyl transfer probed with $Phe^{52} \rightarrow Ala$ and $Phe^{52} \rightarrow Asn$ mutants

FEBS Letters 585 (2011) 499–504

ELSEVIER

FEBS Letters

journal homepage: www.FEBSLetters.org

Aromatic interactions at the catalytic subsite of sucrose phosphorylase: Their roles in enzymatic glucosyl transfer probed with Phe^{52} → Ala and Phe^{52} → Asn mutants

Patricia Wildberger, Christiane Luley-Goedl, Bernd Nidetzky *

Institute of Biotechnology and Biochemical Engineering, Graz University of Technology, Petersgasse 12/1, A-8010 Graz, Austria

ARTICLE INFO

Article history:
Received 3 November 2010
Revised 23 December 2010
Accepted 29 December 2010
Available online 8 January 2011

Edited by Judit Ovádi

Keywords:
Sucrose phosphorylase
GH-13
Cation-π interaction
Oxocarbenium ion
Aromatic stacking
Glycoside hydrolase
Glycosyltransferase

ABSTRACT

Mutants of *Leuconostoc mesenteroides* sucrose phosphorylase having active-site Phe^{52} replaced by Ala (F52A) or Asn (F52N) were characterized by free energy profile analysis for catalytic glucosyl transfer from sucrose to phosphate. Despite large destabilization (⩾3.5 kcal/mol) of the transition states for enzyme glucosylation and deglucosylation in both mutants as compared to wild-type, the relative stability of the glucosyl enzyme intermediate was weakly affected by substitution of Phe^{52}. In reverse reaction where fructose becomes glucocylated, "error hydrolysis" was the preponderant path of breakdown of the covalent intermediate of F52A and F52N. It is proposed, therefore, that Phe^{52} facilitates reaction of the phosphorylase through (1) positioning of the transferred glucosyl moiety at the catalytic subsite and (2) strong cation-π stabilization of the oxocarbenium ion-like transition states flanking the covalent enzyme intermediate.

1. Introduction

Recognition of carbohydrates by proteins often involves π-interactions from aromatic side chains of Phe, Tyr, and Trp. Aromatic rings undergo stacking with pyranoses and furanoses whereby their π-electron cloud interacts with aliphatic protons of the sugar ring [1–4]. The resulting interaction energies were reported to vary between −0.5 and −0.8 kcal/mol, depending on the nature of the aromatic ring and the carbohydrate [5]. Not surprisingly, therefore, carbohydrate-π interactions are widely utilized by glycoside hydrolases (e.g. [6,7]), glycosyltransferases (e.g. [8–10]) and carbohydrate-binding modules [11,12] to achieve recognition and specificity for their natural substrates. A striking commonality among the diverse families of glycoside hydrolases is the occurrence of a family-specific hydrophobic motif in their catalytic subsites. This motif usually consists of one or more aromatic residues and is found irrespective of whether the glycoside hydrolase utilizes an α or β-configured pyranosyl substrate and hydrolyzes it with retention or inversion of anomeric configuration [13]. Its proposed role in catalysis is to aid in the conformational itinerary of the glycopyranoside upon moving from the ground state (e.g. $^4C_1$ chair) to the oxocarbenium ion-like transition state (e.g. $^4H_3$ half-chair). Non-polar contacts with the hydrophobic C_4–C_5-hydroxymethyl moiety of the glycopyranoside that become tightened in the transition state are believed to be the source of the catalytic facilitation provided. In addition to this *conformational* stabilization derived from carbohydrate-π interactions, there is the interesting question if aromatic side chains contributed to the catalytic subsite might also be important for *electrostatic* stabilization of the transition state of the glycoside hydrolase reaction.

Family GH-13 constitutes a large group of retaining hydrolases and transglycosidases that act on α-*O*-glycosidic substrates such as starch and sucrose [14]. Its members contain a special aromatic motif (Fig. 1; [15–21]) where a highly conserved Phe/Tyr is positioned at the B-face of the glucopyranosyl ring bound in the catalytic subsite. Sucrose phosphorylase (from *Leuconostoc mesenteroides*; LmSPase) was chosen for examining with site-directed mutagenesis the function of the relevant aromatic residue (Phe^{52}) in the catalytic mechanism. Note: the aromatic motif in Fig. 1 must be distinguished from the likewise present hydrophobic

Abbreviations: Glc1P, α-D-glucopyranosyl phosphate; Glc1F, α-D-glucopyranosyl fluoride; SPase, sucrose phosphorylase (EC 2.4.1.7); BaSPase, *Bifidobacterium adolescentis* SPase; LmSPase, *Leuconostoc mesenteroides* SPase

* Corresponding author. Fax: +43 316 873 8434.
E-mail address: bernd.nidetzky@tugraz.at (B. Nidetzky).

0014-5793/$36.00 © 2011 Federation of European Biochemical Societies. Published by Elsevier B.V. All rights reserved.
doi:10.1016/j.febslet.2010.12.041

A

Enzyme	Organism GenBank	Sequence
Amylosucrase [15]	*Neisseria polysaccharea* AAT15258.1	EGKSDGG**Y**^{155}AVSSYRD
Sucrose hydrolase [16]	*Xanthomonas axonopodis pv. Glycines* AAQ93678.1	AGDNDGG**F**^{133}AVSDYGQ
α-Glucosidase [17]	*Geobacillus sp. HTA-462* BAE48285.1	--NADNG**Y**^{62}DISDYYA
Isomaltulose synthase [18]	*Klebsiella sp. LX3* AAK82938.1	--NTDNG**Y**^{104}DISNYRQ
Cyclodextrin glycosyltransferase [19]	*Bacillus circulans* CAA48401.1	TNTAYHG**Y**^{133}WARDFKK
α-Amylase [20]	*Bacillus licheniformis* AAA22226.1	GYGAYDL**Y**^{90}DLGEFHQ
Sucrose phosphorylase [21]	*Bifidobacterium adolescentis* AAO33821.1	FDGADAG**F**^{53}DPIDHTK

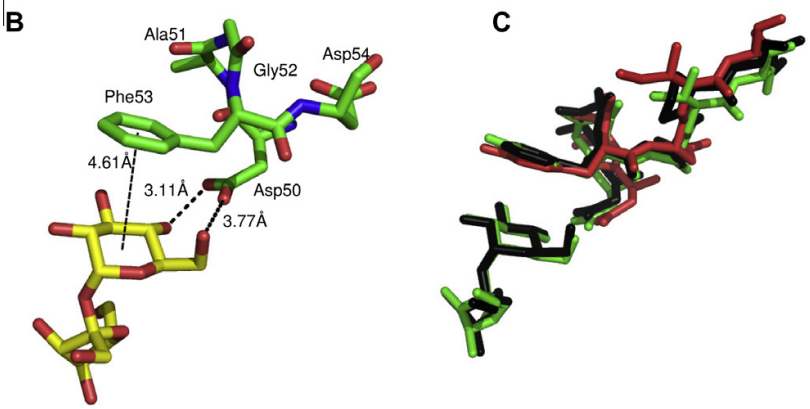

Fig. 1. The aromatic motif at the catalytic subsite of selected glucoside hydrolases and transglucosidases from family GH-13, revealed by Phe/Tyr residue conservation in both sequence (A) and three-dimensional structure (B and C). Panel B shows relevant interactions with the glucopyranosyl moiety of sucrose in the catalytic subsite of *B. adolescentis* sucrose phosphorylase (BaSPase). Note: Phe^{52} of LmSPase is homologous to the shown Phe^{53} of BaSPase. Panel C is a structural overlay of the corresponding catalytic subsite parts of BaSPase (2GDU; black), *N. polysaccharea* amylosucrase (1JGI; green) and *Klebsiella sp.* isomaltulose synthase (1M53; red).

motif (Phe^{160} in LmSPase) of conformational stabilization [13] that is not considered herein. LmSPase belongs to a particular group of transglycosidases within family GH-13 that promote reversible glucosyl transfer from sucrose to phosphate (P_i), yielding α-D-glucopyranosyl phosphate (Glc1P) and D-fructose as products [22]. Like in other GH-13 enzymes [23–26], catalytic reaction of LmSPase involves formation (*glucosylation*) and breakdown (*deglucosylation*) of a covalent β-glucosyl enzyme intermediate [27]. The proposed role of Phe^{52} involves stabilization, by strong cation-π interactions, of the oxocarbenium ion-like transition states leading to and from the glucosylated enzyme.

2. Materials and methods

Materials used have been described elsewhere [22]. α-D-Glucopyranosyl fluoride (Glc1F) was prepared by Zemplen deprotection from 2,3,4,6-tetra-*O*-α-D-glucopyranosyl fluoride that was obtained from TCI Europe.

2.1. Site-directed mutagenesis and enzyme preparation

Mutations resulting in substitution of Phe^{52} by Ala (F52A) or Asn (F52N) were introduced using a reported two-stage PCR protocol [28] in which a pQE30 expression vector encoding wild-type LmSPase was used as template [22]. Oligonucleotide primers and details of conditions used for PCR are summarized in Supplementary data. For expression, we subcloned native and mutated genes, via *Bam*HI and *Pst*I restriction sites, from pQE30 into pASK-IBA7+ (IBA GmbH). The pASK-IBA7+ constructs introduce *Strep*-tag II at the N-terminus of each enzyme. The new tag (8 amino acids) is comparable in length to the previously used His-tag (11 amino acid), which however did not facilitate protein isolation [22]. All inserts were confirmed by sequencing in sense and antisense directions. *Escherichia coli* Top10 cells harboring pASK-IBA7+ construct were cultivated under standard conditions (Supplementary data) using induction with 200 μg/l anhydrotetracycline (6 h, 25 °C). Crude cell extract was prepared with a French press and protein was purified using chromatography on a Strep-Tactin Superflow column (bed volume 5 ml) (for details, see the Supplementary data). Purification was monitored by SDS–PAGE.

2.2. Assays

Enzyme activity in direction of phosphorolysis of sucrose was determined at 30 °C using a continuous coupled enzymatic assay with phosphoglucomutase and glucose-6-phosphate dehydrogenase [22]. Protein concentration was measured with the BioRad dye-binding method referenced against BSA. Glucose was determined using an assay with hexokinase and glucose-6-phosphate dehydrogenase [22]. Glucose in the presence of fructose was determined using an assay with glucose oxidase and peroxidase [29]. Glc1P was assayed using phosphoglucomutase and glucose-6-phosphate dehydrogenase [22]. Phosphate was determined colorimetrically at 850 nm [22]. Other analytical methods (NMR, HPLC)

were described elsewhere [27] and specific details are provided in Supplementary data.

2.3. Initial-rate studies and steady-state kinetic analysis

Reactions were performed at 30 °C in 50 mM MES buffer, pH 7.0, and monitored by product formation (phosphorolysis: Glc1P; synthesis: P_i) in discontinuous assays. The typical concentration of wild-type LmSPase was 0.001 mg/ml, that of F52A and F52N was 0.3 mg/ml. Initial-rate measurements were done under conditions in which conversion of limiting substrate was less than 5% and increase in product concentration was linearly dependent on incubation time. Glucosyl donor and acceptor concentrations were varied in a suitable range, depending on the enzyme used: sucrose (0.01–800 mM), P_i (0.01–250 mM), Glc1P (0.01–250 mM), fructose (0.01–800 mM), Glc1F (0.1–250 mM). Control reactions lacking the enzyme or one of the substrates were performed, and enzymatic initial rates were corrected as required. Kinetic parameters (V_{max}, K_m) were obtained from non-linear fits of data to the Michaelis–Menten equation. When enzyme was not saturable with substrate and independent determination of V_{max} and K_m therefore not possible, V_{max}/K_m was obtained from data acquired under substrate-limited reaction conditions where the rate increases in linear dependence on substrate concentration. The catalytic constant was calculated from the relationship $k_{cat} = V_{max}/E$ where E is the molar enzyme concentration based on a molecular mass of 59 kDa for the LmSPase subunit.

2.4. Construction of free energy profiles

A 1-M standard state was assumed for all reactants. Temperature (T) was 303.15 K. K_{eq_kin} and K_{eq_therm} are kinetic and thermodynamic expressions of the equilibrium constant for the phosphorylase reaction (Eq. (1)) at pH 7.0.

$$\text{Sucrose} + \text{phosphate} \leftrightarrow \text{Glc1P} + \text{fructose} \quad (1)$$

K_{eq_therm} was determined from a series ($N = 9$) of phosphorolysis experiments that used different initial concentrations of sucrose (0.05–0.5 M) and phosphate (0.05–0.5 M) dissolved in 50 mM MES buffer, pH 7.0. The concentration of Glc1P at apparent equilibrium was measured, and K_{eq_therm} was calculated according to Eq. (1). A value of 9 (±61%) was obtained. Gibbs free energies (ΔG) were calculated using Eqs. (2) and (3) where R is gas constant (8.314 J/(mol K)), k is the Boltzmann constant (1.38×10^{-23} J/K) and h is the Planck constant (6.626×10^{-34} Js). ΔG^{eq} and $\Delta G^{\#}$ are equilibrium and transition-state energies, respectively.

$$\Delta G^{eq} = -\text{RT In } K_{eq\_kin} \quad (2)$$

$$\Delta G^{\#} = \text{RT In}(k_B T/h) - RT \text{ In}(k_{cat}/K_m) \quad (3)$$

Eq. (4) was used to calculate the Gibbs free energy for the covalent intermediate where k_{cat}/K_m (P_i) and k_{cat}/K_m (Glc1P) are catalytic efficiencies for P_i and Glc1P, respectively.

$$\Delta G^{int} = \Delta G^{eq} + \text{RT In}[k_{cat}/K_m(P_i)/k_{cat}/K_m(\text{Glc1P})] \quad (4)$$

3. Results and discussion

Strep-tagged phosphorylases were purified to apparent electrophoretic homogeneity in a single step of affinity chromatography (Supplementary Fig. 1). Protein isolation was therefore made much simpler than it was when working with His-tagged LmSPase that needed to be purified through a multiple-step procedure [27]. Kinetic parameters for phosphorolysis and synthesis of sucrose by the *Strep*-tagged form of wild-type LmSPase are summarized in Table 1. Although the numbers are not identical to those reported in earlier work using the His-tagged enzyme [30], it is clear that exchange of the N-terminal tag went along with useful retention of the known kinetic properties of wild-type LmSPase. However, data for the wild-type enzyme are required as reference for analysis of kinetic consequences in LmSPase mutants that also harbor *Strep*-tag II.

Table 1
Kinetic parameters in phosphorolysis and synthesis direction catalyzed by wild-type LmSPase and Phe[52] mutants thereof.

Reaction		Wild-type	F52A	F52N
Phosphorolysis of sucrose				
Glucosylation from sucrose[1]	k_{cat} [s^{-1}]	117	n.a.	n.a
	K_m [mM^{-1}]	9.8	n.a.	n.a.
	k_{cat}/K_m [s^{-1} mM^{-1}]	12	2.3×10^{-3}	3.0×10^{-3}
Deglucosylation by phosphate[2]	k_{cat} [s^{-1}]	145	3.3[a]	3.1[c]
	K_m [mM^{-1}]	6.0	46	42
	k_{cat}/K_m [s^{-1} mM^{-1}]	24	7.2×10^{-2} [b]	7.4×10^{-2} [d]
Synthesis of sucrose				
Glucosylation from Glc1P[3]	k_{cat} [s^{-1}]	39	9.8×10^{-3}	3.5×10^{-2}
	K_m [mM^{-1}]	4.7	0.4	18
	k_{cat}/K_m [s^{-1} mM^{-1}]	8.3	2.5×10^{-2}	1.9×10^{-3}
Deglucosylation by fructose[4]	k_{cat} [s^{-1}]	47	n.a.	n.a.
	K_m [mM^{-1}]	13	n.a.	n.a.
	k_{cat}/K_m [s^{-1} mM^{-1}]	3.7	(7.1×10^{-4})[e]	(1.3×10^{-2})[e]
	k_{catH}[5] [s^{-1}]	1.5	4.4×10^{-3}	3.4×10^{-3}
Phosphorolysis of Glc1F				
Glucosylation from Glc1F[6]	k_{cat} [s^{-1}]	121	n.a.	n.a.
	K_m [mM^{-1}]	22	n.a.	n.a.
	k_{cat}/K_m [s^{-1} mM^{-1}]	5.5	3.3×10^{-3}	4.3×10^{-3}

The S.D. for k_{cat} and k_{cat}/K_m was equal or smaller than 3.5% and 14% of the reported values, respectively, with the exception of [a]22%, [b]31%, [c]19%, [d]29%. [e]The values in parenthesis were calculated with the Haldane relationship, assuming a value of 9 for K_{eq_kin}.

[1] Sucrose was varied at 14 levels between 0.01 and 120 mM for the wild-type enzyme. For the mutants, sucrose was varied at 10 levels between 5 and 800 mM. Phosphate was constant at 50 mM.

[2] Phosphate concentration was varied at 17 levels between 0.01 and 140 mM for the wild-type enzyme. For the mutants, phosphate was varied at 11 levels between 1 and 250 mM. Sucrose was constant at 500 mM.

[3] Glc1P was varied at 12 levels between 0.5 and 250 mM for the wild-type enzyme. For F52A, Glc1P was varied at 10 levels between 0.01 and 10 mM. For F52N, Glc1P was varied at 16 levels between 0.01 and 250 mM. Fructose was constant at 100 mM.

[4] Fructose was varied at 12 levels between 1 and 200 mM. Glc1P was constant at 100 mM.

[5] Hydrolysis of Glc1P was determined under conditions when no fructose was present. Glc1P was used at 50 mM.

[6] Glc1F was varied at 14 levels between 0.1 and 250 mM for both wild-type enzyme and mutants. Phosphate was constant at 50 mM.

3.1. Kinetic consequences of substitution of Phe^{52} in LmSPase

Purified preparations of F52A and F52N showed specific activities for phosphorolysis of sucrose under standard assay conditions (50 mM of each sucrose and P_i) that were 221- (F52A) and 145-fold (F52N) below the wild-type level of 98 U/mg, suggesting that Phe^{52} has an important role for substrate binding and/or catalysis by LmSPase. Kinetic parameters of the two mutants were determined for each direction of enzymatic glucosyl transfer, and the results are shown in Table 1. The phosphorolysis rate of both F52A and F52N showed a linear dependence on the sucrose concentration up to a level of 800 mM, indicating that K_m for this substrate was dramatically increased in the mutants, substantially more than 80-fold (= 800/10) as compared to the K_m for the wild-type enzyme, and that it was raised to a value far outside of the experimental range. Expressed in k_{cat}/K_m terms, F52A was about 5200-fold and F52N was about 4000-fold less efficient than the wild-type enzyme.

Using P_i as varied substrate when the sucrose level was constant, the K_m value for P_i of both mutants was about 8-times higher than the wild-type K_m. The phosphorolysis rate of each mutant showed substrate inhibition by P_i, the corresponding inhibition constant K_{iS} being 66 mM for F52A and 87 mM for F52N. The catalytic efficiency of the two mutants was decreased about 330-fold as compared to k_{cat}/K_m (P_i) of the wild-type enzyme. The effect of substitution of Phe^{52} on kinetic parameters for the synthesis direction was interesting because it involved a large decrease in both k_{cat} and k_{cat}/K_m (Glc1P) relative to the corresponding parameters of wild-type LmSPase while at the same time the K_m for Glc1P was only moderately changed. We describe later why it was not possible to determine kinetic parameters of the two mutants for fructose.

3.2. Enzymatic phosphorolysis of Glc1F

Glc1F is a highly active glucosyl donor substrate for wild-type LmSPase [31]. It was examined here as alternative substrate for the phosphorolysis reaction catalyzed by the Phe^{52} mutants. Just like when sucrose was utilized as glucosyl donor, the phosphorolysis rate of F52A and F52N was linearly dependent on the Glc1F concentration. In terms of k_{cat}/K_m (Table 1), both mutants were about 1000-fold less active than the wild-type enzyme that employs Glc1F with an efficiency comparable to that for the reaction with sucrose. Glc1F differs from sucrose with respect to chemical nature and molecular size of the leaving group, fluoride in contrast with fructose. Because site-directed substitution of Phe^{52} had a similar disruptive effect of comparable magnitude on apparent binding of both donor substrates, it seems highly unlikely that loss of stabilizing interactions with the fructose moiety at subsite +1 accounts for the large increase in K_m for sucrose in F52A and F52N as compared to the corresponding K_m for wild-type enzyme.

3.3. Free energy profiles for reactions of wild-type and mutated enzymes

Interpretation of kinetic data for F52A and F25N is done on the basis of the Ping-pong bi-bi kinetic mechanism of wild-type LmSPase [31]. Therefore, k_{cat}/K_m for donor and acceptor substrate represents formation and breakdown of the glucosyl enzyme intermediate, respectively. Because limitation in acceptor substrate results in accumulation of a high steady-state concentration of glucosylated enzyme irrespective of the saturation level of donor substrate, k_{cat}/K_m of F52A and F52N for P_i are useful despite the very high K_m for sucrose. The ratio of k_{cat}/K_m for sucrose and fructose is the equilibrium constant of enzyme glucosylation from sucrose (K_{eq_glu}). The ratio of k_{cat}/K_m for P_i and Glc1P is the equilibrium constant for enzyme deglucosylation by P_i (K_{eq_deglu}). Data from Table 1 are used to calculate that in the reaction of the wild-type enzyme, K_{eq_glu} and K_{eq_deglu} have similar values of 3.24 and 2.89, respectively. The kinetic expression (Haldane relationship) for the overall equilibrium constant (K_{eq_kin}) is $K_{eq\_glu} \times K_{eq\_deglu}$ and has a value of 9. K_{eq_kin} is validated by useful agreement with an experimentally determined value of 10 for K_{eq_therm}. The discrepancy between this K_{eq_therm} and the K_{eq_therm} of 44 reported by us in an earlier paper [22] is brought to knowledge. The source of problem in determination of K_{eq_therm} in the previous study is not known.

Free energy profiles were constructed by applying kinetic data in Table 1 to Eqs. (2)–(4), and results are displayed in Fig. 2. Substitution of Phe^{52} caused a large destabilization of the transition state for enzyme glucosylation by sucrose ($\Delta\Delta G^{\#} \approx +5$ kcal/mol). This destabilization was uniform among the two mutants. The transition state for glucosylation by Glc1P was destabilized by +3.5 kcal/mol in F52A and even more so ($\approx$ +5 kcal/mol) in F52N. Interestingly, therefore, the stability of the covalent intermediate was not affected (F52A) or only slightly decreased (F52N; 1.6 kcal/mol) in the mutants as compared to wild-type enzyme. We are not aware of studies that have measured the thermodynamic stability of covalent reaction intermediates in glycoside hydrolases and transglycosidases of family GH-13. We therefore believe that Fig. 2 could be of a general interest in this respect. It is also worth pointing out that glucosylation of the wild-type enzyme by sucrose is thermodynamically favored whereas "reverse" glucosylation from Glc1P must proceed energetically uphill.

The results in Fig. 2 support the suggestion that stabilization by Phe^{52} is selective for the transition states of the reaction catalyzed by LmSPase. Cation-π interactions between the aromatic ring of the Phe and the glucopyranosyl oxocarbenium ion-like species that is thought to be formed in each transition state [31] are the probable source of this stabilization. Both the distance of about 4.6 Å between the interacting groups (Fig. 1) and the apparent amount of stabilization energy derived from the proposed interaction (Fig. 2) would be in useful agreement with literature on geometrical and energetic features of the cation-π interaction [32–35]. However, interpretation of kinetic consequences resulting from site-directed substitutions of Phe^{52} in terms of loss of local interaction energy must be made with caution. It is crucial to consider the possibility of a proximally disruptive effect of the Phe^{52} replacement, on interactions of the nearby Asp^{49} with the transferred

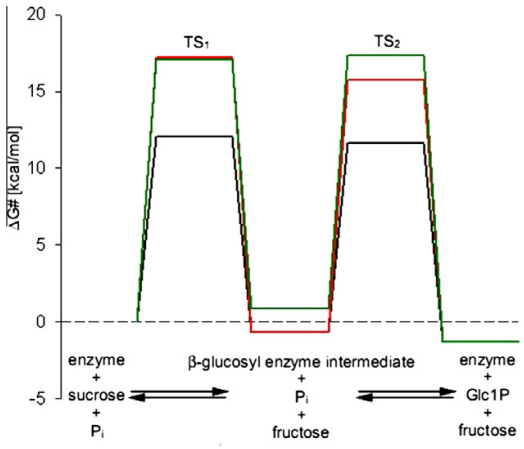

Fig. 2. Standard free energy profile for phosphorolysis of sucrose catalyzed by wild-type LmSPase (black), F52A (red), and F52N (green) at 30 °C and pH 7.0. TS, transition state.

glucosyl moiety (Fig. 1B), for example. However, crystallographic data for *Bifidobacterium adolescentis* SPase (BaSPase) [21,23] reveal that Phe^{52} and Asp^{49} (LmSPase numbering) as well as the entire loop containing the two residues are almost perfectly superimposed in a structural overlay of the catalytic subsites in free, sucrose-bound and glucosylated enzyme forms (Supplementary Fig. 3). The positions of Asp^{50} and Phe^{52} are further stabilized by a turn structure that involves residues 49–52 (Fig. 1B). We therefore believe that effects of substitution of Phe^{52} on catalytic function of LmSPase are predominantly due to a local structural disruption.

3.4. "Error hydrolysis" during glucosyl transfer to fructose

When F52A or F52N was assayed in direction of synthesis of sucrose, it was found that the initial rate of P_i release was hardly changed from "background level" (50 mM Glc1P, no fructose) upon the addition of fructose in concentrations ranging from 10 μM to 800 mM. We therefore used NMR and HPLC to analyze samples that were taken from a 72 h-long synthesis reaction (20 mM Glc1P, 100 mM fructose) catalyzed by the two mutants. Despite substantial conversion of Glc1P (F52A: 85%; F52N: 66%), sucrose was produced in very low amounts (F52A: 1.5 mM; F52N: 4.5 mM). The analysis also revealed that donor substrate utilization by the two mutants was mainly via hydrolysis. Luley-Goedl and Nidetzky [36] have determined a partition coefficient of 36.4 M^{-1} for reaction of the β-glucosyl enzyme intermediate of wild-type LmSPase with fructose and water. Observations for F52A and F52N imply that the analogous partition coefficient for the mutants must have been decreased dramatically as result of substitution of Phe^{52}. Using data in Table 1 we can apply the Haldane relationship, $K_{eq\_glu} \times K_{eq\_deglu} = K_{eq\_therm}$, to estimate that k_{cat}/K_m for fructose is on the order of 7×10^{-4} $mM^{-1}s^{-1}$ (F52A) and 1×10^{-2} $mM^{-1}s^{-1}$ (F52N). When we now calculate the ratio of k_{cat}/K_m (fructose) and the k_{cat} for hydrolysis of Glc1P (k_{catH}, Table 1), partition coefficients of 161 M^{-1} and 3800 M^{-1} are obtained for F52A and F52N, respectively. The analogously calculated partition coefficient for the wild-type enzyme is 2467 M^{-1}, differing from the experimentally determined partition coefficient [36] by almost two orders of magnitude. A tentative explanation for this discrepancy is that hydrolysis of glucosylated LmSPase can take place from a complex of the enzyme intermediate and fructose, and this hydrolysis is substantially ($\geqslant 10^2$-fold) faster than hydrolysis of the intermediate under conditions when no fructose is present (k_{catH}). Note: fructose could bind to glucosylated LmSPase in several of its different conformations (e.g. α/β-furanose; α/β-pyranose) in aqueous solution. It is speculative but certainly possible that enzyme complexes with fructose unable to form sucrose might show enhanced tendency towards hydrolysis. The change in enzyme selectivity for reaction with fructose as compared to reaction with water that results from substitution of Phe^{52} and is clearly observable in the synthesis experiments described above would thus be determined by altered reactivity of the complex between glucosylated enzyme and fructose for undergoing conversion via transfer to acceptor or hydrolysis. It would *not* be determined by competition between mutually exclusive nucleophiles, that is, fructose and water, for binding to the enzyme intermediate.

We also examined if hydrolysis was a relevant side reaction during phosphorolysis of sucrose by the two mutants. However, like wild-type LmSPase, both F52A and F52N did not produce glucose within limits of error as long as P_i was present in the reaction mixture. Therefore, these findings imply that substitution of Phe^{52} was selective in opening up competition from reaction with water during enzyme deglucosylation to fructose as compared to enzyme deglucosylation to P_i. Aromatic interactions from Phe^{52} appear to be required for precise positioning of the transferred glucosyl moiety such that productive nucleophile attack from fructose can take place and "error hydrolysis" is suppressed effectively. Reaction with P_i may not be dependent on similar positioning effects from Phe^{52} or the binding of P_i could prevent nucleophilic water from entering the active site.

4. Conclusions

Aromatic interactions from Phe^{52} in the catalytic subsite of LmSPase facilitate enzymatic catalysis of reversible phosphorolysis of sucrose in two different ways. Each of the two oxocarbenium ion-like transition states leading to and from the β-glucosyl enzyme intermediate appears to recruit a large amount of stabilization from cation-π interaction with Phe^{52}. Making the error of reacting with water instead of reacting with fructose becomes strongly favored upon replacement of Phe^{52}. We therefore suggest that uncharged π interaction with the β-glucosyl moiety of the covalent enzyme intermediate contribute to precise positioning of the transferred glucosyl residue relative to fructose acceptor, thereby reducing possible interception from water. There is a high degree of conservation for the aromatic motif at the subsites −1 of various glycoside hydrolases and transglycosidases of family GH-13 (Fig. 1). Stabilization of oxocarbenium ion-like transition states by cation-π interactions could therefore be a common theme of catalysis by the members of this family. Several other enzymes [10,37–41], among them glycosyltransferases [8,10] that show significant mechanistic analogy to glycoside hydrolases [42], have been proposed to stabilize (partial) positive charges in intermediates or transition states of their reaction, by up to 4 kcal/mol [37], with the help of π bonding interactions.

Acknowledgements

Financial support from the Austrian Science Funds FWF (Project L586-B03 to B.N.) is gratefully acknowledged. Prof. Lothar Brecker (Institute of Organic Chemistry, University of Vienna) is thanked for NMR analysis.

Appendix A. Supplementary data

Supplementary data associated with this article can be found, in the online version, at doi:10.1016/j.febslet.2010.12.041.

References

[1] Quiocho, F.A. (1986) Carbohydrate-binding proteins: tertiary structures and protein-sugar interactions. Annu. Rev. Biochem. 55, 287–315.
[2] Ramirez-Gualito, K., Alonso-Rios, R., Quiroz-Garcia, B., Rojas-Aguilar, A., Diaz, D., Jimenez-Barbero, J. and Cuevas, G. (2009) Enthalpic nature of the CH/π interaction involved in the recognition of carbohydrates by aromatic compounds, confirmed by a novel interplay of NMR, calorimetry, and theoretical calculations. J. Am. Chem. Soc. 131, 18129–18138.
[3] Diaz, M.D., Fernandez-Alonso, M.D., Cuevas, G., Canada, F.J. and Jimenez-Barbero, J. (2008) On the role of aromatic-sugar interactions in the molecular recognition of carbohydrates: a 3D view by using NMR. Pure Appl. Chem. 80, 1827–1835.
[4] Sujatha, M.S., Sasidhar, Y.U. and Balaji, P.V. (2005) Insights into the role of the aromatic residue in galactose-binding sites: MP2/6–311G++** study on galactose- and glucose-aromatic residue analogue complexes. Biochemistry 44, 8554–8562.
[5] Laughrey, Z.R., Kiehna, S.E., Riemen, A.J. and Waters, M.L. (2008) Carbohydrate-π interactions: what are they worth? J. Am. Chem. Soc. 130, 14625–14633.
[6] Muraki, M., Harata, K., Sugita, N. and Sato, K.I. (2000) Protein-carbohydrate interactions in human lysozyme probed by combining site-directed mutagenesis and affinity labeling. Biochemistry 39, 292–299.
[7] Spiwok, V., Lipovova, P., Skalova, T., Buchtelova, E., Hasek, J. and Kralova, B. (2004) Role of CH/π interactions in substrate binding by *Escherichia coli* β-galactosidase. Carbohydr. Res. 339, 2275–2280.
[8] Zhang, Y.N., Deshpande, A., Xie, Z.H., Natesh, R., Acharya, K.R. and Brew, K. (2004) Roles of active site tryptophans in substrate binding and catalysis by α-1, 3 galactosyltransferase. Glycobiology 14, 1295–1302.
[9] Ravaud, S., Robert, X., Watzlawick, H., Haser, R., Mattes, R. and Aghajari, N. (2007) Trehalulose synthase native and carbohydrate complexed structures provide insights into sucrose isomerization. J. Biol. Chem. 282, 28126–28136.

[10] Heroux, A., White, E.L., Ross, L.J., Kuzin, A.P. and Borhani, D.W. (2000) Substrate deformation in a hypoxanthine–guanine phosphoribosyltransferase ternary complex: the structural basis for catalysis. Structure 8, 1309–1318.
[11] Hashimoto, H. (2006) Recent structural studies of carbohydrate-binding modules. Cell. Mol. Life Sci. 63, 2954–2967.
[12] Boraston, A.B., Bolam, D.N., Gilbert, H.J. and Davies, G.J. (2004) Carbohydrate-binding modules: fine-tuning polysaccharide recognition. Biochem. J. 382, 769–781.
[13] Nerinckx, W., Desmet, T. and Claeyssens, M. (2003) A hydrophobic platform as a mechanistically relevant transition state stabilising factor appears to be present in the active centre of all glycoside hydrolases. FEBS Lett. 538, 1–7.
[14] Stam, M.R., Danchin, E.G., Rancurel, C., Coutinho, P.M. and Henrissat, B. (2006) Dividing the large glycoside hydrolase family 13 into subfamilies: towards improved functional annotations of α-amylase-related proteins. Protein Eng. Des. Sel. 19, 555–562.
[15] Mirza, O., Skov, L.K., Remaud-Simeon, M., Potocki de Montalk, G., Albenne, C., Monsan, P. and Gajhede, M. (2001) Crystal structures of amylosucrase from *Neisseria polysaccharea* in complex with D-glucose and the active site mutant Glu328Gln in complex with the natural substrate sucrose. Biochemistry 40, 9032–9039.
[16] Kim, M.I., Kim, H.S., Jung, J. and Rhee, S. (2008) Crystal structures and mutagenesis of sucrose hydrolase from *Xanthomonas axonopodis pv Glycines*: insight into the exclusively hydrolytic amylosucrase fold. J. Mol. Biol. 380, 636–647.
[17] Shirai, T., Hung, V.S., Morinaka, K., Kobayashi, T. and Ito, S. (2008) Crystal structure of GH13 α-glucosidase GSJ from one of the deepest sea bacteria. Proteins Struct. Funct. Bioinf. 73, 126–133.
[18] Zhang, D., Li, N., Lok, S.M., Zhang, L.H. and Swaminathan, K. (2003) Isomaltulose synthase (*PalI*) of *Klebsiella sp. LX3*. Crystal structure and implication of mechanism. J. Biol. Chem. 278, 35428–35434.
[19] Klein, C. and Schulz, G.E. (1991) Structure of cyclodextrin glycosyltransferase refined at 2.0 Å resolution. J. Mol. Biol 217, 737–750.
[20] Machius, M., Wiegand, G. and Huber, R. (1995) Crystal structure of calcium-depleted *Bacillus licheniformis* α-amylase at 2.2 Å resolution. J. Mol. Biol. 246, 545–559.
[21] Sprogoe, D., van den Broek, L.A., Mirza, O., Kastrup, J.S., Voragen, A.G., Gajhede, M. and Skov, L.K. (2004) Crystal structure of sucrose phosphorylase from *Bifidobacterium adolescentis*. Biochemistry 43, 1156–1162.
[22] Goedl, C., Schwarz, A., Minani, A. and Nidetzky, B. (2007) Recombinant sucrose phosphorylase from *Leuconostoc mesenteroides*: characterization, kinetic studies of transglucosylation, and application of immobilised enzyme for production of α-D-glucose 1-phosphate. J. Biotechnol. 129, 77–86.
[23] Mirza, O., Skov, L.K., Sprogoe, D., van den Broek, L.A., Beldman, G., Kastrup, J.S. and Gajhede, M. (2006) Structural rearrangements of sucrose phosphorylase from *Bifidobacterium adolescentis* during sucrose conversion. J. Biol. Chem. 281, 35576–35584.
[24] Jensen, M.H., Mirza, O., Albenne, C., Remaud-Simeon, M., Monsan, P., Gajhede, M. and Skov, L.K. (2004) Crystal structure of the covalent intermediate of amylosucrase from *Neisseria polysaccharea*. Biochemistry 43, 3104–31010.
[25] Zhang, R., Li, C., Williams, L.K., Rempel, B.P., Brayer, G.D. and Withers, S.G. (2009) Directed "in situ" inhibitor elongation as a strategy to structurally characterize the covalent glycosyl-enzyme intermediate of human pancreatic α-amylase. Biochemistry 48, 10752–10764.
[26] Uitdehaag, J.C., Mosi, R., Kalk, K.H., van der Veen, B.A., Dijkhuizen, L., Withers, S.G. and Dijkstra, B.W. (1999) X-ray structures along the reaction pathway of cyclodextrin glycosyltransferase elucidate catalysis in the α-amylase family. Nat. Struct. Biol. 6, 432–436.
[27] Schwarz, A. and Nidetzky, B. (2006) Asp-196 → Ala mutant of *Leuconostoc mesenteroides* sucrose phosphorylase exhibits altered stereochemical course and kinetic mechanism of glucosyl transfer to and from phosphate. FEBS Lett. 580, 3905–3910.
[28] Wang, W. and Malcolm, B.A. (1999) Two-stage PCR protocol allowing introduction of multiple mutations, deletions and insertions using QuikChange Site-Directed Mutagenesis. Biotechniques 26, 680–682.
[29] Goedl, C., Sawangwan, T., Mueller, M., Schwarz, A. and Nidetzky, B. (2008) A high-yielding biocatalytic process for the production of 2-*O*-(α-D-glucopyranosyl)-*sn*-glycerol, a natural osmolyte and useful moisturizing ingredient. Angew. Chem. Int. Ed. 47, 10086–10089.
[30] Schwarz, A., Brecker, L. and Nidetzky, B. (2007) Acid-base catalysis in *Leuconostoc mesenteroides* sucrose phosphorylase probed by site-directed mutagenesis and detailed kinetic comparison of wild-type and Glu237 → Gln mutant enzymes. Biochem. J. 403, 441–449.
[31] Goedl, C. and Nidetzky, B. (2009) Sucrose phosphorylase harbouring a redesigned, glycosyltransferase-like active site exhibits retaining glucosyl transfer in the absence of a covalent intermediate. ChemBioChem 10, 2333–2337.
[32] Prajapati, R.S., Sirajuddin, M., Durani, V., Sreeramulu, S. and Varadarajan, R. (2006) Contribution of cation-π interactions to protein stability. Biochemistry 45, 15000–15010.
[33] Gallivan, J.P. and Dougherty, D.A. (1999) Cation-π interactions in structural biology. Proc. Natl. Acad. Sci. U.S.A. 96, 9459–9464.
[34] Ma, J.C. and Dougherty, D.A. (1997) The cation-π interaction. Chem. Rev. 97, 1303–1324.
[35] Poliakov, E., Gentleman, S., Chander, P., Cunningham Jr., F.X., Grigorenko, B.L., Nemuhin, A.V. and Redmond, T.M. (2009) Biochemical evidence for the tyrosine involvement in cationic intermediate stabilization in mouse ß-carotene 15, 15′-monooxygenase. BMC Biochem. 10, 31.
[36] Luley-Goedl, C. and Nidetzky, B. (2010) Small-molecule glucosylation by sucrose phosphorylase: structure-activity relationships for acceptor substrates revisited. Carbohydr. Res. 345, 1492–1496.
[37] Iismaa, S.E., Holman, S., Wouters, M.A., Lorand, L., Graham, R.M. and Husain, A. (2003) Evolutionary specialization of a tryptophan indole group for transition-state stabilization by eukaryotic transglutaminases. Proc. Natl. Acad. Sci. USA 100, 12636–12641.
[38] Zacharias, N. and Dougherty, D.A. (2002) Cation-π interactions in ligand recognition and catalysis. Trends Pharmacol. Sci. 23, 281–287.
[39] Barrett, J.E., Lucero, C.M. and Schultz, P.G. (1999) A model for hydride transfer in thymidylate synthase based on unnatural amino acid mutagenesis. J. Am. Chem. Soc. 121, 7965–7966.
[40] Ogura, K. and Koyama, T. (1998) Enzymatic aspects of isoprenoid chain elongation. Chem. Rev. 98, 1263–1276.
[41] Soderberg, T. and Poulter, C.D. (2001) *Escherichia coli* dimethylallyl diphosphate:tRNA dimethylallyltransferase: site-directed mutagenesis of highly conserved residues. Biochemistry 40, 1734–1740.
[42] Lairson, L.L. and Withers, S.G. (2004) Mechanistic analogies amongst carbohydrate modifying enzymes. Chem. Commun., 2243–2248.

SUPPLEMENTARY INFORMATION FOR

Aromatic interactions at the catalytic subsite of sucrose phosphorylase: Their roles in enzymatic glucosyl transfer probed with Phe^{52} → Ala and Phe^{52} → Asn mutants

Patricia Wildberger, Christiane Luley-Goedl and Bernd Nidetzky*

Institute of Biotechnology and Biochemical Engineering, Graz University of Technology, Petersgasse 12/1, A-8010 Graz, Austria

*Corresponding author
E-mail: bernd.nidetzky@tugraz.at; Tel. +43-316-873-8400; Fax +43-316-873-8434

S1 Site-directed mutagenesis, production and purification of enzymes

A pair of complementary oligonucleotide primers, each introducing the desired site-directed substitution at the protein level, was used. The mismatched bases are underlined.

F52A forward: 5′-GGTGATCGCGGTGCTGCGCCAGC-3′
F52A reverse: 5′-GCTGGCGCAGCACCGCGATCACC-3′
F52N forward: 5′-GGTGATCGCGGTAATGCGCCAGC-3′
F52N reverse: 5′-GCTGGCGCATTACCGCGATCACC-3′

The two-stage protocol involved in the first step, two separate PCR reactions with the forward and reverse primer. These reactions consisted of a preheating step at 95°C for 60 s followed by 4 reaction cycles (95°C, 50 s/60°C, 50 s/72°C, 10 min). In the second step, PCR reactions were combined and continued for 18 reaction cycles (95°C, 50 s/60°C, 50 s/72°C, 10 min). The amplification product was subjected to parental template digest by *Dpn*I and transformed into electro-competent *E. coli* Top10 cells. Mini-prep plasmid DNA was sequenced in order to verify the introduction of the desired substitutions. Isolated pQE30 vectors harboring genes for wild-type and mutated LmSPase were digested using Fast Digest restriction enzymes *BamH*I and *Pst*I (Promega, Madison, USA). The genes excized in that way were ligated into dephosphorylated pASK-IBA7+ expression vector (IBA, Göttingen, Germany) using a T4-DNA ligase (Promega, Madison, USA). Sequencing in sense and antisense directions was used to confirm the resulting inserts.

E. coli Top10 cells harboring one of the pASK-IBA7+ expression vectors were cultivated in 1-L baffeled shaken flasks at 37°C and 110 rpm using LB-media and 115 mg/L ampicillin. When OD_{550} reached 0.5-0.6, temperature was decreased to 25°C and gene expression was induced with 200 μg/L anhydrotetracycline for 6 h. Cells were harvested by centrifugation at 4°C and 5,000 rpm for 30 min in a Sorvall RC-5B Refrigerated Superspeed centrifuge. Resuspended cells were frozen at -20°C, thawed and the suspension was passed twice through a French pressure cell press (American Instruments, Silver Springs, USA) at 150 bar. Cell debris was removed by centrifugation at 4°C, 14,000 rpm for 45 min. The resulting supernatant was used for further enzyme purification.

S2 Enzyme purification

Protein purification was done at 6°C using a Bio-Rad Duoflow system. Elution of proteins was monitored automatically at 280 nm. All buffers were degassed and filtered using 0.45 μm cellulose-acetate and 0.2 μm Sartolon polyamide filters. The crude cell extract was passed through an 1.2 μm cellulose-

acetate filter (Sartorius) before loading on a *Strep*-Tactin Superflow column (binding capacity 100 nmol/mL; bed volume 5 mL). Note that *Strep*-tagged LmSPase has a molecular weight of 59 kDa, which results in a loading capacity of 30 mg. Results of a typical chromatography are shown in Supplementary Figure 1.

S3 NMR spectroscopic analysis

Reaction mixtures contained F52A or F52N (0.4 mg/mL), 20 mM glucose 1-phosphate and 100 mM fructose in 50 mM MES buffer (pH 7.0) and were incubated at 30°C for 72 h. Samples were lyophilized, dissolved in D_2O (99.95%, 0.7 mL) and used for NMR spectroscopic data recording without further purification. Samples were transferred into 5 mm high precision NMR sample tubes (Promochem, Wesel, Germany). All spectra were recorded on a Bruker DRX-400 AVANCE spectrometer (Bruker, Rheinstetten, Germany) at 300K and 400.13 MHz (^{1}H), 100.61 MHz (^{13}C) or 161.98 MHz (^{31}P) using the Bruker Topspin 1.3 software. For 1D-spectra, 32k data points were acquired using a relaxation delay of 1.0 s and an appropriate number of scans for reasonable signal to noise ratios. After zero filling to 64k data points and Fourier transformation, spectra with a range of 7,200 Hz (^{1}H), 20,000 Hz (^{13}C) and 16,200 Hz (^{31}P) were obtained, respectively. To determine the 2D COSY, TOCSY, NOESY, HMQC, and HMBC as well as ^{1}H/^{31}P-HMQC spectra, 128 experiments with 8 scans and 1024 data points each were performed. After linear forward prediction to 256 data points in the f_2-dimension and appropriate sinusoidal multiplication in both dimensions, the data were Fourier transformed in order to obtain 2D-spectra with ranges of 4,000 Hz (^{1}H), 20,000 Hz (^{13}C) and 8,100 Hz (^{31}P). Chemical proton and carbon shifts were referenced to external acetone (^{1}H: δ_H 2.225 ppm; ^{13}C: δ_C 31.45 ppm) and phosphorus shifts were referenced to external aqueous 85% phosphoric acid (^{31}P: δ_P 0.00 ppm).

S4 HPLC

The same reaction mixtures described above (S3 NMR spectroscopic analysis) were analyzed by HPLC. This was performed on a Shimadzu CTO-20AC system equipped with an Aminex HPX-87C column (Bio-Rad, Vienna, Austria) that was operated at 75°C. Water was the mobile phase and was applied at a constant flow rate of 0.6 mL/min. Refractive index detection (Shimadzu RID-10A) was used for all compounds. Under the conditions applied, the following retention times were obtained: 7.7 min for sucrose, 9.7 min for glucose, 12.3 min for fructose and 6.2 min for glucose 1-phosphate.

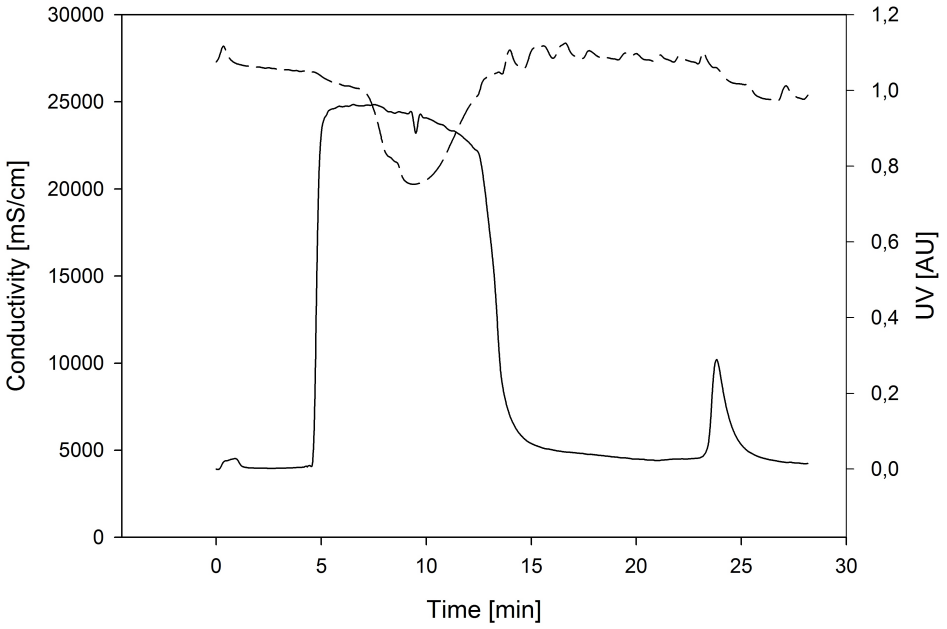

Supplementary Figure S1. Typical chromatogram for all enzymes isolated. Chromatogram recorded during purification of F52N by *Strep*-Tactin affinity chromatography. The column was equilibrated with buffer W (100 mM Tris/HCl, 150 mM NaCl, 1 mM EDTA, pH 8.0) at a flow rate of 3 mL/min (5 column volumes). The crude cell extract was applied (2.5-12.5 min) at a flow rate of 1 mL/min. After washing with buffer W (12.5-20.5 min) at a flow rate of 2 mL/min (5 column volumes), fractions containing the enzyme (59-kDa band in SDS-PAGE) were eluted (20.5-28 min) with buffer E (100 mM Tris/HCl, 150 mM NaCl, 1 mM EDTA, 2.5 mM desthiobiotin, pH 8.0) at a flow rate of 2 mL/min (3 column volumes). Pooled fractions were concentrated and desalted using a HiPrep 26/10 desalting column (Amersham Biosciences, Uppsala, Sweden), and again concentrated to about 2-5 mg/mL in 50 mM MES buffer, pH 7.0. Stock solutions of wild-type and mutants were stored at -20°C. The yield of pure protein from one liter culture was about 6 mg.

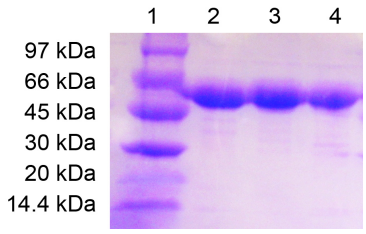

Supplementary Figure S2. Purification monitored by SDS-PAGE. Lane 1: molecular mass standard; 2: purified wild-type LmSPase; 3: purified F52A; 4: purified F52N.

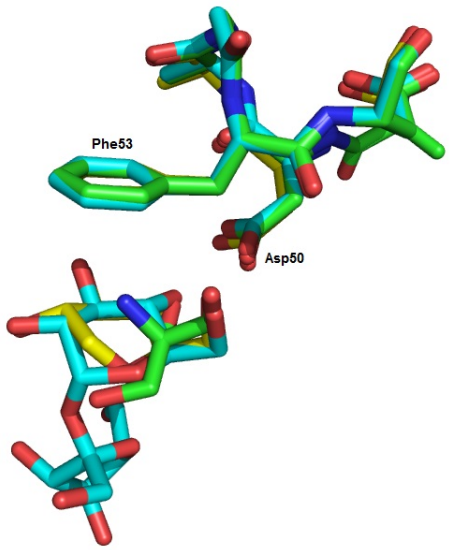

Supplementary Figure S3. Structural overlay of the catalytic subsites in free (green), sucrose bound (blue) and glucosylated (yellow) SPase from *Bifidobacterium adolescentis*.

4 Construction of active-site mutants of sucrose phosphorylase to investigate the interplay between aromatic interactions from Phe^{52} and the residues of the catalytic triad

Patricia Wildberger and Bernd Nidetzky*

Institute of Biotechnology and Biochemical Engineering, Graz University of Technology, Petersgasse 12/1, A-8010 Graz, Austria

*Corresponding author

E-mail: bernd.nidetzky@tugraz.at; Tel. +43-316-873-8400; Fax +43-316-873-8434

Abstract

Sucrose phosphorylase catalyzes the reversible reaction of sucrose and phosphate to glucose 1-phosphate and fructose. The reaction proceeds via a double displacement-like reaction mechanism that involves formation and breakdown of a β-glucosyl enzyme intermediate. Three active-site residues constitute the catalytic triad, acting as nucleophile (Asp196), acid-base catalyst (Glu237) and transition state stabilizer (Asp295). An aromatic amino acid residue, Phe52, is situated at the B-face of the glucopyranosyl ring of the donor substrate bound at the catalytic subsite. Phe52 is proposed to facilitate the reaction by stabilizing the oxocarbenium ion-like transition states flanking the β-glucosyl enzyme intermediate. To investigate the interplay between the aromatic side chain of Phe52 and the residues of the catalytic triad on substrate binding and/or catalysis, three double mutants, F52A-D196A, F52A-E237A and F52A-D295A, were designed and subjected to a detailed kinetic characterization. Double mutants, in which Phe52 and Asp196 or Glu237, respectively, were substituted by Ala resulted in non-active mutants. Interpretation of the data for the F52A-D295A mutant revealed drastic changes compared to the kinetic pattern of LmSPase. In particular, the catalytic efficiency for glucosylation from glucose 1-phosphate was strongly affected. Based on these findings docking studies were performed to thoroughly investigate the accommodation of glucose 1-phosphate in the active-site of LmSPase and the corresponding mutants. The structural investigations provided an unexpected opportunity to gain insight on binding of glucose 1-phosphate and revealed how important the conformation of glucose 1-phosphate may be for catalysis.

INTRODUCTION

Molecular interactions between proteins and carbohydrates are critical in many physiological and pathological processes (1), including protein trafficking, cell adhesion, fertilization, infection and different aspects of the immune response (2). However, although of great biological relevance the general understanding of these protein-carbohydrate interactions is still limited (3). Therefore, great effort takes currently place to contribute to a better understanding of protein-carbohydrate interactions and to elucidate the mechanisms underlying carbohydrate recognition in the binding sites of the receptor proteins (1, 2, 4, 5).

Recognition of saccharides by proteins is mainly achieved via hydrogen-bonding interactions, however, noncovalent interactions mediated from aromatic rings were found to be pivotal too (2). A rich source for investigating aromatic-carbohydrate interactions are carbohydrate-active enzymes, in particular glycoside hydrolases and glycosyltransferases (6), which use carbohydrate-aromatic interactions to achieve recognition and specificity for their natural substrates. Selective binding of carbohydrates to aromatic residues is mainly accomplished via CH-π interactions, in which the aromatic ring of phenylalanine, tyrosine or tryptophan can stack with the planar face of the carbohydrate ring (2). Next to this conformational stabilization mediated by CH-π interactions, aromatic residues can provide electrostatic stabilization of the transition states of the reaction. The proposed source of the electrostatic stabilization is a cation-π interaction, an interaction between aromatic amino acid residues and partial positive charges of intermediates or transition states (7).

Sucrose phosphorylase from *Leuconostoc mesenteroides* (LmSPase, EC 2.4.1.7) (8), a representative of the glycoside hydrolase family 13 (GH-13), contains an aromatic motif, Phe52, which is positioned at the B-face of the glucopyranosyl ring bound in the catalytic subsite. In a former study, we evaluated the role of this aromatic motif and analyzed its contribution on ligand binding as well as on catalysis (9). Therefore, we substituted Phe52 to Ala and Asn, respectively. The corresponding mutants, F52A and F52N, were characterized by free energy profile analysis. Interpretation of the free energy profile was done on the basis of the Ping-pong bi-bi kinetic mechanism of wild-type LmSPase (10). α-D-Glucopyranosyl 1-phosphate and D-fructose are converted reversibly into sucrose (α-D-glucopyranosyl-1,2-β-D-fructofuranoside) and phosphate (Scheme 1). In the first step (enzyme glucosylation), the glucosyl moiety of sucrose (phosphorolysis) or glucose 1-phosphate (synthesis), respectively, is transferred to Asp196, thereby forming the β-glucosyl enzyme intermediate. In the second step (enzyme deglucosylation), the glucosyl moiety is transferred from the β-glucosyl enzyme intermediate to fructose (synthesis) or phosphate (phosphorolysis), respectively (8). Both steps proceed through an oxocarbenium-ion like transition state. The aromatic interactions from Phe were found to facilitate enzymatic catalysis

of reversible phosphorolysis of sucrose through (1) positioning of the transferred glucosyl moiety at the catalytic subsite and (2) strong cation-π stabilization of the oxocarbenium ion-like transition states flanking the covalent enzyme intermediate. The amount of stabilization of the oxocarbenium ion-like transition states from cation-π interactions with Phe52 was found to be 5.0 kcal/mol for enzyme glucosylation by sucrose and 3.5 kcal/mol for glucosylation by glucose 1-phosphate (9). The observation that Phe52 is selective for transition state stabilization may be a common theme of catalysis by the GH-13 family members, as the presence of an aromatic amino acid residue at the subsite -1 is not just a characteristic in LmSPase but present in various members of the GH-13 family (Supplementary Figure S1). To expand our understanding on aromatic-carbohydrate interactions, we further investigated the role of Phe52, in particular we examined the influence of Phe52 on the functionality of the catalytic triad. The residues representing the catalytic triad were identified in former studies as the nucleophile (Asp196) (11), the acid-base catalyst (Glu232) (12) and the transition state stabilizer (Asp295) (13). To examine whether the known properties of these active-site residues are affected by the substitution of Phe52, we substituted the corresponding residues and generated three doubly mutated enzymes, F52A-D196A, F52A-E237A and F52A-D295A. Proper folding at the secondary structural level was ensured after extensive rebuilding of the active-site in the doubly mutated enzymes, before a detailed kinetic analysis followed.

RESULTS AND DISCUSSION

Protein production, folding and characterization

Asp196, Glu232 and Asp295 were unambiguously identified as nucleophile, acid-base catalyst and transition state stabilizer in former studies (11-13). To examine whether their known properties are affected by the substitution of Phe52, we have performed site-directed mutagenesis of the three residues on the F52A (9) template to generate the three doubly mutated enzymes, F52A-D196A, F52A-E237A and F52A-D295A. *Strep*-tagged phosphorylases were purified to apparent electrophoretic homogeneity in a two step-purification procedure (Supplementary Figure S2). The second purification step was introduced after we noted the problem of co-purification of phosphatase activities in some batches after the single *Strep*-tag purification. The phosphatase hydrolyzed glucose 1-phosphate into glucose and phosphate. This activity was completely absent in samples purified via the two-step purification procedure.

Correct folding of purified LmSPase and mutants was ensured by circular dichroism (CD) spectroscopy. Far-UV spectra of the purified mutated enzymes were super-imposable on the corresponding spectrum of LmSPase. The relative proportions of secondary structural elements between LmSPase and mutants were conserved (Table 1) and agreed with the anticipated data observed in the crystal structure of LmSPase, which characterizes LmSPase by a mixed α-β composition, whereas the amount of α-helices (37%) slightly exceeds the amounts of β-sheets (20%) (14, 15).

The specific activities of purified preparations of LmSPase and mutants were evaluated in the standard assay of phosphorolysis of sucrose (8). As expected, the introduction of the second purification step went along with an increase in specific activity. In LmSPase, the additional purification step resulted in an enhancement of specific activity by around 14% to 114 U/mg. This increase was uniform in F52A, which specific activity was around 200-fold (0.6 U/mg) decreased compared to LmSPase. The additional substitution of the transition state stabilizer (F52A-D295A) decreased the specific activity by around 1.6-fold (0.4 U/mg) compared to F52A and by around 300-fold compared to LmSPase. The site-directed replacement of the nucleophile (F52A-D196A) and acid-base catalyst (F52A-E237A) resulted in mutants not active within limits of detection of the used assay which corresponds to $\geq$ 0.0004% of the activity of LmSPase.

Enzyme-ligand interactions in LmSPase and mutants

We start by presenting some structural investigations, performed to support the subsequent kinetic interpretations. Based on the crystal structure of the closely related sucrose phosphorylase from *Bifidobacterium adolescentis* (BaSPase; PDB entry 2gdu) (14), homology models of LmSPase and mutants

were prepared. Subsequently, the deprotonated form of glucose 1-phosphate was docked into the active-site of LmSPase and mutants (Figure 1). Several binding modes with comparable energies were obtained for each enzyme. The selection of the chosen binding mode was done on the basis of best structural alignment between the glucopyranosyl ring of the docked glucose 1-phosphate and the glucopyranosyl ring of sucrose, the ligand which was co-crystallized in the structure of BaSPase. The approach for selecting the binding mode on basis of structural alignment was verified by the STD-NMR measurements performed with glucose 1-phosphate as ligand and LmSPase and mutants as receptors. Figure 2 shows the results of the STD-NMR measurements, which were performed to identify the ligand-binding epitopes of glucose 1-phosphate when bound to LmSPase and mutants. The protons of glucose 1-phosphate, which are in close contact to the receptor, receive a higher degree of saturation via the protein resulting in the observation of stronger STD-NMR signals compared with ligand protons that do not interact with the protein surface. The STD-NMR pattern resulting from the binding of glucose 1-phosphate to LmSPase was then compared to the corresponding binding pattern of glucose 1-phosphate to the mutants. Overall, the binding behavior of glucose 1-phosphate to LmSPase (Figure 2B) was very comparable of glucose 1-phosphate binding to F52A (Figure 2C), F52A-E237A (Figure 2D) and F52A-D295A (Figure 2E); a significant different pattern was just observed when F52A-D196A was employed as ligand (Figure 2F).

In LmSPase, the reactive group arrangement relative to glucose 1-phosphate seems to be optimal for catalysis (Figure 1A). Glucose 1-phosphate is positioned such that the nucleophilic attack by Asp196 on the anomeric carbon of the glucosyl moiety (distance 3.2 Å) is highly plausible. Furthermore, the binding of glucose 1-phosphate is supported by hydrogen bonding interactions from the carboxylate side chain of Asp295 to the hydroxyl groups at C2 (distance 2.8 Å) and C3 (distance 3.2 Å) of the glucosyl residue. Interestingly, the phosphate of glucose 1-phosphate is positioned in a "tucked-under" conformation on the A-face of the glucopyranosyl moiety, thereby enabling an interaction between the phosphate group and the C2-OH of glucose 1-phosphate (distance 2.7 Å). Such a conformation is proposed to provide some ground-state destabilization and to assist the acid/base catalysis of glycosyl transfer (16). The finding of this relatively unusual disposition in LmSPase is surprising, as it hints structural parallels to several retaining GTs (α-galactosyltransferase LgtC and glucosyltransferase OtsA) (17, 18) and retaining glycosidases classified as GTs (glycogen phosphorylase, maltodextrin phosphorylase) (19, 20), in which crystal structures the "tucked-under" conformation of the phosphate moiety was already observed. The phosphate group of glucose 1-phosphate also interacts with the side chain of Arg137, which presumably neutralizes the negative charge that develops during catalysis.

In a previous study Phe52 was substituted by Ala. As this mutant served as template for the introduc-

tion of the substitutions of the residues from the catalytic triad, we investigated the binding of glucose 1-phosphate in F52A (Figure 1C). Consistent with the in the former study obtained K_m values for glucose 1-phosphate (4.7 mM for LmSPase and 0.4 mM for F52A) (9), which reflected no drastic changes in substrate binding, the conformation and the binding pattern of glucose 1-phosphate in LmSPase was very similar compared with F52A.

Note: Glucose 1-phosphate has a pK of 6.13. All reactions for the kinetic characterizations were performed at pH 7.0. The corresponding docking studies were accordingly performed with the dianion of glucose 1-phosphate as ligand. In addition, a separate docking study was performed in which glucose 1-hydrogenphosphate was employed as ligand (see Supplementary Figure S3). With exception for F52A-E237A, all other docking studies resulted in the same outcome irrespective if the deprotonated form of glucose 1-phosphate or glucose 1-hydrogenphosphate was used.

In addition to glucose 1-phosphate as traditional substrate for LmSPase, a phosphono analogue of glucose 1-phosphate, in which the glycosidic oxygen atom was substituted by a carbon atom, was used as ligand in STD-NMR measurements, molecular docking studies and kinetic characterizations. The STD-NMR measurement employing the glucose 1-phosphate analogue as ligand and LmSPase as receptor did not result in any STD-effects, which means that either the ligand inhibits LmSPase or does not bind to the active-site. Subsequently, the hydrolytic activity of LmSPase towards glucose 1-phosphate and the phosphono analogue of glucose 1-phosphate (both present in a concentration of 5 mM) was tested and compared to the hydrolytic activity of LmSPase towards glucose 1-phosphate without supplement. The k_{cat} for both reactions was determined as 1.1 s^{-1}, thereby supporting the hypothesis that the glucose 1-phosphate analogue does not productively bind to the active-site of LmSPase. This outcome is supported by the docking of the glucose 1-phosphate analogue to the active-site of LmSPase (Figure 1B). Compared to glucose 1-phosphate, the conformation and alignment of the glucose 1-phosphate analogue shows significant differences. The glucose 1-phosphate analogue adopts a relaxed conformation and its alignment is not supported by a strong hydrogen bonding network.

Kinetic characterization of LmSPase and mutants

Kinetic characterization of F52A-D196A. Substitution of the catalytic nucleophile, Asp196, to Ala on the template of the F52A mutant resulted in a doubly mutated enzyme, F52A-D196A, which was not active above detection limits, irrespective if fructose (synthesis) or phosphate (phosphorolysis) was used as acceptor. This finding is in agreement with a former study, in which the Asp196 was unambiguously identified as the catalytic nucleophile and which substitution to Ala, D196A, resulted in

an inactive variant of LmSPase (11). The performed STD-NMR measurements (Figure 2F) intended to compare the binding behavior of glucose 1-phosphate in LmSPase and mutants revealed a significant different binding pattern of F52A-D196A compared to LmSPase. This result is in agreement with the predicted binding of glucose 1-phosphate in subsite -1 of LmSPase (Figure 1D), which assumes that glucose 1-phosphate binds in a flipped position, the phosphate group pointing towards the Ala52 rather than binding to the phosphate binding site.

Kinetic characterization of F52A-E237A. The role of Glu237 as acid-base catalyst in the two-step enzymatic mechanism of LmSPase has been carefully analyzed in a former study (12). Assistance from the acid-base catalyst affects both half reactions of the canonical two-step mechanism, enzyme glucosylation from sucrose or glucose 1-phosphate and enzyme deglucosylation by phosphate or fructose. Substitution of Glu237 by Gln (E237Q) resulted in a 10^5-fold decrease in wild-type activity in both directions (12). To get more detailed information about the role of Glu237, enzyme glucosylation and deglucosylation were examined as two kinetically isolated steps. The catalytic efficiency (k_{cat}/K_m) for the glucosyl donor and acceptor substrate represents the formation (enzyme glucosylation) and breakdown (enzyme deglucosylation) of the covalent glucosyl-enzyme intermediate, respectively. In the event of enzyme glucosylation, Glu237 has to provide protonic assistance to the departure of the leaving group, either fructose (phosphorolysis) or phosphate (synthesis). In the event of enzyme deglucosylation, Glu237 has to deprotonate the incoming acceptor, phosphate (phosphorolysis) or fructose (synthesis). The catalytic efficiency for enzyme glucosylation is mainly correlated to the leaving group ability of the donor substrate. The glucosyl transfer from fructose, an example of a poor leaving group, was strongly affected in E237Q (10^4-fold decreased compared to LmSPase), whereas the glucosyl transfer from phosphate to the enzyme was only moderately affected in E237Q (23-fold decreased compared to LmSPase) (12). Under conditions when a donor substrate with a good leaving group ability (glucose 1-phosphate) was used, the deprotonation of the acceptor substrate was the rate limiting step. To circumvent this rate limitation, chemical rescue reagents, which were meant to compensate for the loss of the carboxylate side chain of Glu237, were added to the reaction with glucose 1-phosphate. The addition of azide, acetate and formate was found to restore catalytic activity up to 300-fold in E237Q compared to the wild-type level. The double mutant F52A-E237A showed no activity in either phosphorolysis or synthesis direction. In analogy to E237Q, we tried to restore activity in F52A-E237A by adding external reagents. Acetate, chloride, bromide, azide, cyanide and formate were tested as external nucleophiles, however, none of the reagents could restore activity. Finally we added arsenate

to glucose 1-phosphate and F52A-E237A. Arsenate, a closely related nucleophile to phosphate with similar natural bond orbital charges for the nucleophilic oxygens and similar pK values (21), was used as replacement for fructose and is expected to intercept the glucosyl-enzyme intermediate to form α-D-glucose 1-arsenate, which decomposes spontaneously to free glucose and arsenate. Consistent with the expectations that both steps, glucosylation and deglucosylation, are just weakly affected in the arsenolysis of glucose 1-phosphate, the catalytic efficiency of E237Q (k_{cat}/K_m = 0.6 s^{-1} mM^{-1}) was just minorly decreased compared to LmSPase (k_{cat}/K_m = 5.5 s^{-1} mM^{-1}). In contrast, no activity could be detected for arsenolysis of glucose 1-phosphate catalyzed by F52A-E237A. Hence, several characteristics which defined Glu237 as acid-base catalyst in the former study with E237Q could not be regained in F52A-E237A.

The results obtained from the kinetic characterization are supported by the structural investigations of the predicted binding of glucose 1-phosphate in the active-site of F52A-E237A. Compared to LmSPase and F52A, further rebuilding of LmSPase active-site by substituting the acid-base catalyst by alanine (Figure 1E) had two consequences: The glucopyranosyl ring of glucose 1-phosphate is significantly shifted, reflected by an increased distance (up to 4.1 Å compared to LmSPase) between the carboxylate side chain of Asp295 to the hydroxyl groups at C2 and C3. Secondly, the orientation of the phosphate group in F52A-E237A is distorted compared to the "tucked-under" conformation observed in LmSPase reflected by an increased distance from 2.7 to 5.2 Å between the C2-OH of glucose 1-phosphate and the oxygen of phosphate. The obtained results let assume that the presence of both residues, Phe52 and Glu237, is required for forcing glucose 1-phosphate into the reactive conformation. If these structural elements are missing, glucose 1-phosphate adopts a rather relaxed conformation, which precludes the release of the leaving group. As direct consequence the β-glucosyl enzyme intermediate cannot be formed, resulting in an inactive mutant. In this case, the addition of arsenate cannot have any effect, as arsenate can just be active after the β-glucosyl enzyme intermediate has formed. Chemical rescue reagents, intended to compensate for the loss of the carboxylate side chain of Glu237 and to attack the glycosidic oxygen atom, are restricted in their function as the glycosidic oxygen atom is far out of their range.

Kinetic characterization of F52A-D295A. In addition to Asp196 and Glu237, two residues which are directly involved in the catalytic reaction of LmSPase, Asp295 is characterized as the third residue belonging to the catalytic triad. In literature, Asp295 is often described as transition state stabilizer, a residue which provides charged hydrogen bonding interactions to the C2 and C3 of the glucosyl

moiety of the donor substrate (13). These charged hydrogen bonding interactions assist substrate distortion and stabilize the transition states flanking the β-glucosyl enzyme intermediate. To investigate the interplay between Phe52 and Asp295 on substrate binding and catalysis, the corresponding double-mutant F52A-D295A was subjected to a steady-state kinetic analysis for phosphorolysis and synthesis of sucrose. The results are summarized in Table 2, along with the data for LmSPase and F52A, which were determined in an earlier study (9).

We begin by analyzing kinetic consequences in direction of phosphorolysis by sucrose. Compared to the single mutant F52A, the additional substitution of Asp295 to Ala had no major further effect on the kinetic parameters. Enzyme glucosylation from sucrose was strongly impaired in F52A and in analogy in F52A-D295A. The initial rate of reaction showed a linear dependence on the sucrose concentration, up to a high level of 800 mM. This result suggested that the K_m for sucrose was increased substantially, up to 81-fold (800/9.8) compared to the K_m of LmSPase. Expressed in k_{cat}/K_m terms, the F52A mutant showed a 5,200-fold reduced efficiency, the F52A-D295A mutant showed a 7,500-fold reduced catalytic efficiency compared to LmSPase. When the acceptor substrate phosphate was used as variable substrate, the catalytic efficiencies for enzyme deglucosylation by phosphate were similar in both mutants, F52A and F52A-D295A. Expressed in k_{cat}/K_m terms, the F52A mutant showed a 333-fold reduced efficiency, the F52A-D295A mutant showed a 480-fold reduced efficiency compared to LmSPase. In contrast to F52A and LmSPase, which displayed "normal" Michaelis-Menten behavior, F52A-D295A was subjected to a substrate inhibition of phosphate. Fit of the data with Equation 2 resulted in a substrate inhibition constant of 12 mM.

Analysis of kinetic consequences of F52A-D295A in direction of synthesis of sucrose depicted marked differences to the kinetic pattern of F52A. Compared to LmSPase and F52A, F52A-D295A showed a linear dependence on the glucose 1-phosphate concentration up to a level of 800 mM. This result suggested that the K_m for glucose 1-phosphate was increased significantly, up to 178-fold (800/4.5) compared to the K_m of LmSPase and up to even 2,000-fold (800/0.4) compared to the K_m of F52A. Expressed in k_{cat}/K_m terms, the F52A-D295A mutant showed a 120-fold decreased catalytic efficiency for enzyme gluosylation from glucose 1-phosphate compared to F52A and a 40,000-fold decreased catalytic efficiency compared to LmSPase. Figure 1F shows the proposed binding of glucose 1-phosphate in the substrate binding site of F52A-D295A. Compared to the binding of glucose 1-phosphate in LmSPase and F52A, the accommodation of glucose 1-phosphate in the active-site is very similar in terms of conformation and alignment. The observed "tucked-under" conformation of the phosphate moiety is still preserved and the interactions to Asp196, Glu237 and Arg137 are very comparable. However, loss of hydrogen bonding interactions from the carboxylate side chain of Asp295 to the hydroxyl groups at

C2 and C3 of the glucosyl residues as well as from the carboxylate side chain of Asp295 to the oxygen of the phosphate group, resulted in a less productive binding of glucose 1-phosphate. The loss of stabilization towards the hydroxyl groups at carbons 2 and 3 may explain the dramatic increase in K_m for binding of glucose 1-phosphate.

The effects of enzyme deglucosylation from fructose were less severe compared to the effect of enzyme glucosylation from glucose 1-phosphate. Initial rates in the direction of synthesis showed a hyperbolic dependence of the concentration of fructose, allowing an independent determination of K_m and k_{cat}. The around 130-fold decrease in catalytic efficiency compared to LmSPase was mainly attributed to an around 5,200-fold decreased k_{cat}.

In summary it can be said that all kinetic steps in phosphorolysis direction were affected to a similar extent, irrespective if Phe52 alone or Phe52 and Asp295 were substituted by Ala. However in synthesis direction, substitution of Asp295 to Ala on the F52A template had a major effect. The binding of glucose 1-phosphate was significantly affected and hence, the catalytic efficiency for enzyme glucosylation from glucose 1-phosphate was greatly decreased. Sucrose and glucose 1-phosphate differ in their leaving group, fructose versus phosphate. For LmSPase it is known that the structural requirements for binding of phosphate are less stringent than those for binding of fructose. Phosphate can be accommodated in subsite +1 in a variety of reactive conformations, still recruiting stabilization from residues present in subsite +1. The binding of fructose, however, is restricted to one certain conformation. For F52A-D295A it seems that the presence of fructose as leaving group has a positive effect on the binding of the donor substrate, which is missing when phosphate is present as leaving group. The catalytic efficiency for glucosylation from sucrose was decreased in F52A-D295A around 7,500-fold compared to LmSPase. The catalytic efficiency for glucosylation from glucose 1-phosphate, however, was decreased around 40,000-fold compared to LmSPase. These results suggest that the binding of fructose to the acceptor binding site can somehow compensate for the loss of stabilization of the glucopyranosyl moiety due to the substitution of Asp295 to Ala. Phosphate cannot compensate for this stabilization loss, resulting in an unproductive binding of glucose 1-phosphate. However, although the binding of glucose 1-phosphate is strongly affected and the catalytic efficiency is dramatically decreased, sucrose is formed. The road to productive catalysis in direction of synthesis seems to be dependent on the conformation of glucose 1-phosphate. The phosphate moiety of glucose 1-phosphate is proposed to be aligned in the "tucked-under" conformation. This disposition seems to be the reactive conformation for glucose 1-phosphate and seems to be required for catalysis.

CONCLUSION

The study presented herein shows how well-orchestrated active-site residues in LmSPase interact with each other. Slight changes in active-site architecture have tremendous effects on substrate binding and/or catalysis. Based on the evidence obtained in the present study the conformation of glucose 1-phosphate in its binding mode seems to be decisive for functional catalysis. The disposition in which the phosphate moiety is "tucked-under" the sugar is proposed to be the reactive conformation of glucose 1-phosphate. Although unusual, this alignment has already been observed in several retaining GTs and retaining phosphorylases classified as GTs but not yet in a retaining phosphorylase classified as GHs, to which class LmSPase belongs to.

MATERIALS AND METHODS

Chemicals and reagents

Pfu DNA polymerase and *Dpn*I were purchased from Promega (Madison, USA) and Fermentas (Burlington, Canada), respectively. Oligonucleotide synthesis was performed by Invitrogen (Carlsbad, USA). DNA sequencing was performed at LGC Genomics (Berlin, Germany). The plasmid vector pASK-IBA7+, anhydrotetracycline and all materials used for *Strep*-tag purification were obtained from IBA (Göttingen, Germany). Fractogel EMD-DEAE column (2.6 x 9.5 cm) was purchased from Merck (Darmstadt, Germany). Amicon Ultra-15 Centrifugal Filter Units with a 10,000-molecular-weight cutoff were from Millipore (Billerica, USA). Phosphoglucomutase from rabbit muscle (PGM) and glucose-6-phosphate dehydrogenase from *Leuconostoc mesenteroides* (G6PDH) were obtained from Sigma-Aldrich (Vienna, Austria). Glucose oxidase from *Aspergillus niger* (GOD), peroxidase from horseradish (POD) and 2,2'-azino-bis(3-ethylbenzothiazoline-6-sulfonic acid) diammonium salt (ABTS) were purchased from Sigma-Aldrich. The phosphono analogue of glucose 1-phosphate was synthesized as described by Beaton et al (22).

All other chemicals were obtained from Sigma-Aldrich or Roth (Karlsruhe, Germany) in highest purity available.

Site-directed mutagenesis, enzyme production and purification

The point mutation Phe52 to Ala, for the generation of F52A, was introduced according to reported procedures (9). The F52A plasmid encoded in the pASK-IBA7+ expression vector served as template for substitution of Asp196 to Ala, Glu237 to Ala and Asp295 to Ala, respectively. The PCR was carried out in the same way as for F52A (9), except for an annealing temperature of 47.6°C for F52A-D196A and 61.8°C for F52A-E237A and F52A-D295A. The following mutagenic primers and their reverse complementary ones were used, whereby the mismatched codons are underlined:

F52A-D196A: 5'-ATTCGTTTGGCTGCCTTTGCG-3';

F52A-E237A: 5'-CCATTAAAGGCTGAAATTTTACCAGCAATTCATG-3';

F52A-D295A: 5'-GGACACGCATGCAGGTATTGGTG-3'.

All four amplified plasmid vectors (F52A, F52A-D196A, F52A-E237A and F52A-D295A) harboring the sequence-proven mutated gene were transformed into electro-competent cells of *Escherichia coli* BL21-Gold (DE3). *E. coli* BL21-Gold (DE3) cells harboring one of the pASK-IBA7+ expression vectors were cultivated in 1-L baffeled shaken flasks at 37°C and 110 rpm using LB-media and 115 mg/L ampicillin. When OD_{550} reached 0.8-1.0 temperature was decreased to 22°C and gene expression was induced with

200 μg/L anhydrotetracycline for 20 h. Cells were harvested by centrifugation at 4°C and 5,000 rpm for 30 min in a Sorvall RC-5B Refrigerated Superspeed centrifuge (Du Pont Instruments, Wilmington, USA). Resuspended cells were frozen at -20°C, thawed and the suspension was passed twice through a French pressure cell press (American Instruments, Silver Springs, USA) at 150 bar. Cell debris was removed by centrifugation at 4°C, 14,000 rpm for 30 min. The resulting supernatant was used for further enzyme purification.

LmSPase and mutants were purified via a two-step purification procedure. The clear supernatant of LmSPase and mutants was applied on a *Strep*-Tactin Sepharose column, like described previously (23). Pooled fractions of eluted LmSPase and mutants were concentrated, loaded on Fractogel EMD-DEAE and purified according to reported procedures (11). Buffer exchange to 50 mM MES, pH 7.0 was performed using Amicon Ultra-15 Centrifugal Filter Units. Purification was monitored by SDS-PAGE.

Assays and analytical methods

Enzyme activity in direction of phosphorolysis of sucrose was determined at 30°C using a continuous coupled enzymatic assay with PGM and G6PDH (detection limit: 0.05 mM) (8). The quantity of inorganic phosphate present was determined colorimetrically at 850 nm (detection limit: 0.0025 mM) (24). D-Glucose was determined using a colorimetric GOD-POD assay (detection limit: 0.005 mM) (25), glucose 1-phosphate was assayed in a coupled enzymatic system with PGM and G6PDH (26). Formation of sucrose was measured using high performance anion exchange chromatography with pulsed amperometric detection (HPAE-PAD; detection limit of sucrose: 0.005 mM) (23). Protein concentration was measured with the BioRad dye-binding method referenced against BSA.

Characterization of LmSPase and mutants

Hydrolysis in the presence and absence of the glucose 1-phosphate analogue. LmSPase displays hydrolase activity towards glucose 1-phosphate under conditions in which a suitable nucleophile is lacking. The hydrolytic activity of LmSPase towards glucose 1-phosphate (5 mM) and glucose 1-phosphate in the presence of glucose 1-phosphate analogue (both substrates were present in a concentration of 5 mM) was determined in 50 mM MES, pH 7.0. The release of phosphate was measured in dependence of time of incubation up to 50 min.

Chemical rescue studies using exogenous nucleophiles. In an attempt to restore activity in F52A-E237A we added external reagents to a reaction mixture containing 10 mM glucose 1-phosphate and

0.3 mg/mL F52A-E237A in 50 mM MES, pH 7.0. The sodium salts of acetate, chloride, bromide, azide, cyanide and formate were tested as external nucleophiles, each present in a concentration of 50 mM. The release of phosphate was measured in dependence of time of incubation up to 24 h. The reported values are corrected for the amount of phosphate produced by spontaneous hydrolysis of glucose 1-phosphate.

Enzymatic reaction with arsenate. Arsenate replaced fructose as glucosyl acceptor in the reaction of F52A-E237A with glucose 1-phosphate. In contrast to the natural, reversible reaction, arsenolysis is a completely irreversible process as α-D-glucose 1-arsenate is spontaneously hydrolyzed to glucose and arsenate. The rate of arsenolysis was determined at 30°C in 50 mM MES, pH 7.0, in discontinuous assays containing 50 mM arsenate and 50 mM glucose 1-phosphate. The concentration of F52A-E237A used was 0.3 mg/mL. The release of glucose was measured in dependence of time of incubation up to 24 h. The reported values are corrected for the amount of glucose produced by spontaneous hydrolysis of glucose 1-phosphate.

Initial-rate studies and steady-state kinetic analysis. Reactions were performed at 30°C in 50 mM MES, pH 7.0, and monitored by product formation (phosphorolysis: glucose 1-phosphate; synthesis: phosphate) in discontinuous assays. The typical concentration of F52A-D295A used was 0.3 mg/mL. All reactions were incubated for 1 h. The concentrations of donor and acceptor substrate were varied in a suitable range: sucrose (5-800 mM), phosphate (1-250 mM), glucose 1-phosphate (1-800 mM) and fructose (0.01-100 mM). Control reactions lacking the substrate or the enzyme were recorded in all cases and initial rates were corrected as required. Kinetic parameters (V_{max}, K_m) for the glucosylation from sucrose and glucose 1-phosphate, respectively as well as the deglucosylation by fructose were obtained from non-linear fits of data to equation 1. When substrate inhibition from phosphate occurred, kinetic parameters (V_{max}, K_m) were determined using a Lineweaver-Burk plot. V_{max} and K_m were set constant and the substrate inhibition constant was calculated by using equation 2. k_{cat} is defined in equation 3.

$$v = \mathrm{V}_{max} \cdot \frac{S}{K_m + S} \tag{1}$$

$$v = \mathrm{V}_{max} \cdot \frac{S}{K_m + S \cdot \frac{1+S}{K_i}} \tag{2}$$

$$k_{cat} = \frac{V_{max}}{E} \tag{3}$$

where v is the observed reaction rate [mM/min], V_{max} is the maximal initial rate [mM/min], S is the substrate concentration [mM], K_m is the apparent Michaelis-Menten constant [mM], K_i is the substrate-inhibition constant [mM], k_{cat} is the catalytic constant [s^{-1}] and E is the total molar enzyme concentration based on a molecular mass of 59 kDa for the wild-type LmSPase subunit [mM]. When enzyme was not saturable with substrate and an independent determination of V_{max} and K_m therefore not possible, V_{max}/K_m was obtained from data acquired under substrate-limited reaction conditions where the rate increases in linear dependence on substrate concentration.

Circular dichroism (CD) spectroscopy

Far-UV CD spectra of protein solutions of LmSPase and mutants (0.1 mg/mL; 50 mM MES, pH 7.0) were recorded at 22°C on a Chirascan Plus system (Applied Photophysics, Leatherhead, UK). CD spectra were collected at a scan speed of 20 nm/min at 1.0 nm bandwidth and response time of 0.5 s. All spectra were recorded in a 0.1 cm cuvette between 200 and 280 nm. All data shown here represent the average of 5 recorded spectra, corrected with a buffer spectrum before converting the CD signal to molar ellipticity using the program CDNN (27).

Homology modeling and molecular docking

The homology models of LmSPase, F52A, F52A-D196A, F52A-E237A and F52A-D295A were build using SwissModel (28). The crystal structure of the closely related sucrose phosphorylase from *Bifidobacterium adolescentis* (BaSPase; PDB entry 2gdu) (14) was manually selected as template. AutoDock 4.2 (29) as implemented in Yasara V 11.11.21 was used for the enzyme-ligand docking. The AMBER03 force field (30) and the default parameters provided by the standard docking macro were used, except that the number of runs was increased to 50. The homology models of LmSPase, F52A, F52A-D196A, F52A-E237A and F52A-D295A were used as macromolecules in a molecular docking experiment that employed deprotonated glucose 1-phosphate and glucose 1-hydrogenphosphate as ligand. The 3D coordinates for the ligands was generated from SMILES strings using Chimera (http://www.cgl.ucsf.edu/chimera). The ligand was flexible placed into the active-site of LmSPase and mutants. A search space of 15 x 15 x 25 Å around the C1 atom of Asp196 was used. The same set-up was used to dock the phosphono analogue of glucose 1-phosphate (in the deprotonated and glucose 1-hydrogenphosphate form) to the active-site of LmSPase. When the deprotonated form of glucose 1-phosphate was used as ligand, the docking algorithm resulted in 5 binding modes for F52A-E237A, 6 binding modes for LmSPase, 7 binding modes for F52A-D295A, 8 binding modes for F52A-D196A and 11 binding modes

for F52A. When glucose 1-hydrogenphosphate was used as ligand, the docking algorithm resulted in 6 binding modes for F52A-E237A, 7 binding modes for LmSPase and F52A-D295A, 8 binding modes for F52A-D196A and 12 binding modes for F52A. The docking of the deprotonated form and glucose 1-hydrogenphosphate form of the glucose 1-phosphate analogue resulted in 9 binding modes. The selection of the best-fit binding mode was done on the basis of best structural alignment between the glucopyranosyl ring of the docked glucose 1-phosphate and the glucopyranosyl ring of sucrose, the ligand which was co-crystallized in the structure of BaSPase.
PyMOL (http://pymol.sourceforge.net) was used for visualization.

Saturation Transfer Difference (STD) NMR

STD spectra were recorded as described earlier (31). Samples were prepared in D_2O (pH 6.65) and contained 50 mM MES, 7 μM enzyme and 5 mM ligand. Selective protein saturation was achieved by a series of 40 Gaussian pulses (50 ms length) with a 1 ms delay resulting in a 2.04 s total irradiation time. On and off resonance irradiations were made by concomitant change of the irradiation frequencies at -2.0 ppm and 40.0 ppm, respectively. Each experiment was performed with two times 256 scan. A spin lock (30 ms) after the 90°C pulse was used to eliminate the protein frequencies. No water suppression was applied to avoid influences of signals close to HDO signal. Subtraction of the spectra was performed after the measurement. For the interpretation the largest signal in all comparable experiments was set to 100% and the relative intensities were determined in steps of 5% (31, 32).

Acknowledgements

We acknowledge financial support from the Austrian Science Funds FWF (project L586-B03); David Jakeman (College of Pharmacy, Dalhousie University, Nova Scotia, Canada) for synthesis of the phosphono analogue of glucose 1-phosphate; Lothar Brecker (Institute of Organic Chemistry, University of Vienna, Austria) for performing the STD-NMR measurements; and Can Araman (Institute of Biological Chemistry, University of Vienna, Austria) for help in recording CD spectra.

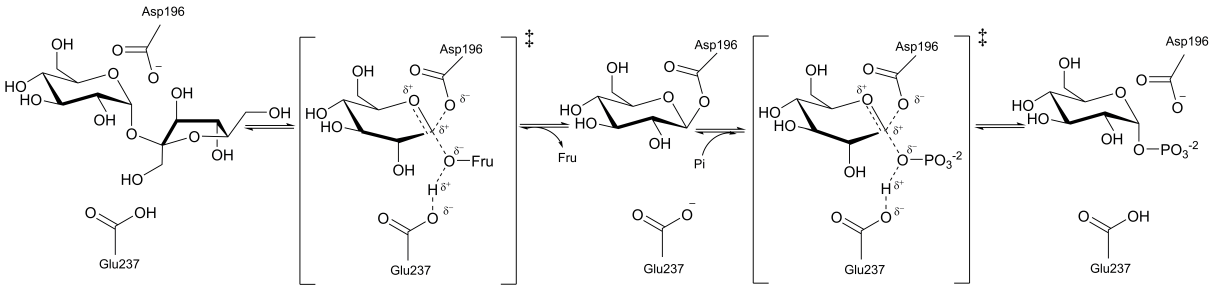

Scheme 1. Proposed catalytic mechanism of LmSPase. The reaction proceeds in two steps via a covalent β-glucosyl enzyme intermediate. Asp196 adopts the catalytic role of the nucleophile, Glu237 of the acid-base catalyst.

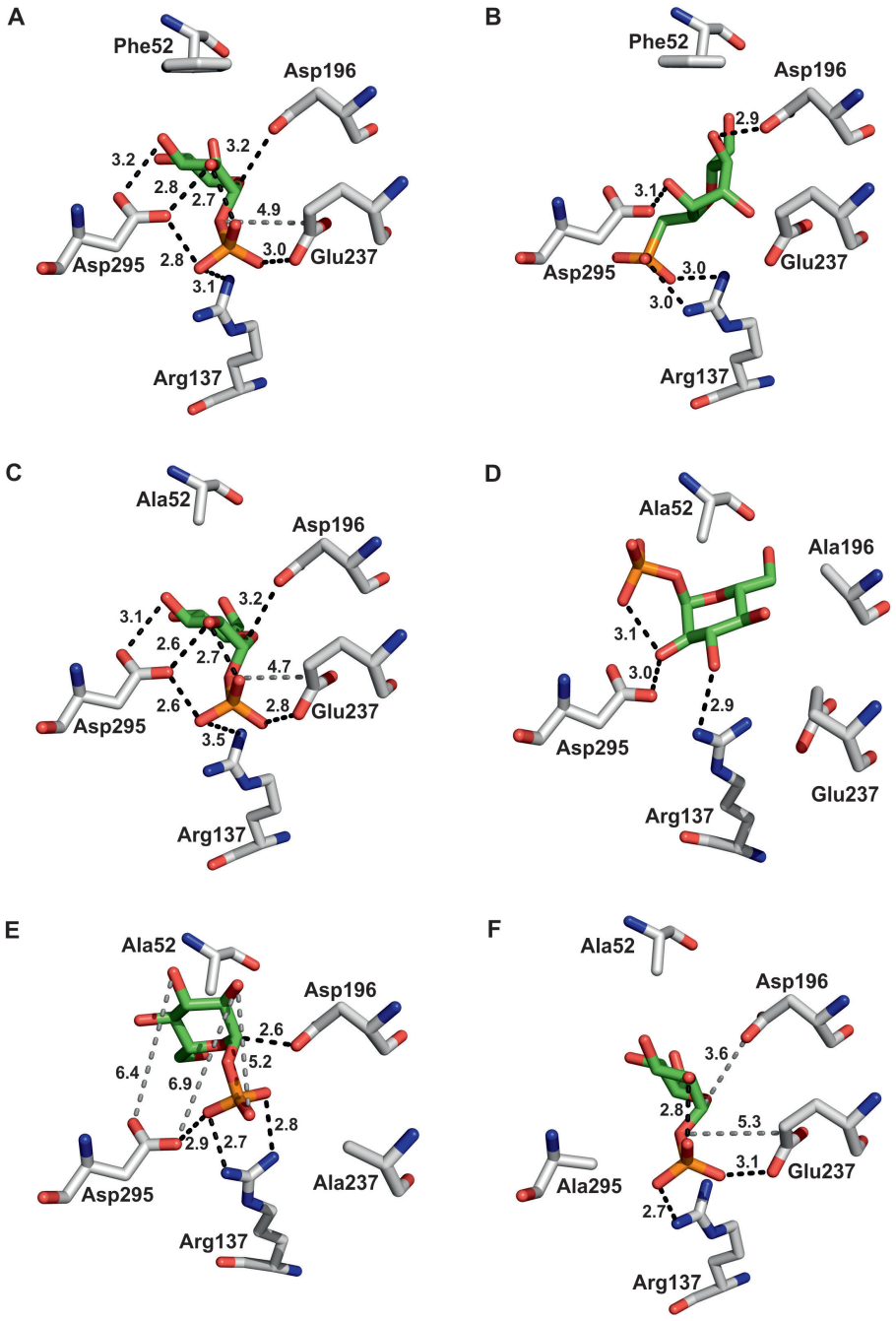

Figure 1. Close-up view of predicted binding of (deprotonated) glucose 1-phosphate (green) in subsite -1 of LmSPase (A), F52A (C), F52A-D196A (D), F52A-E237A (E) and F52A-D295A (F). The predicted binding of the phosphono analogue of glucose 1-phosphate in the active-site of LmSPase is shown in B. Hydrogen bonds ($\leq$ 3.5 Å) are shown as black-dashed lines. Interactions potentially relevant for catalysis are shown as gray-dashed lines. Distances are given in Å.

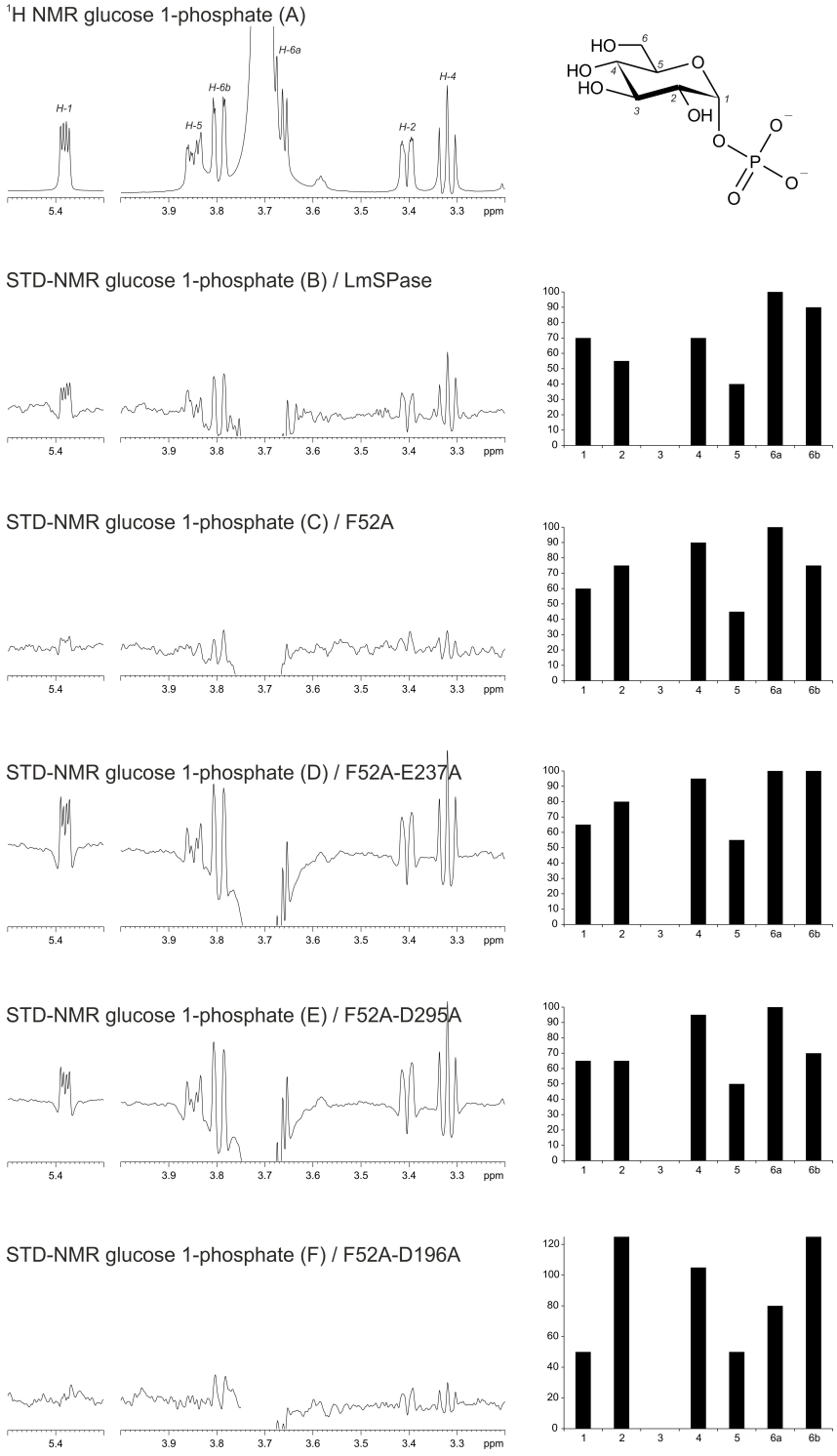

Figure 2. Analysis of glucose 1-phosphate binding to LmSPase and mutants. Values are relative STD effects of glucose 1-phosphate bound to LmSPase and mutants. Each STD effect is calculated as a quotient of signal intensities in the STD spectrum and in the reference proton spectrum. The effects are normalized to the respective largest effect in the sample.

Table 1. Far UV-CD spectra were recorded on an Applied Photophysics Chirascan Plus system. The analysis of the secondary structure was performed with the CD deconvolution software CDNN.

Secondary structure	LmSPase [%]	F52A [%]	F52A-D196A [%]	F52A-E237A [%]	F52A-D295A [%]
Alpha helices	38.3	42.5	35.6	41.3	34.3
Beta strands	15.1	13.6	16.1	14.1	16.4
Turns	16.2	15.8	16.6	16.0	16.7
Unordered	30.4	28.1	31.7	28.6	32.6

Table 2. Kinetic parameters in phosphorolysis and synthesis direction catalyzed by LmSPase, F52A and F52A-D295A.

Reaction		LmSPase	F52A	F52A-D295A
Phosphorolysis of sucrose				
Glucosylation from sucrose[1]	k_{cat} [s^{-1}]	117	n.a.	n.a.
	K_m [mM]	9.8	n.a.	n.a.
	k_{cat}/K_m [s^{-1} mM^{-1}]	12	$2.3 \cdot 10^{-3}$	$1.6 \cdot 10^{-3}$
Deglucosylation by phosphate[2]	k_{cat} [s^{-1}]	145	3.3	5.4 [a]
	K_m [mM]	6	46	107
	k_{cat}/K_m [s^{-1} mM^{-1}]	24	$7.2 \cdot 10^{-2}$	$5.0 \cdot 10^{-2}$
	K_i [mM]	-	-	12
Synthesis of sucrose				
Glucosylation from glucose 1-phosphate[3]	k_{cat} [s^{-1}]	39	$9.8 \cdot 10^{-3}$	n.a.
	K_m [mM]	4.7	0.4	n.a.
	k_{cat}/K_m [s^{-1} mM^{-1}]	8.3	$2.5 \cdot 10^{-2}$	$2.1 \cdot 10^{-4}$
Deglucosylation by fructose[4]	k_{cat} [s^{-1}]	47	n.a.	$9.1 \cdot 10^{-3}$ [b]
	K_m [mM]	13	n.a.	0.3
	k_{cat}/K_m [s^{-1} mM^{-1}]	3.7	$4.4 \cdot 10^{-3}$	$2.9 \cdot 10^{-2}$

The S.D. for k_{cat} and k_{cat}/K_m was equal or smaller than 3.2% and 8.3% of the reported values respectively, with the exception of [a] 5.4%, [b] 7.3%. n.a., not applicable.

Kinetic parameters in phosphorolysis and synthesis direction catalyzed by LmSPase and F52A were determined in an earlier study (9).

[1] For F52A-D295A, sucrose was varied at 10 levels between 5 mM and 800 mM. Phosphate was constant at 50 mM.

[2] For F52A-D295A, phosphate was varied at 11 levels between 1 mM and 250 mM. Sucrose was constant at 500 mM.

[3] For F52A-D295A, glucose 1-phosphate was varied at 10 levels between 1 mM and 800 mM. Fructose was constant at 100 mM.

[4] For F52A-D295A, fructose was varied at 8 levels between 0.01 mM and 100 mM. Glucose 1-phosphate was constant at 20 mM.

SUPPLEMENTARY INFORMATION

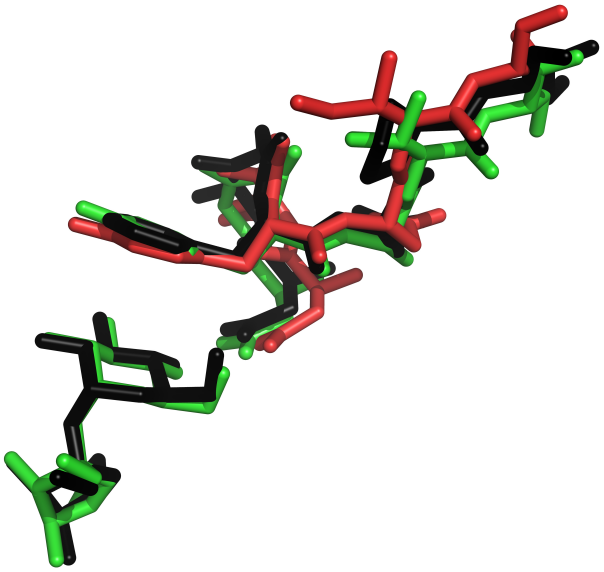

Supplementary Figure S1. The aromatic motif at the catalytic subsite of selected GH-13 glucoside hydrolases and transglucosidases is revealed by Phe/Tyr residue conservation. A structural overlay of the corresponding catalytic subsite parts of BaSPase (pdb entry 2gdu; black), *N. polysaccharea* amylosucrase (pdb entry 1jgi; green) and *Klebsiella sp.* isomaltulose synthase (pdb entry 1m53; red) is shown.

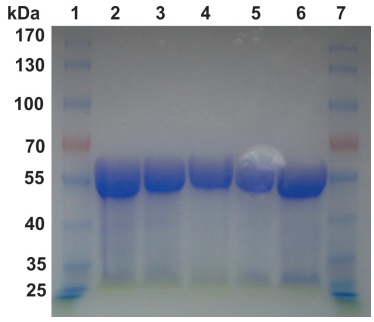

Supplementary Figure S2. Enzyme purification monitored by SDS-PAGE. Lane 1: molecular mass standard; 2: LmSPase; 3: F52A; 4: F52A-D196A; 5: F52A-E237A; 6: F52A-D295A; 7: molecular mass standard.

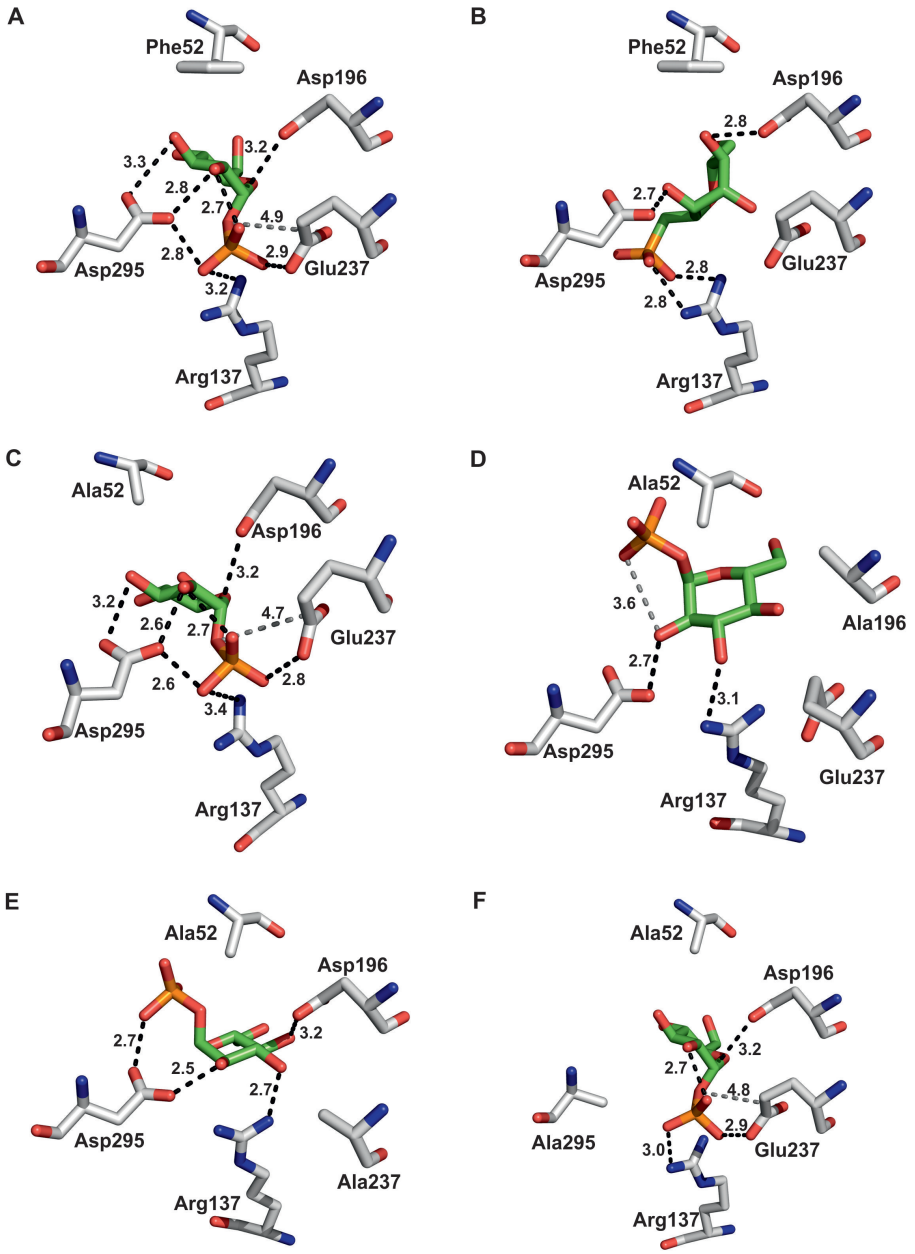

Supplementary Figure S3. Close-up view of the predicted binding of glucose 1-hydrogenphosphate (green) in subsite -1 of LmSPase (A), F52A (C), F52A-D196A (D), F52A-E237A (E) and F52A-D295A (F). The predicted binding of the glucose 1-hydrogenphosphate analogue in the active-site of LmSPase is shown in B. Hydrogen bonds ($\leq$ 3.5 Å) are shown as black-dashed lines. Interactions potentially relevant for catalysis are shown as gray-dashed lines. Distances are given in Å.

References

1. Kamiya Y, Yagi-Utsumi M, Yagi H, Kato K. 2011. Structural and molecular basis of carbohydrate-protein interaction systems as potential therapeutic targets. Curr Pharm Des 17:1672-1684.

2. Asensio JL, Arda A, Canada FJ, Jimenez-Barbero J. 2013. Carbohydrate-aromatic interactions. Acc Chem Res 46:946-954.

3. Laederach A, Reilly PJ. 2005. Modeling protein recognition of carbohydrates. Proteins 60:591-597.

4. Kumari M, Sunoj RB, Balaji PV. 2012. Conformational mapping and energetics of saccharide-aromatic residue interactions: implications for the discrimination of anomers and epimers and in protein engineering. Org Biomol Chem 10:4186-4200.

5. Payne CM, Bomble YJ, Taylor CB, McCabe C, Himmel ME, Crowley MF, Beckham GT. 2011. Multiple functions of aromatic-carbohydrate interactions in a processive cellulase examined with molecular simulation. J Biol Chem 286:41028-41035.

6. Henrissat B, Davies GJ. 2000. Glycoside hydrolases and glycosyltransferases. Families, modules, and implications for genomics. Plant Physiol 124:1515-1519.

7. Dougherty DA. 2007. Cation-π interactions involving aromatic amino acids. J Nutr 137:1504S-1508S.

8. Goedl C, Schwarz A, Minani A, Nidetzky B. 2007. Recombinant sucrose phosphorylase from *Leuconostoc mesenteroides*: characterization, kinetic studies of transglucosylation, and application of immobilised enzyme for production of α-D-glucose 1-phosphate. J Biotechnol 129:77-86.

9. Wildberger P, Luley-Goedl C, Nidetzky B. 2011. Aromatic interactions at the catalytic subsite of sucrose phosphorylase: their roles in enzymatic glucosyl transfer probed with Phe52 $\rightarrow$ Ala and Phe52 $\rightarrow$ Asn mutants. FEBS Lett 585:499-504.

10. Mieyal JJ, Abeles RH. 1970. The mechanism of action of sucrose phosphorylase. Isolation and properties of a β-linked covalent glucose-enzyme complex. J Biol Chem 245:1020-1031.

11. Schwarz A, Nidetzky B. 2006. Asp-196 $\rightarrow$ Ala mutant of *Leuconostoc mesenteroides* sucrose phosphorylase exhibits altered stereochemical course and kinetic mechanism of glucosyl transfer to and from phosphate. FEBS Lett 580:3905-3910.

12. Schwarz A, Brecker L, Nidetzky B. 2007. Acid-base catalysis in *Leuconostoc mesenteroides* sucrose phosphorylase probed by site-directed mutagenesis and detailed kinetic comparison of wild-type and Glu237 $\rightarrow$ Gln mutant enzymes. Biochem J 403:441-449.

13. Mueller M, Nidetzky B. 2007. The role of Asp-295 in the catalytic mechanism of *Leuconostoc mesenteroides* sucrose phosphorylase probed with site-directed mutagenesis. FEBS Lett 581:1403-1408.

14. Mirza O, Skov LK, Sprogøe D, van den Broek LA, Beldman G, Kastrup JS, Gajhede M. 2006. Structural rearrangements of sucrose phosphorylase from *Bifidobacterium adolescentis* during sucrose conversion. J Biol Chem 281:35576-35584.

15. Sprogøe D, van den Broek LA, Mirza O, Kastrup JS, Voragen AG, Gajhede M, Skov LK. 2004. Crystal structure of sucrose phosphorylase from *Bifidobacterium adolescentis*. Biochemistry 43:1156-1162.

16. Lairson LL, Withers SG. 2004. Mechanistic analogies amongst carbohydrate modifying enzymes. Chem Comm:2243-2248.

17. Persson K, Ly HD, Dieckelmann M, Wakarchuk WW, Withers SG, Strynadka NC. 2001. Crystal structure of the retaining galactosyltransferase LgtC from *Neisseria meningitidis* in complex with donor and acceptor sugar analogs. Nat Struct Biol 8:166-175.

18. Gibson RP, Turkenburg JP, Charnock SJ, Lloyd R, Davies GJ. 2002. Insights into trehalose synthesis provided by the structure of the retaining glucosyltransferase OtsA. Chem Biol 9:1337-1346.

19. Geremia S, Campagnolo M, Schinzel R, Johnson LN. 2002. Enzymatic catalysis in crystals of *Escherichia coli* maltodextrin phosphorylase. J Mol Biol 322:413-423.

20. Martin JL, Johnson LN, Withers SG. 1990. Comparison of the binding of glucose and glucose 1-phosphate derivatives to T-state glycogen phosphorylase b. Biochemistry 29:10745-10757.

21. Silva RG, Hirschi JS, Ghanem M, Murkin AS, Schramm VL. 2011. Arsenate and phosphate as nucleophiles at the transition states of human purine nucleoside phosphorylase. Biochemistry 50:2701-2709.

22. Beaton SA, Huestis MP, Sadeghi-Khomami A, Thomas NR, Jakeman DL. 2009. Enzyme-catalyzed synthesis of isosteric phosphono-analogues of sugar nucleotides. Chem Commun:238-240.

23. Wildberger P, Todea A, Nidetzky B. 2012. Probing enzyme-substrate interactions at the catalytic subsite of *Leuconostoc mesenteroides* sucrose phosphorylase with site-directed mutagenesis: the roles of Asp49 and Arg395. Biocatal Biotransform 30:326-337.

24. Saheki S, Takeda A, Shimazu T. 1985. Assay of inorganic phosphate in the mild pH range, suitable for measurement of glycogen phosphorylase activity. Anal Biochem 148:277-281.

25. Werner W, Rey HG, Wielinger H. 1970. Properties of a new chromogen for determination of glucose in blood according to god/pod-Method. Z Anal Chem 252:224-228.

26. Eis C, Nidetzky B. 1999. Characterization of trehalose phosphorylase from *Schizophyllum commune*. Biochem J 341:385-393.

27. Bohm G, Muhr R, Jaenicke R. 1992. Quantitative analysis of protein far UV circular dichroism spectra by neural networks. Protein Eng 5:191-195.

28. Arnold K, Bordoli L, Kopp J, Schwede T. 2006. The SWISS-MODEL workspace: a web-based environment for protein structure homology modelling. Bioinformatics 22:195-201.

29. Morris GM, Goodsell DS, Halliday RS, Huey R, Hart WE, Belew RK, Olson AJ. 1998. Automated docking using a Lamarckian genetic algorithm and an empirical binding free energy function. J Comput Chem 19:1639-1662.

30. Duan Y, Wu C, Chowdhury S, Lee MC, Xiong G, Zhang W, Yang R, Cieplak P, Luo R, Lee T, Caldwell J, Wang J, Kollman P. 2003. A point-charge force field for molecular mechanics simulations of proteins based on condensed-phase quantum mechanical calculations. J Comput Chem 24:1999-2012.

31. Brecker L, Straganz GD, Tyl CE, Steiner W, Nidetzky B. 2006. Saturation-transfer-difference NMR to characterize substrate binding recognition and catalysis of two broadly specific glycoside hy-

drolases. J Mol Catal B: Enzym 42:85-89.

32. Brecker L, Schwarz A, Goedl C, Kratzer R, Tyl CE, Nidetzky B. 2008. Studying non-covalent enzyme carbohydrate interactions by STD NMR. Carbohydr Res 343:2153-2161.

5 Chiral resolution through stereoselective transglycosylation by sucrose phosphorylase: application to the synthesis of a new biomimetic compatible solute, (*R*)-2-*O*-α-D-glucopyranosyl glyceric acid amide

Graphical abstract

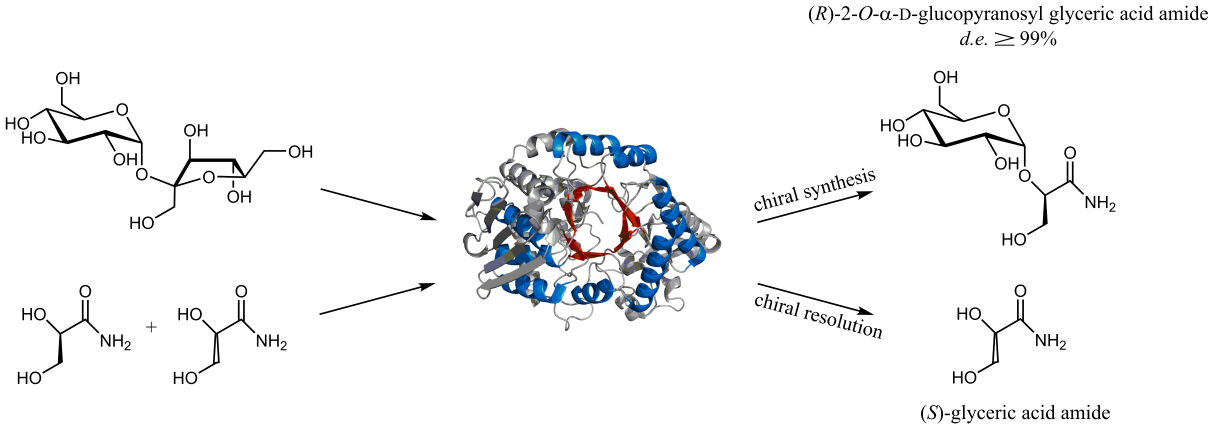

Cite this: DOI: 10.1039/c0xx00000x

www.rsc.org/xxxxxx

COMMUNICATION

Chiral resolution through stereoselective transglycosylation by sucrose phosphorylase: application to the synthesis of a new biomimetic compatible solute, (*R*)-2-*O*-α-D-glucopyranosyl glyceric acid amide

Patricia Wildberger,[a] Lothar Brecker[b] and Bernd Nidetzky*[a]

Received (in XXX, XXX) Xth XXXXXXXXX 20XX, Accepted Xth XXXXXXXXX 20XX
DOI: 10.1039/b000000x

Sucrose phosphorylase catalyses glucosylation of glyceric acid amide with complete regio- and diastereo-selectivity, giving exclusively (*R*)-2-*O*-α-D-glucopyranosyl glyceric acid amide (up to 250 mM) in near theoretical yield from a single-step transformation of racemic glyceric acid amide and sucrose. Non-productive binding of (*S*)-glyceric acid amide underlies strict enantiodiscrimination by the enzyme, thus supporting chiral resolutions based on stereoselective transglycosylation.

Biocatalytic transglycosylations constitute highly expedient transformations in synthetic organic chemistry. Transglycosylations can be applied broadly to the targeted modification of small molecules, polymers and even materials through covalent attachment of sugar moieties.[1-4] Chemically, transglycosylations proceed via transfer of a glycosyl residue from a donor glycoside onto a suitable functional group, typically an alcohol, on an acceptor substrate (Scheme 1). Biocatalytic transglycosylations usually involve robust and co-substrate-independent enzymes that utilise inexpensive donor substrates. They are therefore regarded as practical methodology of glycoside synthesis that can be applied readily across scales. A number of glycosidic products prepared through biocatalytic transglycosylation have important industrial applications in the food, cosmetic and fine-chemicals sectors.[5, 6] Despite these clear advantages, however, there exists a significant gap in the scope of biocatalytic transglycosylations, in that known enzymes are often lacking in acceptor substrate regioselectivity, stereoselectivity, or both.[7] Site-heterogeneous glycosylation of acceptor substrates offering more than a single reactive group severely restricts practicability of the method. Also, chiral resolution of racemic alcohols through diastereoselective glycosylation has not so far been a useful option for biocatalytic synthesis.

We herein provide a first-time example of enzymatic transglycosylation with complete regio- and stereo-selectivity. When offered sucrose (**1**) as glucosyl donor and racemic glyceric acid amide (**2**) as acceptor (Scheme 1), sucrose phosphorylase was highly specific for formation of (*R*)-2-*O*-α-D-glucopyranosyl glyceric acid amide (**3**) as single diastereomerically pure glucosyl transfer product. The enzymatic reaction thus supports different chiral resolution strategies for **2** in which synthesis of a structurally and stereochemically well defined glycoside **3** or recovery of unreacted acceptor (*S* enantiomer of **2**) is targeted. Based on results of molecular docking analysis we explain how sucrose phosphorylase achieves strict discrimination between *R* and *S* enantiomers of **2**. We also provide evidence on the role of the acceptor's 1,2-diol group for substrate binding recognition and positioning for regio- and stereo-selective catalytic glycosylation. Our findings suggest that sucrose phosphorylase-catalysed chiral synthesis from racemic diols (for which **2** is a representative example) could be an interesting novel strategy for application of enzymatic transglycosylations in organic synthesis. Work of Franssen and co-workers has recently shown that the enzyme promotes 2-*O*-α-D-glucosylation of various diols with useful stereoselectivity.[8] Glycoside **3** was synthesized herein for the first time. It is a close structural analogue of (*R*)-2-*O*-α-D-mannopyranosyl glyceric acid amide (**4**), also called Firoin-A, which was reported from the thermophilic bacterium *Rhodothermus marinus*. Firoin-A is an intracellular compatible solute that the organism accumulates in response to high salt environment. Firoin-A is described as a useful stabilizer of proteins in different applications, refolding processes in particular.[9]

Sucrose phosphorylase promotes transglucosylation from sucrose in a two-step catalytic mechanism, depicted in Scheme 1, that involves formation of a β-glucosyl enzyme intermediate.[10] In the natural reaction of the enzyme, phosphate is the terminal glucosyl acceptor and α-D-glucose 1-phosphate is formed. In the absence of phosphate, when an alternative acceptor alcohol is present, a new *O*-α-D-glucoside is synthesized, provided that the acceptor competes effectively with water for reaction with the enzyme intermediate. Acceptor **2** was synthesized chemically as described in the ESI (Materials). Purified sucrose phosphorylase from *Leuconostoc mesenteroides*, recombinantly produced in *Escherichia coli* as described in earlier work, was used. We incu-

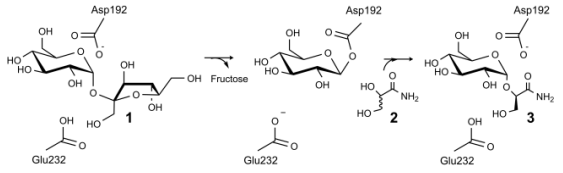

Scheme 1. Proposed mechanism of sucrose phosphorylase for kinetic resolution of **2** and chiral synthesis of **3**.

bated a mixture of **1** and **2** (each 500 mM) in the presence of enzyme (30 units of activity/mL; see the ESI for methods and reaction conditions used) and analyzed samples from the reaction mixture with liquid chromatography. Release of fructose from conversion of **1** exceeded by up to 2-fold the concurrent formation of glucose, providing indirect evidence for the occurrence of transglucosylation next to a significant hydrolysis of the enzyme intermediate. Product mixture in which about 45 - 50% of **2** had been consumed was analyzed by NMR, and Figure 1 summarizes pertinent results. The glucosylation of **2** was confirmed and it was shown that only a single main transglucosylation product had been formed in the enzymatic reaction. Identity of this product was established as 2-*O*-α-D-glucopyranosyl glyceric acid amide. The interglycosidic linkage was identified by the $^{3}J_{H\text{-}C}$ couplings determined from HMBC spectra showing interactions between the H-1 of the glycoside and C-2' of the aglycon, as well as between the C-1 of the glycoside and H-2' of the aglycon. Furthermore, the two protons in these positions have an intensive dipolar interaction, detected in the 2D NOESY spectrum. The α-anomeric form of the glucopyranosyl moiety was determined from the typical ^{13}C and ^{1}H chemical shifts as well as from the small coupling constant (3.8 Hz) between the protons in position one and two of the glycoside (Figure 1). Although the absolute configuration of C-2' could not be elucidated from the NMR data, the absent signal splitting of H-1 of the glycoside and H-2' of the aglycon strongly hinted the presence of a diasteromerically pure glycoside (*d.e.* ≥ 99%). A racemic mixture would have led to a double set of signals with slightly different chemical shifts (ESI, Figure S1).

In a next step, we applied chiroptical techniques for the determination of the transglucosylation product's absolute configuration. Due to unavailable reference data for the product, an indirect approach was chosen. Residual **2** was recovered from the reaction mixture as described in the ESI (conversion of **2** ≥ 35%) and the optical rotation $[\alpha]_D^{22}$ of the sample was determined as +15°. The significant sign of the measurement can be compared with literature where an optical rotation of $[\alpha]_D^{20}$ = –63° was reported for (*R*)-**2**.[11] A circular dichroism spectrum of the sample (ESI, Figure S2) showed only one extremum at λ = 230 nm with Δε = +15.7. Data can be compared to circular dichroism spectra of (*R*) and (*S*)-serine because serine shares some structural similarity with **2**. The *S* enantiomer of serine shows a similar positive circular dichroism band as the purified residual sample whereas the circular dichroism band of (*R*)-serine is negative.[12, 13] In summary, therefore, strong evidence is presented supporting the suggestion that **2** recovered from the reaction with sucrose phosphorylase has *S* configuration. Stereochemical structure of the glucosylation product is assigned accordingly as (*R*)-2-*O*-α-D-glucopyranosyl glyceric acid amide (**3**). Synthesis of pure **3** necessitates that sucrose phosphorylase provides complete regio- and diastereo-selectivity in the reaction with **2** which is a combination of selectivity properties not previously observed in other transglycosidase-catalysed conversions. Remaining **2** was recovered in excellent yield from the reaction (> 40%), suggesting the possibility of kinetic resolution via stereoselective transglucosylation.

To gain a molecular interpretation of the phosphorylase's remarkable selectivity, we performed energy-minimised docking studies on the high-resolution crystal structure of the enzyme (from *Bifidobacterium adolescentis*)[10] whereby the *R* and *S* enantiomers of **2** were placed flexibly into the acceptor-binding pocket of the β-glucosyl enzyme intermediate. Figure 2 illustrates the obtained best-fit binding modes for (*R*)-**2** and (*S*)-**2**. Reactive group arrangement was highly plausible for the (*R*)-**2** pose where the 2-OH was well aligned for nucleophilic attack on the glucosyl anomeric carbon, catalytically assisted by Glu-232 functioning as a general base, consistent with the proposed catalytic mechanism of the enzyme. The primary hydroxyl of (*R*)-**2** was coordinated tightly by Asp-290 and Gln-345. The amide group of (*R*)-**2** was bound weakly by comparison. For (*S*)-**2** the predicted binding mode was characterized by a conspicuously large distance between the reactive carbon and oxygen, clearly indicating that the (*S*)-**2** pose was non-productive for reaction. As in (*R*)-**2**, however, the primary hydroxyl of (*S*)-**2** was accommodated through hydrogen bonding interactions with Asp-290 and Gln-

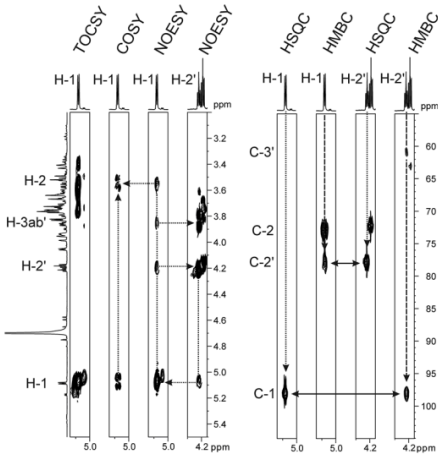

Figure 1. Details of 2D NMR spectra recorded from the reaction mixture to determine the product's glycosidic linkage. TOCSY and COSY traces of the anomeric proton H-1 allow for determination of further protons in the glycosidic moiety. The NOESY trace indicates spatial closeness of H-1 to H-2' and H-3ab' of the glyceric acid amide aglycon. Concomitant trace of H-2' is shown. HSQC and HMBC trace indicates the $^{1}J_{H\text{-}C}$ and $^{3}J_{H\text{-}C}$ couplings of H-1 and H-2', respectively. The long-range coupling over three bonds clearly indicates the glycosidic bond to be formed to the secondary alcohol of the glyceric acid amide. The signal group directly neighboured to those of H-2' belongs to the H-2 of not transformed educt.

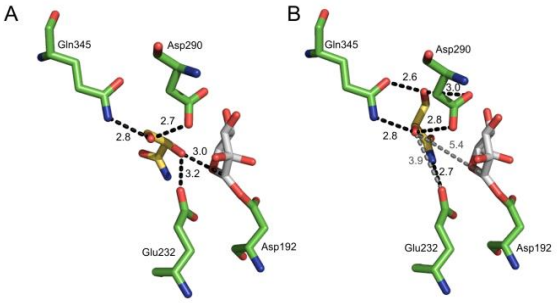

Figure 2. Best-fit docking poses for binding of (*R*)-**2** (A) and (*S*)-**2** (B) to a trapped covalent intermediate of sucrose phosphorylase having β-glucosyl residue linked to Asp-192 (PDB-entry 2gdv, molecule A).

345. Other acceptors harbouring a terminal diol moiety (Figure 3) were previously shown to be glucosylated by the enzyme with useful stereoselectivity, resulting in 2-*O*-α-D-glucosidic products of high diastereomeric purity.[8, 14] Molecular docking of (*R*)- and *S*-forms of glyceric acid and 3-methoxy-1,2-propanediol to sucrose phosphorylase underpins the observed preference for reaction with one enantiomer of the acceptor, suggesting this to be the *R*-form in each case (ESI, Figure S3). In search of an interpretable structural parameter of enzyme stereoselectivity in reactions with different acceptors, we compared reactive atom distances (glucosyl carbon and acceptor oxygen; C1…O2) in the respective (*R*)- and (*S*)-acceptor poses. The C1…O2 distance in the (*S*)-acceptor pose was highly variable across the different acceptors used (ESI; Figure S3), while the corresponding C1…O2 distance in the (*R*)-acceptor pose was constant at about 3.0 Å. The ratio of C1…O2 distance in the (*S*)- and (*R*)-acceptor pose appears to correlate to the observed diastereoselectivity of the enzyme, as shown in Figure 3. The docking data suggest that Gln-345 might be generally important for chiral recognition by the enzyme.[15, 16] Use of sucrose phosphorylase in chiral synthesis and chiral resolution strategies for diol-containing acceptor substrates is therefore supported, and this presents a new type of application for enzymatic transglycosylations. Protein engineering that has been employed widely for selectivity enhancement in esterases and lipases should be useful to improve existing (not highly selective) transglycosylation catalysts.[17]

We examined synthesis of **3** as biomimetic analogue of **4**. Reaction optimisation was complex, because antagonising effects of the concentration of **2** on formation of **3** needed to be balanced. Donor substrate hydrolysis was suppressed optimally at high concentrations of **2** (ESI, Figure S4). Release of glucose due to hydrolysis is known to cause strong product inhibition and glucose can serve as acceptor substrate to become glucosylated from the enzyme.[6] In addition, non-productive binding of (*S*)-**2** can also result in inhibition of the enzyme at high levels of racemic **2**. Figure S4 in ESI shows a full time course of synthesis of **3** when **2** was present in 2.5-fold molar excess over **1** (400 mM). Two-thirds of the offered **1** was utilized for glucosylation of (*R*)-**2** while the remainder substrate was lost to hydrolysis. Product **3** was obtained in a concentration of about 250 mM. Glucosylation of glucose occurred to a minor extent under these conditions (< 5%). Production of **3** was lowered substantially (≤140 mM) upon decreasing the concentration of **2** to 400 mM, now equaling the applied concentration of **1** (ESI, Figure S4), or when using **1** (1000 mM) in excess over **2** (400 mM). Use of **2** in excess over **1** is therefore supported. Procedures for efficient preparative work-up of reaction mixtures from sucrose phosphorylase-catalyzed transglucosylations have previously been developed.[5, 14]

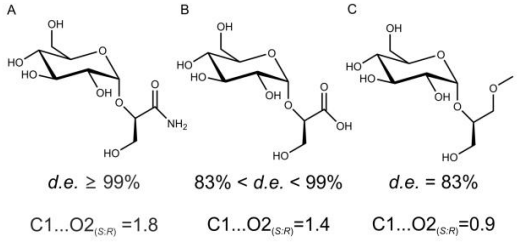

Figure 3. Diastereoselectivity of sucrose phosphorylase in the glucosylation of 1,2-diols correlated to the ratio of reactive atom distances (C1…O2) in (*S*)- and (*R*)-acceptor poses from molecular docking.

Summarizing, single-step diastereoselective glucosylation of **2** provides convenient access to the new biomimetic glycoside **3** through chiral synthesis. The same reaction could be exploited through chiral resolution to obtain (*S*)-**2**. Chiral 1,2-diols are important target molecules in organic chemistry, and their preparation through chiral resolution is therefore of considerable interest.[18] Relying on the selectivity of enzymes, biocatalytic glycosylation might present a useful alternative to reported two-step esterification processes catalysed by lipases/esterases.[19]

We acknowledge financial support from the Austrian Science Funds FWF (project L586-B03); V. N. Belov (Max Planck Institute for Biophysical Chemistry, Goettingen, Germany) for synthesis of **2**; S. Felsinger (Institute of Organic Chemistry, University of Vienna, Austria) for recording several NMR spectra; and C. Araman and N. K. Chu (Institute of Biological Chemistry, University of Vienna, Austria) for help in recording CD spectra.

Notes and references

[a] *Institute of Biotechnology and Biochemical Engineering, Graz University of Technology, Petersgasse 12/1, A-8010 Graz, Austria; E-mail:bernd.nidetzky@tugraz.at*

[b] *Institute of Organic Chemistry, University of Vienna, Währingerstraße 38, A-1090 Vienna, Austria*

† Electronic Supplementary Information (ESI) available: [Experimental procedures used; NMR spectra of **3**; CD spectrum of residual **2** isolated from reaction mixture; docking poses of *R* and *S*-forms of 1,2-diol acceptors stereoselectively glucosylated by sucrose phosphorylase; time course of synthesis of **3**]. See DOI: 10.1039/b000000x/

1. P. Bojarova, R. R. Rosencrantz, L. Elling and V. Kren, *Chem Soc Rev* 2013, **42**, 4774-4497.
2. T. Desmet, W. Soetaert, P. Bojarova, V. Kren, L. Dijkhuizen, V. Eastwick-Field and A. Schiller, *Chem Eur J*, 2012, **18**, 10786-10801.
3. J. Kadokawa, *Chem Rev*, 2011, **111**, 4308-4345.
4. C. A. Weijers, M. C. Franssen and G. M. Visser, *Biotechnol Adv*, 2008, **26**, 436-456.
5. C. Goedl, T. Sawangwan, M. Mueller, A. Schwarz and B. Nidetzky, *Angew Chem Int Ed Engl*, 2008, **47**, 10086-10089.
6. C. Luley-Goedl, T. Sawangwan, L. Brecker, P. Wildberger and B. Nidetzky, *Carbohyr Res*, 2010, **345**, 1736-1740.
7. F. van Rantwijk, M. W. V. Oosterom and R. A. Sheldon, *J Mol Catal B: Enzym*, 1999, **6**, 511-532.
8. R. Renirie, A. Pukin, B. van Lagen and M. C. R. Franssen, *J Mol Catal B: Enzym*, 2010, **67**, 219-224.
9. G. Lentzen and T. Schwarz, *Appl Microbiol Biotechnol*, 2006, **72**, 623-634 (and references therein).
10. O. Mirza, L. K. Skov, D. Sprogøe, L. A. van den Broek, G. Beldman, J. S. Kastrup and M. Gajhede, *J Biol Chem*, 2006, **281**, 35576-35584.
11. P. F. Frankland, F. M. Whartin and H. Aston, *J Chem Soc*, 1901, **79**, 266-274.
12. W. Gaffield, *Chem Ind*, 1964, 1460-1461.
13. E. Iizuka and J. T. Yang, *Biochemistry*, 1964, **3**, 1519-1524.
14. T. Sawangwan, C. Goedl and B. Nidetzky, *Org Biomol Chem*, 2009, **7**, 4267-4270.
15. C. Luley-Goedl and B. Nidetzky, *Carbohydr Res*, 2010, 1492-1496.
16. T. Verhaeghe, M. Diricks, D. Aerts, W. Soetaert and T. Desmet, *J Mol Catal B: Enzym*, 2013, **96**, 81-88.
17. U. T. Bornscheuer, *Curr Opin Biotechnol*, 2002, **13**, 543-547.
18. Y. Zhao, A. W. Mitra, A. H. Hoveyda and M. L. Snapper, *Angew Chem Int Ed Engl*, 2007, **46**, 8471-8474.
19. F. Theil, J. Weidner, S. Ballschuh, A. Kunath and H. Schick, *J Org Chem*, 1994, **59**, 388-393.

SUPPLEMENTARY INFORMATION FOR

Chiral resolution through stereoselective transglycosylation by sucrose phosphorylase: application to the synthesis of a new biomimetic compatible solute, (*R*)-2-*O*-α-D-glucopyranosyl glyceric acid amide

Patricia Wildberger[a], Lothar Brecker[b] and Bernd Nidetzky[a,*]

[a] Institute of Biotechnology and Biochemical Engineering, Graz University of Technology, Petersgasse 12/1, A-8010 Graz, Austria

[b] Institute of Organic Chemistry, University of Vienna, Währingerstraße 38, A-1090 Vienna, Austria

*Corresponding author

E-mail: bernd.nidetzky@tugraz.at; Tel. +43-316-873-8400; Fax +43-316-873-8434

Chemicals and reagents

Glyceric acid amide was prepared from commercially available 2,3-dihydroxypropanoic acid (40% solution in water; TCI Europe nv, Antwerp, Belgium), which was dissolved in methanol and methylated with an excess of the etheral solution of diazomethane. Methyl 2,3-dihydroxy-propanoate was isolated from the concentrated reaction mixture and purified by column chromatography on silica gel with chloroform-methanol mixture as eluent. Then, methyl 2,3-dihydroxypropanoate was dissolved in methanol, and an equal volume of 25 - 28% aq. NH_3 was added to this solution. The reaction mixture was kept overnight at room temperature, concentrated in vacuo, and the residue was crystallized from water (from concentrated solution). No impurities have been determined in the ^{1}H NMR spectrum, indicating a glyceric acid amide purity of $> 97\%$.

Glyceric acid amide: ^{1}H NMR (D_2O, 600.13 MHz): δ 4.16 (dd, J = 4.8, 3.6 Hz, 1H, H-2), 3.75 (dd, J = 12.0, 3.6 Hz, 1H, H-3a), 3.73 (dd, J = 12.0, 4.8 Hz, 1H, H-3b). ^{13}C NMR (D_2O, 150.90 MHz): 177.5 (C-1), 72.0 (C-2), 63.1 (C-3).

All other chemicals used were of highest purity available from Sigma-Aldrich (Vienna, Austria) or Roth (Karlsruhe, Germany).

Biocatalyst production

Recombinant wild-type sucrose phosphorylase from *Leuconostoc mesenteroides*, encoded in pASK-IBA7+ (IBA GmbH) (1), was produced in *Escherichia coli* BL21-Gold(DE3) and purified to apparent homogeneity according to reported procedures (2). Enzymatic activity of the purified preparation was determined at 30°C using a continuous coupled enzymatic assay with phosphoglucomutase and glucose-6-phosphate dehydrogenase (3). Protein concentration of the purified preparation was measured with the BioRad dye-binding method referenced against BSA.

Product identification

For product identification by NMR analysis, 30 U/mL of sucrose phosphorylase (specific activity: 100 U/mg) were incubated with equimolar concentrations (500 mM) of sucrose and a racemic mixture of glyceric acid amide for 24 h and the content of the mixture was lyophilized and analyzed as described under NMR measurements.

The resulting spectra indicate a complete transformation of sucrose. Analysis also indicates the presence of fructose (1.00 eq., mixture of both isomers), glucose (0.50 eq., mixture of both isomers), four not further identified disaccharides (in sum $<$ 0.05 eq.), glyceric acid amide (0.55 eq.), and (*R*)-2-*O*-*α*-

D-glucopyranosyl glyceric acid amide (0.45 eq.).

(*R*)-2-*O*-*α*-D-glucopyranosyl glyceric acid amide (determined from crude reaction mixture): ^{1}H NMR (D_2O, 400.13 MHz): δ 5.08 (d, J = 3.8 Hz, 1H, H-1), 4.21 (dd, J = 4.2, 3.7 Hz, 1H, H-2'), 3.97 (dd, J = 12.2, 2.5 Hz, 1H, H-6a), 3.94 (m, 1H, H-5), 3.88 (dd, J = 12.4, 3.7 Hz, 1H, H-3a'), 3.82 (dd, J = 12.4, 4.2 Hz, 1H, H-3b'), 3.75 (dd, J = 9.8, 9.9 Hz, 1H, H-3), 3.65 (dd, J = 12.2, 4.5 Hz, 1H, H-6b), 3.56 (dd, J = 9.8, 3.8 Hz, 1H, H-2), 3.39 (dd, J = 9.9, 9.5 Hz, 1H, H-4). ^{13}C NMR (D_2O, 100.61 MHz): 174.9 (C-1'), 98.2 (C-1), 77.9 (C-2'), 72.8 (C-3), 71.6 (C-2), 69.6 (C-5), 69.5 (C-4), 63.7 (C-6), 60.8 (C-3').

High performance anion exchange chromatography with pulsed amperometric detection (HPAE-PAD)

HPAE-PAD was performed using a Dionex BioLC system (Dionex Corporation, Sunnyvale, USA) equipped with a CarboPac PA10 column (4 x 250 mm) and an Amino Trap guard column (4 x 50 mm). Glucose, fructose, sucrose, (*R*)- and (*S*)-glyceric acid amide and (*R*)-2-*O*-*α*-D-glucopyranosyl glyceric acid amide were detected with an ED50A electrochemical detector using a gold working electrode and a silver/silver chloride reference electrode by applying the predefined waveform for carbohydrates. Elution was carried out at a flow rate of 0.3 mL/min at an isocratic flow of 52 mM NaOH for 50 min. Under the conditions applied, the following retention times were obtained: 3.0 min for (*R*)- and (*S*)-glyceric acid amide, 25.4 min for glucose, 28.8 min for fructose and 41.2 min for sucrose. Authentic standards for glucose, fructose and sucrose were used for peak identification and quantification was based on peak area that was suitably calibrated with standards of known concentration dissolved in 50 mM MES buffer pH 7.0. The two enantiomers of glyceric acid amide co-eluted in the analysis and could neither separated nor quantified by using the described procedure. The formation of (*R*)-2-*O*-*α*-D-glucopyranosyl glyceric acid amide was indicated by the appearance of a shoulder (on the right) of the acceptor peak, but could not be quantified directly from the HPAE-PAD chromatogram. The concentration of (*R*)-2-*O*-*α*-D-glucopyranosyl glyceric acid amide was therefore determined indirectly from the difference in the concentration of fructose and glucose. Release of fructose paralleled the consumption of sucrose; the formation of glucose indicated that glucosylated sucrose phosphorylase had also reacted with water. The portion of sucrose utilised for transglucosylation was assumed to have resulted in glucosylation of (*R*)-glyceric acid amide. Results of NMR analysis support the assumption. However, minor formation of disaccharide by-products ($< 5\%$) was not considered in the analysis of the HPAE-PAD data.

NMR measurements

The reaction mixture was dissolved in D_2O (99.95%, 0.7 mL) and transferred into 5 mm NMR sample tubes (Promochem, Wesel, Germany). Spectra were measured with Topspin 3.1 on Bruker DRX-400 AVANCE or AV-III 600 (Bruker, Rheinstetten, Germany). Measurement frequencies were 400.13 MHz and 100.61 MHz for ^{1}H and ^{13}C, respectively, or 600.13 MHz and 150.90 MHz for ^{1}H and ^{13}C, respectively. Measurement temperature was 298.1 $\pm$ 0.1 K. For the 1D proton spectrum 32k data points were recorded and Fourier transformed to spectra with a range of 6,000 Hz (^{1}H). 2D DQF-COSY, TOCSY, NOESY, HMQC, and HMBC spectra were measured by 256 experiments with 1,024 data points each. Appropriate linear forward prediction, sinusoidal multiplication and Fourier transformation led to 2D-spectra with a range of 4,800 Hz and 20,000 Hz for ^{1}H and ^{13}C, respectively. Acetone was used as external standard for ^{1}H (δH 2.225) and ^{13}C (δC 30.89) spectra.

Molecular Docking

AutoDock 4.2 (4) as implemented in Yasara V 11.11.21 was used for the enzyme-ligand docking. The AMBER03 force field (5) and the default parameters provided by the standard docking macro were used, except that the number of runs was increased to 40. The X-ray crystal structure of sucrose phosphorylase from *Bifidobacterium adolescentis* having a β-glucosyl enzyme intermediate linked to Asp192 (pdb entry 2gdv, molecule A) (6) was used as macromolecule in a molecular docking experiment that employed (*R*)- and (*S*)-glyceric acid amide, the protonated form of (*R*)- and (*S*)-glyceric acid and (*R*)- and (*S*)-3-methoxy-1,2-propanediol, respectively, as ligand. The 3D coordinates for the ligands were generated from SMILES strings using Chimera (http://www.cgl.ucsf.edu/chimera). The ligands were flexibly placed into the active site of sucrose phosphorylase. A search space of 10 x 10 x 10 Å around the C1 atom of the glucosyl moiety of the β-glucosyl enzyme intermediate was used. The docking algorithm resulted in 3 binding modes for (*R*)-glyceric acid amide, 2 for (*R*)- and (*S*)-glyceric acid as well as for (*R*)- and (*S*)-3-methoxy-1,2-propanediol and in 1 binding mode for (*S*)-glyceric acid amide. In case the docking algorithm resulted in more than 1 binding mode, the binding modes had comparable energies. Best-fit binding modes were selected on the basis of reactive-group arrangement. Distances between the C2-OH of the ligand to the anomeric carbon of the β-glucosyl residue and distances between the C2-OH of the ligand to the oxygen of the ionized side chain of Glu232 were determined in all cases. Based on the distances determined, the binding modes in which the accommodation of the ligand appeared to be highly plausible for catalysis were selected. The criterions for the selection comprised that the distance of the reactive 2-OH of the acceptor to the catalytic base (Glu232) was $\leq$ 3.2

Å and that the distance of the reactive 2-OH of the acceptor to the anomeric carbon of the β-glucosyl residue was $\leq$ 3.1 Å. PyMOL (http://pymol.sourceforge.net) was used for visualization.

Isolation of the residual educt from the reaction mixture

400 mM sucrose were incubated with 400 mM of a racemic mixture of glyceric acid amide in the presence of 7 U/mL sucrose phosphorylase in 50 mM MES, pH 7.0 at 550 rpm for 65 h. The residual educt was isolated from the reaction mixture on a Shimadzu CTO-20AC system equipped with an Aminex HPX-87C column (Bio-Rad, Vienna, Austria) that was operated at 75°C. Deionized water was the mobile phase and was applied at a constant flow rate of 0.3 mL/min. Refractive index detection (Shimadzu RID-10A) was used for all compounds. Under the conditions applied, the following retention times were obtained: 17.2 min for sucrose, 20.7 min for glucose, 26.9 min for fructose and 36.8 min for the residual glyceric acid amide. The reaction product co-eluted with sucrose. Samples containing the purified residual educt were pooled. The presence of the purified residual educt and the removal of all other components were shown by HPAE-PAD and further proved by NMR analysis. A ^{1}H NMR spectrum was recorded to confirm that no organic impurities have been present. Hence no further optical active impurities influenced chiroptic measurements.

Optical rotatory dispersion and circular dichroism (CD) spectroscopy

The purified residual educt was then subjected to an optical rotation measurement. For that purpose, the purified residual educt was lyophilized, dissolved in methanol and the optical rotation was determined by using a Perkin Elmer Automatic Polarimeter 241 (Perkin Elmer Austria GmbH, Vienna, Austria). Data were recorded at the sodium D line using a 100 mm path length cell. Results are reported as $[\alpha]_{D,}^{T}$, concentration (g/100 mL, CH_3OH).

Far-UV CD spectra were recorded at 25°C on an Applied Photophysics Chirascan Plus system (Applied Photophysics Ltd, Surrey, UK). The purified residual educt was diluted in acetonitrile to a final concentration of 50 mM. CD spectra were collected at a scan speed of 20 nm/min at 1 nm bandwidth and response time of 4 s. All spectra were recorded in a 0.1 cm cuvette between 180 nm and 300 nm. The data shown are the average of 10 recorded spectra.

Reaction optimization

To find conditions in which glucosyl transfer to (*R*)-glyceric acid amide is favored over hydrolysis, three time-profiles were recorded in which sucrose and a racemic mixture of glyceric acid amide were

present in the following concentrations: 1) 400 mM sucrose and 1,000 mM glyceric acid amide, 2) equimolar concentrations of sucrose and glyceric acid amide (400 mM each) and 3) 1,000 mM sucrose and 400 mM glyceric acid amide. The reactions were started by addition of 7 U/mL purified sucrose phosphorylase. Incubations were performed in 50 mM MES, pH 7.0 using an Eppendorf Thermomixer comfort set at 30°C and an agitation rate of 550 rpm. Samples were taken after appropriate time intervals for up to 48 h, heat-treated (at 99°C for 5 min) to inactivate the enzyme and centrifuged at 13,000 rpm for 10 min to remove precipitated protein prior to further analysis. Quantification of substrate consumption and product formation was done like described (section: HPAE-PAD); the presence of the reaction product was verified by NMR analysis.

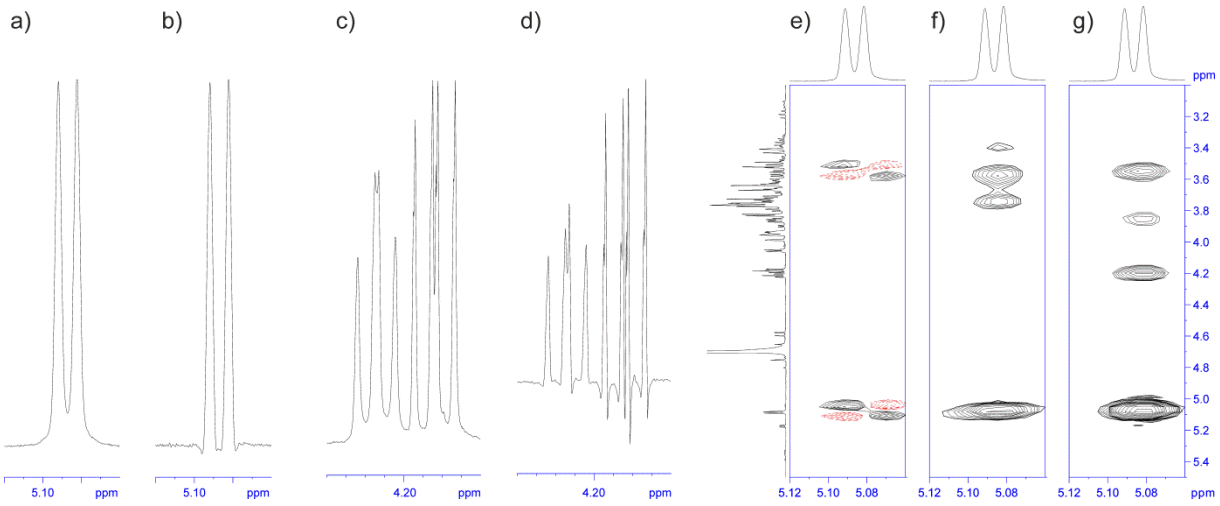

Supplementary Figure S1. 1D and 2D homonuclear proton spectra of the reaction mixture obtained upon conversion of 500 mM sucrose and 500 mM glyceric acid amide. The conversion of glyceric acid amide was about 45%. The data are consistent with exclusive formation of one diastereomer resulting from glucosylation of glyceric acid amide.

All signals of the product recorded from crude reaction mixture do not show any shoulder. Additionally no further signals are present. Hence there is no indication for the presence of a second diastereomer. (a) Proton signal H-1 of the glycoside after direct Fourier transformation showing Lorentzian line shape signal group without presence of any additional signals and shoulders, which would indicate the presence of a second diastereomer. (b) Proton signal H-1 of the glycoside after Gaussian multiplication (LB = -0.3; GB = 0.2) and Fourier transformation leading to narrower line width at half height. There is also no indication for a second signal. (c) Proton signal H-2′ of the glycoside as well as proton signal of the free glyceric acid amide after direct Fourier transformation showing Lorentzian line shape signal group without any additional signals and shoulders, which would indicate a second diastereomer. (d) Proton signal H-2′ of the glycoside as well as proton signal of the free glyceric acid amide after Gaussian multiplication (line broadening factor (LB) = -0.3; Gaussian broadening factor (GB) = 0.2) and Fourier transformation leading to narrower line width at half height. There is also no indication for a second signal. (e) DQF-COSY trace of proton signal H-1 of the glycoside indicating the diagonal peak and the cross peak, which shows the coupling to H-2. (f) TOCSY (100 ms mixing time) trace of proton signal H-1 of the glycoside, which indicates all protons in the glycoside spin system. (g) NOESY (800 ms mixing time) trace of proton signal H-1 of the glycoside. It indicates the spatial closeness to other protons, in particular to H-2′ of the aglycon moiety.

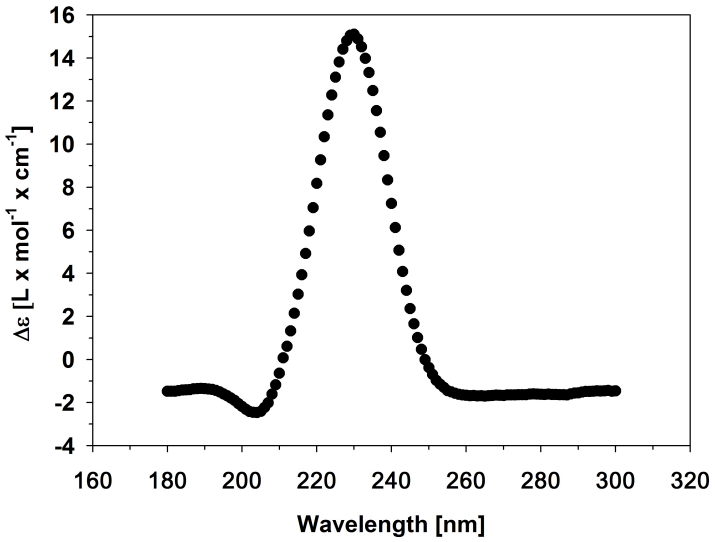

Supplementary Figure S2. The CD-spectrum of the purified residual educt is shown.

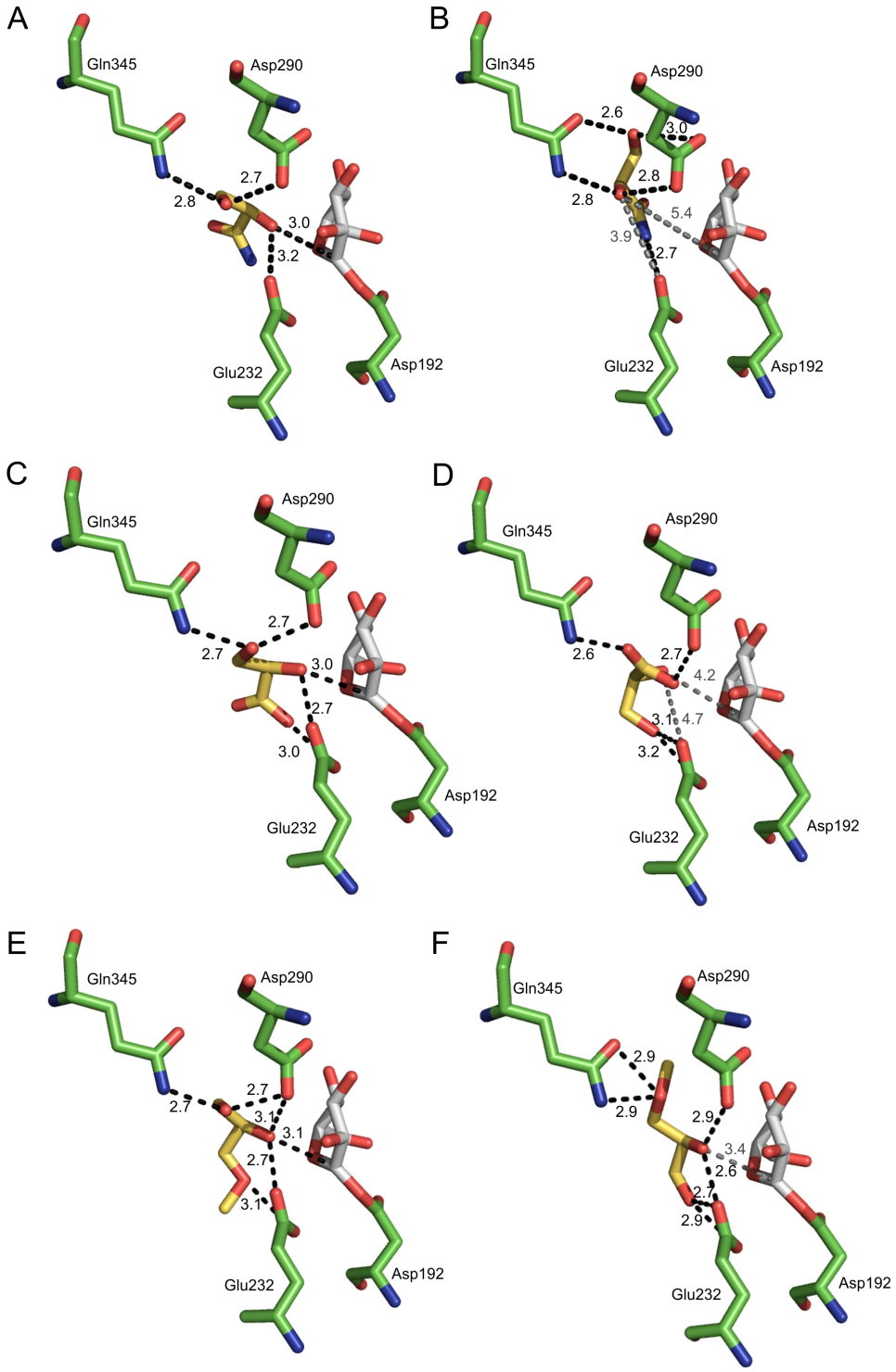

Supplementary Figure S3. Close-up view of predicted best-fit molecular docking poses of (*R*,*S*)-glyceric acid amide (A, B), (*R*,*S*)-glyceric acid (C, D) and (*R*,*S*)-3-methoxy-1,2-propanediol (E, F) with the β-glucosyl enzyme intermediate of sucrose phosphorylase (pdb entry 2gdv, molecule A). Hydrogen bonds ($\leq$ 3.2 Å) are shown as black-dashed lines. Interactions potentially relevant for catalysis are

shown as gray-dashed lines. Distances are given in Å.

Note: When glyceric acid was employed as ligand, the docking experiment was performed with the protonated and deprotonated form of the *R* and *S*-enantiomer of glyceric acid. The protonated form of both enantiomers resulted in higher binding energies (up to 1.9 kcal/mol), assuming that the protonated form of glyceric acid is the preferred form. The docking results presented here employed the protonated form of the *R* and *S*-enantiomer of glyceric acid as ligand.

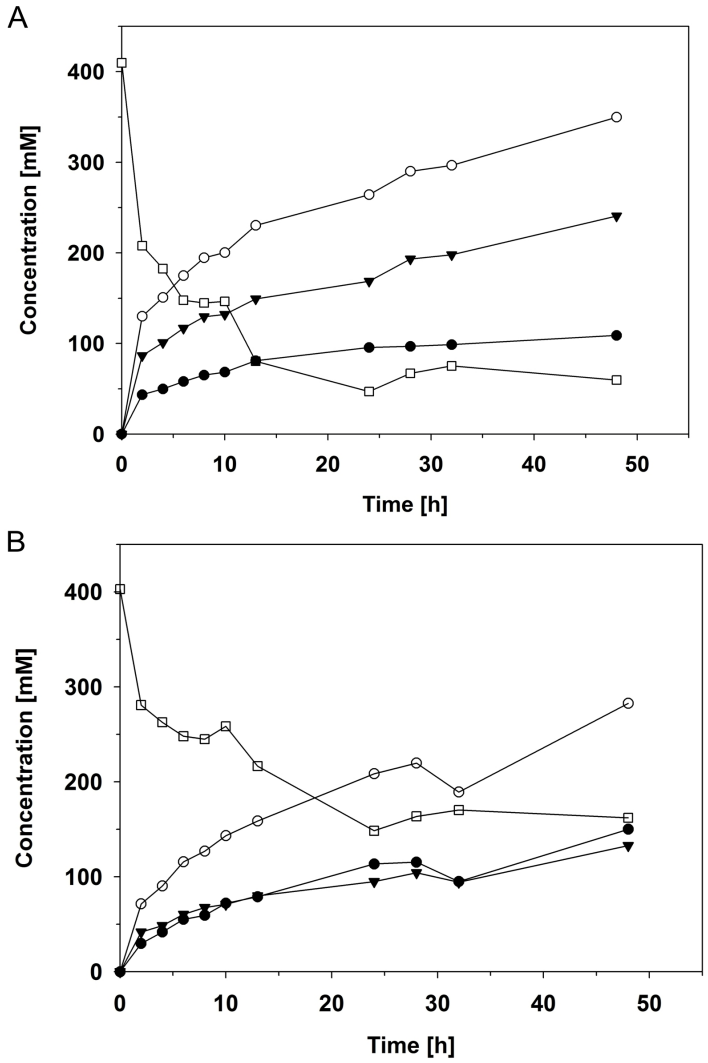

Supplementary Figure S4. Time courses for the enzymatic synthesis of (*R*)-2-*O*-*α*-D-glucopyranosyl glyceric acid amide from 400 mM sucrose and 1,000 mM glyceric acid amide (A) and equimolar concentrations of sucrose and glyceric acid amide (400 mM, B), respectively. The symbols indicate sucrose (□), fructose (○), glucose (●) and (*R*)-2-*O*-*α*-D-glucopyranosyl glyceric acid amide (▼).

References

1. Wildberger P, Luley-Goedl C, Nidetzky B. 2011. Aromatic interactions at the catalytic subsite of sucrose phosphorylase: their roles in enzymatic glucosyl transfer probed with Phe52 → Ala and Phe52 → Asn mutants. FEBS Lett 585:499-504.

2. Wildberger P, Todea A, Nidetzky B. 2012. Probing enzyme-substrate interactions at the catalytic subsite of *Leuconostoc mesenteroides* sucrose phosphorylase with site-directed mutagenesis: the roles of Asp49 and Arg395. Biocatal Biotransform 30:326-337.

3. Goedl C, Schwarz A, Minani A, Nidetzky B. 2007. Recombinant sucrose phosphorylase from *Leuconostoc mesenteroides*: characterization, kinetic studies of transglucosylation, and application of immobilised enzyme for production of α-D-glucose 1-phosphate. J Biotechnol 129:77-86.

4. Morris GM, Goodsell DS, Halliday RS, Huey R, Hart WE, Belew RK, Olson AJ. 1998. Automated docking using a Lamarckian genetic algorithm and an empirical binding free energy function. J Comput Chem 19:1639-1662.

5. Duan Y, Wu C, Chowdhury S, Lee MC, Xiong G, Zhang W, Yang R, Cieplak P, Luo R, Lee T, Caldwell J, Wang J, Kollman P. 2003. A point-charge force field for molecular mechanics simulations of proteins based on condensed-phase quantum mechanical calculations. J Comput Chem 24:1999-2012.

6. Mirza O, Skov LK, Sprogøe D, van den Broek LA, Beldman G, Kastrup JS, Gajhede M. 2006. Structural rearrangements of sucrose phosphorylase from *Bifidobacterium adolescentis* during sucrose conversion. J Biol Chem 281:35576-35584.

6 Examining the role of phosphate in glycosyl transfer reactions of *Cellulomonas uda* cellobiose phosphorylase using D-glucal as donor substrate

Graphical abstract

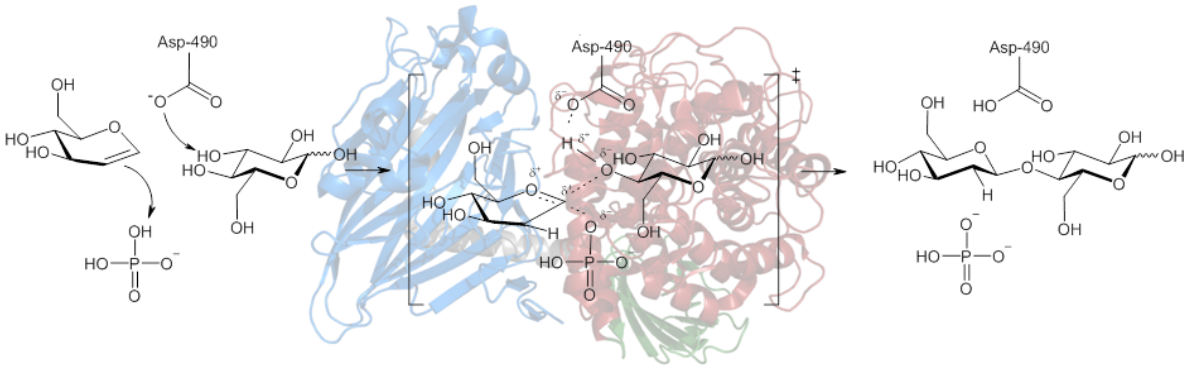

Highlights

- Cellobiose phosphorylase (from *Cellulomonas uda*) catalyzes transfer of 2-deoxy-D-glucosyl from glucal to phosphate in a single-step transformation.
- The resulting 2-deoxy-α-D-glucose 1-phosphate is difficult to synthesize chemically.
- Proposed enzymatic mechanism involves direct protonation of glucal by enzyme-bound phosphate.
- Proton transfer occurs from below the substrate ring in a *re* side attack on C2.
- Catalytic concentration of phosphate stimulate regioselective 2-deoxy-D-glucosyl transfer from glucal to the 4-hydroxyl of glucose.

Carbohydrate Research 356 (2012) 224–232

Contents lists available at SciVerse ScienceDirect

Carbohydrate Research

journal homepage: www.elsevier.com/locate/carres

Examining the role of phosphate in glycosyl transfer reactions of *Cellulomonas uda* cellobiose phosphorylase using D-glucal as donor substrate

Patricia Wildberger [a], Lothar Brecker [b], Bernd Nidetzky [a,*]

[a] Institute of Biotechnology and Biochemical Engineering, Graz University of Technology, Petersgasse 12/1, A-8010 Graz, Austria
[b] Institute of Organic Chemistry, University of Vienna, Währingerstraße 38, A-1090 Vienna, Austria

ARTICLE INFO

Article history:
Received 1 March 2012
Received in revised form 3 April 2012
Accepted 4 April 2012
Available online 13 April 2012

Keywords:
Cellobiose phosphorylase
Glycoside hydrolase family GH-94
D-Glucal
Catalytic mechanism
Stereospecific protonation
2-Deoxy-D-glucosyl transfer

ABSTRACT

Cellobiose phosphorylase from *Cellulomonas uda* (*Cu*CPase) is shown to utilize D-glucal as slow alternative donor substrate for stereospecific glycosyl transfer to inorganic phosphate, giving 2-deoxy-α-D-glucose 1-phosphate as the product. When performed in D_2O, enzymatic phosphorolysis of D-glucal proceeds with incorporation of deuterium in equatorial position at C-2, implying a stereochemical course of reaction where substrate becomes protonated from below its six-membered ring through stereoselective *re* side attack at C-2. The proposed catalytic mechanism, which is supported by results of docking studies, involves direct protonation of D-glucal by the enzyme-bound phosphate, which then performs nucleophilic attack on the reactive C-1 of donor substrate. When offered D-glucose next to D-glucal and phosphate, *Cu*CPase produces 2-deoxy-β-D-glucosyl-(1→4)-D-glucose and 2-deoxy-α-D-glucose 1-phosphate in a ratio governed by mass action of the two acceptor substrates present. Enzymatic synthesis of 2-deoxy-β-D-glucosyl-(1→4)-D-glucose is effectively promoted by catalytic concentrations of phosphate, suggesting that catalytic reaction proceeds through a quaternary complex of *Cu*CPase, D-glucal, phosphate, and D-glucose. Conversion of D-glucal and phosphate presents a convenient single-step synthesis of 2-deoxy-α-D-glucose 1-phosphate that is difficult to prepare chemically.

1. Introduction

Cellobiose phosphorylase (CPase; EC 2.4.1.20) catalyzes reversible phosphorolysis of cellobiose into α-D-glucose 1-phosphate and D-glucose.[1] Like the majority of known disaccharide phosphorylases, CPase is an inverting enzyme that forms a glycosidic product having the opposite anomeric configuration as the substrate.[2] The stereochemical course of cellobiose conversion involves a β-to-α change in anomeric configuration, proposed to result from a single displacement-like reaction that produces an equatorial-to-axial substitution at the anomeric carbon.[3] The canonical catalytic mechanism of enzymatic glycosyl transfer with inversion (used by glycoside hydrolases, for example) involves a pair of acidic residues, typically Asp or Glu, that are positioned in the active site so that one can function as the general catalytic acid and the other as the general catalytic base.[4,5] CPase is thought to employ a modified version of this mechanism, in which only one catalytic residue (Asp) is used, and this has the role of a general acid.[2] Since the acceptor substrate, phosphate, is already ionized at physiological pH, it does not need to be activated by deprotonation from a catalytic base, therefore explaining the absence of a corresponding residue in the CPase active site. CPase crystal structures reveal a distinct phosphate recognition site in the enzyme, rich in positively charged amino acids (Fig. 1b). Once accommodated at this site, phosphate is optimally positioned for direct nucleophilic attack on the glycosidic carbon of cellobiose (Scheme 1).

In an original classification based on sequence analysis, CPase was classified as a member of the glycosyltransferase families and further categorized into family GT-36. This classification, which is in accordance with CPase catalytic function of glucosyl transfer to and from phosphate, as also reflected in the EC number, needed to be revised when the first crystal structure of an enzyme from the CPase group, *Vibrio proteolyticus* chitobiose phosphorylase (*Vb*ChPase), became available.[6] Evidence that *Vb*ChPase was structurally similar to certain glycoside hydrolases, in particular to maltose phosphorylase and glucoamylase from glycoside hydrolase family GH-65 and GH-15, respectively, necessitated reclassification of CPase as a glycoside hydrolase, forming a new family GH-94.[6] It is worth noting therefore that CPase enzymes usually show no or just scant glycoside hydrolase activity. As of today, family GH-94 consists of four principal members, CPase (EC 2.4.1.20), cellodextrin phosphorylase (EC 2.4.1.49), ChPase (EC 2.4.1.-), and cyclic β-1,2-glucan synthase (EC 2.4.1.-) (http://www.cazy.org/CAZY). Among individual enzymes belonging to family GH-94, CPase from *Cellvibrio gilvus* (*Cg*CPase) is the one most extensively studied.[7–9] Two crystal structures of *Cg*CPase are available, one containing

* Corresponding author. Tel.: +43 316 873 8400; fax: +43 316 873 8434.
E-mail address: bernd.nidetzky@tugraz.at (B. Nidetzky).

0008-6215/$ - see front matter © 2012 Elsevier Ltd. All rights reserved.
http://dx.doi.org/10.1016/j.carres.2012.04.003

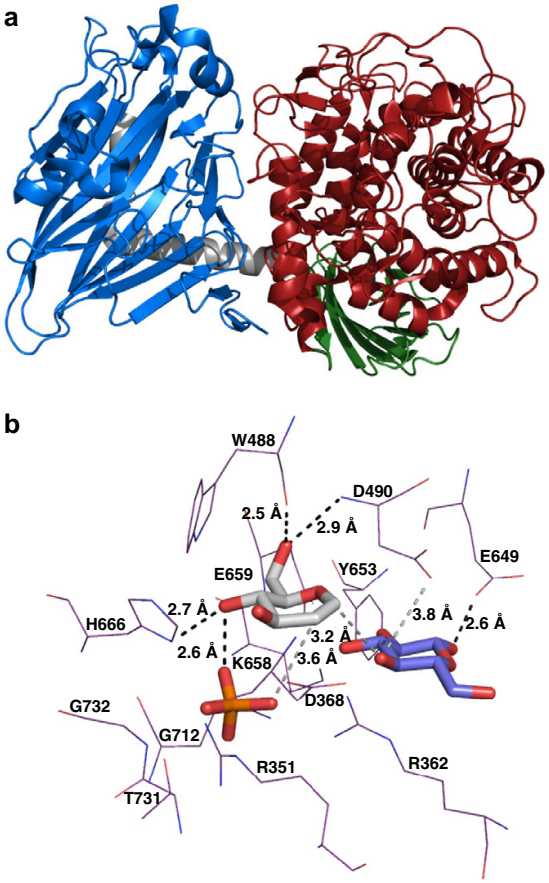

Figure 1. (a) Three-dimensional fold of the protein subunit of *Cg*CPase (PDB-entry 2cqt, molecule B). *Cg*CPase consists of an N-terminal domain (blue), linker helices (gray), an α-helix barrel domain (red), and a C-terminal domain (green). (b) Close-up view of the predicted binding of D-glucal (gray) in subsite -1 of *Cg*CPase (PDB-entry 2cqt, molecule B) complexed with phosphate (orange) and D-glucose (purple) in subsite +1. Interactions potentially relevant for catalysis and the reaction are shown as gray-dashed lines, and strong hydrogen bonds stabilizing the quaternary complex are shown as black-dashed lines. (For interpretation of the references to colour in this figure legend, the reader is referred to the web version of this article.)

sulfate (PDB-entry 2cqs) and one containing phosphate (PDB-entry 2cqt) at the catalytic site.[2] The structure of *Cg*CPase monomer is shown in Figure 1a and consists of four distinct regions: an N-terminal domain, a helical linker region, an α-helix barrel domain, and a C-terminal domain.

The substrate specificity of CPase has been examined in a number of biochemical studies using enzymes from different sources.[1,10–12] It was convenient to analyze the reverse direction of reaction where a glycosyl residue is transferred from sugar 1-phosphate donor to acceptor. The various CPases are similar in that relatively relaxed specificity for the acceptor substrate is contrasted with highly restricted use of glycosyl donors.[7,13] Two relevant examples of active donor substrate analogues are α-D-glucose 1-fluoride[14] and α-D-galactose 1-phosphate.[15] Note that ChPase has of course different structural requirements to its donor substrate as compared to CPase where in particular 2-hydroxyl in α-D-glucose 1-phosphate is replaced by 2-acetamido in α-D-*N*-acetylglucosamine 1-phosphate.[6] In a recent paper, Kitaoka and co-workers reported the interesting observation that the endocyclic enitol D-glucal was accepted by *Cg*CPase as donor substrate for 2-deoxy-glucosyl transfer to D-glucose and other sugar acceptors (e.g. D-xylose, D-mannose) used normally in the reaction with α-D-glucose 1-phosphate.[16] They also demonstrated the transfer products to have β-(1→4) glycosidic structure. Using *Cellulomonas uda* CPase (*Cu*CPase), Nidetzky and co-workers had earlier examined reactivity toward D-glucal as donor substrate for glycosyl transfer to phosphate or D-glucose but were unable to detect any.[14] Inspired by Kitaoka's findings, the topic of utilization of D-glucal was therefore revisited herein, and we would like to communicate results of a comprehensive analysis that provide deepened insight into the underlying reaction mechanism. We in particular clarify the role of phosphate in promoting the enzymatic reaction with D-glucal and show that depending on reaction conditions used, D-glucal serves as donor substrate for 2-deoxy-D-glucosyl transfer to phosphate or sugar acceptor. Requirement for phosphate to essentially 'activate' *Cu*CPase reaction with D-glucal explains negative findings of our previous experiments that in direction of disaccharide synthesis were all performed in the absence of phosphate. In addition, the amount of native enzyme (isolated from the natural host *C. uda*) and the analytical method used (TLC) may have been insufficient for identification of D-glucal as donor substrate for phosphorolysis. We herein also show that conversion of D-glucal in the presence of phosphate constitutes a convenient single-step method for preparation of 2-deoxy-α-D-glucose 1-phosphate (**1**) that is difficult to synthesize chemically.

In chemical terms, D-glucal and related glycals are characterized as 1,2-unsaturated derivatives of pentoses or hexoses. These compounds have been widely used as mechanistic probes for study of glycoside hydrolases and phosphorylases.[17–23] Their unique feature of structure and function lies in the half-chair conformation of the typically six-membered ring that contains a highly reactive double bond between C-1 and C-2. It is known from seminal work

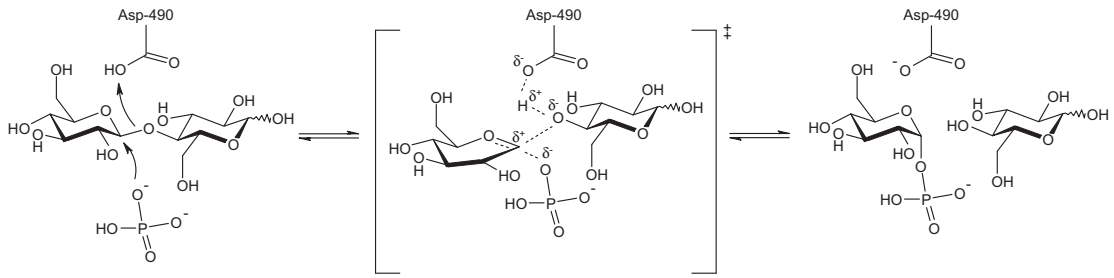

Scheme 1. Proposed catalytic mechanism of *Cu*CPase. Asp^{490} is thought to adopt the catalytic role of a general acid and base in direction of cellobiose phosphorolysis and synthesis, respectively. See Ref. 2 for a detailed discussion.

of Hehre, Lehmann, Legler and their co-workers performed as early as the 1970s that glycals are substrates to become hydrated by many glycoside hydrolases.[18,24,25] D-Glucal is utilized by α-glucosidase from *Candida tropicalis* and β-glucosidase from sweet almond.[18] Disaccharide analogues of maltose (maltal) and cellobiose (cellobial) in which D-glucal replaces the original 'reducing-end' D-glucose moiety are hydrated by, respectively, sweet potato β-amylase[19] and *exo*- as well as *endo*-type cellulases.[26] Work of Klein et al. on α-glucan phosphorylase[27] and glycogen phosphorylase[28] provided a first case for reaction of a phosphorylase with D-glucal. Unlike the hydrolases that promoted double bond hydration only, the phosphorylase catalyzed transfer of the 2-deoxy-glucosyl-moiety generated from D-glucal upon protonation at C-2. Depending on relative abundance of acceptor substrates present in the reaction, transfer occurred preferentially to phosphate or α-(1→4)-D-glucosyl oligo/polysaccharide.[27,28] The exocyclic enitol heptenitol (2,6-anhydro-1-deoxy-D-gluco-hept-1-enitol) was applied in the study of different glycoside hydrolases and glycogen phosphorylase. It is particularly relevant for this work that the phosphorylase catalyzed glycosyl transfer to phosphate, forming heptulose 2-phosphate as product.[29]

Mechanistic proposals for enzymatic utilization of glycals share a common initial step that is chemical 'activation' of the glycal by protonation at C-2. Analysis of stereospecifity of this protonation event has therefore been an important component of the mechanistic characterization of different enzymes, including α- and β-glucosidases[18], *exo*-α-glucanases,[30] and glycogen phosphorylase.[27] To examine the stereochemical course of the transformation, reactions were performed in D_2O and their progress analyzed by NMR spectroscopy. The same methodology was applied in this work to monitor *Cu*CPase-catalyzed 2-deoxy-D-glucosyl-transfer to phosphate. We show that deuterium from solvent is incorporated stereospecifically in equatorial position of **1**, revealing that proton attack occurs on the *re* side of C-2, that is from below the ring of D-glucal.

2. Results and discussion

2.1. Single-step purification of recombinant *Cu*CPase

Using the procedures described under 3.2 enzyme preparation, we obtained *Cu*CPase in a highly purified form. The isolated enzyme migrated as single protein band in SDS PAGE (Supplementary Fig. 1), and its specific activity of 14.4 U/mg was in useful agreement with the value of 19.2 U/mg reported for the same His-tagged *Cu*CPase in a previous paper from this laboratory.[31] It should be noted that *Cu*CPase isolation was possible with only a single purification step via the enzyme's His-tag, using Ni-chelating Sepharose Fast Flow chromatography with a His-Trap HP column. In previous work using Cu-loaded chelating Sepharose CL-4B, a second chromatographic step on hydroxyapatite resin was necessary to obtain highly purified enzyme. Elution of *Cu*CPase occurred at a higher concentration of imidazole (250 mM) using the 'new' method as compared to the published protocol (120 mM imidazole), suggesting that interaction of the His-tagged protein with the chromatographic material was enhanced under the conditions used herein. Overall, the purification of *Cu*CPase was made simpler and more time-efficient as compared to the reported protocol. In some batches of enzyme purified according to literature, we noted the problem of co-purification of phosphorylase and phosphatase activities. The phosphatase hydrolyzed α-D-glucose 1-phosphate into D-glucose and phosphate. It was important to confirm therefore that the purified *Cu*CPase used herein was absolutely devoid of such phosphatase activity.

2.2. Identification of D-glucal as *Cu*CPase substrate for 2-deoxy-D-glucosyl transfer to phosphate

When offered D-glucal (50 mM) and phosphate (50 mM) as substrates, *Cu*CPase (5 μM) catalyzed formation of a single main product that eluted in analytical high performance anion exchange chromatography with pulsed amperometric detection (HPAED-PAD) at a position comparable to that of elution of an authentic α-D-glucose 1-phosphate standard. We determined that product formation took place at the expense of D-glucal (HPAED-PAD). NMR analysis from a reaction mixture in which about 20% of the original substrate had been converted identified the product to be a phosphorylated sugar. Results depicted in Figure 2a establish identity of the phospho-sugar product as **1**. Presence of the phosphate group was indicated by a ^{31}P signal at 2.4 ppm, which showed a $^{3}J_{P\text{-}H}$ coupling in $^{1}H/^{31}P$-HSQC to proton H-1 with a coupling constant of 7.6 Hz. The $^{3}J_{H\text{-}H}$ coupling of 3.0 Hz between H-1 and H2a pointed to α-anomeric configuration at C-1. In Figure 2a the TOCSY trace of protons H-1 is shown, which indicates all protons in the respective spin system. Several scalar couplings can be deduced from additionally shown separated proton signals of **1**. NMR spectroscopic data are summarized in Supplementary Table 1.

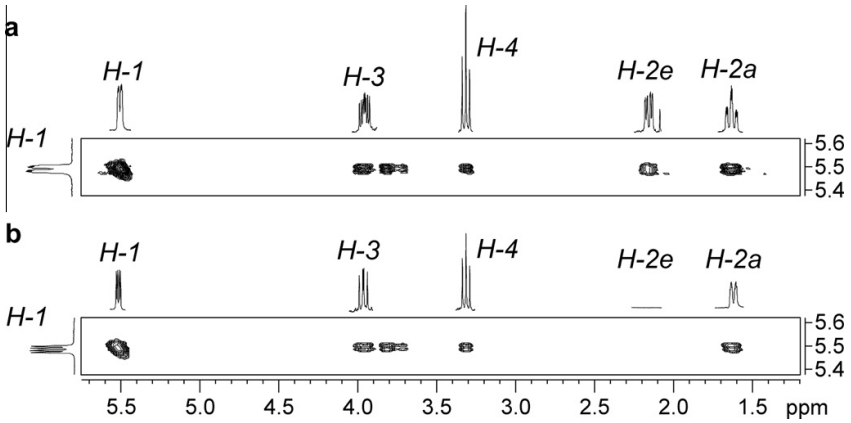

Figure 2. NMR spectroscopy based identification of 2-deoxy-α-D-glucose 1-phosphate (**1**) (panel a) and 2-deoxy-α-D-[(2e)-D]-glucose 1-phosphate (**4**) (panel b). Shown are the 2D TOCSY traces of protons H-1 in f_2-dimension. Additionally, the separated and not overlapped ^{1}H NMR signals are attached to the axes, respectively. Indicative shifts and coupling constants are listed in Supplementary Table 1.

NMR analysis revealed that 2-deoxy-D-glucose (**2**) was a minor additional product of the conversion of D-glucal that was formed in low abundance (⩽2%) relative to **1**. Careful controls performed under otherwise identical reaction conditions in the absence of enzyme showed that D-glucal was stable over the entire timespan of the experiment, eliminating the possibility that spontaneous, non-enzymatic reactions are responsible for the observed product pattern. These results indicate that *Cu*CPase promotes conversion of D-glucal via 2-deoxy-D-glucosyl transfer to phosphate whereby D-glucal serves as donor substrate for phosphorolysis. From time-course data presented in Figure 3 we estimated that the reactivity of D-glucal as substrate for phosphorolysis by *Cu*CPase is roughly three orders of magnitude lower than reactivity of the native donor substrate cellobiose used under otherwise identical conditions (50 mM of each cellobiose and phosphate). A plausible explanation for formation of **2** during phosphorolysis of D-glucal is that slow non-enzymatic hydrolysis of the relatively unstable **1** takes place as a secondary reaction of the overall transformation. The alternative possibility is that *Cu*CPase catalyzes direct hydration of D-glucal at a rate much slower than the phosphorolysis rate. In experiments described later where *Cu*CPase was incubated with D-glucal and D-glucose in the absence of phosphate, the enzyme synthesized tiny amounts of a product that was shown by HPAED-PAD analysis to consist of **2** next to 2-deoxy-β-D-glucosyl-(1→4)-D-glucose (**3**). Product **2** is quite unlikely to have originated from hydrolysis of the trace amounts of **3** formed under these conditions. Direct hydration of D-glucal by *Cu*CPase is therefore supported. The hydration product is assumed to be 2-deoxy-α-D-glucose, which then undergoes mutarotation in solution, yielding the α- and β-anomers of **2** in the reaction mixture, as observed in the NMR analysis.

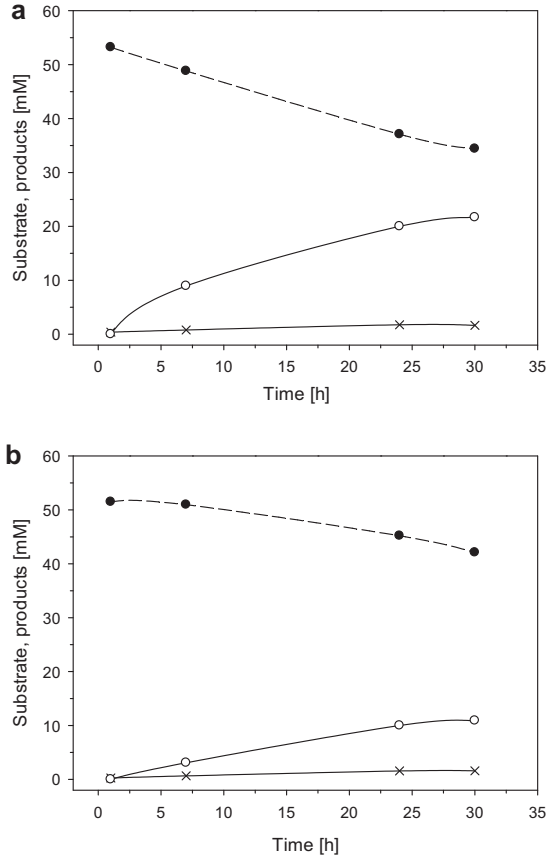

Figure 3. Time-courses for 2-deoxy-α-D-glucose 1-phosphate (**1**) (○) and 2-deoxy-D-glucose (**2**) (x) production from 50 mM D-glucal (●) in the presence of 250 mM phosphate (a) and 50 mM phosphate (b). The enzyme concentration was 5 μM. Lines show trend of the data.

2.3. Enzymatic synthesis of 1 from D-glucal

Figure 3a shows time courses of conversion of 50 mM D-glucal in the presence of the same molar concentration of phosphate and a fivefold molar excess of phosphate. Reaction rate was enhanced (twofold) by increasing the initial phosphate concentration from 50 mM to 250 mM. The final concentration of **1** obtained in the enzymatic conversion was doubled from 10 mM to around 20 mM by the same increase in phosphate concentration, indicating a mass action effect. The maximum conversion of D-glucal under the conditions used was around 40%. Despite this rather modest yield, single-step production by *Cu*CPase appears to be the currently most convenient synthesis of **1**. We will show later under 2.5 enzymatic reaction with D-glucal in the presence of D-glucose and phosphate, that the presence of D-glucose further stimulates catalytic formation of **1**, making the synthesis even more efficient.

2.4. Stereochemical course of enzymatic reaction with D-glucal

A plausible mechanism of utilization of D-glucal for 2-deoxy-D-glucosyl transfer to phosphate involves substrate activation by protonation at C-2 prior to or concomitant with nucleophilic attack of phosphate oxygen on C-1. To probe the stereoselectivity of the protonation event, we performed enzymatic reaction in D_2O using 50 mM of each D-glucal and phosphate, and analyzed with NMR the incorporation of deuterium in the resulting **1** obtained after 24 h of incubation. The obtained NMR spectrum identified the formed product as 2-deoxy-α-D-[(2e)-D]-glucose 1-phosphate (**4**). This compound has the same anomeric configuration as **1** and shows a ^{31}P signal at 2.5 ppm. It shows the proton signal of H-2a, while no signal of H-2e is detectable (Fig. 2b). Concomitant the signal of H-1 and H-3 show only scalar couplings to H-2a as well as to H-2a and H-4, respectively. Furthermore, C-2 has a typical $^1J_{C\text{-}D}$ coupling (data not shown). NMR spectroscopic ^1H and ^{13}C data of **4** are summarized in Supplementary Table 1.

Our results indicate that protonation of D-glucal by *Cu*CPase is highly stereoselective. They also suggest a stereochemical course of the protonation where the proton is delivered from below the six-membered ring of substrate in a *re* side attack on C-2 (Scheme 2B). We will discuss later with the help of molecular docking that the most plausible mechanistic scenario is that enzyme-bound phosphate serves as proton donor in the reaction.

2.5. Enzymatic reaction with D-glucal and D-glucose in the absence and presence of phosphate

Kitaoka et al. have shown exploitation of *Cg*CPase-catalyzed 2-deoxy-β-D-glucosyl transfer from D-glucal to different acceptors (D-glucose, D-xylose, D-mannose, and 2-deoxy-D-arabino-hexose) for synthesis of rare disaccharide analogs of cellobiose.[16] We used *Cu*CPase to perform the same synthesis using D-glucal and D-glucose (50 mM each), but obtained poor yields (⩽4%). Analysis by HPAED-PAD of a sample taken after 30 h of incubation confirmed formation of a disaccharide product that eluted at a position similar, yet not identical to that of elution of authentic cellobiose. However, this product was present in a concentration of only about

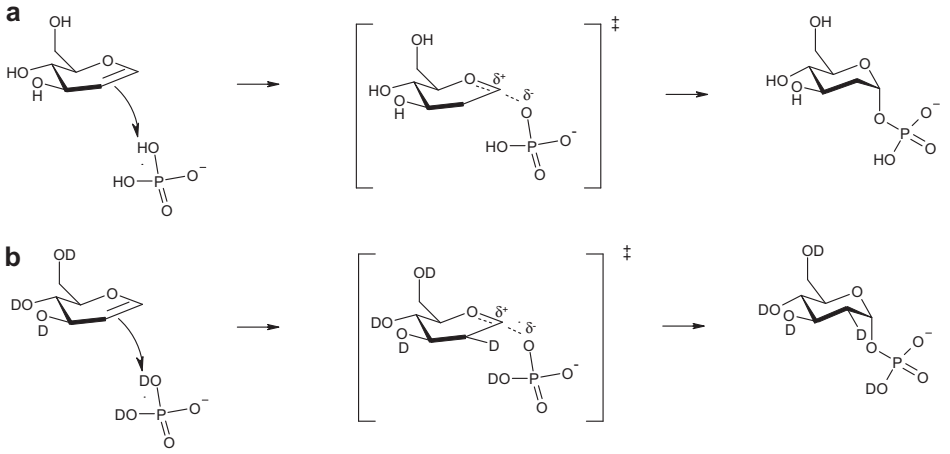

Scheme 2. Reaction course for 2-deoxy-D-glucosyl transfer from D-glucal to phosphate catalyzed by *Cu*CPase in H_2O (a) and D_2O (b). In D_2O, all acidic protons are assumed to be exchanged by deuterium.

2 mM (calibrated as cellobiose). We also noticed formation of **2**, presumably resulting from hydration of D-glucal (see Fig. 4f).

The reaction was then repeated in the presence of phosphate. Interestingly and at first unexpectedly, disaccharide synthesis was substantially enhanced under these conditions as compared to the control lacking phosphate. Two main products were formed: a disaccharide whose identity was revealed by NMR as **3**, and **1**, re-confirmed by the NMR data. The molar ratio of synthesis and phosphorolysis products was dependent on the initial phosphate concentration used; it decreased as the phosphate concentration was raised (see Fig. 4). NMR data for the disaccharide product identify the constituent 2-deoxy-β-D-glucosyl group from the typical large coupling constants between the axial protons present in each position, including C-1. The additional equatorial oriented proton on position C-2 shows concomitant smaller $^3J_{H\text{-}H}$ couplings and leads to a high field shift of the C-2 ^{13}C signal. The terminal saccharide is a glucose moiety, present in a typical 2:3 mixture of α- and β-anomers. The interglycosidic linkage has been determined by a weak NOE between the H-1 of the 2-deoxy-β-D-glucosyl moiety and H-4 of the terminal glucose. We isolated **3** from the product mixture, however, only in small amounts that were not sufficient to determine $^3J_{C\text{-}H}$ couplings between the two sugar units. In spite of that, all NMR spectroscopic data (Supplementary Table 2) indicate the disaccharide to be a **3** and are in very good accordance with an earlier reported analysis of this compound.[16]

Figure 4 summarizes time-course data for conversion of D-glucal and D-glucose (50 mM each) in the presence of different phosphate concentrations in the range 1.00–250 mM. A control lacking phosphate is also shown (panel f). Each time course in Figure 4 (panels a–e) was characterized by relatively fast drop of D-glucal concentration in the first 5 h of reaction. Depending on the phosphate concentration used, D-glucose was consumed at roughly the same rate (1 and 5 mM phosphate) or at a rate much lower (⩾50 mM phosphate) than the D-glucal utilization rate. The products **3** and **1** were formed according to mass balance. At low phosphate concentration, **3** was essentially the only product derived from D-glucal. At phosphate concentrations of 50 mM and greater, the distribution of transfer products varied in dependence of the phosphate concentration. While at 50 mM phosphate the products were formed in almost identical amounts, use of 250 mM phosphate rendered **1** as the predominant reaction product. In each of the time courses in Figure 4 (panels a–e) at 10 h and above, the reaction rate became stalled and the concentrations of substrates and products remained constant over time. Therefore, this suggested that an apparent equilibrium had been reached in each of the reactions. The results in Figure 4 are interesting as they hint a catalytic role of phosphate and D-glucose during conversion of D-glucal into **3** (panels d and e compared to panel f) and **1** (panel a compared to Fig. 3), respectively. A plausible scenario is that quaternary complex between *Cu*CPase, phosphate, D-glucal, and D-glucose shows substantially enhanced activity as compared to the corresponding ternary complexes (enzyme/D-glucal/D-glucose; enzyme/D-glucal/phosphate). Preferred direction of reaction, 2-deoxy-D-glucosyl transfer to D-glucose or phosphate, is determined by prevalence of acceptor substrate for synthesis or phosphorolysis. Reaction of *Cu*CPase with D-glucal therefore appears to occur under thermodynamic control (see later under 2.6 molecular docking studies).

Kinetic analysis of the data in Figure 4 reveals that *Cu*CPase activity was lowest for reaction with D-glucal and D-glucose in the absence of phosphate. An approximate turnover number (k_{app}) of $3.5 \times 10^{-3}\ s^{-1}$ was calculated from data in Figure 4f. Using D-glucal and phosphate in the absence of D-glucose (Fig. 3b), k_{app} was approximately $1.8 \times 10^{-2}\ s^{-1}$. Presence of phosphate (150 mM) and D-glucose next to D-glucal (Fig. 4f compared to Fig. 3b) resulted in a roughly 15-fold increase in k_{app} to a value of $0.27\ s^{-1}$. At 1.00 mM phosphate, k_{app} was still $0.2\ s^{-1}$.

Reaction of CPase with D-glucal is of interest to be applied for synthesis of 2-deoxy-D-glucosyl saccharides, as already demonstrated by Kitaoka and co-workers. This work adds to their previous study showing that **1** can also be synthesized. Generally, deoxy-sugars in which a particular hydroxy group has been substituted by hydrogen have proven to be valuable tools in the biochemical study of substrate binding recognition and catalysis by carbohydrate-active enzymes.[32,33] The OH→H replacement can be viewed as chemical mutagenesis of substrate, resulting in selective removal of hydrogen-bonding interactions that the original hydroxy group had with the enzyme. Considering the central physiological role of α-D-glucose 1-phosphate at the interface of cellular catabolism and anabolism, **1** presents an interesting analog of α-D-glucose 1-phosphate that could be used in the examination of various enzymes utilizing α-D-glucose 1-phosphate as their native substrate (e.g., phosphoglucomutase,

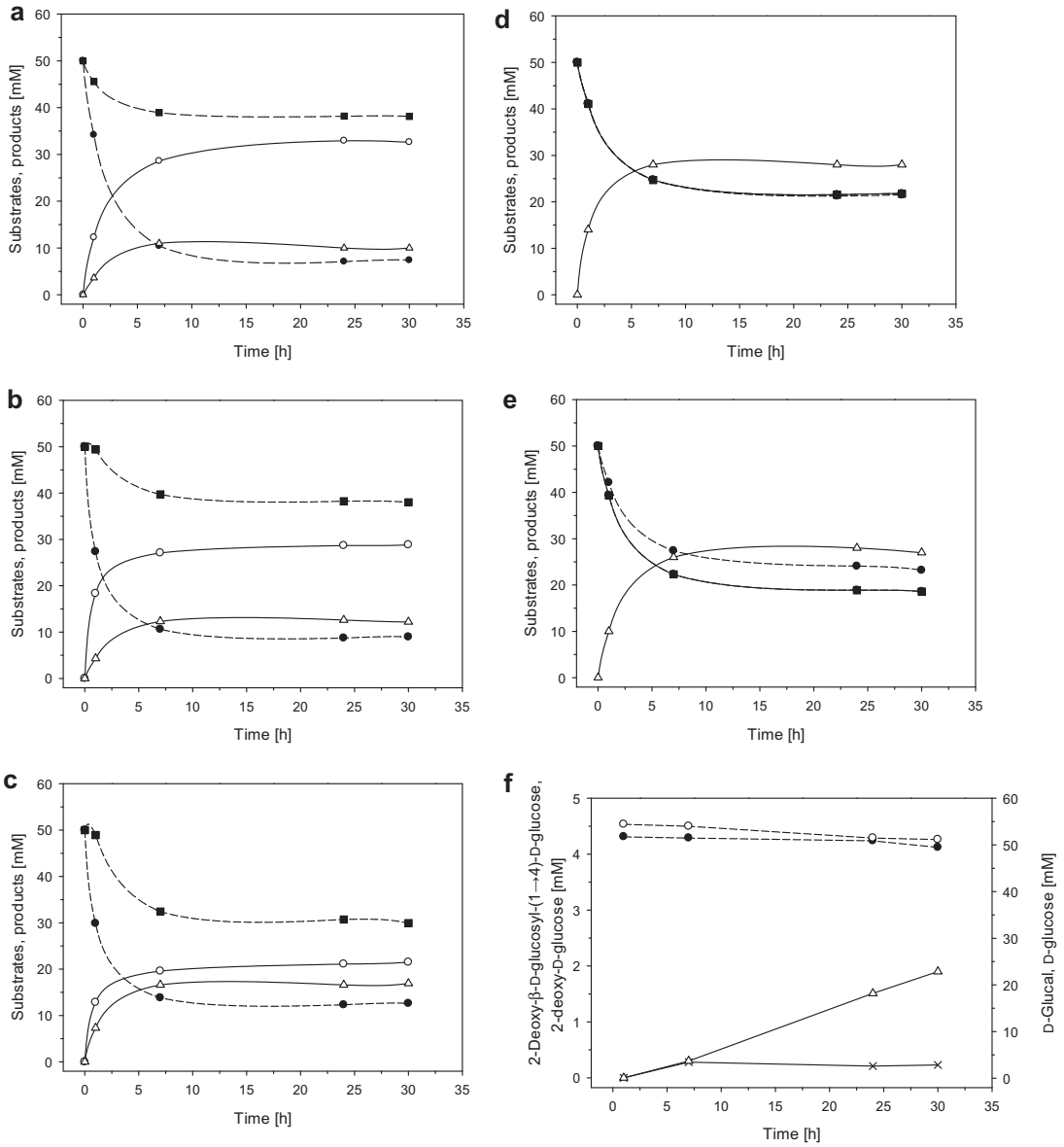

Figure 4. Time-courses for 2-deoxy-β-D-glucosyl-(1→4)-D-glucose (**3**) (△) and 2-deoxy-α-D-glucose 1-phosphate (**1**) (○) production from 50 mM D-glucal (●) and 50 mM D-glucose (■) in the presence of 250 mM phosphate (a), 150 mM phosphate (b), 50 mM phosphate (c), 5 mM phosphate (d) and 1 mM phosphate (e), respectively. (f) shows the time-course of 2-deoxy-β-D-glucosyl-(1→4)-D-glucose (**3**) (△) and 2-deoxy-D-glucose (**2**) (x) production from 50 mM D-glucal (●) and 50 mM D-glucose (■) in the absence of phosphate. Lines show trend of the data.

NDP-glucose pyrophosphorylase, phosphatase, phosphorylase). However, applying purely chemical approaches, synthesis of **1** has turned out to be remarkably difficult due to compound instability.[34–38] Percival and Withers used an enzymatic approach that involved five enzymes and proceeded via 2-deoxy-D-glucose 6-phosphate and 2-deoxy-UDP-D-glucose.[39] Thiem and co-workers exploited reaction of glycogen phosphorylase with D-glucal.[40] The enzyme used is special in that its activity is dependent on an α-1,4-oligo-D-glucoside primer. Maltotetraose, which is the smallest primer utilized by the phosphorylase, and starch were used. Applying maltotetraose, authors reported synthesis of **1** in two steps: a 2-deoxy-D-glucosyl polysaccharide having an average degree of polymerization of 20 was prepared first and separated from the reaction mixture; polysaccharide was then used for phosphorolysis, giving **1** in a yield of 50%. An issue of using starch, which is cheaper than maltotetraose, was formation of α-D-glucose 1-phosphate next to **1** and difficulty of separation of the two sugar phosphates. Therefore, synthesis of **1** using *Cu*CPase under conditions as in Figure 4 (panels a and b) is promising.

2.6. Molecular docking studies and proposal for the enzymatic reaction mechanism

The crystal structure of *Cg*CPase (PDB-entry 2cqt) in complex with phosphate and D-glucose (bound at subsite +1) was used for an energy-minimized docking experiment in which D-glucal was rigidly placed into subsite −1 of the enzyme. Inherent ambiguity of the used docking procedure notwithstanding, predicted accommodation of D-glucal at the catalytic subsite −1 of *Cg*CPase appears to be highly plausible. Compared to the PDB structure, no conformational changes were observed in the docked structure. Figure 1b shows the resulting enzyme–ligand interaction map. The docking provides useful insight into formation of and possible reactive group arrangement in a quaternary complex, enzyme/phosphate/D-glucal/D-glucose, that might be catalytically competent. D-Glucal is positioned through a network of hydrogen bonds that involves protein residues (D368; W488, D490; H666), but also phosphate and D-glucose. D-Glucal makes contacts from each of its hydroxy groups, whereby the 4-OH and 6-OH show strong interactions with, respectively, phosphate and the main-chain NH of D490 in particular. Both phosphate and D-glucose (indirectly via D490) are therefore expected to contribute to binding affinity of D-glucal in the quaternary complex.

Figure 1b supports a catalytic mechanism for reaction of *Cu*CPase with D-glucal. The proposed mechanism is shown in Scheme 3. D-Glucal is accommodated in a position that allows the bound phosphate molecule to serve as proton donor for stereospecific *re*-face protonation at C-2. From previous studies of inverting glycoside hydrolases and glycosyltransferases,[41–43] the subsequent glycosyl transfer is expected to proceed through an oxocarbenium ion-like transition state. Partial negative charges at the reactive O atoms of phosphate and D-glucose will stabilize this transition state. The ionized side chain of D490 will provide general base catalytic assistance to the reaction through partial deprotonation of the glucose 4-OH. Regioselective 2-deoxy-D-glucosyl transfer to D-glucose is therefore explained. The proposed role of D490 during conversion of D-glucal is analogous to its role in the natural reaction when cellobiose is synthesized.[2]

A kinetic mechanism for reaction of *Cu*CPase with D-glucal is proposed in Scheme 4. 'Activation' of donor substrate to formally generate a 2-deoxy-D-glucosyl cation is thought to be completely rate-limiting and therefore, 2-deoxy-D-glucosyl transfer between phosphate and D-glucose comes to equilibrium at all times during the reaction. The thermodynamic equilibrium constant for conversion of 2-deoxy-cellobiose into **1** at given pH (K_{eq}) is defined in kinetic terms as the ratio of third-order rate constants in direction of phosphorolysis and synthesis (see Scheme 4). It is interesting that glycogen phosphorylase differs from *Cu*CPase in that its reaction with D-glucal is kinetically controlled, where initial 2-deoxy-D-glucosyl transfer occurs exclusively on the carbohydrate acceptor substrate (e.g., maltotetraose).[27,40] Compound **1** is formed only in a subsequent step, as required by reaction thermodynamics. A possible explanation for switch from thermodynamic to kinetic control in two otherwise similar phosphorylase-catalyzed transformations of D-glucal could be that, when compared on the basis of turnover number for reaction with the natural donor substrate α-D-glucose 1-phosphate, glycogen phosphorylase (relative k_{cat}: 0.1–0.4)[27] is by far (⩾100-fold) more reactive toward D-glucal than *Cu*CPase (relative k_{cat}: 0.001). Mechanistic differences between the two phosphorylases, reflected in a different stereochemical course of the reaction catalyzed, could also be responsible. Glycogen phosphorylase is a retaining enzyme that promotes an axial-to-axial substitution at C-1 of the transferred glycosyl residue. Unlike *Cu*CPase that is reactive with D-glucal and phosphate in the absence of sugar acceptor, glycogen phosphorylase *must* form a quaternary complex of enzyme, phosphate, D-glucal, and oligosaccharide acceptor (primer) to become detectably active. Arrangement of reactive groups in this complex may be such that phosphate, which is thought to serve a proton donor function in the reaction with D-glucal analogous to that proposed for *Cu*CPase,[27] cannot directly participate as nucleophilic acceptor of the transferred 2-deoxy-D-glucosyl moiety. Initial formation of oligosaccharide elongated by 2-deoxy-D-glucosyl residues may thus be a necessity of the mechanism utilized. It is interesting that glycogen phosphorylase promotes conversion of heptenitol to heptulose-2-phosphate in the absence of primer molecule,[29] using a reaction course highly similar to that of direct **1** formation by *Cu*CPase from D-glucal and phosphate.

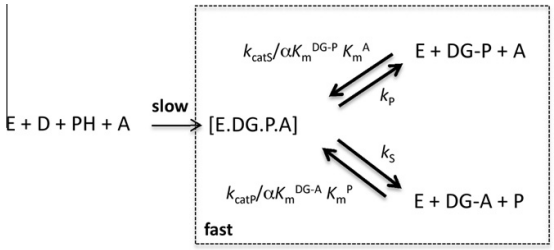

Scheme 4. Proposed kinetic mechanism for reaction of *Cu*CPase with D-glucal. E: *Cu*CPase; D: D-glucal; PH: phosphate, protonated; A: D-glucose; DG: transient 2-deoxyglucosyl oxocarbenium ion (**2**); DG-P: 2-deoxy-α-D-glucose 1-phosphate (**1**); DG-A: 2-deoxy-β-D-glucose-(14)-D-glucose (**3**); P: deprotonated phosphate. [E.DG.P.A] is the quaternary transition state complex. The parameter α is an interaction coefficient describing the effect of binding of one substrate to the enzyme on the binding of the respective other substrate.

3. Experimental

3.1. Materials

Unless otherwise stated, all chemicals used have been described elsewhere.[44] D-Glucal was purchased from Sigma, 2-deoxy-α-D-glucose (**2**) from Roth.

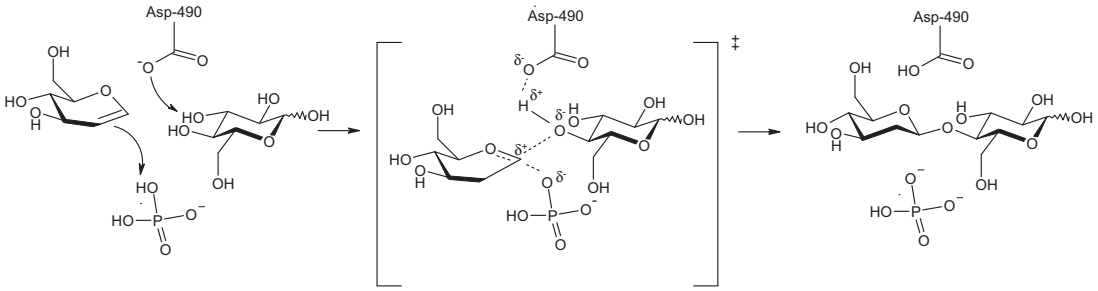

Scheme 3. Proposed catalytic mechanism for reaction of *Cu*CPase with D-glucal, D-glucose and phosphate.

3.2. Enzyme preparation

Recombinant *Cellulomonas uda* CPase (*Cu*CPase) was prepared by a modification of a procedure reported elsewhere.[31] Details of the protocol were as follows. *Escherichia coli* BL21-Gold(DE3) expression cells harboring the pQE30-vector encoding *Cu*CPase were cultivated in 1-L baffled shaken flasks at 37 °C and 110 rpm using LB-media and 115 mg/L ampicillin. When OD_{600} reached 0.9–1.0, temperature was decreased to 22 °C and gene expression was induced with 0.1 mM IPTG for 20 h. Cells were harvested by centrifugation at 4 °C and 5000 rpm for 30 min in a Sorvall RC-5B Refrigerated Superspeed centrifuge. Resuspended cells were frozen at −20 °C, thawed and the suspension was passed twice through a French pressure cell press (Aminco) at 150 bar. Cell debris was removed by centrifugation at 4 °C, 14,000 rpm for 45 min. The resulting supernatant was used for further enzyme purification after it was passed through a 1.2 μm cellulose-acetate filter (Sartorius). As the pQE30-vector encoding *Cu*CPase has a His-tag fused to the N-terminus of the enzyme, *Cu*CPase was purified by using a Ni-chelating Sepharose Fast Flow chromatography (His-Trap HP, GE Healthcare) at 4 °C. All buffers were degassed and filtered using 0.45 μm cellulose-acetate filters (Sartorius). The column was equilibrated with buffer A (20 mM Tris–HCl, 20 mM imidazole, 500 mM NaCl, pH 7.4) at a flow rate of 5 mL/min (5 column volumes). The crude cell extract was applied at a flow rate of 1 mL/min. After washing with buffer A at a flow rate of 5 mL/min (5 column volumes), fractions containing the enzyme (91-kDa band in SDS–PAGE) were eluted with buffer E (20 mM Tris–HCl, 250 mM imidazole, 500 mM NaCl, pH 7.4) at a flow rate of 2 mL/min (6 column volumes). Pooled fractions were concentrated and desalted using a Vivaspin ultrafiltration tube (10 kDa cutoff; Vivascience) and again concentrated to about 40 mg/mL in 50 mM MES buffer, pH 6.6. Stock solutions of *Cu*CPase were stored at −20 °C. The yield of pure protein from one liter culture was about 50 mg. Purification was monitored by SDS–PAGE and the measurement of the specific activity (see Supplementary Fig. 1). To further check the preparation's purity and specifically the absence of a phosphatase related impurity, *Cu*CPase (1 μM) was incubated with 50 mM α-D-glucose 1-phosphate in 50 mM MES buffer, pH 6.6 for 24 h and the reaction mixture was analyzed by high performance anion exchange chromatography with pulsed amperometric detection (HPAED-PAD) (see below). No hydrolytic activity of α-D-glucose 1-phosphate into D-glucose and phosphate could be detected with purified *Cu*CPase prepared with the protocol just described.

3.3. Assays

Enzyme activity in direction of phosphorolysis of cellobiose was determined at 30 °C using a continuous coupled enzymatic assay with phosphoglucomutase and glucose-6-phosphate dehydrogenase.[14] Protein concentration was measured with the BioRad dye-binding method referenced against BSA.

3.4. Analytical methods

All synthesis products were analyzed by high performance anion exchange chromatography with HPAED-PAD. The analysis was performed using a Dionex BioLC system equipped with a CarboPac PA10 column (4 × 250 mm) and an Amino Trap guard column (4 × 50 mm) thermostated at 30 °C. D-Glucal, **2**, D-glucose, **3,** and **1** were detected with an ED50A electrochemical detector using a gold working electrode and a silver/silver chloride reference electrode by applying the predefined waveform for carbohydrates. Elution was carried out at a flow rate of 1 mL/min with the following method: isocratic flow of 52 mM NaOH for 20 min, followed by an isocratic flow of 100 mM NaOH and 100 mM NaOAc for 5 min, and a linear gradient from 100 mM NaOAc to 400 mM NaOAc applied within 15 min in an isocratic background of 100 mM NaOH. The column was washed 10 min with 52 mM NaOH. Under the conditions applied, the following retention times were obtained: 2.6 min for D-glucal, 5.8 min for **2**, 7.9 for D-glucose, 11.2 min for **3,** and 23.0 min for **1**.

3.5. Reactions with D-glucal and phosphate

D-Glucal was tested as a possible glycosyl donor in phosphorolysis direction catalyzed by *Cu*CPase. 5 μM *Cu*CPase were incubated with 50 mM D-glucal and different concentrations of phosphate (50 mM, 250 mM) in 50 mM MES buffer, pH 6.6. The formation of a new product for *Cu*CPase, **1**, was monitored by HPAED-PAD after the reaction mixture was incubated at 30 °C, 550 rpm for up to 30 h.

To determine the stereochemical course of the reaction, we performed a reaction using 50 mM D-glucal, 50 mM phosphate, 50 mM MES (pH 6.6), and 5 μM *Cu*CPase in 99% (v/v) D_2O. The mixture was incubated at 30 °C, 550 rpm for 24 h and the content of the mixture was analyzed by NMR analysis (see 3.8).

3.6. Reactions with D-glucal and D-glucose in presence and absence of phosphate

To test whether *Cu*CPase still utilizes D-glucal when phosphate and D-glucose is present, 5 μM *Cu*CPase were incubated with 50 mM D-glucal, 50 mM D-glucose, and different concentrations of phosphate (1 mM, 5 mM, 50 mM, 150 mM, 250 mM) in 50 mM MES buffer, pH 6.6, at 30 °C for 30 h. The reaction mixture was analyzed by HPAED-PAD and the synthesis products were identified by NMR-analysis as **3** and **1**. To test the role of phosphate in the reaction, *Cu*CPase was incubated with only D-glucal and D-glucose (without phosphate). 5 μM *Cu*CPase were incubated with 50 mM D-glucal and 50 mM D-glucose in 50 mM MES buffer, pH 6.6, at 30 °C and after 24 h the reaction was stopped and the reaction mixture was analyzed by HPAED-PAD.

3.7. Energy-minimized molecular docking

Yasara V 11.11.21 was used for the determination of energy-minimized structure and the enzyme–ligand docking. PyMOL (http://pymol.sourceforge.net) was used for visualization. The X-ray crystal structure of *Cg*CPase having a D-glucose and phosphate bound in subsite +1 and phosphate binding site, respectively (PDB-entry 2cqt) was used as macromolecule in a rigid molecular docking experiment that employed D-glucal as the ligand. A search space of 15 × 12 × 12 Å was used, spanning the enzyme's active site. The docking algorithm resulted in 4 binding modes with comparable energies. From these, the most accurate model was selected on the basis of the binding mode of *N*-acetylglucosamine in subsite −1 of *Vp*ChPase.[6]

3.8. NMR measurements

NMR spectroscopic measurements were made from crude or partially purified reaction mixtures. Lyophilized samples were dissolved in D_2O (99.95%, 0.7 mL) and transferred into 5 mm NMR sample tubes (Promochem, Wesel, Germany). All spectra were recorded on a Bruker DRX-400 AVANCE spectrometer (Bruker, Rheinstetten, Germany) at 400.13 MHz (^1H), 100.61 MHz (^{13}C), and 161.98 MHz (^{31}P) using the Bruker Topspin 1.3 software. Measurements temperature was 300 ± 0.1 K. For 1D-spectra, 32k data points were acquired using a relaxation delay of 1.0 s and appropriate number of scans. After zero filling to 64k data points and Fourier transformation, spectra with a range of 7200 Hz (^1H),

20,000 Hz (^{13}C), and 16,200 Hz (^{31}P) were obtained, respectively. To determine the 2D COSY, TOCSY, NOESY, HMQC, and HMBC as well as ^{1}H/^{31}P-HSQC spectra, 128 experiments with 8 scans and 1024 data points each were performed. After linear forward prediction to 256 data points in the f_2-dimension and appropriate sinusoidal multiplication in both dimensions, the data were Fourier transformed to obtain 2D-spectra with ranges of 4000 Hz (^{1}H), 20,000 Hz (^{13}C), and 8100 Hz (^{31}P). Chemical ^{1}H and ^{13}C shifts were referenced to external acetone (δ_H 2.225 ppm; δ_C 31.45 ppm) and phosphorus shifts were referenced to external aq 85% phosphoric acid (^{31}P: δ_P 0.00 ppm).

Acknowledgements

Financial support from the Austrian Science Funds FWF (project L586-B03) is gratefully acknowledged. We thank Susanne Felsinger for kind help with measurement of NMR spectra.

Supplementary data

Supplementary data associated with this article can be found, in the online version, at http://dx.doi.org/10.1016/j.carres.2012.04.003.

References

1. Alexander, J. K. *J. Bacteriol.* **1961**, *81*, 903–910.
2. Hidaka, M.; Kitaoka, M.; Hayashi, K.; Wakagi, T.; Shoun, H.; Fushinobu, S. *Biochem. J.* **2006**, *398*, 37–43.
3. Stam, M. R.; Blanc, E.; Coutinho, P. M.; Henrissat, B. *Carbohydr. Res.* **2005**, *340*, 2728–2734.
4. Henrissat, B.; Davies, G. *Curr. Opin. Struct. Biol.* **1997**, *7*, 637–644.
5. McCarter, J. D.; Withers, S. G. *Curr. Opin. Struct. Biol.* **1994**, *4*, 885–892.
6. Hidaka, M.; Honda, Y.; Kitaoka, M.; Nirasawa, S.; Hayashi, K.; Wakagi, T.; Shoun, H.; Fushinobu, S. *Structure* **2004**, *12*, 937–947.
7. Kitaoka, M.; Sasaki, T.; Taniguchi, H. *J. Biochem.* **1992**, *112*, 40–44.
8. Liu, A. M.; Tomita, H.; Li, H. B.; Miyaki, H.; Aoyagi, C.; Kaneko, S.; Hayashi, K. *J. Ferment. Bioeng.* **1998**, *85*, 511–513.
9. Percy, A.; Ono, H.; Hayashi, K. *Carbohydr. Res.* **1998**, *308*, 423–429.
10. Alexander, J. K. *J. Biol. Chem.* **1968**, *243*, 2899–2904.
11. Sih, C. J.; McBee, R. H. *Proc. Montana Acad. Sci.* **1955**, *15*, 21–22.
12. Sih, C. J.; McBee, R. H. *Bacteriol. Proc.* **1955**, 126.
13. Alexander, J. K. *Arch. Biochem. Biophys.* **1968**, *123*, 240–246.
14. Nidetzky, B.; Eis, C.; Albert, M. *Biochem. J.* **2000**, *351*, 649–659.
15. De Groeve, M. R. M.; De Baere, M.; Hoflack, L.; Desmet, T.; Vandamme, E. J.; Soetaert, W. *Protein Eng. Des. Sel.* **2009**, *22*, 393–399.
16. Kitaoka, M.; Nomura, S.; Yoshida, M.; Hayashi, K. *Carbohydr. Res.* **2006**, *341*, 545–549.
17. Fritz, H.; Lehmann, J.; Schlesselmann, P. *Carbohydr. Res.* **1983**, *113*, 71–92.
18. Hehre, E. J.; Genghof, D. S.; Sternlicht, H.; Brewer, C. F. *Biochemistry* **1977**, *16*, 1780–1787.
19. Hehre, E. J.; Kitahata, S.; Brewer, C. F. *J. Biol. Chem.* **1986**, *261*, 2147–21453.
20. Kasumi, T.; Tsumuraya, Y.; Brewer, C. F.; Kerstershilderson, H.; Claeyssens, M.; Hehre, E. J. *Biochemistry* **1987**, *26*, 3010–3016.
21. Kitahata, S.; Brewer, C. F.; Genghof, D. S.; Sawai, T.; Hehre, E. J. *J. Biol. Chem.* **1981**, *256*, 6017–6026.
22. Lai, E. C. K.; Morris, S. A.; Street, I. P.; Withers, S. G. *Bioorg. Med. Chem.* **1996**, *4*, 1929–1937.
23. Lehmann, J.; Zieger, B. *Carbohydr. Res.* **1977**, *58*, 73–78.
24. Legler, G.; Roeser, K. R.; Illig, H. K. *Eur. J. Biochem.* **1979**, *101*, 85–92.
25. Lehmann, J.; Schroter, E. *Carbohydr. Res.* **1972**, *23*, 359–368.
26. Kanda, T.; Brewer, C. F.; Okada, G.; Hehre, E. J. *Biochemistry* **1986**, *25*, 1159–1165.
27. Klein, H. W.; Palm, D.; Helmreich, E. J. *Biochemistry* **1982**, *21*, 6675–6684.
28. Palm, D.; Klein, H. W.; Schinzel, R.; Buehner, M.; Helmreich, E. J. *Biochemistry* **1990**, *29*, 1099–1107.
29. Klein, H. W.; Im, M. J.; Palm, D.; Helmreich, E. J. M. *Biochemistry* **1984**, *23*, 5853–5861.
30. Chiba, S.; Brewer, C. F.; Okada, G.; Matsui, H.; Hehre, E. J. *Biochemistry* **1988**, *27*, 1464–1469.
31. Nidetzky, B.; Griessler, R.; Schwarz, A.; Splechtna, B. *J. Mol. Catal. B: Enzym.* **2004**, *29*, 241–248.
32. Niggemann, J.; Lindhorst, T. K.; Walfort, M.; Laupichler, L.; Sajus, H.; Thiem, J. *Carbohydr. Res.* **1993**, *246*, 173–183.
33. Nikaido, H.; Hassid, W. Z. *Adv. Carbohydr. Chem. Biochem.* **1971**, *26*, 351–483.
34. McDonald, D. L. *J. Org. Chem.* **1962**, *27*, 1107–1109.
35. Sabesan, S.; Neira, S. *Carbohydr. Res.* **1992**, *223*, 169–185.
36. Schmidt, R. R.; Stumpp, M. *Liebigs Ann. Chem.* **1984**, 680–691.
37. Westerduin, P.; Veeneman, G. H.; Vandermarel, G. A.; Vanboom, J. H. *Tetrahedron Lett.* **1986**, *27*, 6271–6274.
38. Withers, S. G.; Percival, M. D.; Street, I. P. *Carbohydr. Res.* **1989**, *187*, 43–66.
39. Percival, M. D.; Withers, S. G. *Can. J. Biochem.* **1988**, *66*, 1970–1972.
40. Evers, B.; Mischnick, P.; Thiem, J. *Carbohydr. Res.* **1994**, *262*, 335–341.
41. Brüx, C.; Ben-David, A.; Shallom-Shezifi, D.; Leon, M.; Niefind, K.; Shoham, G.; Shoham, Y.; Schomburg, D. *J. Mol. Biol.* **2006**, *359*, 97–109.
42. Vasella, A.; Davies, G. J.; Bohm, M. *Curr. Opin. Chem. Biol.* **2002**, *6*, 619–629.
43. Withers, S. G. *Carbohydr. Polym.* **2001**, *44*, 325–337.
44. Goedl, C.; Schwarz, A.; Minani, A.; Nidetzky, B. *J. Biotechnol.* **2007**, *129*, 77–86.

SUPPLEMENTARY INFORMATION FOR

Examining the role of phosphate in glycosyl transfer reactions of *Cellulomonas uda* cellobiose phosphorylase using D-glucal as donor substrate

Patricia Wildberger[a], Lothar Brecker[b] and Bernd Nidetzky[a,*]

[a] Institute of Biotechnology and Biochemical Engineering, Graz University of Technology, Petersgasse 12/1, A-8010 Graz, Austria

[b] Institute of Organic Chemistry, University of Vienna, Währingerstraße 38, A-1090 Vienna, Austria

*Corresponding author

E-mail: bernd.nidetzky@tugraz.at; Tel. +43-316-873-8400; Fax +43-316-873-8434

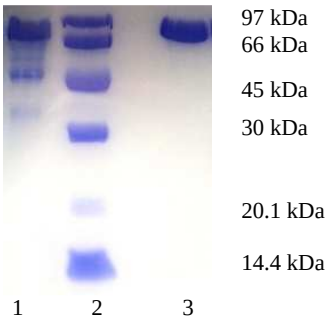

Supplementary Figure S1. Purification of recombinant CuCPase documented by SDS-PAGE. Lane 1: crude cell extract of CuCPase; lane 2: molecular mass standard; lane 3: purified CuCPase.

Supplementary Table 1. Proton and carbon NMR spectroscopic data of 2-deoxy-α-D-glucose 1-phosphate (1) and 2-deoxy-α-D-[(2e)-D]-glucose 1-phosphate (4).

proton	Compound **1**[a]	Compound **4**[a]	carbon	Compound **1**[b]	Compound **4**[b]
H-1	5.49, 1H, ddd, 7.6; 3.0; 1.3	5.52, 1H, dd, 7.5; 3.3	C-1	91.9, d	92.3, d
H-2a	1.62, 1H, dddm, 12.7; 11.7; 3.0	1.63, 1H, dm, 11.6	C-2	38.1, t	38.2, t(t)
H-2e	2.15, 1H, ddd, 12.7; 5.1; 1.3	-			
H-3	3.96, 1H, ddd, 11.7; 9.0; 5.1	3.96, 1H, dd, 11.6; 9.3	C-3	67.1, d	66.8,d
H-4	3.31, 1H, dd, 9.0; 9.0	3.31, 1H, dd, 9.3; 9.3	C-4	71.2, d	70.0, d
H-5	3.83, 1H, m	3.83, 1H, m	C-5	72.0, d	71.8, d
H-6a	3.81, 1H, m	3.81, 1H, m	C-6	60.5, t	60.2, t
H-6b	3.72, 1H, m	3.72, 1H, m			

[a]: chemical shift [ppm], integral, multiplicity, coupling constants [Hz]

[b]: chemical shift [ppm], multiplicity

Supplementary Table 2. Proton and carbon NMR spectroscopic data of 2-deoxy-β-D-glucosyl-(1→4)-D-glucose (3).

proton	α anomer (α-3)[a]	β anomer (β-3)[a]	carbon	α anomer (α-3)[b]	β anomer (β-3)[b]
2-deoxy-β-D-glucosyl-(1→					
H-1	4.83, 1H, dd, 10.0; 2.0	4.82, 1H, dd, 10.0; 2.0	C-1	101.8, d	101.8, d
H-2a	1.59, 1H, ddd, 12.5; 12.0; 10.0	1.61, 1H, ddd, 12.5; 12.0; 10.0	C-2	39.5, t	39.5, t
H-2e	2.37, 1H, ddd, 12.5; 5.0; 2.0	2.38, 1H, ddd, 12.5; 5.0; 2.0			
H-3	3.80, 1H, ddd, 12.0; 9.0; 5.0	3.80, 1H, ddd, 12.0; 9.0; 5.0	C-3	72.0, d	72.0, d
H-4	3.33, 1H, dd, 9.0; 9.0	3.33, 1H, dd, 9.0; 9.0	C-4	72.5, d	72.5, d
H-5	3.45, 1H, m	3.45, 1H, m	C-5	77.9, d	77.9, d
H-6a	3.90, 1H, m	3.90, 1H, m	C-6	60.5, t	60.2, t
H-6b	3.80, 1H, m	3.80, 1H, m			
→4)-D-glucose					
H-1	5.26, 1H, d, 3.9	4.67, 1H, d, 7.8	C-1	93.4, d	97.8, d
H-2	3.60, 1H, dd, 9.7; 3.9	3.29, 1H, dd, 9.5, 7.8	C-2	72.7, d	76.0, d
H-3	3.83, 1H, dd, 9.7; 9.0	3.66, 1H, dd, 9.5; 9.0	C-3	73.1, d	76.0, d
H-4	3.70, 1H, dd, 9.9; 9.0	3.70, 1H, dd, 9.1; 9.0	C-4	80.3, d	80.3, d
H-5	3.90, 1H, m	3.60, 1H, m	C-5	72.0, d	76.4, d
H-6a	3.82, 1H, m	3.88, 1H, m	C-6	61.0, t	61.1, t
H-6b	3.77, 1H, m	3.77, 1H, m			

[a]: chemical shift [ppm], integral, multiplicity, coupling constants [Hz]

[b]: chemical shift [ppm], multiplicity; [determined from $^{1}H/^{13}C$-HSQC]

7 Phosphoryl transfer from glucose 1-phosphate catalyzed by *Escherichia coli* sugar-phosphate phosphatases from two phosphatase-superfamily types

Patricia Wildberger[a], Martin Pfeiffer[a], Lothar Brecker[b], Gerald N. Rechberger[c], Ruth Birner-Gruenberger[d] and Bernd Nidetzky[a,*]

[a] Institute of Biotechnology and Biochemical Engineering, Graz University of Technology, Petersgasse 12/1, A-8010 Graz, Austria

[b] Institute of Organic Chemistry, University of Vienna, Währingerstraße 38, A-1090 Vienna, Austria

[c] Institute of Molecular Biosciences, University of Graz, Humboltstraße 50/2, A-8010 Graz, Austria

[d] Institute of Pathology and Center for Medical Research, Medical University Graz, Stiftingtalstrasse 24, A-8010 Graz, Austria

*Corresponding author

E-mail: bernd.nidetzky@tugraz.at; Tel. +43-316-873-8400; Fax +43-316-873-8434

Abstract

The gene *agp* encodes for glucose-1-phosphatase from *Escherichia coli*, a member of the high molecular weight histidine acid phosphatase family. The periplasmic enzyme was cytoplasmically expressed and purified by affinity chromatography. Proper folding at the secondary structural level was ensured by circular dichroism spectroscopy and correct formation of the three intramoelcular disulfide bonds was revealed by LC-MS/MS. Glucose-1-phosphatase and two representatives of the haloacid dehydrogenase-like phosphatase family, HAD4 and HAD13, were benchmarked by their hydrolytic activities towards various donor substrates. Glucose 1-phosphate was among the substrates, which was hydrolyzed most efficiently by all three phosphatases. In a next step we used glucose 1-phosphate as donor substrate and tested the phosphoryl transfer potential of the three phosphatases to fructose as phosphoryl transfer acceptor substrate. Whereas HAD4 and HAD13 displayed no phosphoryl transfer activity, we could decipher glucose-1-phosphatase as a bifunctional enzyme, displaying hydrolytic and synthetic activity. By using G1Pase as biocatalyst, we were able to establish an one-step reaction process for the efficient synthesis of fructose 1-phosphate, in a yield of up to 60%, based on the initial glucose 1-phosphate concentration. Fructose 1-phosphate is a high-value metabolite which is difficult to prepare chemically and difficult to access biocatalytically.

INTRODUCTION

Phosphate esters are essential for all living organisms (1). Their diverse roles range from providing stability to the genome, lipids and the skeletal structure to being indispensible for protein regulation and signaling (2). Considering the importance of phosphoryl transfer reactions in biology, it is not surprising that phosphoryl transferring enzymes have attracted considerable interest in recent years. The classes of enzymes involved in reactions on phosphate monoesters mainly comprise phosphatases, kinases and mutases (3). The general understanding of how these enzymes catalyze the formation and hydrolysis of phosphate esters is constantly growing (3-6). Besides of deepening the insights on the reaction mechanism utilized by these enzymes, significant progress was made to exploit the enzymes for the synthesis of phosphorylated compounds, which are often used as prodrugs to improve drug delivery, nutritional supplements or taste enhancers in the food industry and as cosmetic ingredients in moisturizers, detergents and new polymers (7, 8).

Enzymes catalyzing phosphoryl transfer reactions have in common that they are dependent on phosphate containing activated donor substrates. In biological systems, kinases are the main enzymes responsible for catalyzing the transfer of a phosphoryl group from the high-energy donor molecule ATP to a variety of alcohols. Several kinases are exploited in synthetic applications thereby providing access to valuable metabolic intermediates like glucose 6-phosphate synthesized by hexokinase (9) or ribose 5-phosphate by ribokinase (10). The accompanied bottlenecks of kinase catalyzed phosphoryl transfer reactions include high expenses for the nucleoside triphosphates and potential inhibitory effects of the resulting nucleoside diphosphates. ATP regeneration evolved as strategy to circumvent these limitations (11), however, is restricted by introducing additional complexity into the kinase-catalyzed reaction system. Phosphatases, enzymes catalyzing the *in vivo* hydrolysis of phosphomonoesters to inorganic phosphate and the corresponding free alcohol, are used as alternatives to kinases in biocatalytic reactions. They use pyrophosphate as donor substrate and transfer the phosphate group to a variety of acceptor substrates, thereby enabling the economic synthesis of products like D-glucose 6-phosphate (12), *N*-acetyl-D-glucosamine and allylphosphate (13). Another group of activated donor substrates, employing a phosphate moiety, are sugar phosphates. Whereas no phosphoryl transferring enzyme is known to transfer the phosphate group of sugar phosphates to an acceptor, an analogous mechanism for glycosyl transferring enzymes is well described. Dissaccharide phosphorylases are known to utilize sugar phosphates and to transfer the glycosyl groups from the sugar phosphate to a variety of acceptors (14).

In this study we introduce three sugar phosphate utilizing phosphatases from *Escherichia coli*. Two of them, HAD4 and HAD13, belong to the haloacid dehalogenase-like phosphatase (HAD) family,

whereas G1Pase is classified as an enzyme from the histidine acid phosphatase superfamily. The selection of the chosen enzymes was made on the ability to display activity towards glucose 1-phosphate (15, 16), which substrate we used as precursor for comparing and benchmarking the three phosphatases and on the availability of the crystal structure, which is solved for all three enzymes (pdb entry 2boc: HAD4 in complex with glucose 1-phosphate; pdb entry 1rkq: HAD13; pdb entry 1nt4: G1Pase in complex with glucose 1-phosphate).

Based on a structural level, both enzyme families are well characterized and the family-internal conserved motifs are defined. Interestingly, although both enzyme families are almost exclusively restricted to phosphoryl transfer, their structural topologies and their active-site signature displays significant differences.

Figure 1A shows the overall structure of HAD13 (the structure of HAD4 is not considered due to inconsistencies), which is characterized, like all HAD phosphotransferases, by an α/β-core domain consisting of a modified Rossmann fold, with two, unique key structural features essential for catalysis: an almost complete α-helical turn, a so-called squiggle and a β-hairpin turn, termed flap (17, 18). The active-site is located at the interface of this core domain and a second domain, the cap domain. The two domains are flexibly linked, they enclose the active-site for catalysis and open for product dissociation and subsequent substrate binding (17). Figure 1B zooms into the active-site of HAD13 to display the conserved residues of the sequence motifs. The catalytic scaffold accommodates two conserved aspartic acid residues, one acting as nucleophile (Asp10), the other as acid-base catalyst (Asp12) (19, 20). Furthermore, the active-site accommodates a Thr (Thr44) and a Lys (Lys198), which are required to bind the phosphoryl group of the substrate and to position the nucleophile. Two carboxylate groups (Asp221 and Asp225) are required to bind the Mg^{2+} cofactor, which forms a coordinate with the nucleophile and the phosphoryl group of the substrate, thereby orienting and shielding the negative charges in the ground and transition state (21).

In contrast to HAD13, the periplasmic glucose-1-phosphatase (G1Pase, EC 3.1.3.10) is characterized by a typical histidine acid phosphatase-like overall folding architecture. The overall topology comprises two domains, an α-domain and an α/β domain, embedding the central catalytic shaft (22) (Figure 1C). The common structural features include a conserved nucleophilic histidine (His18, substituted by Ala in Figure 1D) and a proton donor (Asp290), next to a catalytic domain filled by positively charged residues (Arg17, Arg21, Arg94 and His289) (see Figure 1D). Both enzyme families share a double displacement-like reaction mechanism that involves the formation of a covalently bound phosphoryl enzyme intermediate to either the nucleophilic aspartic acid (HAD4 and HAD13, Scheme 1A) (23) or the nucleophilic histidine (G1Pase, Scheme 1B) (24, 25).

In summary, the representatives selected for this study are known to be three glucose 1-phosphate hydrolyzing enzymes classified in two enzyme families, whereas each family is well characterized on a structural and mechanistic level. To gain a better understanding on why evolution has developed two enzyme families with different structural topologies but an apparently similar function, we compared the three phosphatases by their hydrolytic activities towards several donor substrates. In addition, we tested the potential of the three phosphatases to catalyze phosphoryl transfer from glucose 1-phosphate as donor substrate to a terminal acceptor different from water. The observed differences on substrate specificity between G1Pase and HAD4 and HAD13, respectively, are interpreted on a structural level.

RESULTS

Molecular cloning, expression and purification of recombinant G1Pase

Encoded by the *agp* gene, glucose-1-phosphatase from the histidine acid phosphatase family hydrolyzes glucose 1-phosphate in the periplasmic space of *E. coli* (26). For recombinant, cytoplasmic enzyme production, the G1Pase gene was amplified from the genomic DNA of *E. coli* BL21-Gold (DE3). The 66 bp native N-terminal signal sequence, required for exporting the native G1Pase to the periplasmic space of *E. coli*, was predicted using SignalIP-4.1 and removed to prevent cytoplasmic export. A *Strep*-tactin affinity tag was fused to the N-terminus and the resulting construct was cloned into a pMS470_dsbC vector under control of the *tac* promoter. To enhance the folding of G1Pase, the expression vector used contains a polycistronic operon in which the disulfide bond isomerase (DsbC) is encoded on the first open reading frame and *Strep*-tagged G1Pase (without signal sequence) on the second one. G1Pase was inducibly expressed in the cyctoplasm of *E. coli* Origami B cells. Purification to apparent homogeneity of *Strep*-tagged G1Pase (molecular mass: 45 kDa) was accomplished via an one-step or two-step purification procedure. *Strep*-tactin affinity chromatography was used as first step, anion exchange chromatography as second. The one-step purification procedure resulted in a protein yield of 6 mg from 1 L of culture; the two-step purification procedure resulted in a protein yield of 1 mg from 1 L of culture. The specific activities of the two preparations, purified via the one-step and two-step procedure, respectively, were identical (1.1 U/mg).

Molecular cloning, expression and purification of recombinant HAD4 and HAD13

HAD4 (*yihX*) was cloned into a pT7-Z_{basic2} under control of the T7 promoter, thereby fused to a strongly positively charged mini-protein called Z_{basic2} (27-29). HAD13 (*yidA*), encoded by the recombinant vector p15TvL-yida (15, 30), and HAD4 were inducibly expressed in the cytoplasm of *E. coli* BL21-Gold (DE3). Purification to apparent homogeneity of Z_{basic2}-tagged HAD4 (molecular mass: 31 kDa) was accomplished via a cation exchange chromatography step. Purification of *His*-tagged HAD13 (molecular mass: 31 kDa) was accomplished via a two step purification procedure, using a Cu^{2+}-chelat followed by an anion exchange chromatography step. The yield of protein from one litre of culture was 26 mg for HAD4 and 0.5 mg for HAD13, respectively.

The purity of the three phosphatases was verified by SDS-PAGE (Figure 2).

Circular dichroism (CD) spectroscopy analysis of the three phosphatases

Correct folding of purified G1Pase and HAD13 was ensured by CD-spectroscopy (Figure 3). Both

enzymes contained the anticipated secondary structure elements previously observed in the corresponding crystal structure (Table 1). G1Pase is characterized by a mixed α-β composition, whereas the amount of α-helices exceeds the amount of β-sheets by more than two times. HAD13 has a mixed α-β composition with similar amounts of α-helices and β-sheets. HAD13 shows a large proportion of unordered structure (28%) which may result from the flexible HAD-like cap domain. Analysis of the recorded CD-spectrum for HAD4 revealed discrepancies to the data observed in the crystal structure and hint a state of partial unfolding of the expressed HAD4.

Formation of disulfide bonds in G1Pase

The sequence of G1Pase contains six cysteines, involved in three intramolecular disulfide bonds (Figure 1). To map the disulfide bonds, purified G1Pase was proteolytically digested with trypsin, chymotrypsin or both. The resulting peptides were separated by nano LC-MS/MS and analyzed in an Orbitrap velos mass spectrometer. Mass spectrometry analysis proved the presence of one disulfide bond formed between Cys189 and Cys195 (sequence: KDSPA**C**KEKQQ**C**SLVDGKNTF; ion score: 34; expect 0,00042; see spectrum and ion table in Figure 4). The other two disulfide bridges could not be detected directly, however, better sequence coverage in reduced samples in the regions around the cysteines indirectly indicates a higher probability of correct formation (Figure 5) as proteolytic enzymes access regions without disulfide bonds easier than in the presence of disulfide bonds.

Hydrolytic activity towards various substrates

The specific activity of G1Pase, HAD4 and HAD13 was assayed by following the enzyme-catalyzed dephosphorylation of a generic phosphatase substrate, *p*-nitrophenyl phosphate and was determined as 1.1 U/mg for G1Pase and 0.1 U/mg for HAD4 and HAD13, respectively. In a next step, we tested the hydrolytic activities of the three phosphatases towards various donor substrates by measuring the release of free phosphate (Table 2). G1Pase was the most active phosphatase towards all sugar phosphates tested as substrates, except for β-glucose 1-phosphate, which was not hydrolyzed by G1Pase. Glucose 1-phosphate and glucose 6-phosphate were hydrolyzed with a hydrolytic activity of 40 s^{-1} and 56 s^{-1}, respectively, the corresponding fructose analogues with 22 s^{-1}. Phytate and pyrophosphate were tested as non-sugar phosphate donor substrates. Under the conditions described, G1Pase hydrolyzed neither phytate, nor pyrophosphate. A decrease of pH from 7.0 to 4.5 (going along with a buffer change from 50 mM MES to 100 mM NaOAc) resulted in a measureable hydrolytic activity of G1Pase towards phytate, which was hydrolyzed with a k_{cat} of 2.1 s^{-1}. A catalytic activity towards

pyrophosphate, which is in general a donor substrate utilized by different bacterial acid phosphatases (31), was not measureable (detection limit $\leq$ 2.5 μM free phosphate).

In contrast to G1Pase, HAD4 and HAD13 were active towards all provided sugar phosphates and could not discriminate between the α- and β-configurated glucose 1-phosphate, hydrolyzing both substrates, however, with a clear preference for the α-configurated form. HAD4 and HAD13 displayed the highest hydrolytic activity towards glucose 1-phosphate, with a k_{cat} of 2.3 s^{-1} for HAD4 and 12 s^{-1} for HAD13, respectively. Both HADs did not catalyze hydrolysis of the tested non-sugar phosphate substrates.

^{18}O incorporation

The hydrolysis of glucose 1-phosphate catalyzed by G1Pase and HAD13 was studied in more detail by ^{18}O incorporation in the presence of $H_2{}^{18}O$. Subsequent analysis by GC-MS revealed the nucleophilic attack to occur at the phosphorus (Figure 6).

Phosphoryl transfer activity from glucose 1-phosphate to fructose

In a subsequent step, we tested the potential of the phosphatases to transfer the phosphoryl moiety from glucose 1-phosphate to fructose as acceptor substrate. HAD4 and HAD13 showed no detectable phosphoryl transfer activity, incubation of glucose 1-phosphate and fructose resulted in the hydrolysis of glucose 1-phosphate to phosphate and glucose. The hydrolytic activity towards glucose 1-phosphate was not dependent on the presence of fructose in the reaction; the catalytic activities for hydrolysis of glucose 1-phosphate in the absence and presence of fructose were highly comparable (k_{cat} = 2.2 s^{-1} for HAD4 and 12 s^{-1} for HAD13).

Then, we incubated glucose 1-phoshate and fructose in the presence of G1Pase, followed the reaction over time and analyzed samples from the reaction mixture. In a first step, the concentration of glucose 1-phosphate and phosphate was determined by using spectrophotometric assays. An unclosed phosphate balance (the sum of glucose 1-phosphate and free phosphate did not correspond to the initial phosphate concentration at t = 0 min) evolved and increased over the reaction time, thereby providing indirect evidence for the formation of a new reaction product. Samples were then analyzed with liquid chromatography, which verified the formation of a new reaction product. The elution pattern of the new reaction product corresponded to the retention time of fructose 1-phosphate, which identity was further confirmed by NMR analysis. It was identified using 1D and 2D NMR, which were compared with NMR spectra derived from commercially gained fructose 1-phosphate. Next to fructose 1-phosphate as main reaction product, glucose 6-phosphate and fructose 6-phosphate were formed

as side products. The formation of the side products over time was followed by spectrophotometric assays and verified by liquid chromatography. Figure 7 shows a time-profile for fructose 1-phosphate synthesis. 20 mM glucose 1-phosphate and 200 mM fructose were incubated in the presence of 0.1 μM G1Pase in 50 mM MES, pH 7.0 at 37°C. Under these conditions a maximal concentration of fructose 1-phosphate of 12 mM was achieved after 60 min of incubation, which corresponds to a fructose 1-phosphate yield of 60% based on the inital glucose 1-phosphate concentration. The concentration of side products was determined to be 1.0 mM for glucose 6-phosphate and 2.7 mM for fructose 6-phosphate. Spoken in catalytic activities, G1Pase consumed glucose 1-phosphate with a k_{cat} of 119 s^{-1} and formed fructose 1-phosphate with a k_{cat} of 88 s^{-1}. The catalytic activities for formation of the side products was determined as 20 s^{-1} for fructose 6-phosphate and 6 s^{-1} for glucose 6-phosphate. The hydrolytic activity of G1Pase in presence of fructose was determined by 18 s^{-1}.

DISCUSSION

The study reported herein describes the first cytoplasmic expression of G1Pase fused to an N-terminal *Strep*-tag to facilitate enzyme expression and purification, thereby providing a time-efficient improvement over the previous purification system, which was based on native periplasmic production of G1Pase followed by purification via dialysis (22). The introduction of the second purification step after affinity chromatography of *Strep*-tagged G1Pase and *His*-tagged HAD13 was introduced to remove any contaminations which may have co-eluted with the target protein during the first purification step. The isolated enzymes migrated at single protein bands in SDS-PAGE (Figure 2). Visualization was done by using the sensitive silver-staining method to document the purity of the target enzymes and the absence of any contaminating proteins. Correct folding of G1Pase and HAD13 was ensured by CD spectroscopy. The CD-spectrum of the expressed HAD4 hinted a state of partial unfolding, which may be explained by a disturbing interference during the folding process caused by the highly positively charged Z_{basic2}-tag. Being aware that HAD4 may not be folded correctly, we determined the specific activity towards the synthetic substrate *p*-nitrophenylphosphate with 0.1 U/mg. This is in agreement with a former study, which determined the activity of HAD4 with 0.2 U/mg (15), thereby supporting our decision to use the present preparation of HAD4 for further studies. The specific activity of HAD13 and G1Pase was determined as 0.1 U/mg and 1.1 U/mg, respectively. Compared to the literature value, the specific activities of the preparations used in this study were decreased around 14-fold for HAD13 and decreased around 65-fold for G1Pase (15, 32). Whereas the reason for the decreased activity of HAD13 is not known, the decreased activity observed for G1Pase can be attributed to the pH value. The optimal pH for G1Pase for hydrolysis of *p*-nitrophenylphosphate was determined by 3.5 (32); in our study we used a pH value of 7.0.

In a next step, we tested the hydrolytic activity of the three phosphatases on various intermediates of central metabolic pathways, like on glucose 1-phosphate, glucose 6-phosphate and fructose 6-phosphate. The three phosphatases have in common to hydrolyze all tested α-configurated donor substrates. β-Glucose 1-phosphate was utilized by HAD4 and HAD13, however, not by G1Pase indicating that G1Pase is specific for α-configurated sugar phosphates. The HADs hydrolyzed both anomers of glucose 1-phosphate, although displaying an up to 230-fold preference for the α-configurated form of glucose 1-phosphate. The hydrolysis of phytate catalyzed by G1Pase was pH dependent. Hydrolytic activity towards phytate was just detected when the pH value was set to 4.5. The non detected activity at higher pH values is most probably caused by repulsion between the negatively charged phytate and the gating residue Glu196, which is negatively charged at neutral pH (16). The HADs showed no activity towards phytate, which may be explained by the quite narrow and well structured active-site

(see Figure 1B), which excludes a bulky substrate, like phytate. Pyrophosphate was not accepted as donor substrate neither by the HADs, nor by G1Pase, which may be caused by the highly negative charge of pyrophosphate, which may prevent pyrophosphate from entering the active-site.

The proposed reaction mechanism of the three enzymes is a double displacement-like reaction mechanism that involves the formation of a phosphoryl enzyme intermediate, followed by a nucleophilic attack of an activated water molecule on the phosphorus atom of the phosphoryl enzyme intermediate. To provide evidence for the dephosphorylation step, an inorganic phosphate-water medium ^{18}O exchange was performed. G1Pase and HAD13, respectively, were incubated with glucose 1-phosphate in the presence of $H_2{}^{18}O$. In accordance with the reaction mechanism, the nucleophilic attack from the activated labelled water molecule resulted in ^{18}O incorporation in phosphate, which was detected by GC-MS, after evaporation and derivatization of the reaction mixture with BSTFA/1%TMCS. The ^{18}O enrichment of phosphate groups was measured by analyzing the peak area ratio of the extracted ion chromatograms of m/z 301 (derivatized phosphate with ^{18}O enrichment) and m/z 299 (derivatized phosphate without ^{18}O enrichment). Controls were performed in which G1Pase and HAD13, respectively, were incubated with unlabeled water. In the absence of enrichment, the experimental value for the 301/299 ratio was 0.13. This value mainly reflects the natural abundance of the corresponding isotopes of phosphate. Therefore, 301/299 ratios greater than 0.13 are a measure of ^{18}O enrichment. Figure 6 shows the 301/299 ratios of the reaction of G1Pase and HAD13 in the presence of $H_2{}^{18}O$ as well as in the presence of unlabeled water. ^{18}O enrichment was only observed in the presence of $H_2{}^{18}O$, demonstrating that the nucleophilic attack occurs at the phosphorus atom of the phosphoryl enzyme intermediate.

As a completely novel feature observed in G1Pase we were able to demonstrate its ability to transfer the phosphate moiety from glucose 1-phosphate to an acceptor other than water. By employing fructose as terminal phosphate acceptor, we were able to establish the first biocatalytic process for the efficient synthesis of fructose 1-phosphate (Scheme 1C), a high-value metabolite, which is difficult to synthesize chemically (33). The turnover number for synthesis of fructose under the conditions tested was determined with 88 s^{-1} and the biocatalytic process described resulted in a fructose 1-phosphate yield of 60% based on the initial glucose 1-phosphate concentration.

In contrast to G1Pase, HAD4 and HAD13 did not show any synthetic activity. A comparison of active-site architecture between HAD13 and G1Pase (Figure 1B versus 1D) proposes that the structural requirements for functional catalysis are by far less stringent in G1Pase than in HAD13. HAD13 is a cofactor dependent enzyme and functional catalysis requires the formation of a complex in which the catalytic residues are precisely aligned to Mg^{2+} and the bound substrate. Furthermore, the HADs are

characterized by mobile caps which supply binding determinants for substrate selectivity (23). The cap domain of HAD4 and HAD13 can be classified as C2 cap, characterized by forming a roof over the active site and access to the internal cavities is supposed to be regulated by the movement of the flap (17). The substrate specificity caused by this movement is not described and unpredictable, but may explain the selectivity for water over fructose we observed in our studies.

Determining the substrate specificity and reaction selectivity of the three phosphatases provided a valuable contribution to understand structure-function relationships and to identify subtle differences, which distinguish the HAD enzymes from G1Pase. The unexpected finding that HADs are just hydrolytic enzymes, whereas G1Pase is a promiscuous enzyme displaying hydrolytic and synthetic activity may be of general interest for the spectrum of activities within the superfamilies and may inspire to test other representatives from the histidine acid phosphatase superfamily for catalyzing phosphoryl transfer reactions.

The first evidence on using phosphatases to catalyze phosphoryl transfer reactions dates back in time to the 1960s, when glucose-6-phosphatase was shown to exhibit hydrolytic and synthetic activity (34, 35). These results prompted studies on bacterial phosphatases from the class-A nonspecific acid phosphatase family such as acid phosphatase from *Shigella flexneri* (12, 31), *Salmonella enteric* (31) and *Morgenella morganii* (36). The acid phosphatases were shown to regioselectively transfer the phosphate group from pyrophosphate to a wide range of compounds like inosine, hexoses and pentoses and various alcohols (12, 31, 36). In this study, however, we employed G1Pase, a representative of the histidine acid phosphatase family, thereby providing the first evidence that one member of this family possesses synthetic activity. Furthermore, G1Pase utilizes fructose as acceptor substrate, thereby enabling the efficient synthesis of fructose 1-phosphate. Weaver et al probed the acceptor substrate specificity of the bacterial acid phosphatase from *Shigella flexneri* and tested several carbohydrates, among them fructose (12). However, the phosphorylation efficiency of the bacterial acid phosphatase towards fructose was found to be extremely low; a transfer yield of 5% was reported. Fructokinase is an enzyme which natural reaction involves the synthesis of fructose 1-phosphate from fructose and ATP. The catalytic activity for fructose 1-phosphate synthesis of recombinantly produced fructokinase from *Lycopersicon esculentum* was rather low (k_{cat} = 28 s^{-1}) and displayed severe substrate inhibition when the fructose concentration exceeded 0.5 mM (37), thereby diminishing the use of fructokinase for synthetic exploitations. Our reported biocatalytic process for fructose 1-phosphate synthesis is a clear improvement over the existing chemical and biocatalytic methods.

MATERIALS AND METHODS

Materials

Phusion DNA polymerase and *Dpn*I were obtained from Fermentas (Burlington, Canada). Oligonucleotide synthesis was performed by Sigma-Aldrich (Vienna, Austria). DNA sequencing was performed at LGC Genomics (Berlin, Germany). GeneJET genomic DNA purification kit was purchased from Fermentas. The plasmid vector pASK-IBA7+, anhydrotetracycline and all materials used for *Strep*-tag purification were obtained from IBA (Göttingen, Germany). Lennox medium was purchased from Roth (Karlsruhe, Germany). Fractogel EMD-DEAE column (2.6 x 9.5 cm) was purchased from Merck (Darmstadt, Germany). HiTrap SP, DEAE FF and Cu^{2+}-loaded IMAC Sepharose High Performance columns were obtained from GE Healthcare (Uppsala, Sweden). Amicon Ultra-15 Centrifugal Filter Units with a 10,000-molecular-weight cutoff were from Millipore (Billerica, USA). Phosphoglucomutase from rabbit muscle (PGM) and glucose-6-phosphate dehydrogenase from *Leuconostoc mesenteroides* (G6PDH) were obtained from Sigma-Aldrich.

All other chemicals were obtained from Sigma-Aldrich or Roth in highest purity available.

Molecular cloning, expression and purification of G1Pase

E. coli BL21-Gold (DE3) cells were grown overnight at 30°C in Lennox-medium. The cells were harvested by centrifugation at 10,000 rpm and 4°C for 30 min and the pellet was used for preparation of genomic DNA. The genomic DNA was isolated by using the GeneJET genomic DNA purification kit. The gene encoding G1Pase was amplified from the genomic DNA by PCR using *Phusion* DNA polymerase and the following pair of primers: 5'-ATGAACAAAACGCTAATCACC-3' and 5'-TTATTTCACCGCTTCATTCAAC-3'. PCR consisted of a pre-heating step at 98°C for 5 min and was followed by 30 reaction cycles of denaturation at 98°C for 30 s, annealing at 70°C for 30 s and elongation at 72°C for 1.5 min. The final extension step was carried out at 72°C for 5 min. The presence of an N-terminal, 66 bp long signal sequence was predicted using SignalIP-4.1 at the Center of Biological Sequence Analysis (http://www.cbs.dtu.dk/services/SignalP-4.1/) (38). To remove the N-terminal signal sequence, to add an N-terminal *Strep*-tag and to prepare the insert for Gibson assembly (39), by extending the C-terminus with overlapping regions to the vector, a PCR using *Phusion* polymerase was performed, employing the following pair of primes: 5'-ATGGCTAGCTGGAG CCACCCGCAGTTCGAAAAAATCGAAGGGCGCCAAACCGTACCGGAAGGCTATCAGC-3' and 5'-CATCCGCCAAAACAGCCAAGCTTATTATTTCACCGCTTCATTC-3'. PCR consisted of a pre-heating step at 98°C for 30 s and was followed by 20 reaction cycles of denaturation at 98°C for 15 s, annealing

at 70°C for 30 s and elongation at 72°C for 42 s. The final extension step was carried out at 72°C for 7 min. To prepare the N-terminus for Gibson assembly by extending the 5′-end of the insert with overlapping regions to the vector, a PCR using *Phusion* polymerase was performed, employing the following pair of primers: 5′-GTTTAACTTTAAGAAGGAGATATACATATGGCTAGCTGGAGCCACC-3′ and 5′-CATCCGCCAAAACAGCCAAGCTTATTATTTCACCGCTTCATTC-3′. PCR consisted of a pre-heating step at 98°C for 30 s and was followed by 30 reaction cycles of denaturation at 98°C for 15 s, annealing at 70°C for 30 s and elongation at 72°C for 42 s. The final extension step was carried out at 72°C for 7 min. The final amplification product was subjected to parental template digest by *Dpn*I. The construct encoding G1Pase was cloned into the linearized pMS470_dsbC vector via Gibson assembly (39). Sequenced plasmid vectors harbouring the G1Pase gene were transformed into *E. coli* Origami B cells. Recipient strains were cultivated in 1-L baffeled shaken flasks at 37°C and 110 rpm using Lennox-medium containing 0.15 mg/mL ampicillin. When OD_{600} reached 0.8, temperature was decreased to 18°C and gene induction was induced with 0.01 mM isopropyl-β-D-thiogalactopyranosid (IPTG) for 21 h. Cells were harvested by centrifugation at 4°C and 5,000 rpm for 30 min in a Sorvall RC-5B Refrigerated Superspeed centrifuge (Du Pont Instruments, Newtown, USA). The pellet was resuspended in 50 mM MES, pH 7.0, and frozen at -20°C. Thawed cell suspension was passed twice through a French pressure cell press (American Instruments, Silver Springs, USA) at 150 bar. Cell debris was removed by centrifugation at 4°C, 13,000 rpm for 30 min. The resulting supernatant was used for further enzyme purification. G1Pase was purified via a two-step purification procedure. The clear supernatant of G1Pase was applied on a *Strep*-Tactin Sepharose column, like described previously (40). Pooled fractions of eluted G1Pase were concentrated, loaded on Fractogel EMD-DEAE and purified according to reported procedures (41). Buffer exchange to 50 mM MES, pH 7.0 was performed using Amicon Ultra-15 Centrifugal Filter Units. Purification was monitored by SDS-PAGE.

Molecular cloning, expression and purification of HAD4

To facilitate efficient protein purification an N-terminal Z_{basic2}-HAD4 fusion protein was constructed. The gene encoding HAD4 was amplified from the pCA24N-yihx vector by PCR using *Phusion* DNA polymerase and the following pair of primers: 5′-GAAGCTCTGTTCCAGGGTCCGCTCTATATCTTT GATTTAG-3′ and 5′-CTTTGTTAGCAGCCGGATCTCTTAGCATAACACCTTCG-3′. PCR consisted of a pre-heating step at 98°C for 5 min and was followed by 30 reaction cycles of denaturation at 98°C for 30 s, annealing at 70°C for 30 s and elongation at 72°C for 1.5 min. The final extension step was carried out at 72°C for 5 min. The resulting PCR product comprised 5′- and 3′- overhangs

that were complementary to the target sequence of the pT7ZbQGKlenow destination vector. Vector pT7ZbQGKlenow was amplified by PCR using *Phusion* DNA polymerase and the following pair of primers: 5'-CGGACCCTGGAACAGAGC-3' and 5'-GAGATCCGGCTGCTAACAAAG-3'. PCR consisted of a pre-heating step at 98°C for 5 min and was followed by 30 reaction cycles of denaturation at 98°C for 30 s, annealing at 70°C for 30 s and elongation at 72°C for 3 min. The final extension step was carried out at 72°C for 5 min. Both amplification products were subjected to parental template digest by *Dpn*I, before they were ligated via Gibson assembly. The sequenced plasmid vector encoding the Z_{basic2}-HAD4 fusion protein was transformed into electrocompetent *E. coli* BL21-Gold (DE3) cells. The recipient strain was cultivated in 1-L baffeled shaking flasks at 37°C and 110 rpm using Lennox-medium containing 0.05 mg/mL kanamycin. When OD_{600} reached 0.8, the temperature was decreased to 20°C and protein expression was induced with 0.01 mM IPTG for 20h. Cells were harvested by centrifugation at 4°C and 5,000 rpm for 30 min in a Sorvall RC-5B refrigerated Superspeed centrifuge. The pellet was resuspended in 50 mM potassium phosphate buffer supplemented with 100 mM NaCl, pH 7.0, and frozen at -20°C. Thawed cell suspension was passed through a French pressure cell press at 150 bar. Cell debris was removed by centrifugation at 4°C, 13,000 rpm for 30 min. The resulting supernatant was used for further enzyme purification.

Protein purification was performed at 6°C using an ÄKTA prime plus system (GE Healthcare, Uppsala, Sweden). All buffers were degassed and filtered using 0.45 μm cellulose-acetate and 0.2 μm polyamide filters. Elution of proteins was monitored at 280 nm. The HiTrap SP FF column (column volume: 5 mL) was equilibrated with 50 mM HEPES buffer supplemented with 100 mM NaCl, pH 7.0 at a flow rate of 5 mL/min. The crude cell extract was passed through a 1.2 μm cellulose-acetate filter and loaded onto the column with a flow rate of 2 mL/min. Elution was accomplished using a continuous salt gradient ranging from 0% to 100% of 50 mM HEPES buffer supplemented with 2 M NaCl, pH 7.0, at a flow rate of 4 mL/min. The target protein eluted at 50% B, corresponding to a salt concentration of 1 M. Pooled fractions were collected and buffer exchange to 50 mM MES, pH 7.0, supplemented with 100 mM NaCl, was performed using Amicon Ultra-15 Centrifugal Filter Units. The stock solution was aliquoted and stored at -20°C. Purification was monitored by SDS-PAGE.

Molecular cloning, expression and purification of HAD13

p15TvL-HAD13, encoding an N-terminal *His*-tagged HAD13, was transformed into electrocompetent *E. coli* BL21-Gold (DE3) cells. The recipient strain was cultivated in 1-L baffeled shaking flasks at 37°C and 110 rpm using Lennox-medium supplemented with 0.15 mg/mL ampicillin. When OD_{600} reached

0.6, the temperature was decreased to 18°C and protein expression was induced with 0.4 mM IPTG for 20 h. Cells were harvested by centrifugation at 4°C and 5,000 rpm for 30 min in a Sorvall RC-5B refrigerated Superspeed centrifuge. The pellet was resuspended in 50 mM HEPES buffer, pH 7.0, and frozen at -20°C. Thawed cell suspension was passed through a French pressure cell press at 150 bar. Cell debris was removed by centrifugation at 4°C, 13,000 rpm for 30 min. The resulting supernatant was used for further purification. Protein purification was done at 6°C using a Bio-Logic Duo-Flow system (model 2128; Bio-Rad, Hercules, USA). Elution of proteins was monitored at 280 nm. All buffers were degassed and filtered using 0.45 μm cellulose-acetate and 0.2 μm Sartolon polyamide filters. The crude cell extract was passed through a 1.2 μm cellulose-acetate filter before loading on a Cu^{2+}-loaded IMAC Sepharose High Performance column (column volume: 14 mL). The column was equilibrated with 50 mM Tris/HCl, pH 7.0, supplemented with 300 mM NaCl, at a flow rate of 5 mL/min. The crude cell extract was applied at a flow rate of 1 mL/min. Elution of the target protein was done by using a stepwise gradient with imidazole by applying a 50 mM Tris/HCl, pH 7.0, supplemented with 300 mM NaCl and 400 mM imidazole at a flow rate of 3 mL/min. Fractions containing HAD13 were pooled, concentrated and a buffer exchange to 50 mM HEPES, pH 7.0, was performed prior loading on the Fractogel EMD-DEAE column. Purification was performed according to reported procedures (41). Final buffer exchange to 50 mM HEPES, pH 7.0, was performed using Amicon Ultra-15 Centrifugal Filter Units. Purification was monitored by SDS-PAGE; protein bands were visualized by silver staining.

CD spectroscopy

Far-UV CD spectra of protein solutions of HAD4 (0.7 mg/mL; 5 mM HEPES supplemented with 10 mM NaCl, pH 7.0), HAD13 (0.7 mg/mL; 5 mM HEPES, pH 7.0) and G1Pase (0.4 mg/mL; 5 mM MES, pH 7.0) were recorded at 25°C on a Jasco J715 spectro-polarimeter (JASCO Inst., Gross-Umstadt, Germany). CD spectra were collected at a scan speed of 100 nm/min at 2.0 nm bandwidth and a response time of 1.0 s. All spectra were recorded in a 0.01 cm cuvette between 190 and 260 nm. All data shown here represent the average of 10 recorded spectra and are corrected with a buffer spectrum. The CD data were evaluated by using the online service Dichroweb (42) with reference database No. 4.

Mass spectrometry

Sample preparation. Purified G1Pase (5 μg) was incubated with 5 mM dithiothreitol (DTT) solution for 30 min at 56°C to reduce the disulfide bonds present, followed by incubation with 20 mM

iodoacetamide (IAA) solution for alkylation of free cysteines for 30 min at 37°C. Another sample (5 μg) of G1Pase was not reduced prior to alkylation with IAA. The reduced/alkylated and non-reduced/alkylated samples were digested with modified trypsin (Promega, Madison, USA) according to Shevchenko et al. (43), and/or with 0.5 μg chymotrypsin (Roche Applied Sciences, Penzberg, Germany) in 50 mM ammonium bicarbonate and 10 mM $CaCl_2$.

MS analysis. Single and double digests were acidified to 0.1% formic acid and separated by nano-HPLC (Dionex Ultimate 3000) equipped with a μ-precolumn (C18, 5 μm, 100 Å, 5 x 0.3 mm) and a Acclaim PepMap RSLC nanocolumn (C18, 2 μm, 100 Å, 150 x 0.075 mm) (all Thermo Fisher Scientific, Vienna, Austria). 0.5 μg of digested protein samples were injected and concentrated on the enrichment column for 2 min at a flow rate of 20 μL/min with 0.5% trifluoroacetic acid as isocratic solvent. Separation was carried out on the nanocolumn at a flow rate of 300 nL/min using the following gradient, where solvent A is 0.05% trifluoroacetic acid in water and solvent B is 0.05% trifluoroacetic acid in 80% acetonitrile: 0-2 min: 4% B; 2-70 min: 4-28% B; 70-94 min: 28-50% B, 94-96 min: 50-95% B; 96-116 min: 95% B; 116-116.1 min: 95-4% B; 116.1-140 min: re-equilibration at 4% B. The sample was ionized in the nanospray source equipped with stainless steel emitters (ES528, Thermo Fisher Scientific, Vienna, Austria) and analyzed in a Orbitrap velos mass spectrometer (Thermo Fisher Scientific, Waltham, MA, USA) operated in positive ion mode, applying alternating full scan MS (m/z 400 to 2000) in the ion cyclotron and MS/MS by higher-energy collisional dissociation of the 20 most intense peaks with dynamic exclusion enabled. The LC-MS/MS data were analyzed by searching a database containing the protein sequences of G1Pase and known background proteins with Mascot 2.3 (MatrixScience, London, UK). Search criteria were charge 2+ or 3+, precursor mass error 0.05 Da, and product mass error 0.7 Da, and carbamidomethylation, oxidation on methionine, -2H on cysteine (disulfide) as variable modifications. A maximum false discovery rate of 0.05 using decoy database search, an ion score cut off of 20 and a minimum of 2 identified peptides were chosen as protein identification criteria. As an alternative approach for detection of disulfide bridges the respective database of crosslinked linearized peptides of G1Pase was generated by xComb (44) for trypsin and for chymotrypsin single and double digests, allowing inter- and intramolecular crosslinks and up to three missed cleavage sites, and searched with Mascot 2.3. For the crosslinked peptides Mascot search criteria were as described above except that a Mascot ion score of 15 and 1 identified peptide were used as threshold.

Assays

Phosphatase activities were quantified by using a continuous *p*-nitrophenylphosphate hydrolysis assay

based on a spectrophotometric measurement at 405 nm on a Beckman Coulter DU 800 UV/VIS spectrophotometer (Krefeld, Germany). Reaction mixtures used for assessing the activity of HAD4 and HAD13 contained 4 mM *p*-nitrophenylphosphate and 5 mM $MgCl_2$ in 50 mM HEPES, pH 7.0 and were carried out at 30°C. For G1Pase, the reaction mixture contained 4 mM *p*-nitrophenylphosphate in 50 mM MES, pH 7.0 and was carried out at 30°C. Activity is expressed in U/mg protein. The total protein concentration was determined as described by Bradford (45) employing Roti-Quant referenced against BSA.

The quantity of inorganic phosphate present was determined colorimetrically at 850 nm (46). Glucose 1-phosphate and glucose 6-phosphate were assayed in a coupled enzymatic system with PGM and G6PDH (47). Fructose 6-phosphate was determined using an assay with mannitol 1-phosphate dehydrogenase (48). The concentration of fructose 1-phosphate was quantified indirectly by using equation 1 and directly by using HPAE-PAD and NMR:

Fructose 1-phosphate$_{end}$ = glucose 1-phosphate$_{start}$ - glucose 1-phosphate$_{end}$ - glucose 6-phosphate$_{end}$ - fructose 6-phosphate$_{end}$ - phosphate$_{end}$ (1)

Hydrolysis studies

The hydrolytic activities towards glucose 1-phosphate, β-glucose 1-phosphate, fructose 1-phosphate and fructose 6-phosphate were determined for the three phosphatases. Each substrate was present in a concentration of 20 mM. Reactions employing HAD4 and HAD13 were performed in 50 mM HEPES supplemented with 5 mM $MgCl_2$, pH 7.0, at 37°C and 650 rpm. The reactions were started by addition of 3.2 μM HAD4 and 0.2 μM HAD13, respectively. Reaction mixtures were incubated for 150 min using discontinuous assays. Samples were taken in 30 min intervals and further processed like described below. The reactions with G1Pase were performed in 50 mM MES, pH 7.0, at 37°C and 650 rpm and were started by addition of 0.07 μM G1Pase. Reaction mixtures were incubated for 75 min using discontinuous assays. Samples were taken in 15 min intervals.

All samples were heat-treated at 99°C for 5 min to inactivate the enzyme and centrifuged at 13,000 rpm for 5 min to remove precipitated protein prior to further analysis. To determine the hydrolytic activity (k_{cat}) towards each donor substrate, the release of phosphate was measured. Catalytic activities were calculated by applying equation 2, where k_{cat} is the catalytic constant [s^{-1}], V_{max} is the maximal initial rate [mM min^{-1}] and E is the total molar enzyme concentration based on a molecular mass of 31 kDa for HAD4 and HAD13, respectively and 45 kDa for G1Pase.

$$k_{cat} = \frac{V_{max}}{E} \quad (2)$$

Phosphoryl transfer studies

To investigate the potential of the three posphatases to catalyze phosphoryl transfer from glucose 1-phosphate to fructose, 20 mM glucose 1-phosphate were incubated with 100 mM fructose. Reactions employing HAD4 and HAD13 were performed in 50 mM HEPES supplemented with 5 mM $MgCl_2$, pH 7.0, at 37°C and 650 rpm. The reactions were started by addition of 3.2 μM HAD4 and 0.2 μM HAD13, respectively. Reaction mixtures were incubated for 90 min using discontinuous assays. Samples were taken in 15 min intervals. The reactions with G1Pase were performed in 50 mM MES, pH 7.0, at 37°C and 650 rpm and were started by addition of 0.1 μM G1Pase. Reaction mixtures were incubated for 75 min using discontinuous assays. Samples were taken in 15 min intervals. All samples were heat-treated at 99°C for 5 min to inactivate the enzyme and centrifuged at 13,000 rpm for 5 min to remove precipitated protein prior to further analysis. Concentrations of glucose 1-phosphate, glucose 6-phosphate, fructose 1-phosphate, fructose 6-phosphate and phosphate were determined as described. Catalytic activities were calculated by applying equation 2.

Inorganic phosphate-water medium ^{18}O exchange

Sample preparation. 1 mM glucose 1-phosphate and 50 mM MES, pH 7.0 were solved in 90% $H_2{}^{18}O$. The reaction was started by addition of either G1Pase (0.1 μM), HAD4 (1.0 μM) or HAD13 (0.6 μM) and was incubated at 37°C, 650 rpm for 2 h. After incubation the reaction was stopped by heating the sample at 99°C for 5 min. The control samples with H_2O instead of $H_2{}^{18}O$ were treated in the same way. The resulting assay mixtures were analyzed by GC-MS.

GC-MS analysis. The reaction mixtures were evaporated in a SpeedVac for 3 h and subsequently derivatized with BSTFA/1%TMCS in pyridine (1:2, v:v). GC-MS analysis was performed using a Trace GC and DSQ–MS (Thermo Scientific, Vienna, Austria). The following GC parameters were used: Injection volume: 1 μL, injector temperature: 250°C, carrier gas: He, carrier gas flow: 1mL/min, column: HP-5MS (60m, ID 0.250 mm, film thickness 0.25 μm) (Agilent, Waldbronn, Germany). The temperature gradient was as follows: Starting temperature 110°C for 4 min, up to 300°C at a heating rate of 20°C/min, final hold time 10 min.

The MS was operated in EI mode (source temperature 280°C) and the detected mass range was 50-700 m/z. The extracted ion chromatograms of m/z 299 and m/z 301 were integrated using the Xcalibur 1.4 software (Thermo Scientific, Vienna, Austria).

High performance anion exchange chromatography with pulsed amperometric detection (HPAE-PAD)

To directly detect the formation of fructose 1-phosphate, selected samples were analyzed on a Dionex BioLC system (Dionex Corporation, Sunnyvale, USA) equipped with a CarboPac PA10 column (4 x 250 mm) and an Amino Trap guard column (4 x 50 mm) thermostated at 30°C. Glucose, fructose, glucose 1-phosphate, glucose 6-phosphate, fructose 1-phosphate and fructose 6-phosphate were detected with an ED50A electrochemical detector using a gold working electrode and a silver/silver chloride reference electrode by applying the predefined waveform for carbohydrates. Elution was carried out at a flow rate of 0.9 mL/min with the following method: isocratic flow of 52 mM NaOH for 20 min, followed by a linear gradient from 100 mM NaOAc to 400 mM NaOAc applied within 25 min in an isocratic background of 100 mM NaOH. The column was washed 5 min with 52 mM NaOH. Under the conditions applied glucose eluted after 10.2 min, fructose after 11.8 min, glucose 1-phosphate after 30.3 min, glucose 6-phosphate after 36.6 min, fructose 1-phosphate after 37.2 min and fructose 6-phosphate after 39.1 min.

NMR spectroscopic measurements

Sample preparation. 20 mM glucose 1-phosphate and 200 mM fructose were incubated with 0.1 μM G1Pase in 50 mM MES, pH 7.0. The reaction was kept at 37°C, 650 rpm for 75 min and was stopped by heat-treatment at 99°C for 5 min. After centrifugation at 13,000 rpm for 5 min, the supernatant was applied on a DEAE FF column, pre-equilibrated with deionized water. Unbound, non-charged monosaccharides were removed by washing with deionized water. Elution of phosphorylated reaction products was accomplished by using 50 mM NaCl. Fractions containing the phosphorylated product were pooled and concentrated by lyophilisation (Christ Alpha, Shrewsbury, UK), prior to NMR analysis.

NMR analysis. The isolated compound was dissolved in D_2O (5.0 mg in 0.7 mL) and transferred into 5 mm high precision NMR sample tubes. Measurements were performed on a Bruker DRX-400 at 400.13 MHz (^{1}H) using the Topspin 1.3 software. 1D ^{1}H NMR spectra were recorded by acquisition of 64 k data points and Fourier transformation resulting in spectra with a range of 14 ppm. To determine the 2D COSY, TOCSY, and NOESY spectra 128 experiments with 2048 data points each were recorded and Fourier transformed to 2D-spectra with a range of 10 ppm. Measurement temperature was 298 K +/- 0.05 K and external acetone was used as shift reference standard (δ_H 2.225).

Acknowledgements

We acknowledge financial support from the Austrian Science Funds FWF (project L586-B03); Alexander Yakunin (Department of Chemical Engineering and Applied Chemistry, University of Toronto, Canada) for providing pCA24N_yihx and p15TvL_yida; Harald Pichler (Institute of Molecular Biotechnology, Graz University of Technology, Austria) for providing pMS470_dsbC; Sophia Hober (Department of Biotechnology, Royal Institute of Technology (KTH) Stockholm, Sweden) for providing pT7ZbQG-Klenow; Tom Desmet (Centre for Industrial Biotechnology and Biocatalysis, Ghent University, Belgium) for synthesis of β-glucose 1-phosphate and Christian Fercher (Institute for Molecular Biosciences, Karl-Franzens University Graz, Austria) for help in recording CD spectra.

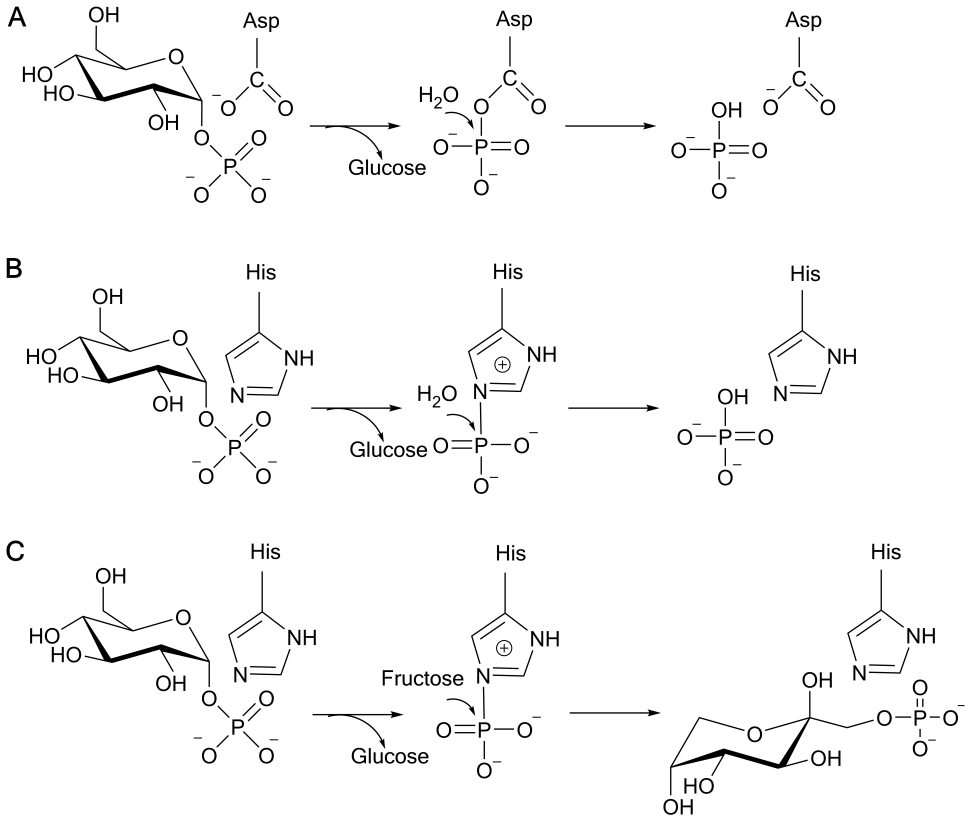

Scheme 1. The proposed reaction mechanisms for hydrolysis of glucose 1-phosphate catalyzed by HAD4 and HAD13, respectively (A), and G1Pase (B). (C) The reaction mechanism for phosphoryl transfer from glucose 1-phosphate to fructose catalyzed by G1Pase.

Note: The theoretical anomeric composition of fructose 1-phosphate in aqueous solution is α-furanose 5%, β-furanose 16%, α-pyranose 5% and β-pyranose 73% (49). Fructose 1-phosphate is shown here in the β-pyranose form.

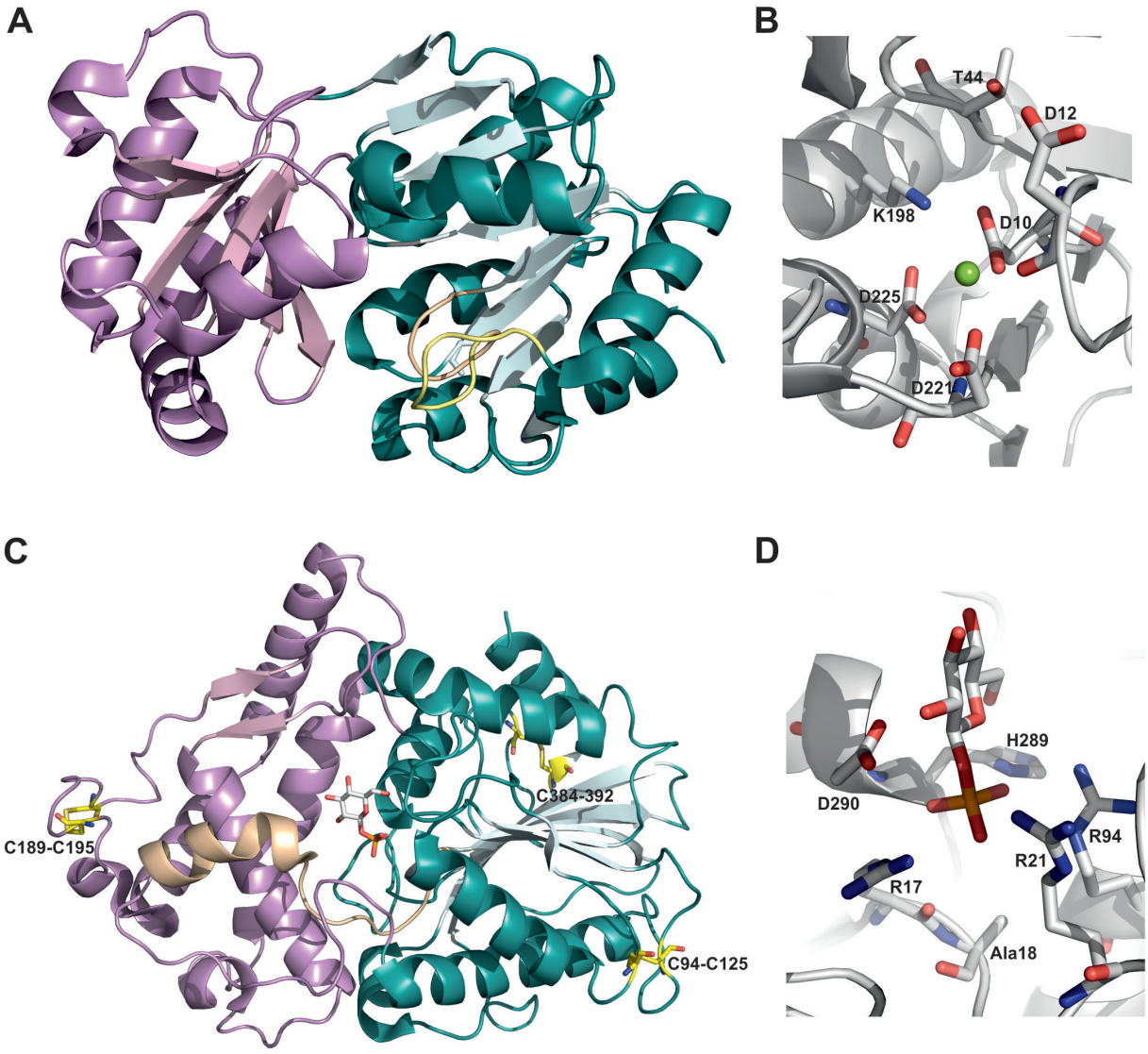

Figure 1. Domain structure and active-site architecture of HAD13 and G1Pase. (A) Three-dimensional fold of *E. coli* HAD13 (pdb entry 1rkq). The cap-domain is colored violet, the α/β domain cyan. The squiggle is indicated in wheat, the flap in yellow. (B) Close-up view on active-site residues of HAD13 complexed with Mg^{2+}. (C) Three-dimensional structure of *E. coli* G1Pase complexed with glucose 1-phosphate (pdb entry 1nt4, chain A). The α-domain is colored violet, the α/β domain cyan and the central catalytic shaft wheat. The three disulfide bonds C94-C125, C189-C195 and C384-C392 are indicated. (D) Stereo view of the active-site of G1Pase containing glucose 1-phosphate in the complex. The catalytic residues are depicted in stick representation.

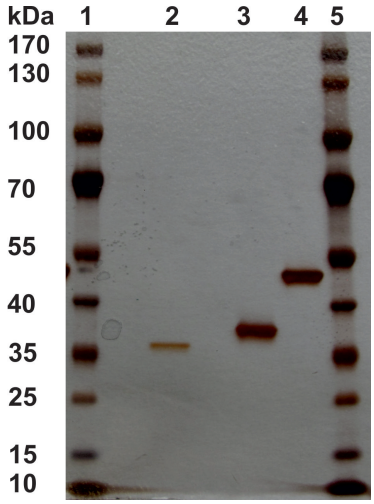

Figure 2. Enzyme purity was verified by SDS-PAGE. Lane 1: molecular mass standard; 2: HAD4; 3: HAD13; 4: G1Pase; 5: molecular mass standard.

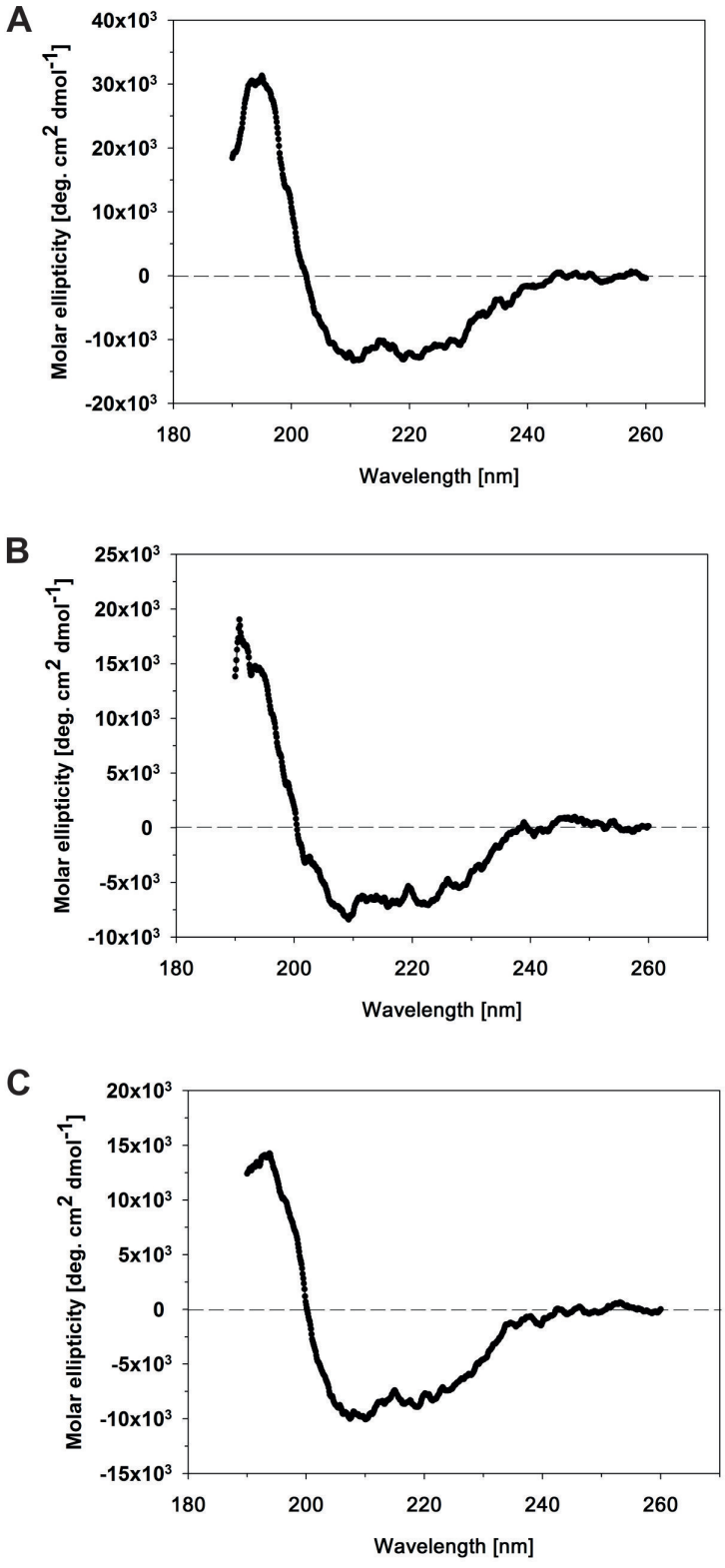

Figure 3. CD-analysis of G1Pase (A), HAD4 (B) and HAD13 (C). The black curve represents the average of ten individual wavelength scans.

A

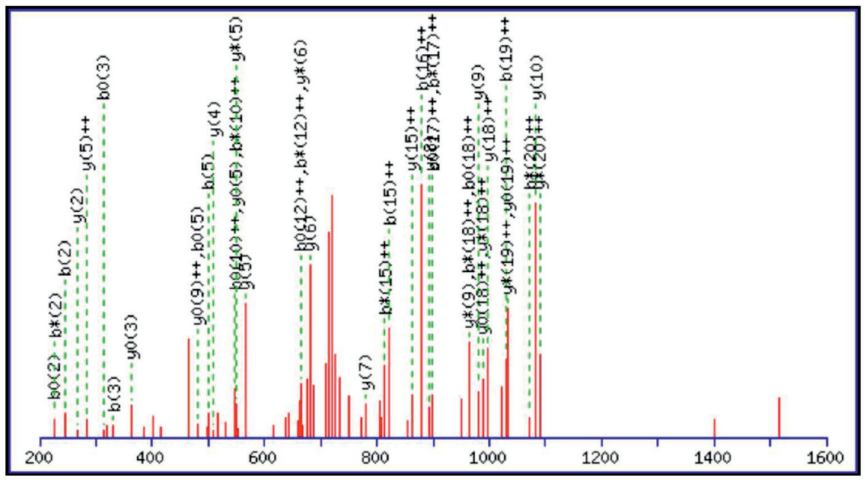

B

#	b	b^{++}	b*	b^{*++}	b^{0}	b^{0++}	Seq.	y	y^{++}	y*	y^{*++}	y^{0}	y^{0++}	#
1	129.1022	65.0548	112.0757	56.5415			K							21
2	***244.1292***	122.5682	227.1026	114.0550	226.1186	113.5629	D	2196.0060	1098.5066	2178.9794	1089.9934	2177.9954	1089.5013	20
3	***331.1612***	166.0842	314.1347	157.5710	313.1506	157.0790	S	2080.9790	1040.9932	2063.9525	1032.4799	2062.9685	1031.9879	19
4	428.2140	214.6106	411.1874	206.0974	410.2034	205.6053	P	1993.9470	997.4771	1976.9205	988.9639	1975.9364	988.4719	18
5	***499.2511***	250.1292	482.2245	241.6159	481.2405	241.1239	A	1896.8942	948.9508	1879.8677	940.4375	1878.8837	939.9455	17
6	600.2446	300.6259	583.2181	292.1127	582.2341	291.6207	C	1825.8571	913.4322	1808.8306	904.9189	1807.8466	904.4269	16
7	728.3396	364.6734	711.3130	356.1602	710.3290	355.6681	K	1724.8636	862.9354	1707.8370	854.4222	1706.8530	853.9302	15
8	857.3822	429.1947	840.3556	420.6815	839.3716	420.1894	E	1596.7686	798.8880	1579.7421	790.3747	1578.7581	789.8827	14
9	985.4771	493.2422	968.4506	484.7289	967.4666	484.2369	K	1467.7260	734.3667	1450.6995	725.8534	1449.7155	725.3614	13
10	1113.5357	557.2715	1096.5092	548.7582	1095.5252	548.2662	Q	1339.6311	670.3192	1322.6045	661.8059	1321.6205	661.3139	12
11	1241.5943	621.3008	1224.5677	612.7875	1223.5837	612.2955	Q	1211.5725	606.2899	1194.5460	597.7766	1193.5619	597.2846	11
12	1344.6035	672.8054	1327.5769	664.2921	1326.5929	663.8001	C	***1083.5139***	542.2606	1066.4874	533.7473	1065.5034	533.2553	10
13	1431.6355	716.3214	1414.6090	707.8081	1413.6249	707.3161	S	***980.5047***	490.7560	963.4782	482.2427	962.4942	481.7507	9
14	1544.7196	772.8634	1527.6930	764.3502	1526.7090	763.8581	L	***893.4727***	447.2400	876.4462	438.7267	875.4621	438.2347	8
15	1643.7880	**822.3976**	1626.7614	813.8844	1625.7774	813.3924	V	***780.3886***	390.6980	763.3621	382.1847	762.3781	381.6927	7
16	1758.8149	**879.9111**	1741.7884	871.3978	1740.8044	870.9058	D	***681.3202***	341.1638	664.2937	332.6505	663.3097	332.1585	6
17	1815.8364	908.4218	1798.8098	899.9086	1797.8258	899.4166	G	***566.2933***	283.6503	549.2667	275.1370	548.2827	274.6450	5
18	1943.9314	972.4693	1926.9048	963.9560	1925.9208	963.4640	K	***509.2718***	255.1395	492.2453	246.6263	491.2613	246.1343	4
19	2057.9743	**1029.4908**	2040.9477	1020.9775	2039.9637	1020.4855	N	381.1769	191.0921	364.1503	182.5788	363.1663	182.0868	3
20	2159.0220	1080.0146	2141.9954	1071.5013	2141.0114	1071.0093	T	***267.1339***	134.0706			249.1234	125.0653	2
21							F	166.0863	83.5468					1

Figure 4. Interpreted MS-MS spectra and detected b and y ions from Mascot search results of the disulfide bond formed between Cys189 and Cys195 are shown.

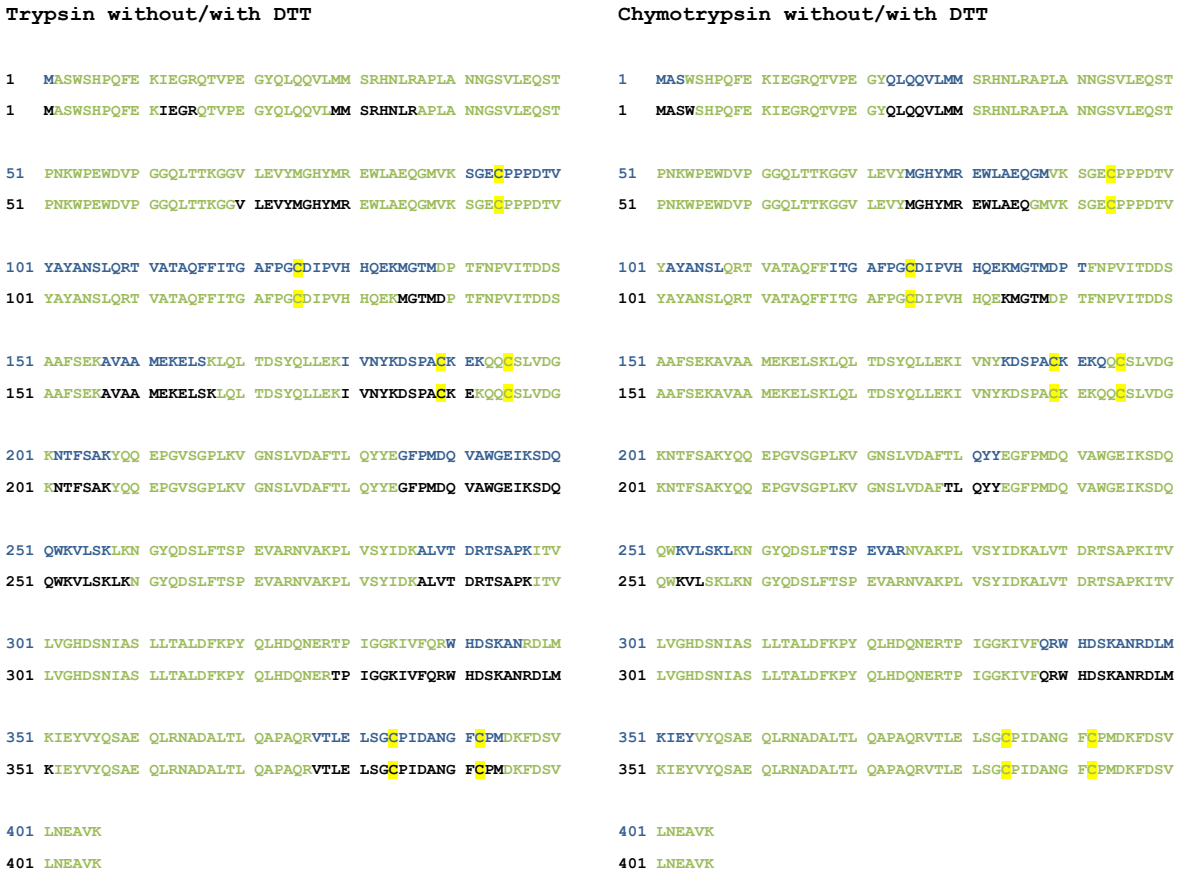

Figure 5. First line (blue): Sample was alkylated with IAA and treated with trypsin/chymotrypsin. Second line (black): Sample was reduced with DTT, alkylated with IAA and digested with trypsin/chymotrypsin. Cysteines involved in disulfide bridges are highlighted yellow. Matched peptides are shown in green.

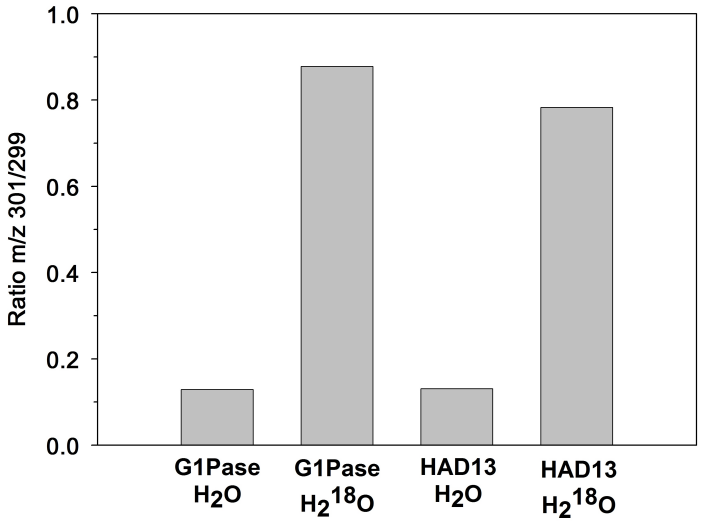

Figure 6. The second step of the reaction mechanism of G1Pase and HAD13 involves hydrolysis of the phosphoryl enzyme intermediate via a nucleophilic attack by an activated water molecule on the phosphorus atom. In line with the proposed mechanism, ^{18}O was incorporated into the phosphate leaving group when the hydrolysis of glucose 1-phosphate was performed in the presence of $H_2{}^{18}O$, reflected by an ^{18}O enrichment in phosphate (m/z $301/299 > 0.13$).

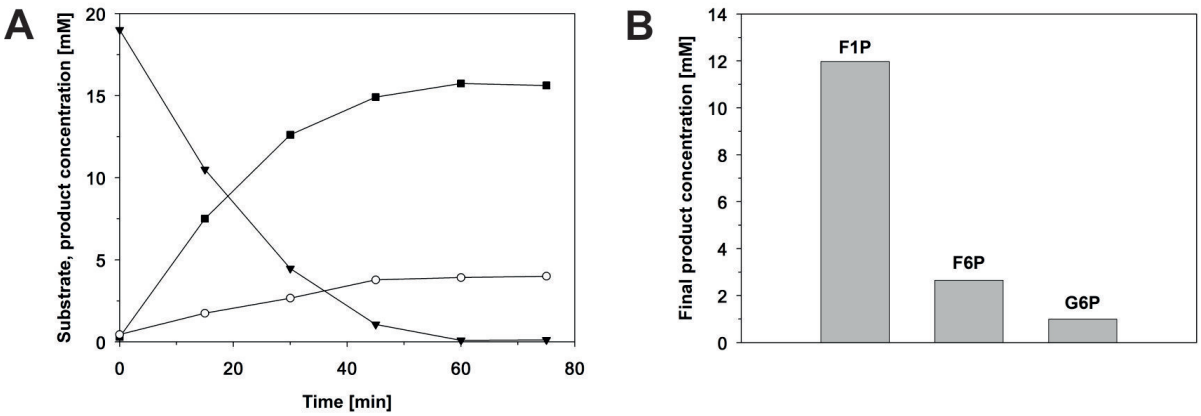

Figure 7. (A) Time-course for the synthesis of phosphorylated products from glucose 1-phosphate and fructose by G1Pase at 37°C. The reaction mixture contained 20 mM glucose 1-phosphate, 200 mM fructose and 0.1 μM G1Pase in 50 mM MES, pH 7.0. Symbols indicate: glucose 1-phosphate (▼), sum of phosphorylated products (■) and phosphate (○). (B) The observed product pattern at the end of the reaction.

Table 1. The secondary structure content for G1Pase, HAD4 and HAD13 as extracted from the CD data is shown and compared with the secondary structural elements as observed in the crystal structures (numbers in parenthesis; amount of turns/unordered not available).

Secondary structure	**G1Pase** [%]	**HAD4** [%]	**HAD13** [%]
Alpha helices	51 (39)	17 (48)	28 (39)
Beta strands	22 (14)	30 (15)	25 (22)
Turns	11	22	19
Unordered	16	31	28

Table 2. Hydrolytic activities of purified phosphatases towards various substrates.

Substrate	**G1Pase** k_{cat} [s^{-1}]	**HAD4** k_{cat} [s^{-1}]	**HAD13** k_{cat} [s^{-1}]
Glucose 1-phosphate	40	2.3 [a]	12
β-Glucose 1-phosphate	n.d.	$1.0\ 10^{-2}$	$6.0\ 10^{-2}$
Glucose 6-phosphate	56	$2.0\ 10^{-2}$	8.6 [b]
Fructose 1-phosphate	22	n.t.	n.t.
Fructose 6-phosphate	22 [d]	$6.0\ 10^{-2}$	4.4 [c]
Phytate	2.1	n.d.	n.d.
Pyrophosphate	n.d.	n.d.	n.d.

The S.D. for k_{cat} was $\leq$ 10% of the reported values respectively, with the exception of [a]23%, [b]18%, [c]24%, [d]14%; n.t. not tested, n.d. no activity above detection limits ($\leq$ 2.5 μM).

References

1. Westheimer FH. 1987. Why nature chose phosphates. Science 235:1173-1178.

2. Bowler MW, Cliff MJ, Waltho JP, Blackburn GM. 2010. Why did Nature select phosphate for its dominant roles in biology? New J Chem 34:784-794.

3. Knowles JR. 1980. Enzyme-catalyzed phosphoryl transfer reactions. Annu Rev Biochem 49:877-919.

4. Allen KN, Dunaway-Mariano D. 2004. Phosphoryl group transfer: evolution of a catalytic scaffold. Trends Biochem Sci 29:495-503.

5. Lassila JK, Zalatan JG, Herschlag D. 2011. Biological phosphoryl-transfer reactions: understanding mechanism and catalysis. Annu Rev Biochem 80:669-702.

6. Thompson PR, Cole PA. 2001. Probing the mechanism of enzymatic phosphoryl transfer with a chemical trick. Proc Natl Acad Sci USA 98:8170-8171.

7. Auriol D, Nalin R, Lefevre F, Ginolhac A, Guembecker DD, Zago C. 2008. Method for preparing C-6 phosphorylated D-aldohexoses and C-6 phosphorylated D-aldohexose derivatives. Libragen FR.

8. Heimbach T, Oh DM, Li LY, Rodriguez-Hornedo N, Garcia G, Fleisher D. 2003. Enzyme-mediated precipitation of parent drugs from their phosphate prodrugs. Int J Pharm 261:81-92.

9. Lunin VV, Li Y, Schrag JD, Iannuzzi P, Cygler M, Matte A. 2004. Crystal structures of *Escherichia coli* ATP-dependent glucokinase and its complex with glucose. J Bacteriol 186:6915-6927.

10. Sigrell JA, Cameron AD, Jones TA, Mowbray SL. 1997. Purification, characterization, and crystallization of *Escherichia coli* ribokinase. Protein Sci 6:2474-2476.

11. Zhao H, van der Donk WA. 2003. Regeneration of cofactors for use in biocatalysis. Curr Opin Biotechnol 14:583-589.

12. van Herk T, Hartog AF, van der Burg AM, Wever R. 2005. Regioselective phosphorylation of carbohydrates and various alcohols by bacterial acid phosphatases; probing the substrate specificity of the enzyme from *Shigella flexneri*. Adv Syn Catal 347:1155-1162.

13. Babich L, Hartog AF, van der Horst MA, Wever R. 2012. Continuous-flow reactor-based enzymatic synthesis of phosphorylated compounds on a large scale. Chem Eur J 18:6604-6609.

14. Luley-Goedl C, Nidetzky B. 2010. Carbohydrate synthesis by disaccharide phosphorylases: reactions, catalytic mechanisms and application in the glycosciences. Biotechnol J 5:1324-1338.

15. Kuznetsova E, Proudfoot M, Gonzalez CF, Brown G, Omelchenko MV, Borozan I, Carmel L, Wolf YI, Mori H, Savchenko AV, Arrowsmith CH, Koonin EV, Edwards AM, Yakunin AF. 2006. Genome-wide analysis of substrate specificities of the *Escherichia coli* haloacid dehalogenase-like phosphatase family. J Biol Chem 281:36149-36161.

16. Lee DC, Cottrill MA, Forsberg CW, Jia Z. 2003. Functional insights revealed by the crystal structures of *Escherichia coli* glucose-1-phosphatase. J Biol Chem 278:31412-31418.

17. Burroughs AM, Allen KN, Dunaway-Mariano D, Aravind L. 2006. Evolutionary genomics of the

HAD superfamily: understanding the structural adaptations and catalytic diversity in a superfamily of phosphoesterases and allied enzymes. J Mol Biol 361:1003-1034.

18. Lu Z, Dunaway-Mariano D, Allen KN. 2008. The catalytic scaffold of the haloalkanoic acid dehalogenase enzyme superfamily acts as a mold for the trigonal bipyramidal transition state. Proc Natl Acad Sci USA 105:5687-5692.

19. Collet JF, Stroobant V, Pirard M, Delpierre G, Van Schaftingen E. 1998. A new class of phosphotransferases phosphorylated on an aspartate residue in an amino-terminal DXDX(T/V) motif. J Biol Chem 273:14107-14112.

20. Lahiri SD, Zhang G, Dunaway-Mariano D, Allen KN. 2006. Diversification of function in the haloacid dehalogenase enzyme superfamily: The role of the cap domain in hydrolytic phosphoruscarbon bond cleavage. Bioorg Chem 34:394-409.

21. Morais MC, Zhang W, Baker AS, Zhang G, Dunaway-Mariano D, Allen KN. 2000. The crystal structure of *Bacillus cereus* phosphonoacetaldehyde hydrolase: insight into catalysis of phosphorus bond cleavage and catalytic diversification within the HAD enzyme superfamily. Biochemistry 39:10385-10396.

22. Jia Z, Cottrill M, Pal GP, Lee D, Sung M, Forsberg CW, Phillips JP. 2001. Purification, crystallization and preliminary X-ray analysis of the *Escherichia coli* glucose-1-phosphatase. Acta Crystallogr, Sect D: Biol Crystallogr 57:314-316.

23. Seifried A, Schultz J, Gohla A. 2013. Human HAD phosphatases: structure, mechanism, and roles in health and disease. FEBS J 280:549-571.

24. Van Etten RL. 1982. Human prostatic acid phosphatase: a histidine phosphatase. Ann N Y Acad Sci 390:27-51.

25. Vincent JB, Crowder MW, Averill BA. 1992. Hydrolysis of phosphate monoesters: a biological problem with multiple chemical solutions. Trends Biochem Sci 17:105-110.

26. Pradel E, Boquet PL. 1991. Utilization of exogenous glucose-1-phosphate as a source of carbon or phosphate by *Escherichia coli* K12: respective roles of acid glucose-1-phosphatase, hexosephosphate permease, phosphoglucomutase and alkaline phosphatase. Res Microbiol 142:37-45.

27. Gräslund T, Ehn M, Lundin G, Hedhammar M, Uhlen M, Nygren PA, Hober S. 2002. Strategy for highly selective ion-exchange capture using a charge-polarizing fusion partner. J Chromatogr A 942:157-166.

28. Gräslund T, Lundin G, Uhlen M, Nygren PA, Hober S. 2000. Charge engineering of a protein domain to allow efficient ion-exchange recovery. Protein Eng 13:703-709.

29. Hedhammar M, Hober S. 2007. Z(basic) - a novel purification tag for efficient protein recovery. J Chromatogr A 1161:22-28.

30. Kuznetsova E, Proudfoot M, Sanders SA, Reinking J, Savchenko A, Arrowsmith CH, Edwards AM, Yakunin AF. 2005. Enzyme genomics: Application of general enzymatic screens to discover new enzymes. FEMS Microbiol Rev 29:263-279.

31. Tanaka N, Hasan Z, Hartog AF, van Herk T, Wever R, Sanders RJ. 2003. Phosphorylation and dephosphorylation of polyhydroxy compounds by class A bacterial acid phosphatases. Org Biomol Chem 1:2833-2839.

32. Cottrill MA, Golovan SP, Phillips JP, Forsberg CW. 2002. Inositol phosphatase activity of the *Escherichia coli agp*-encoded acid glucose-1-phosphatase. Can J Microbiol 48:801-809.

33. Pogell BM. 1953. A new synthesis of fructose-1-phosphate with phosphorus pentoxide. J Biol Chem 201:645-649.

34. Nordlie RC, Arion WJ. 1964. Evidence for the common identity of glucose 6-phosphatase, inorganic pyrophosphatase, and pyrophosphate-glucose phosphotransferase. J Biol Chem 239:1680-1685.

35. Stetten MR, Taft HL. 1964. Metabolism of inorganic pyrophosphate II. The probable identity of microsomal inorganic pyrophosphatase, pyrophosphate phosphotransferase, and glucose 6-phosphatase. J Biol Chem 239:4041-4046.

36. Asano Y, Mihara Y, Yamada H. 1999. A novel selective nucleoside phosphorylating enzyme from *Morganella morganii*. J Biosci Bioeng 87:732-738.

37. Martinez-Barajas E, Krohn BM, Stark DM, Randall DD. 1997. Purification and characterization of recombinant tomato fruit (*Lycopersicon esculentum* Mill.) fructokinase expressed in *Escherichia coli*. Protein Expr Purif 11:41-46.

38. Petersen TN, Brunak S, von Heijne G, Nielsen H. 2011. SignalP 4.0: discriminating signal peptides from transmembrane regions. Nat Methods 8:785-786.

39. Gibson DG, Young L, Chuang RY, Venter JC, Hutchison CA, 3rd, Smith HO. 2009. Enzymatic assembly of DNA molecules up to several hundred kilobases. Nat Methods 6:343-345.

40. Wildberger P, Todea A, Nidetzky B. 2012. Probing enzyme-substrate interactions at the catalytic subsite of *Leuconostoc mesenteroides* sucrose phosphorylase with site-directed mutagenesis: the roles of Asp49 and Arg395. Biocatal Biotransform 30:326-337.

41. Schwarz A, Nidetzky B. 2006. Asp-196 $\rightarrow$ Ala mutant of *Leuconostoc mesenteroides* sucrose phosphorylase exhibits altered stereochemical course and kinetic mechanism of glucosyl transfer to and from phosphate. FEBS Lett 580:3905-3910.

42. Whitmore L, Wallace BA. 2008. Protein secondary structure analyses from circular dichroism spectroscopy: methods and reference databases. Biopolymers 89:392-400.

43. Shevchenko A, Wilm M, Vorm O, Mann M. 1996. Mass spectrometric sequencing of proteins silver-stained polyacrylamide gels. Anal Chem 68:850-858.

44. Panchaud A, Singh P, Shaffer SA, Goodlett DR. 2010. xComb: a cross-linked peptide database approach to protein-protein interaction analysis. J Proteome Res 9:2508-2515.

45. Bradford MM. 1976. A rapid and sensitive method for the quantitation of microgram quantities of protein utilizing the principle of protein-dye binding. Anal Biochem 72:248-254.

46. Saheki S, Takeda A, Shimazu T. 1985. Assay of inorganic phosphate in the mild pH range, suitable for measurement of glycogen phosphorylase activity. Anal Biochem 148:277-281.

47. Eis C, Nidetzky B. 1999. Characterization of trehalose phosphorylase from *Schizophyllum commune*. Biochem J 341:385-393.

48. Krahulec S, Armao GC, Weber H, Klimacek M, Nidetzky B. 2008. Characterization of recombinant *Aspergillus fumigatus* mannitol-1-phosphate 5-dehydrogenase and its application for the stereoselective synthesis of protio and deuterio forms of D-mannitol 1-phosphate. Carbohydr Res 343:1414-1423.

49. Koerner TA, Jr., Voll RJ, Cary LW, Younathan ES. 1980. Carbon-13 nuclear magnetic resonance studies and anomeric composition of ketohexose phosphates in solution. Biochemistry 19:2795-2801.

8 Efficient one-pot synthesis of fructose 1-phosphate from inexpensive starting materials by using a coupled enzymatic system based on sucrose phosphorylase and glucose-1-phosphatase

Patricia Wildberger[a], Martin Pfeiffer[a], Lothar Brecker[b] and Bernd Nidetzky[a,*]

[a] Institute of Biotechnology and Biochemical Engineering, Graz University of Technology, Petersgasse 12/1, A-8010 Graz, Austria

[b] Institute of Organic Chemistry, University of Vienna, Währingerstraße 38, A-1090 Vienna, Austria

*Corresponding author

E-mail: bernd.nidetzky@tugraz.at; Tel. +43-316-873-8400; Fax +43-316-873-8434

Sugar phosphates are essential central metabolites in the non-oxidative pentose phosphate pathway, in the Calvin cycle and of particular interest for the study of metabolic diseases (1-3). However, although highly demanded, their availability is limited. Chemical synthesis of sugar phosphates involves tedious protection and deprotection steps, often accompanied by low product yields, formation of undesired side products and the use of organic solvents and toxic reagents (4-6). Enzymatic methods, however, facilitate mild reaction conditions without the need for complex protection/deprotection strategies. Enzymes employed for the synthesis of sugar phosphates are kinases and phosphatases. β-L-Fucose 1-phosphate (7) or α-D-galactose 1-phosphate (8) are products of successful kinase-catalyzed synthesis reactions, the accompanied bottlenecks include high expenses for the nucleoside triphosphates required as donor substrates and potential inhibitory effects of the resulting nucleoside diphosphates. To circumvent these limitations, phosphatases were considered as alternatives to the use of kinases. Biochemical studies of mammalian glucose-6-phosphatase go back in time to the 1960s, when it was shown for the first time that the enzyme exhibits hydrolytic and synthetic activity towards glucose 6-phosphate (9, 10). Follow-up studies identified glucose-6-phosphatase as multifunctional enzyme, utilizing pyrophosphate, nucleoside di- and triphosphates and sugar phosphate esters as phosphoryl donors and transferring the phosphoryl group to glucose as well as to other polyols or sugars (11). These results prompted studies on bacterial phosphatases from the class-A nonspecific acid phosphatase family such as acid phosphatase from *Shigella flexneri* (12, 13), *Salmonella enterica* (12) and *Morganella morganii* (14). The acid phosphatases were shown to regioselectively transfer the phosphate group from pyrophosphate to a wide range of compounds like inosine, hexoses and pentoses and various alcohols (12-14). The major drawback of the utilization of acid phosphatases in transphosphorylation reactions lies in the reversibility of the reactions, which results in the dephosphorylation of the reaction product upon formation. To circumvent this limitation a continuous-flow reactor-based enzymatic synthesis system was established with which phosphorylated compounds, among them glucose 6-phosphate, *N*-acetyl-D-glucosamine 6-phosphate and glycerol 1-phosphate, were produced on a larger scale by immobilized acid phosphatase (15). In a further step a multi-enzyme continuous process with immobilized acid phosphatase and aldolase was described, which resulted in the efficient, but tedious synthesis of sugar analogues (16).

Herein we present an operationally simple, one-pot, two-step cascade reaction for the efficient synthesis of fructose 1-phosphate from the inexpensive starting materials sucrose and phosphate (Scheme 1), which, in a broader sense, can be adapted to a system applicable for the synthesis of various phosphorylated carbohydrates.

In the first step sucrose and phosphate are converted to glucose 1-phosphate and fructose (transgluco-

sylation). The reaction is catalyzed by sucrose phosphorylase from *Leuconostoc mesenteroides* (SPase, EC 2.4.1.7) and proceeds without formation of any side-products (17). The by SPase catalyzed reaction is an equilibrium based reaction and strongly favors the phosphorolysis of sucrose (K_{eq} = 10) (18). Glucose 1-phosphate and fructose can then be converted directly to the desired fructose 1-phosphate in the second step of the cascade (transphosphorylation) catalyzed by glucose-1-phosphatase from *Escherichia coli* (G1Pase, EC 3.1.3.10). In our previous work, we could provide evidence on the promiscuity of G1Pase, a representative of the histidine acid phosphatase family (19), to exhibit hydrolytic and synthetic activity (22). Interestingly, the donor substrate for phosphoryl transfer utilized by G1Pase is glucose 1-phosphate, a sugar phosphate which was not yet considered and not yet revealed to serve as activated donor substrate in phosphoryl transfer reactions. When glucose 1-phosphate (20 mM) and fructose (200 mM) were incubated with G1Pase, G1Pase catalyzed the formation of fructose 1-phosphate (k_{cat} = 88 s^{-1}) as main reaction product, along with glucose 6-phosphate (k_{cat} = 6 s^{-1}) and fructose 6-phosphate (k_{cat} = 20 s^{-1}) as side products. The yield of fructose 1-phosphate based on the inital glucose 1-phosphate concentration was determined as 60%. The formation of fructose 1-phosphate was followed by using enzymatic and/or HPAE-PAD assays. To increase the process efficiency of the transphosphorylation reaction, process engineering was employed aiming the improvement of the product yield by reducing byproduct formation. Therefore, we investigated the reaction parameters of the transphosphorylation reaction regarding pH and the donor to acceptor ratio. In independent reaction setups, the fructose concentration was varied, while the glucose 1-phosphate and G1Pase concentration as well as pH and temperature was constant. By comparing time-courses in which 100 mM, 200 mM, 400 mM and 600 mM fructose (Supplementary Figure S1, left panel) were used as acceptor in the presence of 20 mM glucose 1-phosphate, we recognized that the catalytic activities for substrate consumption, product synthesis and hydrolysis were dependent on the fructose concentration (Table 1). The catalytic activity for consumption of glucose 1-phosphate increased 2.6-fold by increasing the fructose concentration from 100 mM to 600 mM. Concomitantly, the synthesis of fructose 1-phosphate increased 3.5-times. The corresponding fructose 1-phosphate production rate (r_p) was measured and results are shown in Figure 1A. The half-saturation constant was determined to be 256 mM.

Next, we evaluated the change of the product spectrum in dependency of the donor to acceptor ratio. Therefore, the ratios of fructose 1-phosphate to glucose 6-phosphate (F1P/G6P), fructose 1-phosphate to fructose 6-phosphate (F1P/F6P) and fructose 1-phosphate to free phosphate (F1P/P_i) were determined for each sample of the time-course analysis (Supplementary Figure S1, right panel). The F1P/F6P ratio was determined with 3.6 and remained constant independent on the reaction time and independent on the acceptor concentration. The F1P/P_i ratio was constant within each time-course at

a certain fructose concentration, but increased when the fructose concentration increased; from 1.7 at 100 mM to 7.8 at 600 mM fructose. The F1P/G6P ratio was dependent on both parameters, reaction time and fructose concentration. In the beginning of each reaction (t = 10 min), when the glucose concentration was low, the F1P/G6P ratio was up to 1.6-fold higher compared to the end of the reaction (t = 50 min), when glucose 1-phosphate was consumed. In addition, the increase in fructose concentration influenced the F1P/G6P ratio in favor for synthesis of fructose 1-phosphate. When fructose was present in 5-fold excess to glucose 1-phosphate, the F1P/G6P ratio was determined to be 8.3 (at t = 50 min) and increased to 26 when fructose was present in 30-fold excess. Based on these findings we concluded that an excess of fructose relative to glucose 1-phosphate promotes the reaction rate for fructose 1-phosphate synthesis and suppresses the synthesis of glucose 6-phosphate as well as hydrolysis. A snapshot of the observed product pattern at t = 50 min in dependency on the fructose concentration is shown in Figure 1B. As consequence of suppression of byproduct formation, an increased fructose concentration directly affects the yield of fructose 1-phosphate. Whereas a 5-fold excess of fructose relative to glucose 1-phosphate results in a yield of 52%, a 30-fold excess results in a yield of 67%. Additionally, time-course analysis revealed that secondary hydrolysis of the formed product was inhibited when the fructose concentration was in $\geq$ 10-fold excess to the glucose 1-phosphate concentration (see Supplementary Figure S2). Under conditions, when glucose 1-phosphate was employed in 5-fold excess to fructose, synthesis of fructose 1-phosphate was hardly detectable.

Next, we determined pH-activity dependencies of G1Pase in the direction of synthesis of fructose 1-phosphate. Equimolar concentrations of glucose 1-phosphate and fructose (20 mM) were used and initial rates of phosphoryl transfer were determined at five pH values in the pH range 4.0 - 8.0. The rate of fructose 1-phosphate synthesis was constant at low pH and decreased as the pH was increased above apparent pK (see Supplemenatry Figure S3), which was determined to be 6.8 $\pm$ 0.7. Careful analysis of time-courses at all stages of pH revealed that the product pattern (F1P/G6P, F1P/P_i) was not pH dependent. Based on these results, the one-pot, two-step cascade reaction was performed at pH 7.0, a compromised pH value, which is optimal for SPase (17) and suitable for G1Pase. The temperature was set to 37°C (see Supplementary Figure S4).

Previous studies characterized G1Pase as promiscuous enzyme, hydrolyzing a variety of α-configurated sugar phosphates and non-sugar phosphates like phytate and *p*-nitrophenylphosphate (20, 21). Herein we tested the potential of G1Pase to display promiscuity towards donor and acceptor substrates different from glucose 1-phosphate and fructose, respectively, in phosphoryl transfer reactions. To evaluate the synthetic applicability of glucose 1-phosphate a variety of polyhydroxy compounds were investigated as alternatives to fructose, among them D-arabinose, L-arabinose, D-galactose, D-mannose,

L-arabinose, xylitol and D-xylose. All conversions resulted in the synthesis of phosphorylated products (Supplementary Figure S5A). The transphosphorylation efficiency was dependent on the acceptor substrate used. D-Fructose and L-sorbose, two ketohexoses, which, in equilibrium, mainly exist in their pyranose forms were phosphorylated efficiently to similar extents. The two aldohexoses, D-mannose and D-galactose, in equilibrium mainly present in their pyranose forms were phosphorylated efficiently too. The reaction products were chromatographically purified and analysed by 1D and 2D NMR. Main products were identified as fructose 1-phosphate, sorbose 1-phosphate, mannose 1-phosphate and galactose 1-phosphate, respectively. Aldopentoses, represented by L-arabinose, D-arabinose and D-xylose, as well as a non-cyclic hemiacetal, xylitol, were phosphorylated, however, transphosphorylation strongly competed with hydrolysis. In general, dephosphorylation of the phosphoryl enzyme intermediate takes place by water (primary hydrolysis) or by interception of a suitable acceptor substrate (transphosphorylation). Good acceptor substrates, like the ketohexoses and aldohexoses tested, strongly competed with water and showed a high transphosphorylation to hydrolysis ratio (Supplementary Figure S5B). When aldohexoses or non-cyclic hemiacetals were employed as acceptor substrates, hydrolysis was the predominant reaction. Consequently, these acceptors were phosphorylated in just moderate extent. Although the formation of the phosphorylated products could be proven indirectly (see materials and methods, acceptor substrate studies), the product concentration was too low to allow isolation and product identification by NMR. From these findings we can conclude that G1Pase is characterized by a quite flexible acceptor binding site, therefore being capable of phosphorylating a broad range of acceptor substrates. However, the structure of the acceptor substrates seems to be crucial for the transphosphorylation efficiency; acceptors which are mainly present in their pyranose forms are clearly favoured.

Next, we investigated the donor substrate specificity of G1Pase. Galactose 1-phosphate and xylose 1-phosphate were tested as alternative sugar phosphates to glucose 1-phosphate and *p*-nitrophenylphosphate, phytate and pyrophosphate as representatives of non glycosyl phosphate donors. Glucose was employed as acceptor substrate. Detection of glucose 6-phosphate revealed successful transphosphorylation from the respective donor substrate; the detection of free phosphate was a measure of primary hydrolysis at the level of the phosphoenzyme intermediate (Table 2). Among the donor substrates tested, glucose 1-phosphate showed the highest catalytic activity for phosphoryl transfer combined with the lowest activity for primary hydrolysis. Next to galactose 1-phosphate and xylose 1-phosphate, phytate was utilized as donor substrate for phosphoryl transfer, however, with significant lower catalytic activities and a higher hydrolysis to transfer ratio compared to the use of glucose 1-phosphate. Surprisingly, *p*-nitrophenylphosphate was not utilized as donor substrate for phosphoryl

transfer reactions and was not hydrolyzed as long as fructose was present. In the absence of fructose, *p*-nitrophenylphosphate served as donor substrate and was hydrolyzed with a k_{cat} of 0.6 s^{-1}. From this result we can assume that fructose and *p*-nitrophenylphosphate compete for active-site occupancy and that the presence of fructose prevents binding of *p*-nitrophenylphosphate, which results in unproductive hydrolysis. Cheap pyrophosphate, the preferred donor substrate for phosphoryl transfer reactions catalyzed by the bacterial non-specific acid phosphatases, was not utilized by G1Pase, neither for phosphoryl transfer, nor for hydrolysis. Glucose 1-phosphate is, therefore, the most efficient and economically most justified donor among the substrates tested. To circumvent the use of commercial glucose 1-phosphate as donor substrate and to make the biocatalytic process for fructose 1-phosphate production more cost-effective, the one-pot, two-step cascade reaction was introduced. Table 3 summarizes the results of experiments carried out to optimize the product yield of the one-pot, two-step cascade reaction. In general, there are two ways to perform a cascade reaction: One is the simultaneous mode, the other the sequential mode. We started by applying the simultaneous mode, by adding G1Pase and SPase simultaneously to equimolar concentrations of sucrose and phosphate (Supplementary Figure S6). Thereby, we achieved a moderate fructose 1-phosphate yield of around 40% after 100 min of incubation. In line with the results from the donor/acceptor studies, we observed a significant competition between glucose and fructose as acceptor substrate, reflected in a rather low F1P/G6P ratio of 2.0. In contrast, the F1P/F6P ratio was unexpectedly high (8.0), although the donor/acceptor studies claimed a F1P/F6P ratio of 3.5. This finding lets assume that the furanose form of fructose, as it is released in the reaction catalyzed by SPase, promotes the phosphorylation on C1, rather than on C6. On the basis of our results from the donor/acceptor optimization studies, the above described set-up was adopted by supplementing the reaction with an excess of fructose at t = 0 min (Figure 2A). This resulted in a good fructose 1-phosphate yield of 51% after 100 min. The synthesis of glucose 6-phosphate was suppressed (F1P/G6P = 18), however, as expected the regioselectivity remained poor, reflected by a F1P/F6P ratio of 3.6.

Next, we performed the one-pot, two-step cascade reaction operated in a sequential mode. Here, G1Pase and a surplus of fructose was added after the SPase catalyzed phosphorolysis of sucrose reached its equilibrium (after 100 min, 75% conversion was achieved, Figure 2B). G1Pase efficiently transferred the phosphate group from glucose 1-phosphate to fructose and the overall reaction resulted in an even more efficient fructose 1-phosphate yield of 63% compared to the simultaneous mode. The synthesis of glucose 6-phosphate was effectively suppressed (F1P/G6P = 13), however, the F1P/F6P ratio was still 2.6, which is a result of the poor regioselectivity of G1Pase, which can be hardly overcome by process engineering and may require protein engineering. Procedure for efficient work-up of

reaction mixtures of the one-pot, two-step cascade reactions may employ product purification by using anion exchange chromatography.

In summary, we have developed a strategy for the synthesis of the high-value metabolite fructose 1-phosphate. It is accessible via an one-pot, two-step cascade reaction, starting from the cheap commodity products sucrose and phosphate. Under optimized conditions the sequential cascade employing SPase and G1Pase provided fructose 1-phosphate in a yield of 63%. Formation of glucose 6-phosphate and primary hydrolysis was successfully suppressed.

The presented biocatalytic process can be made applicable to access a broad spectrum of sugar phosphates by exploiting the acceptor promiscuity of G1Pase. At the beginning of step 2, an alternative acceptor to fructose can be added. To prevent competition between the alternative acceptor and fructose, which is still present as consequence of glucose 1-phosphate formation catalyzed by SPase, the alternative acceptor is added in large surplus.

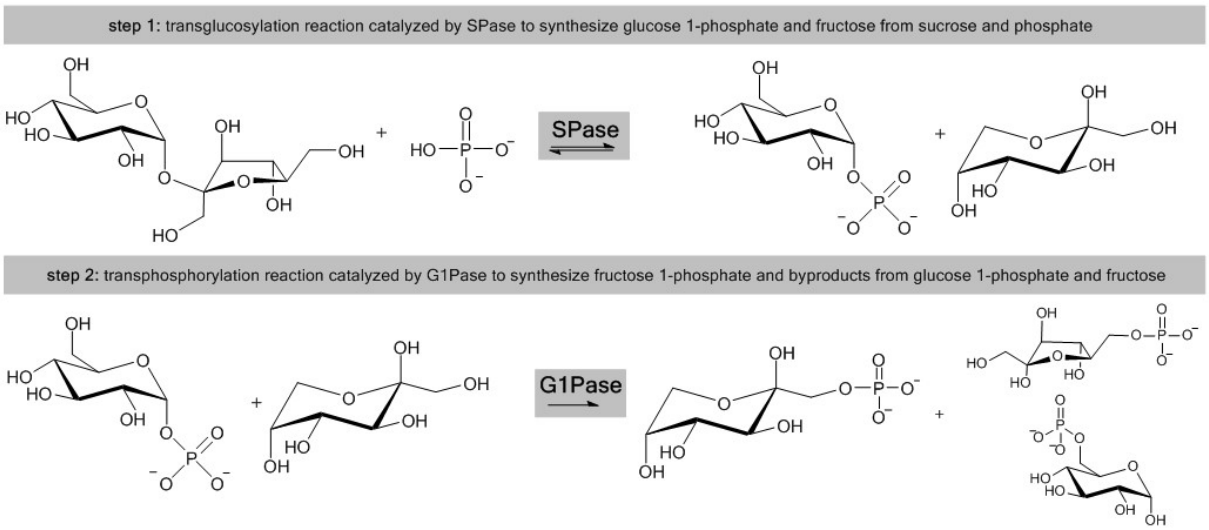

Scheme 1. One-pot, two-step cascade reaction for the synthesis of fructose 1-phosphate from sucrose and phosphate catalyzed by SPase and G1Pase.

Note: The theoretical anomeric composition of fructose 1-phosphate in aqueous solution is *α*-furanose 5%, *β*-furanose 16%, *α*-pyranose 5% and *β*-pyranose 73%; the theoretical anomeric composition of fructose 6-phosphate in aqueous solution is *α*-furanose 19% and *β*-furanose 81% (27). Fructose 1-phosphate is shown here in the *β*-pyranose form; fructose 6-phosphate in the *β*-furanose form.

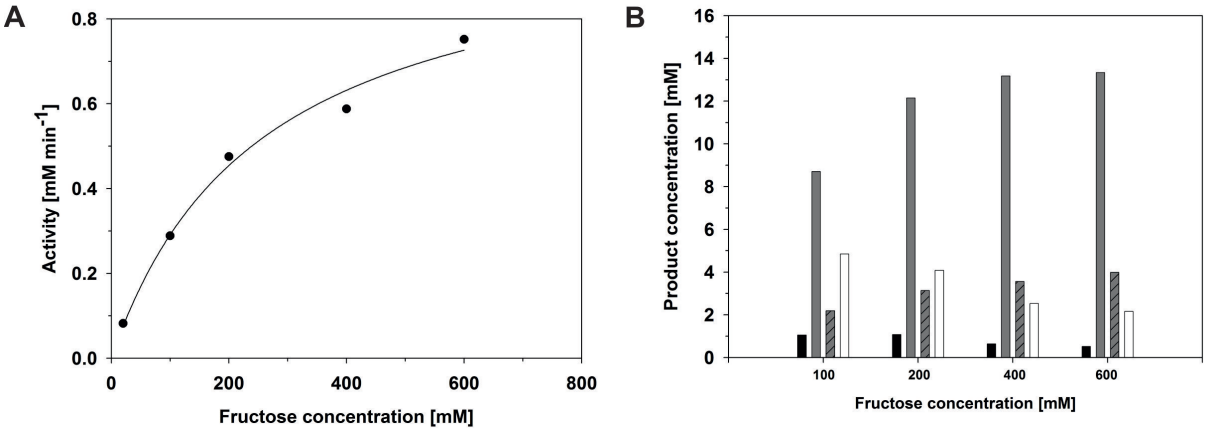

Figure 1. In independent reaction set-ups, the fructose concentration was varied (20 mM, 100 mM, 200 mM, 400 mM and 600 mM), while the glucose 1-phosphate (20 mM) and G1Pase concentration (0.1 μM) were constant. (A) The production rate (r_p) for fructose 1-phosphate is dependent on the fructose concentration. (B) A snapshot (at t = 50 min) of the product spectrum of reactions in which the fructose concentration (100 mM, 200 mM, 400 mM, 600 mM) was varied to display the dependency of the product pattern on the acceptor concentration. Reaction conditions: 50 mM MES, pH 7.0, 37°C, 650 rpm. The bars indicate: fructose 1-phosphate (grey), glucose 6-phosphate (black), fructose 6-phosphate (grey dashed) and phosphate (white).

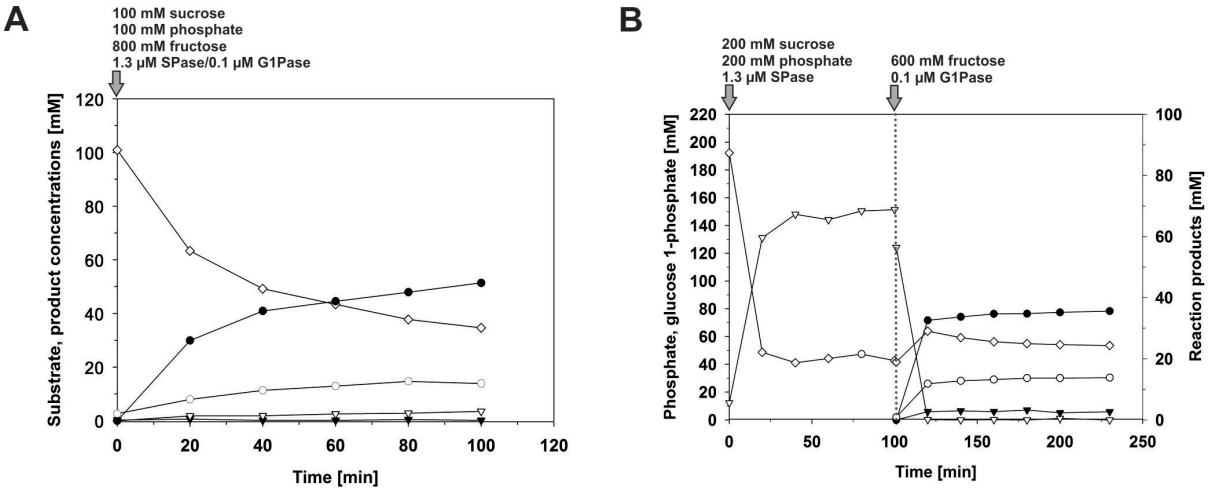

Figure 2. (A) One-pot, two-step cascade reaction operated in simultaneous mode. Substrates (100 mM sucrose, 100 mM phosphate, 800 mM fructose) and enzymes (1.3 μM SPase, 0.1 μM G1Pase) are added simultaneously in the beginning. (B) One-pot, two-step cascade reaction operated in sequential mode. In the first step, sucrose and phosphate (200 mM each) is converted to glucose 1-phosphate and fructose catalyzed by SPase (1.3 μM SPase). In the second step, G1Pase converts glucose 1-phosphate and fructose to fructose 1-phosphate and byproducts. Reaction conditions: 50 mM MES, pH 7.0, 37°C, 650 rpm. Symbols indicate: glucose 1-phosphate (▽), glucose 6-phosphate (▼), fructose 1-phosphate (●), fructose 6-phosphate (○) and phosphate (◊).

Table 1. In independent reaction set-ups, the fructose concentration was varied (100 mM, 200 mM, 400 mM and 600 mM), while the glucose 1-phosphate (20 mM) and G1Pase (0.1 μM) concentrations were constant. The catalytic activities for glucose 1-phosphate consumption, fructose 1-phosphate, glucose 6-phosphate and fructose 6-phosphate synthesis and hydrolysis in dependency on the fructose concentration are shown. Reaction conditions: 50 mM MES, pH 7.0, 37°C, 650 rpm.

Fructose	**Glucose 1-phosphate** k_{cat} [s^{-1}]	**Fructose 1-phosphate** k_{cat} [s^{-1}]	**Glucose 6-phosphate** k_{cat} [s^{-1}]	**Fructose 6-phosphate** k_{cat} [s^{-1}]	**Phosphate** k_{cat} [s^{-1}]
100	73	39	5	11[a]	21
200	119	88	6	20	18
400	148	111[b]	4	28	14
600	189	135	5	36[c]	13

The S.D. for k_{cat} was $\leq$ 10% of the reported values with the exception of [a]16%, [b]11%, [c]20%.

Table 2. Different substrates were tested as potential donors for phosphoryl transfer reactions. Each substrate was present in a concentration of 20 mM in the presence of 200 mM glucose (acceptor). Detection of glucose 6-phosphate revealed successful transphosphorylation from the respective donor substrate to glucose. Detection of free phosphate measured primary hydrolysis at the phosphoenzyme intermediate. Reaction conditions: 50 mM MES, pH 7.0, 37°C, 650 rpm; in case phytate was employed as donor substrate, the pH was 4.5.

Donor substrate	**Glucose 6-phosphate** k_{cat} [s^{-1}]	**Phosphate** k_{cat} [s^{-1}]
Galactose 1-phosphate	19	10
Glucose 1-phosphate	30[a]	4.0
p-Nitrophenyl phosphate	n.d.	n.d.
Phytate	2.1[b]	1.7
Pyrophosphate	n.d.	n.d.
Xylose 1-phosphate	10	5.0[c]

The S.D. for k_{cat} was $\leq 4\%$ of the reported values with the exception of [a]7%, [b]10%, [c]8%.

Table 3. Synthesis of fructose 1-phosphate performed as a simultaneous or sequential one-pot, two-step cascade reaction.

Reaction	Sucrose [mM]	Phosphate [mM]	Fructose [mM]	SPase [μM]	G1Pase [μM]	Yield [%]	F1P/G6P	F1P/F6P
1[a]	100	100	-	0.3	0.1	43[c]	2.0	8.0
2[a]	100	300	-	0.3	0.1	38[d]	2.0	8.0
3[a]	100	100	800	1.3	0.1	51[c]	18	3.6
4[b]	100	100	800	1.3	0.1	63[e]	13	2.6

[a] Cascade reaction was operated in simultaneous mode.

[b] Cascade reaction was operated in sequential mode.

[c] Yield of fructose 1-phosphate based on the initial phosphate concentration.

[d] Yield of fructose 1-phosphate based on the initial fructose concentration (in form of sucrose).

[e] Yield of fructose 1-phosphate based on the glucose 1-phosphate concentration at the beginning of step 2 (after a surplus of fructose was added).

SUPPLEMENTARY INFORMATION

MATERIALS AND METHODS

Chemicals and reagents

Materials used have been described elsewhere (22). All other chemicals were obtained from Sigma-Aldrich (Vienna, Austria) or Roth (Karlsruhe, Germany) in highest purity available.

Expression and purification of G1Pase and SPase

E. coli BL21-Gold (DE3) cells harboring the pASK-IBA7+ expression vector encoding SPase were prepared as described previously (18). The cells were cultivated in 1-L baffeled shaken flasks at 37°C and 110 rpm using LB-media and 115 mg/L ampicillin. When OD_{550} reached 0.8-1.0 temperature was decreased to 22°C and gene expression was induced with 200 μg/L anhydrotetracycline for 20 h. Expression and purification of G1Pase was done as described elsewhere (22).

Assays

The quantity of inorganic phosphate present was determined colorimetrically at 850 nm (23). Glucose 1-phosphate and glucose 6-phosphate were assayed in a coupled enzymatic system with PGM and G6PDH (24). Fructose 6-phosphate was determined using an assay with mannitol 1-phosphate dehydrogenase (25). The concentration of fructose 1-phosphate was quantified indirectly by using equation 1 and directly by using HPAE-PAD. The total protein concentration was determined as described by Bradford (26) employing Roti-Quant referenced against BSA.

$$\text{Fructose 1-phosphate}_{end} = \text{glucose 1-phosphate}_{start} - \text{glucose 1-phosphate}_{end} - \text{glucose 6-phosphate}_{end} - \text{fructose 6-phosphate}_{end} - \text{phosphate}_{end} \quad (1)$$

Reaction optimization

For reaction optimization, glucose 1-phosphate was applied at a constant level of 20 mM and fructose was varied (100 mM, 200 mM, 400 mM, 600 mM). In addition, one sample contained glucose 1-phosphate in excess (100 mM) to fructose. The reactions were started by addition of 0.1 μM G1Pase and were performed in 50 mM MES, pH 7.0, at 37°C and 650 rpm. Reaction mixtures were incubated for 50 min using discontinuous assays. Samples were taken in 10 min intervals, heat-treated at 99°C for 5 min to inactivate the enzyme and centrifuged at 13,000 rpm for 5 min to remove precipitated protein prior to further analysis. Concentrations of glucose 1-phosphate, glucose 6-phosphate, fructose

1-phosphate, fructose 6-phosphate and phosphate were determined as described.

Catalytic activities were calculated by applying equation 2, where k_{cat} is the catalytic constant [s^{-1}], V_{max} is the maximal initial rate [mM min^{-1}] and E is the total molar enzyme concentration based on a molecular mass of 45 kDa for G1Pase.

$$k_{cat} = \frac{V_{max}}{E} \tag{2}$$

Determination of pH-profile

pH-dependences of kinetic parameters for synthesis of fructose phosphate (sum of fructose 1-phosphate and fructose 6-phosphate) were determined from initial rates recorded at constant concentrations of glucose 1-phosphate (20 mM) and fructose (20 mM) in the presence of 0.1 μM G1Pase. All buffer pH values were adjusted at the temperature of measurement (37°C) and controlled before and after recording each enzyme-catalyzed reaction. For pH dependency studies at pH $\leq$ 6.0 and pH $\geq$ 8.0 where MES alone (pK = 6.2) has limited buffering capacity, a buffer mixture consisting of 50 mM MES and 20 mM sodium acetate (pH 4.0-6.0) or 50 mM MES and 50 mM TES (pH 8.0) was used. Reaction mixtures were incubated for 60 min using discontinuous assays. Samples were taken in 15 min intervals, heat-treated at 99°C for 5 min to inactivate the enzyme and centrifuged at 13,000 rpm for 5 min to remove precipitated protein prior to further analysis. The concentrations of glucose 1-phosphate, glucose 6-phosphate and phosphate were determined as described. The concentration of fructose phosphate was determined indirectly as described in equation 1, except that fructose 6-phosphate was not determined and thus not considered in the equation. The concentration of fructose phosphate is the sum of fructose 1-phosphate and fructose 6-phosphate.

For data analysis SigmaPlot 2004 version 9.0 was used. Equation 3 describes a pH dependency where the activity log(k_{cat}) is constant at low pH and decreases above pK. C is the pH-independent value of k_{cat} at the optimum state of protonation, K is the proton dissociation constant and [H^+] is the proton concentration.

$$\log(k_{cat}) = \log\left(\frac{C}{1+\frac{K}{[H^+]}}\right) \tag{3}$$

Acceptor substrate studies

G1Pase catalyzed phosphoryl transfer from glucose 1-phosphate (20 mM) to a variety of polyhydroxy compounds was tested. D-Arabitol, L-arabinose, D-galactose, D-glucose, D-mannose, L-sorbose, xylitol and D-xylose were employed as acceptor substrates, each present in a concentration of 200 mM. The reactions were started by addition of 0.1 μM G1Pase and were performed in 50 mM MES, pH 7.0, at

37°C and 650 rpm. Reaction mixtures were incubated for 75 min using discontinuous assays. Samples were taken in 15 min intervals, heat-treated at 99°C for 5 min to inactivate the enzyme and centrifuged at 13,000 rpm for 5 min to remove precipitated protein prior to further analysis. Concentrations of glucose 1-phosphate, glucose 6-phosphate and phosphate were determined as described. The concentration of the phosphorylated product was quantified indirectly by using equation 4 and directly by NMR.

Phosphorylated product = glucose 1-phosphate$_{start}$ - glucose 1-phosphate$_{end}$ - glucose 6-phosphate$_{end}$ - phosphate$_{end}$ (4)

Donor substrate studies

Galactose 1-phosphate, *p*-nitrophenylphosphate, phytate, pyrophosphate and xylose 1-phosphate were tested as alternative donor substrates to glucose 1-phosphate. 20 mM of each donor substrate was incubated with 200 mM glucose as acceptor substrate. The reactions were started by addition of 0.1 μM G1Pase and were performed in 50 mM MES, pH 7.0, at 37°C and 650 rpm. Reaction mixtures were incubated for 75 min using discontinuous assays. Samples were taken in 15 min intervals, heat-treated at 99°C for 5 min to inactivate the enzyme and centrifuged at 13,000 rpm for 5 min to remove precipitated protein prior to further analysis. The concentrations of glucose 6-phosphate and phosphate were determined as described. Formation of glucose 6-phosphate indicated successful transphosphorylation from the respective donor substrate to glucose; detection of phosphate indicated primary hydrolysis of the donor substrate.

Under the conditions described, phytate was not hydrolyzed. Therefore, reaction conditions were changed to 100 mM sodium acetate buffer adjusted to pH 4.5.

One-pot, two-step cascade reaction operated in simultaneous mode

Standard reaction mixtures contained 100 mM sucrose and 100 mM or 300 mM phosphate in 50 mM MES, pH 7.0. Enzymatic reactions were initiated by the simultaneous addition of 0.3 μM and 1.3 μM SPase, respectively and 0.1 μM G1Pase and were performed at 37°C and 650 rpm. The reaction mixture was incubated for 100 min using a discontinuous assay. Samples were taken in 20 min intervals, heat-treated at 99°C for 5 min to inactivate the enzyme and centrifuged at 13,000 rpm for 5 min to remove precipitated protein prior to further analysis. Concentrations of glucose 1-phosphate, glucose 6-phosphate, fructose 1-phosphate, fructose 6-phosphate and phosphate were determined as described. For reaction optimization the above described set-up was adopted by adding a supplement of 800 mM

fructose to the initial reaction mixture containing 100 mM sucrose and 100 mM phosphate.

One-pot, two-step cascade reaction operated in sequential mode

Equimolar concentrations of sucrose and phosphate (200 mM) were dissolved in 50 mM MES, pH 7.0. The transglucosylation reaction was initiated by adding 1.3 μM SPase and was performed at 37°C and 650 rpm. The reaction mixture was incubated for 100 min using a discontinuous assay. Samples were taken in 20 min intervals, heat-treated at 99°C for 5 min to inactivate the enzyme and centrifuged at 13,000 rpm for 5 min to remove precipitated protein prior to further analysis. Concentrations of glucose 1-phosphate and phosphate were determined as described. The transphosphorylation reaction was started by addition of 0.1 μM G1Pase accompanied by a simultaneous supplement of fructose (final concentration: 600 mM) and was prolonged at 37°C and 650 rpm. The reaction mixture was incubated for additional 130 min. Samples were taken in 20 min intervals, heat-treated at 99°C for 5 min to inactivate the enzyme and centrifuged at 13,000 rpm for 5 min to remove precipitated protein prior to further analysis. Concentrations of glucose 1-phosphate, glucose 6-phosphate, fructose 1-phosphate, fructose 6-phosphate and phosphate were determined as described.

NMR spectroscopic measurements

Sample preparation. For product isolation, 20 mM glucose 1-phosphate and 200 mM of the corresponding acceptor were incubated with 0.1 μM G1Pase in 50 mM MES, pH 7.0. The reaction was kept at 37°C, 650 rpm for 75 min and was stopped by heat-treatment at 99°C for 5 min. After centrifugation at 13,000 rpm for 5 min, the supernatant was applied on a DEAE FF column, pre-equilibrated with deionized water. Unbound, non-charged monosaccharides were removed by washing with deionized water. Elution of phosphorylated reaction products was accomplished by using 50 mM NaCl. Fractions containing the phosphorylated product were pooled and concentrated by lyophilisation, prior to NMR analysis.

NMR analysis. To gain NMR spectroscopic measurements the isolated compounds were dissolved in D_2O (5.0 mg in 0.7 mL) and transferred into 5 mm high precision NMR sample tubes. Measurements were performed on a Bruker DRX-400 at 400.13 MHz (^{1}H), 100.61 MHz (^{13}C), and 161.97 MHz (^{31}P) using the Topspin 1.3 software. The 1D spectra were recorded with 32768 data points. Zero filling to 65536 data points, appropriate exponential multiplication and Fourier transformation led to spectra with ranges of 6000 Hz (^{1}H), 24000 Hz (^{13}C), and 16000 Hz (^{31}P). 2D NMR spectra (COSY; TOCSY; NOESY; HSQC; HMBC) were recorded with 128 experiments, each with 1024 data points and an ap-

propriate number of scans. Zero filling and Fourier transformation led to spectra with ranges of 4000 Hz, 24 000 Hz and 8000 Hz for proton, carbon, and phosphorus, respectively. Measurement temperature was 298 K +/- 0.05 K. Chemical shifts have been referenced to external acetone (δ_H: 2.225 ppm; δ_C: 31.45 ppm) and 85% aqueous phosphoric acid (δ_P: 0.00 ppm).

Product identification β-fructopyranose 1-phosphate - ^{1}H NMR (D_2O): δ = 3.99 (1H, m, H-6a), 3.93 (1H, m, H-3), 3.84 (1H, m, H-4*), 3.82 (1H, m, H-1b), 3.81 (1H, m, H-1a), 3.77 (1H, m, H-5*), 3.65 (1H, m, H-6b); ^{13}C NMR (D_2O): δ = 96.3 (s, C-2), 71.9 (d, C-3), 71.8 (d, C-4*), 70.5 (d, C-5*), 68.6 (t, C-6), 66.2 (t, C-1); ^{31}P NMR (D_2O): δ = 5.5 (R-O-POH_2^-); other isomers regarding anomeric form and pyrano/furano form are present in negligible concentrations; [*] shifts are not univocally assignable.

α-sorbopyranose 1-phosphate - ^{1}H NMR (D_2O): δ = 3.39 (1H, d, 8.6 Hz, H-3), 3.50 (1H, m, H-6b), 3.51 (1H, m, H-5), 3.52 (1H, m, H-4), 3.57 (1H, m, H-6a), 3.63 (1H, dd, 11.1, 5.4 Hz, H-1b), 3.74 (1H, dd, 11.1, 7.3 Hz, H-1a); ^{13}C NMR (D_2O): δ = 97.7 (s, C-2), 73.7 (d, C-5), 71.0 (d, C-3), 69.8 (d, C-4), 66.6 (t, C-1), 62.3 (t, C-6); ^{31}P NMR (D_2O): δ = 5.5 (R-O-POH_2^-); other isomers regarding anomeric form and pyrano/furano form are present in negligible concentrations.

α-mannopyranose 1-phosphate - ^{1}H NMR (D_2O): δ = 5.30 (1H, dd, 8.3, 2.0 Hz, H-1), 3.90 (1H, dd, 3.4, 2.0 Hz, H-2), 3.86 (1H, dd, 9.7, 3.4 Hz, H-3), 3.82 (1H, dd, 11.8, 2,2 Hz, H-6a), 3.79 (1H, ddd, 9.7, 5.9, 2.2 hz, H-5), 3.68 (1H, dd, 11.8, 5.9 Hz, H-6b) 3.57 (1H, dd, 9.7, 9.7 Hz, H-4); ^{13}C NMR (D_2O): δ = 95.4 (s, C-1), 73.2 (d, C-5), 70.8 (d, C-2), 70.0 (d, C-3), 66.8 (d, C-4), 61.0 (t, C-6); ^{31}P NMR (D_2O): δ = 5.1 (R-O-POH_2^-).

α-galactopyranose 1-phosphate - ^{1}H NMR (D_2O): δ = 5.44 (1H, dd, 7.1, 3.6 Hz, H-1), 3.72 (1H, ddd, 10.7, 3.6, 2.3, H-2), 3.83 (1H, ddd, 10.3, 3.6 Hz, H-3), 3.94 (1H, m, 3.6, 0.5 Hz, H-4), 4.08 (1H, ddd, 7.2, 5.2, 0.5 Hz, H-5), 3.68 (1H, dd, 11.9, 7.2 Hz, H-6a), 3.65 (1H, dd, 11.9, 5.2 Hz, H-6b), ^{13}C NMR (D_2O): δ = 94.6 (s, C-1), 71.5 (d, C-5), 69.3 (d, C-3), 69.1 (d, C-4), 68.6 (d, C-2), 61.3 (t, C-6); ^{31}P NMR (D_2O): δ = 4.2 (R-O-POH_2^-).

High performance anion exchange chromatography with pulsed amperometric detection (HPAE-PAD)

To prove the existence of the indirectly calculated fructose 1-phosphate, selected samples were analyzed on a Dionex BioLC system (Dionex Corporation, Sunnyvale, USA) equipped with a CarboPac PA10 column (4 x 250 mm) and an Amino Trap guard column (4 x 50 mm) thermostated at 30°C. Glucose, fructose, glucose 1-phosphate, glucose 6-phosphate, fructose 1-phosphate and fructose 6-phosphate were detected with an ED50A electrochemical detector using a gold working electrode and

a silver/silver chloride reference electrode by applying the predefined waveform for carbohydrates. Elution was carried out at a flow rate of 0.9 mL/min with the following method: isocratic flow of 52 mM NaOH for 20 min, followed by a linear gradient from 100 mM NaOAc to 400 mM NaOAc applied within 25 min in an isocratic background of 100 mM NaOH. The column was washed 5 min with 52 mM NaOH. Under the conditions applied glucose eluted after 10.2 min, fructose after 11.8 min, glucose 1-phosphate after 30.3 min, glucose 6-phosphate after 36.6 min, fructose 1-phosphate after 37.2 min and fructose 6-phosphate after 39.1 min.

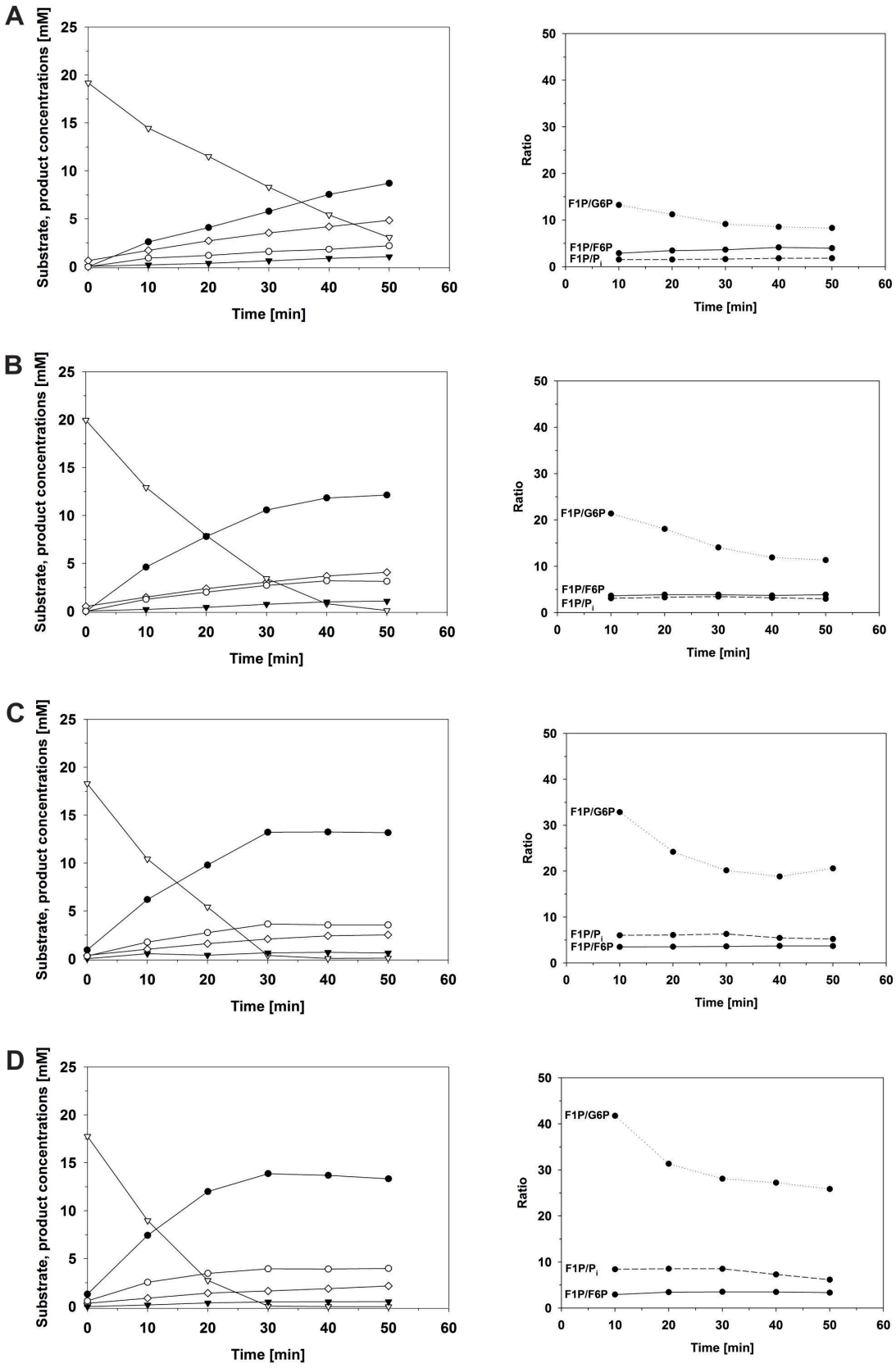
A
B
C
D
Substrate, product concentrations [mM]
Time [min]
Ratio
F1P/G6P
F1P/F6P
F1P/P$_i$

Supplementary Figure S1. Time-courses for fructose 1-phosphate (•) production from 20 mM glucose 1-phosphate (▽) in the presence of 100 mM fructose (A), 200 mM fructose (B), 400 mM fructose (C) and 600 mM fructose (D), respectively. The formation of side products, glucose 6-phosphate (▼), fructose 6-phosphate (○) and phosphate (◊), is indicated. The ratios of fructose 1-phosphate to glucose 6-phosphate (F1P/G6P), fructose 1-phosphate to fructose 6-phosphate (F1P/F6P) and fructose 1-phosphate to free phosphate (F1P/P_i), displayed on the right panel, are extracted from the corresponding time courses displayed on the left panel. Reaction conditions: 50 mM MES, pH 7.0, 37°C, 650 rpm.

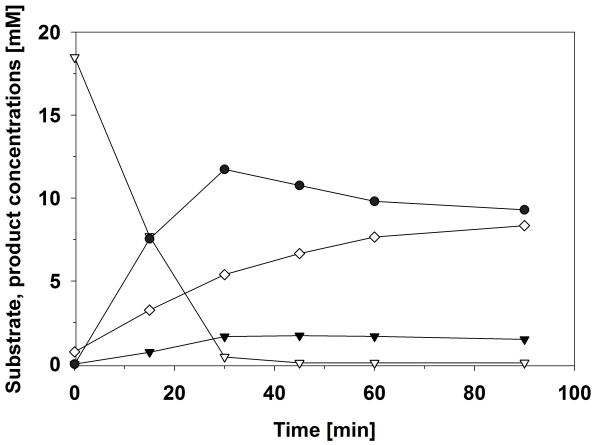

Supplementary Figure S2. Time-course for the synthesis of fructose phosphate (sum of fructose 1-phosphate and fructose 6-phosphate) from glucose 1-phosphate (20 mM) and fructose (100 mM) and subsequent product hydrolysis catalyzed by G1Pase (0.1 μM). The catalytic activity for synthesis of phosphorylated fructose was determined as 42 s^{-1}, the catalytic activity for subsequent secondary hydrolysis was determined as 4.5 s^{-1}. When fructose was used in $\geq$ 10-fold excess to glucose 1-phosphate no product hydrolysis was detectable (see Supplementary Figure S1 B, C, D). Reaction conditions: 50 mM MES, pH 7.0, 37°C, 650 rpm. Symbols indicate: glucose 1-phosphate (▽), sum of fructose 1-phosphate and fructose 6-phosphate (●), glucose 6-phosphate (▼) and phosphate (◊).

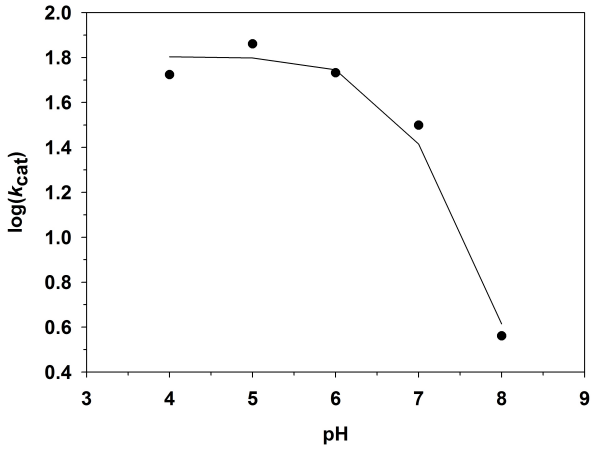

Supplementary Figure S3. pH profile of log(k_{cat}) for the synthesis of fructose phosphate (sum of fructose 1-phosphate and fructose 6-phosphate) from glucose 1-phosphate (20 mM) and fructose (20 mM) catalyzed by G1Pase (0.1 μM). Reaction conditions: 50 mM MES, pH 7.0, 37°C, 650 rpm. The solid line is a fit of equation 3 to the data as described in materials and methods, determination of pH-profile.

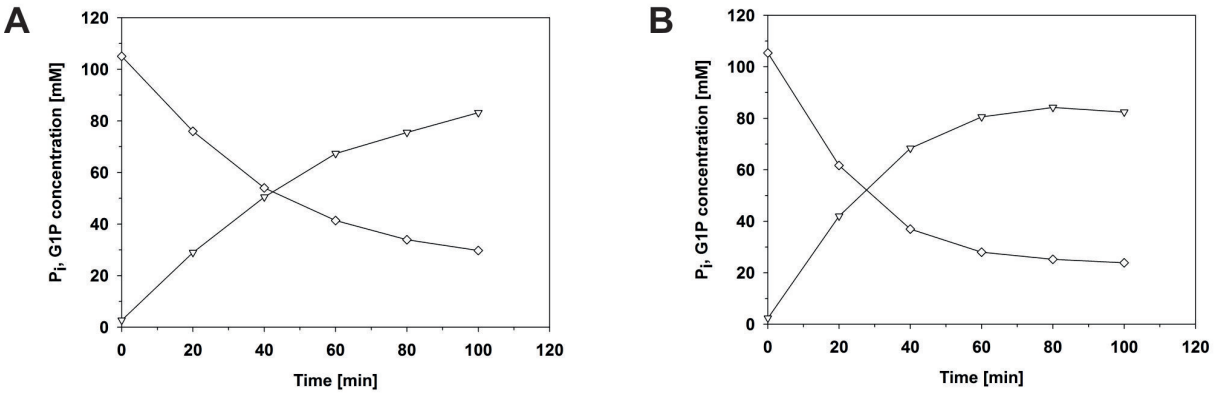

Supplementary Figure S4. Time-course for the synthesis of glucose 1-phosphate (▽) from sucrose and phosphate (◊) (100 mM each) catalyzed by SPase (0.3 μM) at pH 7.0 and 30°C (A) and 37°C (B), respectively. The equilibrium constant (K_{eq}) for both reactions is 11, which is in good agreement to the in a previous study reported value of 10 (18).

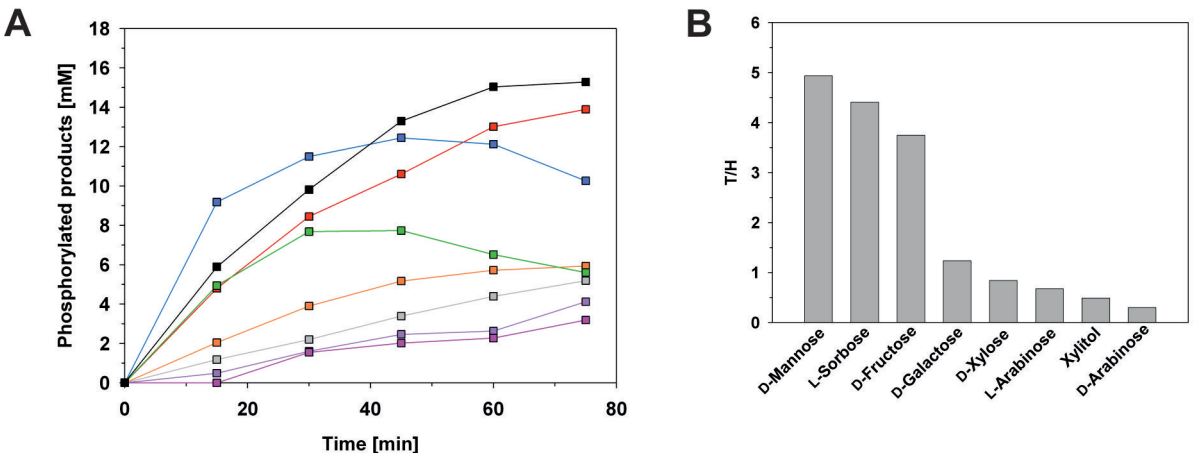

Supplementary Figure S5. (A) Time-courses for the synthesis of different glycosyl phosphates. The reaction mixtures contained glucose 1-phosphate (20 mM), acceptor (200 mM) and G1Pase (0.1 μM). The time-dependent formation of the phosphorylated products of D-arabinose (pink), L-arabinose (orange), D-fructose (black), D-galactose (green), D-mannose (blue), L-sorbose (red), xylitol (purple) and D-xylose (grey) are shown. (B) The transphosphorylation to hydrolysis ratio at t = 75 min of the tested acceptors is shown. Reaction conditions: 50 mM MES, pH 7.0, 37°C, 650 rpm.

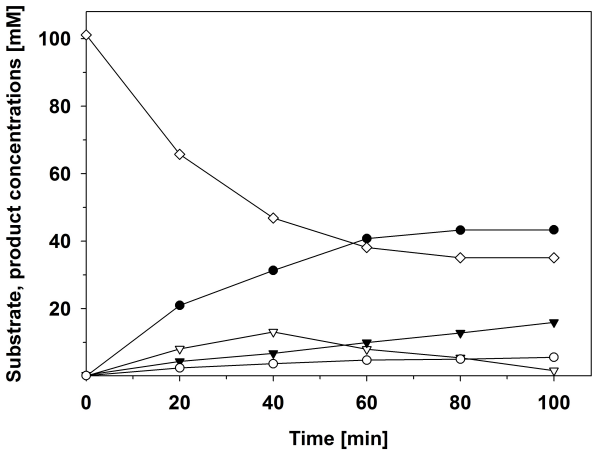

Supplementary Figure S6. One-pot, two-step cascade reaction operated in simultaneous mode. Substrates (100 mM sucrose, 100 mM phosphate) and enzymes (0.3 μM SPase, 0.1 μM G1Pase) are added simultaneously in the beginning. Reaction conditions: 50 mM MES, pH 7.0, 37°C, 650 rpm. Symbols indicate: glucose 1-phosphate (▽), glucose 6-phosphate (▼), fructose 1-phosphate (●), fructose 6-phosphate (○) and phosphate (◊).

References

1. Charmantray F, Helaine V, Legeret B, Hecquet L. 2009. Preparative scale enzymatic synthesis of D-sedoheptulose-7-phosphate from β-hydroxypyruvate and D-ribose-5-phosphate. J Mol Catal B: Enzymatic 57:6-9.

2. Sanchez-Moreno I, Helaine V, Poupard N, Charmantray F, Legeret B, Hecquet L, Garcia-Junceda E, Wohlgemuth R, Guerard-Helaine C, Lemaire M. 2012. One-pot cascade reactions using fructose-6-phosphate aldolase: efficient synthesis of D-arabinose 5-phosphate, D-fructose 6-phosphate and analogues. Adv Synth Catal 354:1725-1730.

3. Shaeri J, Wright I, Rathbone EB, Wohlgemuth R, Woodley JM. 2008. Characterization of enzymatic D-xylulose 5-phosphate synthesis. Biotechnol Bioeng 101:761-767.

4. Nifantiev EE, Grachev MK, Burmistrov SY. 2000. Amides of trivalent phosphorus acids as phosphorylating reagents for proton-donating nucleophiles. Chem Rev 100:3755-3799.

5. van Herk T, Hartog AF, van der Burg AM, Wever R. 2005. Regioselective phosphorylation of carbohydrates and various alcohols by bacterial acid phosphatases; Probing the substrate specificity of the enzyme from *Shigella flexneri*. Adv Synth Catal 347:1155-1162.

6. Yashunsky DV, Nikolaev AV. 2000. Hydrogenphosphonate synthesis of sugar phosphomonoesters. J Chem Soc Perkin Trans 1:1195-1198.

7. Park SH, Pastuszak I, Drake R, Elbein AD. 1998. Purification to apparent homogeneity and properties of pig kidney L-fucose kinase. J Biol Chem 273:5685-5691.

8. Lavine JE, Cantlay E, Roberts CT, Jr., Morse DE. 1982. Purification and properties of galactokinase from *Tetrahymena thermophila*. Biochim Biophys Acta 717:76-85.

9. Nordlie RC, Arion WJ. 1964. Evidence for the common identity of glucose 6-phosphatase, inorganic pyrophosphatase, and pyrophosphate-glucose phosphotransferase. J Biol Chem 239:1680-1685.

10. Stetten MR, Taft HL. 1964. Metabolism of inorganic pyrophosphate II. The probable identity of microsomal inorganic pyrophosphatase, pyrophosphate phosphotransferase, and glucose 6-phosphatase. J Biol Chem 239:4041-4046.

11. Nordlie RC. 1969. Some properties and possible physiological functions of phosphotransferase activities of microsomal glucose-6-phosphatase. Ann N Y Acad Sci 166:699-718.

12. Tanaka N, Hasan Z, Hartog AF, van Herk T, Wever R, Sanders RJ. 2003. Phosphorylation and dephosphorylation of polyhydroxy compounds by class A bacterial acid phosphatases. Org Biomol Chem 1:2833-2839.

13. van Herk T, Hartog AF, van der Burg AM, Wever R. 2005. Regioselective phosphorylation of carbohydrates and various alcohols by bacterial acid phosphatases; probing the substrate specificity of the enzyme from *Shigella flexneri*. Adv Syn Catal 347:1155-1162.

14. Asano Y, Mihara Y, Yamada H. 1999. A novel selective nucleoside phosphorylating enzyme from *Morganella morganii*. J Biosci Bioeng 87:732-738.

15. Babich L, Hartog AF, van der Horst MA, Wever R. 2012. Continuous-flow reactor-based enzymatic synthesis of phosphorylated compounds on a large scale. Chem Eur J 18:6604-6609.

16. Babich L, Hartog AF, van Hemert LJ, Rutjes FP, Wever R. 2012. Synthesis of carbohydrates in a continuous flow reactor by immobilized phosphatase and aldolase. ChemSusChem 5:2348-2353.

17. Goedl C, Schwarz A, Minani A, Nidetzky B. 2007. Recombinant sucrose phosphorylase from *Leuconostoc mesenteroides*: characterization, kinetic studies of transglucosylation, and application of immobilised enzyme for production of α-D-glucose 1-phosphate. J Biotechnol 129:77-86.

18. Wildberger P, Luley-Goedl C, Nidetzky B. 2011. Aromatic interactions at the catalytic subsite of sucrose phosphorylase: their roles in enzymatic glucosyl transfer probed with Phe52 → Ala and Phe52 → Asn mutants. FEBS Lett 585:499-504.

19. Chi H, Tiller GE, Dasouki MJ, Romano PR, Wang J, O'Keefe R J, Puzas JE, Rosier RN, Reynolds PR. 1999. Multiple inositol polyphosphate phosphatase: evolution as a distinct group within the histidine phosphatase family and chromosomal localization of the human and mouse genes to chromosomes 10q23 and 19. Genomics 56:324-336.

20. Cottrill MA, Golovan SP, Phillips JP, Forsberg CW. 2002. Inositol phosphatase activity of the *Escherichia coli agp*-encoded acid glucose-1-phosphatase. Can J Microbiol 48:801-809.

21. Lee DC, Cottrill MA, Forsberg CW, Jia Z. 2003. Functional insights revealed by the crystal structures of *Escherichia coli* glucose-1-phosphatase. J Biol Chem 278:31412-31418.

22. Wildberger P, Pfeiffer M, Rechberger, GN, Birner-Gruenberger R, Nidetzky B. in preparation (see chapter 7).

23. Saheki S, Takeda A, Shimazu T. 1985. Assay of inorganic phosphate in the mild pH range, suitable for measurement of glycogen phosphorylase activity. Anal Biochem 148:277-281.

24. Eis C, Nidetzky B. 1999. Characterization of trehalose phosphorylase from *Schizophyllum commune*. Biochem J 341:385-393.

25. Krahulec S, Armao GC, Weber H, Klimacek M, Nidetzky B. 2008. Characterization of recombinant *Aspergillus fumigatus* mannitol-1-phosphate 5-dehydrogenase and its application for the stereoselective synthesis of protio and deuterio forms of D-mannitol 1-phosphate. Carbohydr Res 343:1414-1423.

26. Bradford MM. 1976. A rapid and sensitive method for the quantitation of microgram quantities of protein utilizing the principle of protein-dye binding. Anal Biochem 72:248-254.

27. Koerner TA, Jr., Voll RJ, Cary LW, Younathan ES. 1980. Carbon-13 nuclear magnetic resonance studies and anomeric composition of ketohexose phosphates in solution. Biochemistry 19:2795-2801.

List of publications

Scientific publications

Sucrose phosphorylase: A powerful transglucosylation catalyst for synthesis of α-D-glucosides as industrial fine chemicals.

C. Goedl, T. Sawangwan, P. Wildberger and B. Nidetzky (2010) Biocatalysis and Biotransformation, 28(1): 10-21.

Regioselective *O*-glucosylation by sucrose phosphorylase: A promising route for functional diversification of a range of 1,2-propanediols.

C. Luley-Goedl, T. Sawangwan, L. Brecker, P. Wildberger and B. Nidetzky (2010) Carbohydrate Research, 345: 1734-1740.

Aromatic interactions at the catalytic subsite of sucrose phosphorylase: Their roles in enzymatic glucosyl transfer probed with Phe^{52} $\rightarrow$ Ala and Phe^{52} $\rightarrow$ Asn mutants.

P. Wildberger, C. Luley-Goedl and B. Nidetzky (2011) FEBS Letters, 585: 499-504.

Examining the role of phosphate in glycosyl transfer reactions of *Cellulomonas uda* cellobiose phosphorylase using D-glucal as donor substrate.

P. Wildberger, L. Brecker and B. Nidetzky (2012) Carbohydrate Research, 356:224-232.

Probing enzyme-substrate interactions at the catalytic subsite of *Leuconostoc mesenteroides* sucrose phosphorylase with site-directed mutagenesis: The roles of Asp^{49} and Arg^{395}.

P. Wildberger, A. Todea and B. Nidetzky (2012) Biocatalysis and Biotransformation, 3:326-337.

Chiral resolution through stereoselective transglycosylation by sucrose phosphorylase: application to the synthesis of a new biomimetic compatible solute, (*R*)-2-*O*-α-D-glucopyranosyl glyceric acid amide.

P. Wildberger, L. Brecker and B. Nidetzky (2013) Chem Comm, submitted.

Construction of active-site mutants of sucrose phosphorylase to investigate the interplay between aromatic interactions from Phe^{52} and the residues of the catalytic triad.

P. Wildberger and B. Nidetzky, in preparation.

Phosphoryl transfer from glucose 1-phosphate catalyzed by *Escherichia coli* sugar-phosphate phosphatases from two phosphatase-superfamily types.
P. Wildberger, M. Pfeiffer, L. Brecker, G. N. Rechberger, R. Birner-Gruenberger and B. Nidetzky, in preparation.

Efficient one-pot synthesis of fructose 1-phosphate from inexpensive starting materials by using a coupled enzymatic system based on sucrose phosphorylase and glucose-1-phosphatase.
P. Wildberger, M. Pfeiffer, L. Brecker and B. Nidetzky, in preparation.

Oral presentations

The role of aromatic interactions in the catalytic mechanism of sucrose phosphorylase.
15^{th} Austrian Carbohydrate Symposium (2011) Graz, Austria.

Aromatic interactions at the catalytic subsite of sucrose phosphorylase: Analysis of their role in enzymatic glucosyl transfer.
16^{th} European Carbohydrate Symposium, Session Glycobiology and Glycomedicine (2011) Sorrento, Italy.

With sucrose phosphorylase to the novel osmolyte (*R*)-2-*O*-α-D-glucopyranosyl glyceramide - an example for a regio- and enantioselective transglucosylation reaction.
10^{th} DocDay (2013) Graz, Austria.

Poster presentations

The role of aromatic stacking interactions at Phe^{52} in the catalytic mechansim of sucrose phosphorylase.
11^{th} European Training Course on Carbohydrates (2010) Wageningen, The Netherlands.

The role of aromatic interactions at the catalytic subsite of sucrose phosphorylase.
9^{th} Carbohydrate Bioengineering Meeting (2011) Lisbon, Portugal.